LUT
Lappeenranta
University of Technology

Jani Siitonen

ADVANCED ANALYSIS AND DESIGN METHODS FOR PREPARATIVE CHROMATOGRAPHIC SEPARATION PROCESSES

Thesis for the degree of Doctor of Science (Technology) to be presented with due permission for public examination and criticism in the Auditorium 1381 at Lappeenranta University of Technology, Lappeenranta, Finland on the 12th of December, 2014, at noon.

Acta Universitatis
Lappeenrantaensis 617

Supervisors Professor Tuomo Sainio
LUT Chemtech
Lappeenranta University of Technology
Lappeenranta, Finland

Professor Mika Mänttäri
LUT Chemtech
Lappeenranta University of Technology
Lappeenranta, Finland

Reviewers Professor Marco Mazzotti
Institute of Process Engineering
ETH Zürich
Zürich, Switzerland

Professor Achim Kienle
Institute of Automation Technology
Otto-von-Guericke University
Magdeburg, Germany

Opponent Professor José Paulo Barbosa Mota
Chemistry Department
Universidade Nova de Lisboa
Caparica, Portugal

Custos Professor Tuomo Sainio
LUT Chemtech
Lappeenranta University of Technology
Lappeenranta, Finland

ISBN 978-952-265-714-5
ISBN 978-952-265-715-2 (PDF)
ISSN-L 1456-4491
ISSN 1456-4491

Lappeenrannan teknillinen yliopisto
Yliopistopaino 2014

ABSTRACT

Jani Siitonen
Advanced analysis and design methods for preparative chromatographic separation processes
Lappeenranta 2014
88 p.
Acta Universitatis Lappeenrantaensis 617
Diss. Lappeenranta University of Technology
ISBN 978-952-265-714-5, ISBN 978-952-265-715-2 (PDF), ISSN 1456-4491

Preparative liquid chromatography is one of the most selective separation techniques in the fine chemical, pharmaceutical, and food industries. Several process concepts have been developed and applied for improving the performance of classical batch chromatography. The most powerful approaches include various single-column recycling schemes, counter-current and cross-current multi-column setups, and hybrid processes where chromatography is coupled with other unit operations such as crystallization, chemical reactor, and/or solvent removal unit. To fully utilize the potential of stand-alone and integrated chromatographic processes, efficient methods for selecting the best process alternative as well as optimal operating conditions are needed.

In this thesis, a unified method is developed for analysis and design of the following single-column fixed bed processes and corresponding cross-current schemes: (1) batch chromatography, (2) batch chromatography with an integrated solvent removal unit, (3) mixed-recycle steady state recycling chromatography (SSR), and (4) mixed-recycle steady state recycling chromatography with solvent removal from fresh feed, recycle fraction, or column feed (SSR–SR). The method is based on the equilibrium theory of chromatography with an assumption of negligible mass transfer resistance and axial dispersion. The design criteria are given in general, dimensionless form that is formally analogous to that applied widely in the so called triangle theory of counter-current multi-column chromatography.

Analytical design equations are derived for binary systems that follow competitive Langmuir adsorption isotherm model. For this purpose, the existing analytic solution of the ideal model of chromatography for binary Langmuir mixtures is completed by deriving missing explicit equations for the height and location of the pure first component shock in the case of a small feed pulse. It is thus shown that the entire chromatographic cycle at the column outlet can be expressed in closed-form.

The developed design method allows predicting the feasible range of operating parameters that lead to desired product purities. It can be applied for the calculation of first estimates of optimal operating conditions, the analysis of process robustness, and the early-stage evaluation of different process alternatives.

The design method is utilized to analyse the possibility to enhance the performance of conventional SSR chromatography by integrating it with a solvent removal unit. It is shown that the amount of fresh feed processed during a chromatographic cycle and thus the

productivity of SSR process can be improved by removing solvent. The maximum solvent removal capacity depends on the location of the solvent removal unit and the physical solvent removal constraints, such as solubility, viscosity, and/or osmotic pressure limits. Usually, the most flexible option is to remove solvent from the column feed.

Applicability of the equilibrium design for real, non-ideal separation problems is evaluated by means of numerical simulations. Due to assumption of infinite column efficiency, the developed design method is most applicable for high performance systems where thermodynamic effects are predominant, while significant deviations are observed under highly non-ideal conditions.

The findings based on the equilibrium theory are applied to develop a shortcut approach for the design of chromatographic separation processes under strongly non-ideal conditions with significant dispersive effects. The method is based on a simple procedure applied to a single conventional chromatogram. Applicability of the approach for the design of batch and counter-current simulated moving bed processes is evaluated with case studies. It is shown that the shortcut approach works the better the higher the column efficiency and the lower the purity constraints are.

Keywords: batch chromatography, steady state recycling, cross-current, solvent removal, equilibrium theory, binary separation, process design

UDC 543.544:66.011:547:004.942

PREFACE

I have had the pleasure to carry out this doctoral thesis in the Laboratory of Separation Technology at Lappeenranta University of Technology during the years 2010–2014. I wish to express my deepest gratitude to my supervisors, Professor Tuomo Sainio and Professor Mika Mänttäri, for the opportunity to focus on this captivating research topic. The guidance, support, and inspiration you have kindly provided has been crucial for the completion of this work.

During my doctoral studies, I have had the privilege to work with some of the greatest researchers in the field of preparative chromatography. My research visits to the Nanyang Technological University, Singapore, in 2011 and to the Max Planck Institute Magdeburg, Germany, in 2013 were some of the most fascinating experiences of my life. I am much obliged to Professor Arvind Rajendran and Professor Andreas Seidel-Morgenstern for welcoming me into their research groups and contributing to my research. Professor Malte Kaspereit from Friedrich-Alexander-Universität deserves warm thanks for all the insightful thoughts he shared with me. The discussions with you were short but always very fruitful.

I thank the reviewers of the manuscript, Professor Marco Mazzotti from ETH Zürich and Professor Achim Kienle from Otto-von-Guericke University for their valuable comments. It has been an honor to have such prestige reviewers for this thesis.

The Graduate School of Chemical Engineering, the Doctoral Program of Green Chemical Technology of LUT Graduate School, the Research Foundation of Lappeenranta University of Technology, and the Finnish Foundation for Technology Promotion are gratefully acknowledged for their generous financial support.

I wish to thank all my current and former co-workers in the Laboratory of Separation Technology for pleasant working atmosphere. Special thanks go to Sam Stade, Elsi Strand, Jussi Lahti, and Timo Laakso. You are all such wonderful persons. Without your brilliant sense of humor and friendly support, the period of my doctoral research would have been much more boring. Moreover, I would like to thank Sanna Hellstén, Jari Heinonen, Esko Makkonen, and Saku Kukkonen for all the help and inspiration they gave me.

I am deeply grateful to my parents Paula and Otto, sister Jenni, other relatives, and friends for providing a counterbalance to my challenging work. My warmest thanks belong to my nephews, Ossi, Kaapo, and Sampo. You are the light of my life. Keep smiling and keep shining!

“Le mieux est l'ennemi du bien.” Voltaire

Lappeenranta, November 26, 2014

Jani Siitonen

LIST OF PUBLICATIONS

This thesis is based on the following peer-reviewed scientific journal articles, which are referred to in the text by Roman numerals:

I Siitonen, J., Sainio, T., and Kaspereit, M., Theoretical analysis of steady state recycling chromatography with solvent removal. *Sep. Purif. Technol.*, 78(2011), 21–32.

II Siitonen, J. and Sainio, T., Explicit equations for the height and position of the first component shock for binary mixtures with competitive Langmuir isotherms under ideal conditions. *J. Chromatogr. A*, 1218(2011), 6379–6387.

III Siitonen, J., Sainio, T., and Rajendran, A., Design of batch chromatography for separation of binary mixtures under reduced purity requirements. *J. Chromatogr. A*, 1286(2013), 55–68.

IV Siitonen, J. and Sainio, T., Steady state recycling chromatography with solvent removal—Effect of solvent removal constraints on process operation under ideal conditions. *J. Chromatogr. A*, 1341(2014), 15–30.

V Siitonen, J. and Sainio, T., Unified design of chromatographic separation processes. *Chem. Eng. Sci.*, 122(2015) 436–451.

VI Siitonen, J., Mänttäri, M., Seidel-Morgenstern, A., and Sainio, T., Robustness of steady state recycling chromatography with an integrated solvent removal unit. Submitted to *J. Chromatogr. A* on October 14, 2014 and revised on December 1, 2014.

Author's contribution in the publications

I The author derived the design equations and performed the simulation study. The manuscript was written together with the co-authors.

II The author derived the analytical equations, coded the simulation tool given as a supplementary material of the paper, and performed the simulation study. The author wrote the first draft of the manuscript.

III The author derived the design equations together with the co-authors and performed the numerical simulations by using a simulation tool developed earlier in the research group. The author wrote the first draft of the manuscript.

IV The author derived the design equations, selected the model systems, and performed the simulation study. The author wrote the first draft of the manuscript.

V The author derived the design equations, performed the simulation study by using a simulation tool developed earlier in the research group, and wrote the first draft of the manuscript.

VI The author developed the simulation tool, performed the simulation study, and wrote the first draft of the manuscript.

Author's other journal publications

Siitonen, J., Sainio, T., and Rajendran, A., Bypass chromatography – design and analysis of an improved strategy for operating batch chromatography processes. *J. Chromatogr. A*, 1230(2012), 77–92.

Hellstén, S., Siitonen, J., Mänttäri, M., and Sainio, T., Steady state recycling chromatography with an integrated solvent removal unit – Separation of glucose and galactose. *J. Chromatogr. A*, 1251(2012), 122–133.

TABLE OF CONTENTS

NOMENCLATURE

Symbols

$\boldsymbol{A}$	coefficient matrix defined by $\boldsymbol{A} = [\sigma_{ij} + Fq_{ij}]$, -
A_{col}	column cross-sectional area, m^2
A_{memb}	membrane area, m^2
A_n	area of section n in Fig. 8, (mol s)/m^3 or (kg s)/m^3
a_n	coefficient of the n^{th}-order term in Eq. (27), -
B_i	solute permeability, $m^3/(m^2\ s)$
B_S	solvent permeability, $m^3/(m^2\ s\ Pa)$
c	concentration in the fluid phase, mol/m^3 or kg/m^3
D_{ax}	axial dispersion coefficient, m^2/s
D_{col}	column diameter, m
EC	specific eluent consumption, m^3/mol or m^3/kg
F	phase ratio, -
H	Henry constant, -
h	an auxiliary parameter defined by $h = (H_1K_2)/(H_2K_1)$, -
J_i	solute flux, mol/(m^2 s) or kg/(m^2 s)
J_S	solvent flux, $m^3/(m^2\ s)$
K	equilibrium parameter, m^3/mol or m^3/kg
K_{SR}	dimensionless solvent removal capacity defined by Eq. (55), -
k	mass transfer coefficient, 1/s
L_{col}	column length, m
L_f	loading factor, -
m_1	dimensionless end of product fraction *B* defined by Eq. (50), -
m_2	dimensionless beginning of product fraction *B* defined by Eq. (51), -
m_3	dimensionless end of product fraction *A* defined by Eq. (52), -
m_4	dimensionless beginning of product fraction *A* defined by Eq. (53), -
m_j	volume of fraction j with respect to the volume of the stationary phase, -
N	saturation capacity of the adsorbent, mol/m^3 or kg/m^3
N_{col}	number of columns, -
$N_{col,tot}$	total number of columns in a multi-column process, -
NTP	number of theoretical plates in a chromatographic column determined under linear conditions for the less strongly adsorbed component, -
n	amount of solute, mol or kg
p	purity, -
PR	productivity, mol/(s m^3) or kg/(s m^3)
Q	volumetric flow rate, m^3/s
q	concentration in the stationary phase, mol/m^3 or kg/m^3
q^{eq}	stationary phase concentration that is in equilibrium with the fluid phase, mol/m^3 or kg/m^3
q_{ij}	partial derivative of adsorption isotherm $q_{ij} = \partial q_i^{eq}/\partial c_j$
R	gas constant, J/(mol K)
T	temperature, K
t	time, s

t_0	elution time of a non-retained component, s
t^*	switch time, s
u	interstitial velocity, m/s
V	volume, m^3
V_{col}	column volume, m^3
x	spatial coordinate, m
x_{col}	width of cross-current true moving bed unit, m
Y	yield, -
y	spatial coordinate, m

Greek letters

α	separation factor, -
Γ	characteristic of a simple wave, -
ΔP_{memb}	transmembrane pressure, Pa
Δt_{cycle}	cycle time, s
Δt_F	duration of a feed pulse, s
$\Delta\pi$	osmotic pressure, Pa
ε	total void fraction of the bed, -
ζ	slope of characteristic in the hodograph plane, -
$\tilde{\zeta}_+^F$	slope of Γ_+ characteristic that passes through the steady state feed composition when no pure products are recycled, -
η	an auxiliary parameters defined by Eq. (76), -
Σ	shock wave, -
σ_{ij}	Kronecker delta, -
ω	characteristic parameter defined by Eqs. (18) and (19), -

Subscripts and superscripts

1, 2	components to be separated
A	first product fraction
*A*1	beginning of product fraction *A*
*A*2	end of product fraction *A*
B	second product fraction
*B*1	beginning of product fraction *B*
*B*2	end of product fraction *B*
C	limit *C*
col	chromatographic column
cycle	chromatographic cycle
design	design chromatogram in shortcut design
E	eluent
*E*1	end of elution profile of component 1
*E*2	end of elution profile of component 2
F	column feed
FF	fresh feed

FF’	concentrated fresh feed
i	component index
in	inlet of reservoir
j	fraction index or reservoir index
L	liquid phase
max	maximum value
memb	membrane
min	minimum value
mix	mixture of fresh feed and recycle fraction
out	outlet of reservoir
perm	permeate
R	recycle fraction
R’	concentrated recycle fraction
*R*1	beginning of elution profile of component 1
*R*2	beginning of elution profile of component 2
ret,feed	retentate that is fed from the membrane unit to the column feed tank
ret,rec	retentate that is recycled
ret,tot	total retentate
S	solid phase
SR	solvent removal
SSR	steady state recycling chromatography without solvent removal
x	spatial direction *x*
y	spatial direction *y*
+	faster wave or shock
−	slower wave or shock

Acronyms

AC	annular chromatography
CMC	carousel multi-column
SMB	simulated moving bed
SSR	steady state recycling
SSR–SR	steady state recycling with solvent removal

1 INTRODUCTION

Preparative liquid chromatography is a highly developed separation technique that is successfully applied to numerous difficult separation tasks in the pharmaceutical, fine chemical, and food industries. Typical examples are isolation and purification of enantiomers, other isomers, sugars, and proteins.

To meet the diverse industrial needs, several process configurations have been developed and applied. They can be roughly categorized to single-column fixed bed techniques, such as classical batch chromatography and various recycling schemes, to continuous counter-current multi-column techniques, such as simulated moving bed chromatography (SMB) and its several modifications, and to continuous cross-current techniques, such as carousel multi-column setup (CMC) and annular chromatography (AC).

The fixed bed batch chromatography is a common setup in many fine chemical and pharmaceutical applications because it is versatile, provides multiple product fractions, and assures rapid method development. The simplicity of the concept is counter-balanced by low productivity, high eluent consumption, and/or low recovery yield. The performance of batch process can be enhanced by employing different single-column recycling or multi-column SMB techniques. The most promising recycling concept is steady state recycling chromatography (SSR). It that can be operated in different injection modes such as mixed-recycle [1], closed-loop [2], or segmented-recycle mode [3, 4]. The counter-current SMB process provides a continuous feed flow and high performance but is rather complex and has high investment costs. The classical four-section SMB scheme is the most studied configuration, but several extensions and modifications have been developed, for example, asynchronous port switching [5, 6], modulation of the flow rates [7–12] or the feed concentration [13, 14], gradient operation [15–17], setups with more [18, 19] or less [20–23] than four sections, and single-column analogies [24–26]. The SMB technique is applied widely for the separation of sugars [27], petrochemicals [28], and fine chemicals, particularly enantiomers of chiral compounds [29]. As to the cross-current concepts, the CMC setup is utilized, for example, in continuous ion exchange [30, 31] and solvent gradient [32] applications. The annular chromatography, in contrast, has not gained an industrial breakthrough due to rather complex implementation and/or negligible performance benefit compared to the batch process [33].

One of the most promising approaches to enhance the performance of chromatographic separations is process integration where two or more unit operations are combined. Many potential chromatography-based hybrid concepts have been proposed such as coupling of chromatography with crystallization, chemical reactor, and/or solvent removal unit. Integration of chromatography with crystallization allows operating the chromatographic step such that only a partial enrichment of the purity is required [34–42]. This leads to higher productivity and lower eluent consumption. Combining separation with a chemical reactor has the advantage to achieve 100% yield of the target component even in the cases where the reaction equilibrium is not beneficial. The possible approaches can be categorized to conventional separator-reactor-recycle systems [43–46], partially integrated processes with side reactors [47], and fully integrated processes with reaction and separation within the same unit [48–50]. As to the solvent removal, membrane filtration or evaporation can be used to

concentrate the internal process streams, and thus enhance the performance of single-column [51], multi-column [52, 53], as well as coupled [44–46, 54, 55] separations.

The design of stand-alone chromatographic separations as well as chromatography-based hybrid processes is challenging due to complex, non-linear dynamics that leads to interactions between the independent process variables. A wide range of models with different levels of complexity are commonly employed in different steps of process development. Simplified models are typically used for estimation of the preliminary operating parameters and early-stage evaluation of the process performance, whereas detailed models are applied for simulation and optimization purposes.

As to the simplified process models, so called equilibrium theory of chromatography [56–60] has provided particularly good results, and established itself as a standard design tool. Within the frame of the theory, the propagation of the concentration states in the column are described by considering phase equilibrium and convection only, while mass transfer resistance and axial dispersion are neglected. The model forms a system of partial differential equations that can be solved by the method of characteristics leading in many cases of interest to simple algebraic equations. The theory provides an understanding of the main features of the non-linear column dynamics such as formation and propagation of concentration shocks, dispersive waves, and their interactions for single, binary, as well as multi-component systems.

The equilibrium theory based triangle method, developed by Storti et al. [61], has been widely used for the design of counter-current multi-column SMB applications both in the academia and industry. The method allows predicting the optimal values of the main operating parameters for a given separation task. Moreover, it specifies a feasible range of operating parameters leading to pure products, which help to analyse the process robustness and the influence of different process variables on the separation performance. The theory has been elaborated for most of the relevant types of adsorption isotherms [62–69], for less than 100% purity constraints [70, 71], and for modified SMB techniques such as gradient operation [16, 72–74], three fraction separations [75], and operation with non-constant flow rates [76, 77]. In addition, it has been used for the design of coupled process configurations, such as combination of SMB unit with crystallization [39], bioreactor [44], or partial solvent removal [53].

As to the design of fixed bed chromatographic processes, the equilibrium theory has been applied by several authors for predicting the optimal operating parameters of different process schemes. Golshan-Shirazi and Guiochon [78] have derived explicit equations for batch chromatography to estimate the feed loading and cut times that lead to complete separation of the feed mixture, *i.e.* touching band operation. They provided also analytical equations to calculate the optimal operating parameters that correspond to arbitrary purity constraints when generation of waste fraction is allowed. The methods hold for binary systems that follow competitive Langmuir isotherm model. In addition, the analytical solution of the ideal model has been used for optimization of batch chromatography under practically relevant non-ideal conditions by combining it with a simple model of band broadening (*e.g.* [79, 80]).

Bailly and Tondeur [1] have employed the equilibrium theory for the design of mixed-recycle SSR chromatography to predict the optimal cut times leading to 100% product purities and recovery yields. Later, Sainio and Kaspereit [81] extended the method for less than 100% purity constraints, and provided a shortcut design approach for non-ideal conditions too [82].

The characteristic features of cross-current chromatographic processes have been analysed in [83–86]. It has been shown that the cross-current chromatography is formally analogous to the classical one-dimensional time dependent fixed bed process when the dispersion in the direction of the solid flow is neglected. This means that the design methods developed originally for the fixed processes can be applied for corresponding cross-current concepts as well.

One of the main research gaps related to the design of preparative chromatographic separations is that the design approaches developed so far for fixed bed, cross-current, and counter-current processes, including the calculation procedure and the way of representing the results, are quite different from each other. For example, the triangle theory of counter-current chromatography allows predicting the entire range of feasible operating parameters, whereas in the cases of fixed bed and cross-current concepts, the discussion is often limited to the choice of the optimal operating conditions only. This shortcoming has made it difficult to generalize the information related to choice of feasible operating parameters for one chromatographic configuration to the design of other process schemes and to analyse the robustness of fixed bed and cross-current schemes.

In addition to this, there is an obvious need for powerful tools for designing hybrid chromatography-based separation concepts. The full potential of coupled processes can be exploited only if both the optimal process configuration and the ideal operating conditions are chosen. This is a challenging task, especially, in the case of integrated processes with internal recycle streams due to interactions between the coupled units that affect the process performance and robustness. The focus of this work is on hybrid schemes where the performance of stand-alone fixed bed or cross-current chromatography is enhanced by integrating it with a solvent removal unit. The equilibrium theory of chromatography has not been applied for the design of such process concepts until now.

2 OBJECTIVES AND SCOPE OF THE THESIS

2.1 Aims of the work

The main objective of this thesis is to create a unified, theoretical frame for the analysis and design of stand-alone single-column and cross-current multi-column chromatographic processes as well as their combinations with an integrated solvent removal unit. For this purpose, the equilibrium theory of chromatography is applied to derive analytical equations for calculating the operating boundaries of various process schemes. The design criteria are given in general, dimensionless form that is formally analogous to that applied in the established triangle theory of counter-current chromatographic processes. The developed design method is applicable for (1) selecting the optimal and robust operating conditions, (2) analysing the influence of different process parameters on the separation performance, and (3) understanding similarities and differences between various chromatographic process schemes.

The developed design method is applied to analyse the possibility to enhance the performance of stand-alone chromatographic separation by coupling it with an integrated solvent removal unit. The focus is on mixed-recycle SSR chromatography where the internal process streams are concentrated by partially removing solvent from them. The process concept will henceforth be abbreviated as SSR–SR. Three alternative SSR–SR configurations, where solvent is removed from the fresh feed, from the recycle fraction, or from the column feed that is obtained by mixing the fresh feed and the recycle fraction, are compared with conventional SSR chromatography and batch process with or without solvent removal.

In addition to the design method based on the equilibrium theory of chromatography, a shortcut approach is developed for the design of chromatographic separations under strongly non-ideal conditions. The method allows predicting first estimates of optimal operating parameters based on a simple procedure applied to a single conventional chromatogram. The applicability of the approach for the design of batch and counter-current SMB processes is evaluated by means of numerical simulations.

2.2 Scope and limitations

The design method based on the equilibrium theory of chromatography is limited to isocratic operation of the following chromatographic process configurations: (1) batch chromatography, (2) batch chromatography with solvent removal from fresh feed, (3) mixed-recycle steady state recycling chromatography, (4) mixed-recycle steady state recycling chromatography with solvent removal from fresh feed, recycle fraction, or column feed, and (5) cross-current chromatography and its modifications that corresponds to the above single-column schemes. The equilibrium design of counter-current SMB units is briefly discussed as a reference.

The analytical design equations derived in the present work holds under ideal conditions for systems that follow competitive Langmuir adsorption isotherm model. The proposed set of dimensionless design criteria, however, is generally applicable also for other isotherm models

and non-ideal conditions. The influence of finite column efficiency on the feasibility of the equilibrium design is briefly discussed with two cases studies.

The shortcut design approach is applicable for the design of stand-alone chromatographic separations under non-ideal conditions. It does not require a dynamic process model and can be applied without knowledge of adsorption isotherm parameters. The method is valid in general for all convex (favourable) and concave (unfavourable) isotherms for which no inflection points or selectivity reversal exist.

Both the design methods are applicable for binary separations under arbitrary purity and/or yield constraints as far as no waste fraction is generated. The discussion is limited to so-called restrictive design, *i.e.* it is assumed that the consecutive chromatograms do not overlap. The bypass aspect, studied in [87], where a part of the feed mixture is overpurified in the chromatographic step and the resulting fractions are blended with fresh feed to match the target purities is not taken into account here.

2.3 Outline

This thesis is based on six scientific journal publications given as appendices. At the beginning of the thesis, basic principles of the process configurations studied in this work are briefly described in Chapter 3. The fundamentals of the applied process models are then reviewed in Chapter 4. The main focus is on the equilibrium theory of chromatography. Special attention has been paid to the novel explicit equations of the height and position of the first component shock derived in Paper II.

The design method based on the equilibrium theory developed in Papers I and III–V is summarized in Chapter 5. The design objectives as well as the unified, dimensionless set of design parameters are given in Chapter 5.1. The procedure to calculate the feasible range of operating parameters corresponding to arbitrary purity and solvent removal constraints is described in Chapters 5.2 and 5.3. Selection of optimal operating parameters, considered in Papers I–V, and selection of robust operating parameters, considered in Paper VI, are discussed in Chapters 5.4 and 5.5, respectively.

The applicability of the design method is demonstrated in Chapter 6 with two case studies. The separation of EMD 53986 enantiomers and the separation of mandelic acid enantiomers are used as model systems. The performance comparison of batch and SSR processes with or without an integrated solvent removal unit under ideal conditions is shown in Chapters 6.1.1 and 6.2.1, and the influence of finite column efficiency on the design of different process configurations is analysed in Chapters 6.1.2 and 6.2.2.

Finally, the shortcut approach proposed in Papers III and V for the design of chromatographic separation processes under strongly non-ideal conditions is reviewed in Chapter 7. The calculation procedure is described in Chapter 7.1, and the applicability of the approach for the design of batch and counter-current SMB units is demonstrated in Chapters 7.2 and 7.3, respectively.

3 PROCESS CONFIGURATIONS

3.1 Batch chromatography

Chromatographic separation is based on differences in the distribution of the target components between a stationary and a mobile phase. In liquid chromatography, the solid stationary phase is typically packed to a fixed bed column, and the sample components travel through it in a carrier liquid called eluent. The migration velocity of each component depends on its specific affinity towards the stationary phase. Retention of components may be caused by different mechanisms, such as adsorption, complex formation, ion-exchange or ligand-exchange, ion-exclusion or size-exclusion, or interactions between the solutes.

A schematic setup of classical elution mode batch chromatography is displayed in Fig. 1a. At given time intervals, the selection valve is switched to introduce a pulse of fresh feed mixture into the column. After the desired volume of the feed pulse, V_F, is realized, the selection valve is switched back to the eluent to elute the feed pulse, and the solutes propagate through the column with different velocities. At the column outlet, the fractionation valve is used to collect the products in independent vessels.

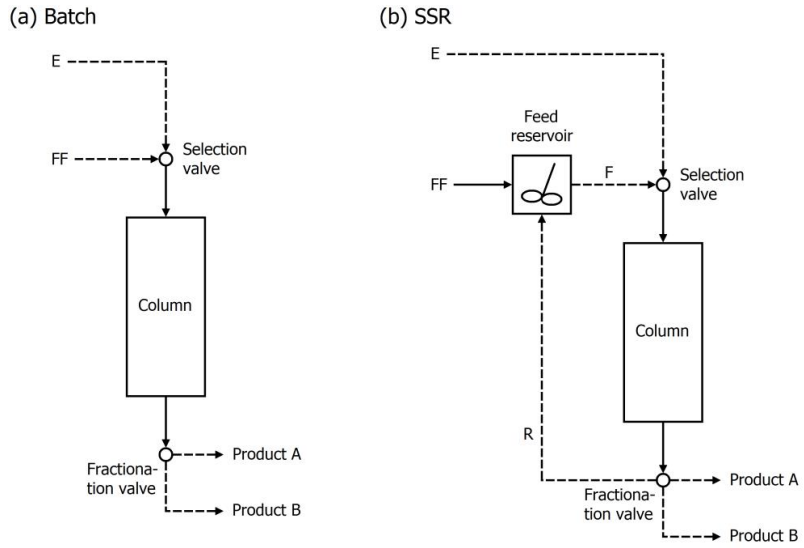

Fig. 1. Schematic setup of (a) batch chromatography and (b) mixed-recycle SSR chromatography. *E*, eluent; *FF*, fresh feed; *F*, column feed; *R*, recycle fraction. Solid line: continuous flow. Dashed line: discontinuous flow.

Batch chromatography can be used for separation of both binary and multi-component mixtures. Different fraction collection strategies can be applied depending on if generation of waste fraction is allowed or not. In this work, only binary separation without generation of

waste fraction is discussed. An example of the fraction collection at the column outlet is illustrated in Fig. 2. The actual chromatographic cycle starts at time t_{A1} when the less strongly retained component begins to elute. The column effluent is directed to product fraction *A* to collect the pure leading section of the chromatogram containing an excess of component 1. When the generation of waste fraction is not allowed, the end of the product fraction *A*, t_{A2}, is equal to the beginning of the product fraction *B*, t_{B1}. After t_{B1}, the product *B* containing an excess of the more retained component 2 is collected until the chromatogram is eluted completely at time t_{B2}.

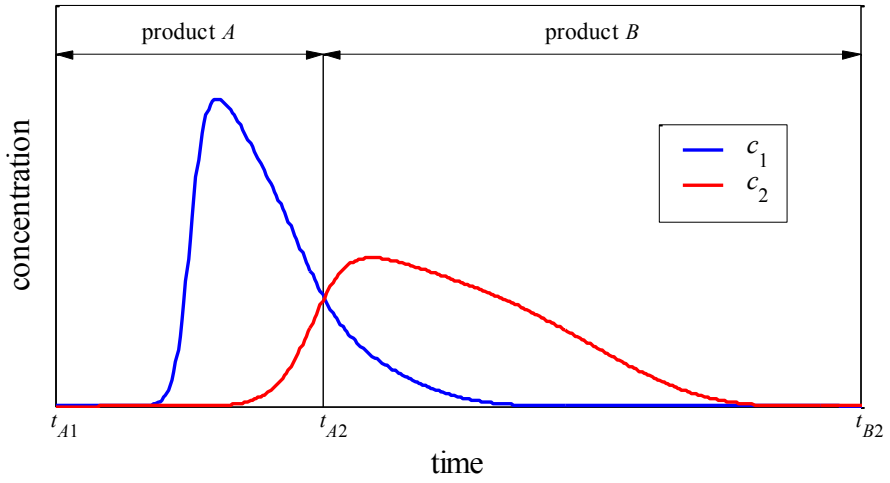

Fig. 2. Individual elution profiles and fraction collection in batch chromatography.

3.2 Steady state recycling chromatography

In steady state recycling chromatography (SSR), shown in Fig. 1b, the volume of the feed pulse is typically larger than in batch process. This leads to only partial separation of the feed mixture. The pure leading and trailing sections of the effluent profile are collected as products, while the unresolved middle zone is recycled. In the mixed-recycle mode, the whole recycle fraction is collected in the feed reservoir, mixed with fresh feed, and then introduced back into the column. Repeating the above procedure forces the process into a periodic steady state in which the column feed concentrations, the elution profiles, and thus the average product compositions do not vary from cycle to cycle.

The start-up behaviour of a mixed-recycle SSR process depends on the initial state of the feed reservoir. An example of the process start-up with a full injection of fresh feed is illustrated in Fig. 3. It is seen that several cycles are required to achieve a periodic steady state. The start-up can be accelerated by initiating the process with a diluted fresh feed or a solution whose composition corresponds to the steady-state feed [81].

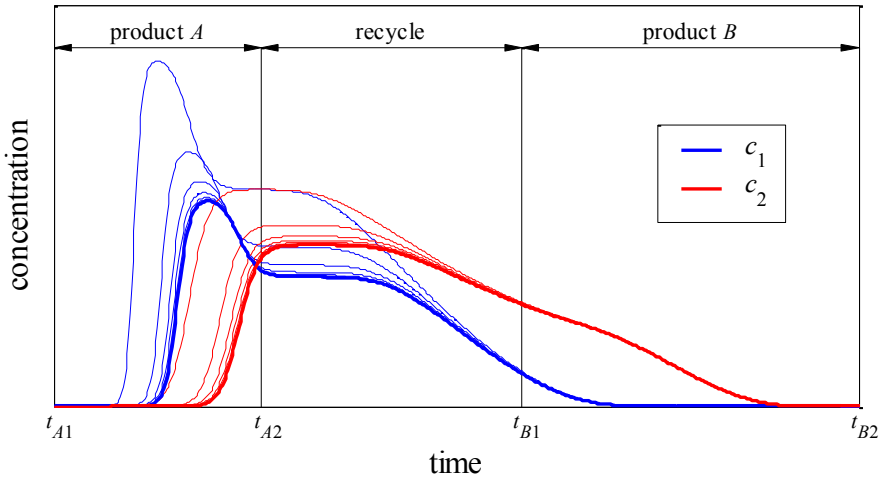

Fig. 3. Start-up behaviour and fraction collection in mixed-recycle SSR chromatography. The diagram shows an overlay of the individual concentration profiles at column outlet for cycles 1–30. Thick solid lines: concentration profiles at steady state (cycle 30).

3.3 Integration of a solvent removal unit with batch and SSR chromatography

The maximum performance in preparative chromatographic separation is typically achieved when the feed concentrations into the chromatographic unit are high [33]. In batch process, the fresh feed mixture can be concentrated by partially removing solvent from it. The solvent can be removed by using, for example, membrane filtration or evaporation. A schematic setup of the process configuration is illustrated in Fig. 4a.

As to the mixed-recycle SSR process, the steady state feed concentrations into the column can be increased by removing solvent either from the fresh feed or from the internal recycle streams. In this work, the design, performance, and robustness of the following three SSR–SR configurations are studied:

I) Solvent is removed from the fresh feed (Fig. 4b).

II) Solvent is removed from the recycle fraction (Fig. 4c).

III) Solvent is removed from the actual feed solution into the column which is obtained by mixing the fresh feed and the recycle fraction (Fig. 4d).

In all three options, the system approaches a cyclic steady state when the amount of removed solvent as well as the amount of fresh feed introduced into the process during a chromatographic cycle are kept constant. The removed solvent can be used as eluent to reduce the need of fresh eluent provided that the removed solvent is pure.

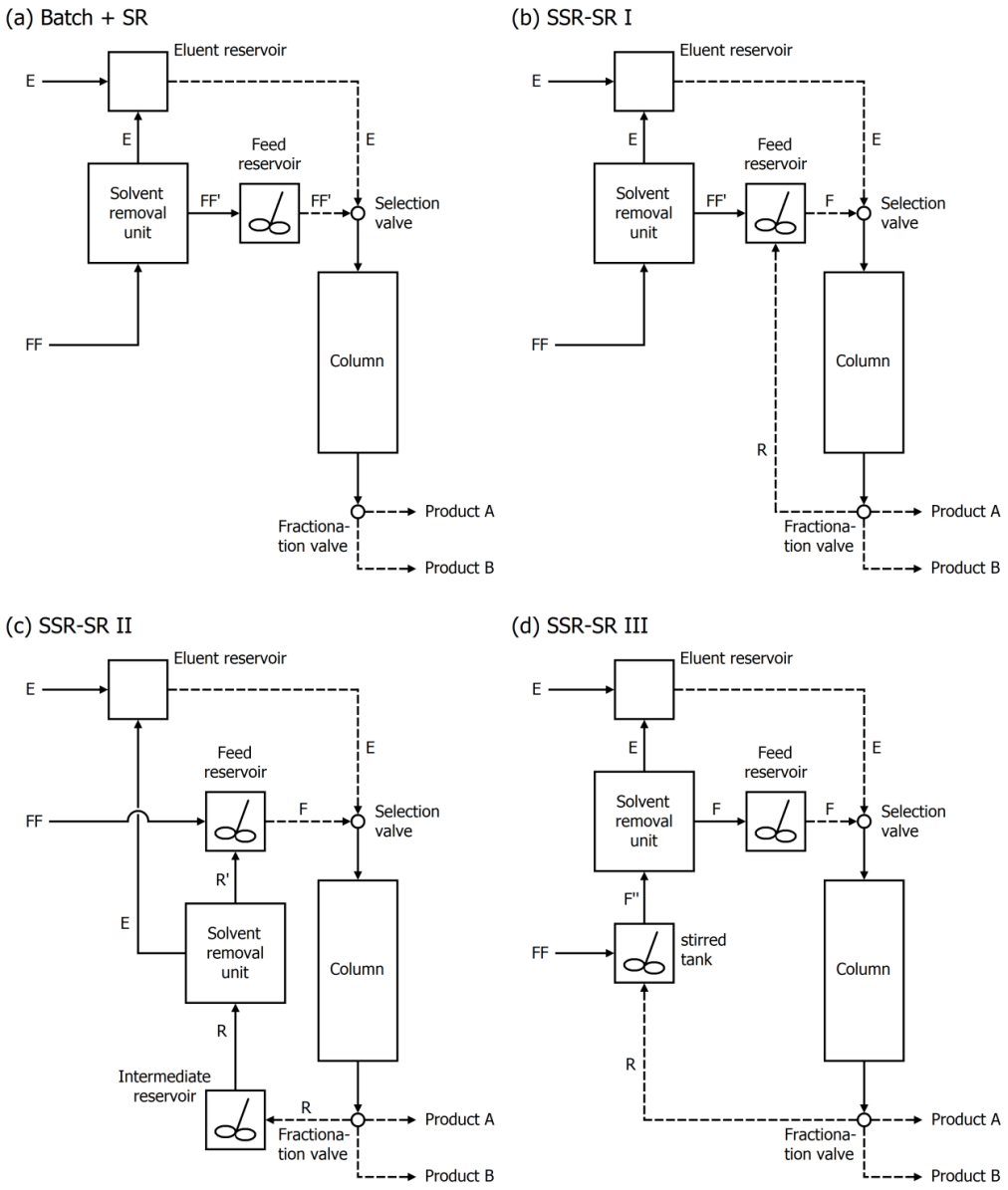

Fig. 4. Schematic setup of (a) batch chromatography with solvent removal from fresh feed, (b) SSR–SR configuration I (solvent is removed from fresh feed), (c) SSR–SR configuration II (solvent is removed from recycle fraction), (d) SSR–SR configuration III (solvent is removed from mixed fraction). *E*, eluent; *FF*, fresh feed; *FF*', concentrated fresh feed; *F*, column feed; *R*, recycle fraction, *R*', concentrated recycle fraction; *F*'', mixed fraction. Solid line: continuous flow. Dashed line: discontinuous flow.

The solvent removal methods are typically continuous by nature, whereas the fixed bed chromatography is operated in a discontinuous manner. For this reason, intermediate buffer reservoirs are needed to ensure a continuous feed flow to the solvent removal unit and a discontinuous feed flow to the chromatographic unit.

The solvent removal unit can be operated either in single-pass mode or in feed and bleed mode where only a part of the concentrated solution is bled continuously from the unit, while the rest is recycled back to the unit inlet. The feed and bleed mode is commonly used in membrane applications, because it allows maintaining high and constant cross-flow velocity across the membrane to prevent concentration polarization irrespective of other process parameters which can vary with time or feed composition.

In addition to single-pass and feed and bleed modes, there exist also a third way to implement the solvent removal step. It is possible to direct the concentrated solution from the outlet of the solvent removal unit back to the feed tank of the unit. This reduces the number of needed reservoirs but causes back-dilution. Qualitatively, the theory discussed in this work is applicable also for this kind of operation as well, but the back-dilution affects the absolute amount of solvent that can be removed without violating solvent removal constraints, such as solubility or viscosity limits.

3.4 Cross-current chromatography

Cross-current chromatography is a separation technique where continuous separation is achieved by employing two spatial directions. The fluid phase flows in crosswise direction with respect to the solid phase, which leads to time independent steady state. The true cross-current operation can be implemented in rotating annular chromatography and simulated cross-current operation in carousel multi-column setup. In practice, the carousel setup is more feasible option because the implementation of annular technique is rather complex.

A carousel multi-column setup (Fig. 5) consists of a series of identical fixed bed columns. The columns are operated parallel under the same conditions. The column node works periodically such that in each time interval a certain number of columns are operated in the loading mode and the remaining ones in the elution mode to assure a continuous fresh feed delivery. This is realized by switching the fresh feed and eluent ports in equal time intervals. The cross-current movement is mimicked better when the number of columns in the carousel is large and the ports are switched at high frequency. The values of the fresh feed and the product flow rates in the unit are multiplication of the corresponding flow rates in single batch column.

As mentioned in Section 1, the two-dimensional cross-current chromatography is formally analogous to the classical one-dimensional time dependent fixed bed process (see *e.g.* [84]). Physically, the analogy is most obvious for the carousel type multi-column setup where each individual column is operated in exactly the same way as a single column. For this reason, also other single-column concepts, such as recycling and hybrid solvent removal techniques described in Sections 3.2 and 3.3, can be easily implemented in cross-current mode as well.

The process schemes are similar to those displayed in Figs. 1 and 4 with the difference that the single-column chromatography is replaced by a cross-current setup.

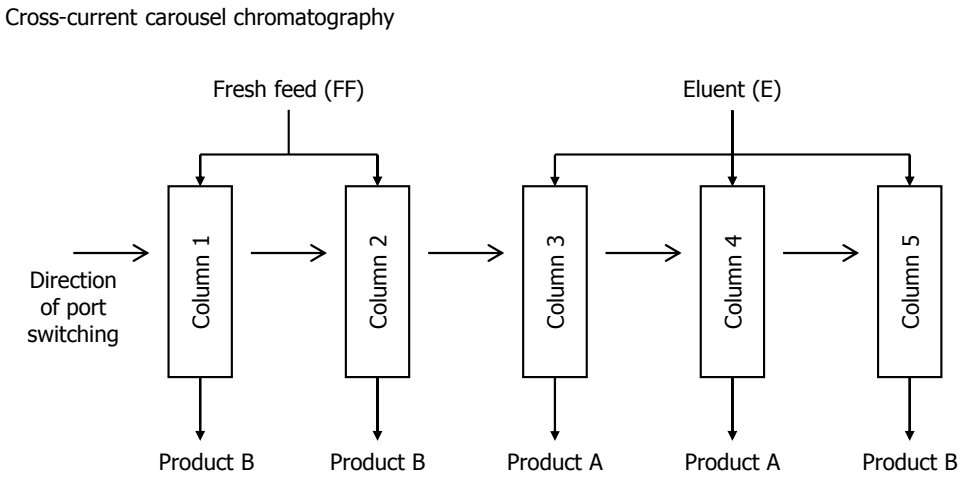

Fig. 5. Schematic setup of a cross-current carousel multi-column chromatography.

3.5 Counter-current chromatography

In counter-current chromatography, the fluid and solid phases flow in opposite directions. The operation mode can be implemented continuously with the true moving bed (TMB) technique or in a discontinuous manner by using the simulated moving bed (SMB) scheme. In practice, however, the TMB mode is not feasible concept because the movement of the solid phase causes mixing and attrition, and the SMB setup is preferred.

The classical SMB process consists of series of conventional fixed bed columns (Fig. 6a). The inlet and outlet ports of the unit are switched periodically in the direction of the fluid phase to mimic the continuous counter-current movement of the solid phase. The continuous movement is simulated better when the number of fixed bed columns in the SMB unit is large and the ports are switched at high frequency. The binary fresh feed mixture is fed continuously between sections 2 and 3. The separation is carried out in the two central sections, 2 and 3, where the less retained component 1 is conveyed to the product fraction *A* (called raffinate) between sections 3 and 4, and the more retained component 2 to the product fraction *B* (called extract) between sections 1 and 2. The eluent is introduced into section 1 to regenerate the solid phase that is then recycled to section 4. The pure eluent that exist section 4 is recycled into section 1. The process is operated in cyclic steady state, in which the unit exhibits the same time dependent behaviour during each time period between two successive switches.

In addition to the conventional multi-column SMB setup, counter-current simulated moving bed mode can be implemented by using only a single chromatographic column [24–26]. The

single-column SMB analogue has one chromatographic column connected to a number of tanks [24, 25] or plug-flow tubes [26] equal to the number of steps of the SMB cycle. These allow recycling of the fluid phase in a pattern that mimics the multi-column SMB operation as displayed in Fig. 6b. It has been shown that an ideal plug-flow single-column analogue is theoretically indistinguishable from the equivalent multi-column SMB unit, and it thus provides the same product purities as those of the analogous multi-column process [26]. In practice, however, the product purities obtained in the single-column setup are often lower due to mixing in the tanks or in the recycling tubes [24–26]. It is worth noting that the single-column SMB analogue can be considered both as a counter-current simulated moving bed unit and as a single-column recycling scheme, thus being an interesting link between single and multi-column chromatographic processes.

a) Counter-current simulated moving bed chromatography

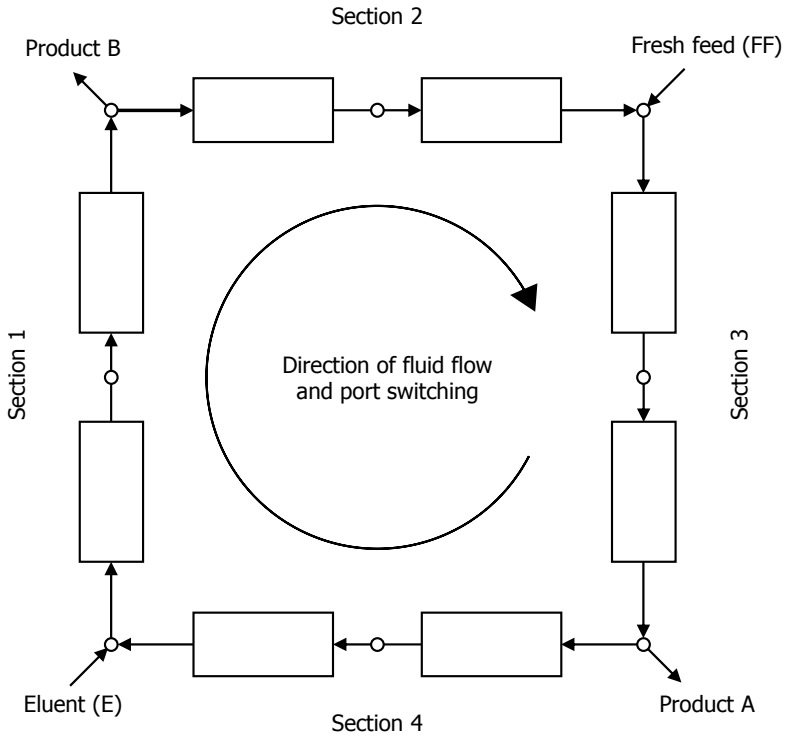

b) Single-column simulated moving bed analogue

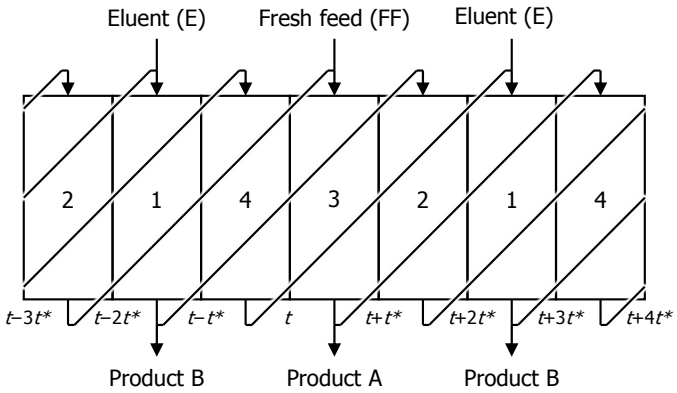

Fig. 6. Schematic setup of (a) four-section counter-current multi-column simulated moving bed chromatography and (b) four-section plug-flow single-column simulated moving bed analogue with recycle lag.

4 MATHEMATICAL MODELLING

4.1 Equilibrium theory of chromatography

4.1.1 Ideal model

The equilibrium theory is based on the ideal model of chromatography with the following assumptions: (1) Axial dispersion and mass transfer resistance in the column are negligible. (2) Conditions in the column are radially homogeneous. (3) Mobile phase flow rate is constant along the column. (4) Isotherm parameters and bed porosity are constant along the column. The mass balance for an individual component *i* in the fixed bed column is given by

$$u_y^L \frac{\partial c_i}{\partial y} + \frac{\partial}{\partial t}\left(c_i + F q_i^{\mathrm{eq}}\right) = 0 \qquad \text{for } i = (1, 2), \tag{1}$$

where c_i is the mobile phase concentration of solute i, q_i^{eq} is the stationary phase concentration that is in equilibrium with the fluid phase, $F = (1-\varepsilon)/\varepsilon$ is the phase ratio, with ε being the total void fraction of the bed, u_y^L is the interstitial velocity, t is the time, and y is the column axial coordinate. The interstitial velocity is related to the volumetric flow rate of the fluid phase in the column, Q_{col}, and to the retention time of a non-retained component, t_0, as follows:

$$u_y^L = \frac{Q_{col}}{\varepsilon A_{col}} = \frac{L_{col}}{t_0}, \tag{2}$$

where A_{col} is the cross-sectional area of the column and L_{col} is the column length.

The discussion of this work is limited to binary systems that follow the competitive Langmuir adsorption isotherm model. The dependence between the stationary phase loading and the mobile phase concentration is given by

$$q_i^{\mathrm{eq}} = \frac{N_i K_i c_i}{1 + K_1 c_1 + K_2 c_2}, \tag{3}$$

where N_i and K_i are the saturation capacity and the equilibrium parameter of solute i, respectively. In the following discussion, it is assumed that the component 1 is the less strongly retained one. This means that $H_2 > H_1$, where $H_i = N_i K_i$ is the Henry constant of component i.

To solve the model equations, the following initial and boundary conditions are used:

$$c_i(y, t = 0) = 0 \quad \text{for } 0 \le y \le L_{col}, \tag{4}$$

$$c_i(y=0,t)=c_i^F \quad \text{for } 0\le t\le \Delta t_F\,, \tag{5}$$

$$c_i(y=0,t)=c_i^E \quad \text{for } t>\Delta t_F\,. \tag{6}$$

In the above equations, c_i^F and c_i^E are the concentrations of solute *i* in the column feed reservoir and eluent reservoir, respectively. In the design method summarized in Section 5, it is assumed that the fresh eluent is pure solvent and the solvent removal unit works ideally such the solute yields are complete, *i.e.* also the removed solvent is pure. This means that the eluent concentrations are zero. In addition, it is assumed that the column feed concentrations are constant during an injection. They are calculated from the following mass balances:

$$c_i^F=\frac{c_i^{FF}V_{FF}+c_i^R V_R}{Q_{col}\Delta t_F}\,, \tag{7}$$

$$V_{FF}=V_F-V_R+V_{SR}\,, \tag{8}$$

$$V_R=(t_{B1}-t_{A2})Q_{col}\,, \tag{9}$$

$$V_{SR}=\Delta t_{cycle}Q_{SR}\,. \tag{10}$$

In the above equations, c_i^{FF} is concentration of solute *i* in the fresh feed, c_i^R is the volume-average concentration of solute *i* in the recycle fraction, V_{FF} is the volume of fresh feed introduced into the process during a chromatographic cycle, V_R is the volume of recycle fraction, V_{SR} is the volume of removed solvent per cycle, Q_{SR} is the solvent removal rate, and Δt_{cycle} is the cycle time. The cycle time, *i.e.* the time interval between the subsequent feed pulses, is selected such that the consecutive chromatograms do not overlap as follows:

$$\Delta t_{cycle}=t_{B2}-t_{A1}\,. \tag{11}$$

The column feed concentrations for conventional batch and SSR processes without solvent removal are obtained from Eqs. (7)–(10) as special cases with V_{SR} = 0.

To describe the cross-current chromatography, true moving bed model is used. It is assumed that the fluid flows with an interstitial velocity u_y^L in the direction *y*, and both the solid phase and the fluid phase move with a velocity $u_x^S = u_x^L$ in the direction *x* that is perpendicular to *y*. The material balance describing the solute movement is

$$\frac{u_y^L}{u_x^L}\frac{\partial c_i}{\partial y}+\frac{\partial}{\partial x}\left(c_i+Fq_i^{\mathrm{eq}}\right)=0\,, \tag{12}$$

where *x* and *y* are the spatial coordinates. The conversion rules for simulated cross-current carousel multi-column concept are given by

$$\frac{N_{col}}{N_{col,tot}} = \frac{x}{x_{col}}, \tag{13}$$

$$t^* = \frac{x_{col}}{u_x^L N_{col,tot}}. \tag{14}$$

In the above equations, $N_{col}/N_{col,tot}$ is the proportion of columns to the total number of columns, x_{col} is the total width of the true moving bed unit in the direction x, and t^* is the switch time. As shown by Wankat [84] the two-dimensional time independent cross-flow model, Eq. (12), is formally analogous to the one dimensional time dependent fixed bed model, Eq. (1). The equations for the latter can be transferred to the former by using the following transform:

$$t = x/u_x^L. \tag{15}$$

The initial and boundary conditions of the cross-current model, Eq. (12), are analogous to those of the fixed bed model, Eq. (1). They can be calculated from Eqs. (4)–(6) by using the above transform, Eq. (15).

4.1.2 Solution of the ideal model

The ideal model described in Section 4.1.1 forms a coupled system of two homogeneous, quasilinear, first-order partial differential equations. When Riemann boundary conditions are used, the model can be solved analytically by the method of characteristics (see *e.g.* [56–60]). The solution is originally derived for the fixed bed model, but it can be applied for the cross-current model as well by using the transform given by Eq. (15).

When a rectangular pulse of a binary mixture that follows competitive Langmuir isotherm model is introduced at the inlet of an initially clean column, two simple wave transitions (Γ_+, Γ_-) and two shock wave transitions (Σ_+, Σ_-) are composed. The solution of the model consists of describing the movement of these waves and their interactions along the column. The image of the chromatographic cycle is conveniently constructed in the so-called hodograph (c_1, c_2) and characteristic (ω_1, ω_2) planes. Examples of these representations and a corresponding chromatogram are given in Fig. 7. Regions of the solution where c_1 and c_2 are constant are represented by single points. The points F and O denote the feed and the initial states, respectively, while P and Q stand for the two intermediate states. The image of the solution path is given by

$$O \overset{\Gamma_-}{\rightarrow} P \overset{\Gamma_+}{\rightarrow} F \overset{\Sigma_-}{\rightarrow} Q \overset{\Sigma_+}{\rightarrow} O. \tag{16}$$

For Langmuir isotherm, the simple wave transitions correspond on the hodograph plane to segments on straight lines, called characteristics. The slopes of the characteristics ($\mathrm{d}c_1/\mathrm{d}c_2$) are obtained from the right eigenvectors of the matrix $\boldsymbol{A} = \left[\delta_{ij} + Fq_{ij}\right]$, where δ_{ij} is the Kronecker

delta, defined as 1 if $i = j$ and 0 if $i \neq j$, and $q_{ij} = \partial q_i^{\mathrm{eq}} / \partial c_j$ is the partial derivative of the adsorption isotherm, Eq. (3). Explicit expressions for the slopes are achieved as roots of the following quadratic equation:

$$K_1 H_2 c_2 \zeta^2 - \left[H_1\left(1 + K_2 c_2\right) - H_2\left(1 + K_1 c_1\right)\right]\zeta - K_2 H_1 c_1 = 0 . \tag{17}$$

The positive and negative slopes of the characteristics are denoted by ζ_+ and ζ_-, respectively. The propagation velocities of the simple waves are calculated from the eigenvalues of the matrix $\boldsymbol{A}$.

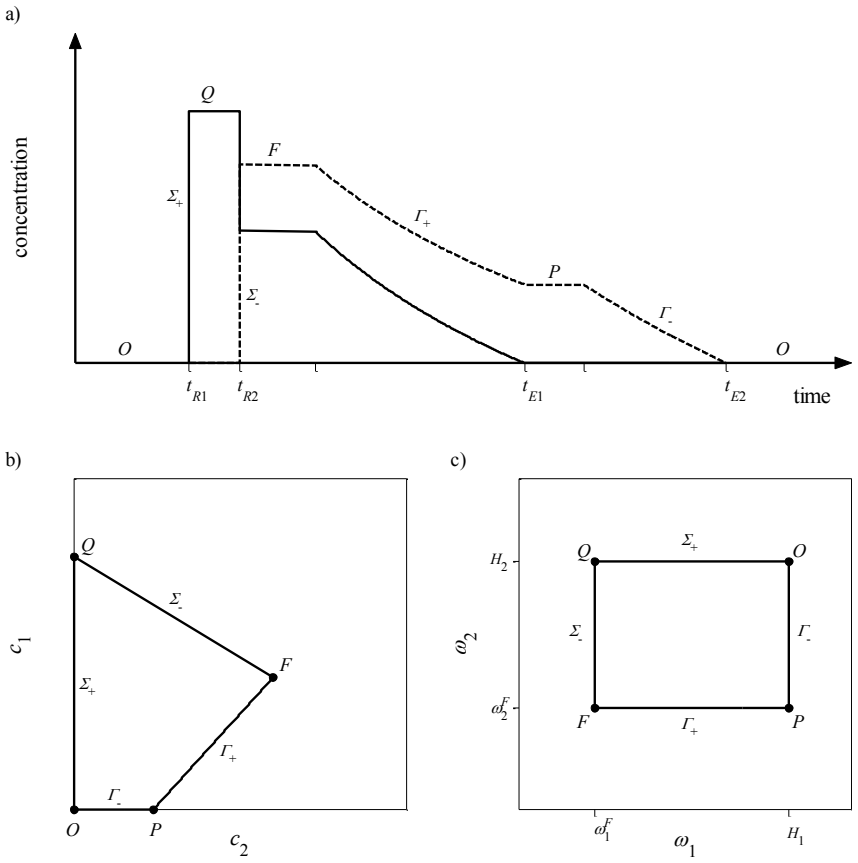

Fig. 7. Chromatographic cycles under ideal conditions for an arbitrary systems that follows competitive Langmuir isotherm models: (a) individual elution profiles; (b) hodograph plane; (c) characteristic plane.

In the case of Langmuir isotherm, the images of the shock transitions Σ_+ and Σ_- coincide with the characteristics Γ_+ and Γ_-, respectively. The propagation velocities of the shock waves are given by the mass balance across the discontinuity.

A convenient way to study the above Riemann problems is to perform a variable transform by introducing pair of characteristic parameters (ω_1, ω_2) defined as

$$\omega_1 = \frac{(\zeta_- + h)H_2}{\zeta_- + h\alpha}, \tag{18}$$

$$\omega_2 = \frac{(\zeta_+ + h)H_2}{\zeta_+ + h\alpha}, \tag{19}$$

where $\alpha = H_2/H_1$ is the separation factor and h is an auxiliary parameter given by $h = (H_1K_2)/(H_2K_1)$. As seen in Eqs. (18) and (19), the parameter ω_1 is constant along the Γ_+ characteristic and ω_2 is constant along the Γ_- characteristic. The limits for ω-values are given by

$$0 < \omega_1 \le H_1 \le \omega_2 \le H_2. \tag{20}$$

It has been shown that there exists a one-to-one mapping between the concentrations (c_1, c_2) and the two characteristics parameters (ω_1, ω_2) [59]. The concentrations are given by the following relationships:

$$c_1 = \frac{-H_2(\omega_1 - H_1)(\omega_2 - H_1)}{\omega_1\omega_2(H_2 - H_1)K_1}, \tag{21}$$

$$c_2 = \frac{H_1(\omega_1 - H_2)(\omega_2 - H_2)}{\omega_1\omega_2(H_2 - H_1)K_2}. \tag{22}$$

4.1.3 Explicit equations for the height and position of the first shock

For decades, there have been available an exact, analytical solution of the ideal model that allows calculating almost the entire chromatographic cycle at the outlet of fixed bed column in the case of binary Langmuir system [58]. The only exception is the height, c_1^S, and retention time, t_{R1}, of the first shock in the case of a relative small feed pulse, *i.e.* in the case when the pure first component plateau (state *Q* in Fig. 7) erodes completely during elution. In Paper II, the existing solution has been completed by deriving the missing closed-form equations for c_1^S and t_{R1}.

Criterion, whether the first component plateau erodes during elution or not, is given in [58]

$$\Delta t_F = \frac{F\omega_1^F \omega_2^F \left(H_2 - \omega_1^F\right)\left(H_1 - \omega_1^F\right)}{H_1 H_2 \left(\omega_2^F - \omega_1^F\right)} t_0 . \tag{23}$$

When the duration of the feed pulse is lower than that given by Eq. (23), the plateau erodes completely, and the first component shock, Σ_+, interacts with the wave, Γ_+. The concentration profile of the resulting pure first component wave is given as follows [58]:

$$t = \Delta t_F + t_0 \left\{ 1 + FH_1 \left[\frac{1}{\left(1 + K_1 c_1\right)^2} - L_{f,2} \frac{1 - 1/\alpha}{\left(1 - 1/\alpha + K_1 c_1\right)^2} \right] \right\}, \tag{24}$$

where symbol $L_{f,i} = \left(c_i^F \Delta t_F\right) / \left(N_i F t_0\right)$ denotes the loafing factor of component *i*.

In principle, the retention time of the first shock could be solved from the mass balance of the first component by integrating the elution profile and solving the floating integration boundary t_{R1} with which the amount of first component that is eluted from the column matches to the injected loading. Eq. (24), however, gives elution time as a function of c_1, while there is no closed-form solution for giving the relationship the other way around. This has complicated the derivation of analytical solution for the first shock.

In Paper II, it has been shown that the height of the first shock can be calculated from the mass balance of the first component, even though Eq. (24) cannot be expressed explicitly in form $c_1 = f(t)$. The idea is to integrate the elution profile piecewise with respect to c_1 from 0 to c_1^S and to subtract the term $c_1^S t_{R1}$ form the value of the integral. The calculation principle is demonstrated in Fig. 8. The areas of hatched regions A_3–A_5 correspond to the values of the integral terms, the area of green region A_1 to the amount of component 1, and the area of orange region A_2 to the difference between these values. For incomplete separation (Fig. 8a), the mass balance is given by

$$c_1^F \Delta t_F = A_1\left(c_1^S\right) = A_5 + A_4 + A_3\left(c_1^S\right) - A_2\left(c_1^S\right), \tag{25}$$

and for complete separation (Fig. 8b) by

$$c_1^F \Delta t_F = A_1\left(c_1^S\right) = A_3\left(c_1^S\right) - A_2\left(c_1^S\right). \tag{26}$$

Integration of Eqs. (25) and (26) leads, in both cases, to the following quartic equation:

$$a_4\left(K_1 c_1^S\right)^4 + a_3\left(K_1 c_1^S\right)^3 + a_2\left(K_1 c_1^S\right)^2 + a_1 K_1 c_1^S + a_0 = 0 , \tag{27}$$

where

$$a_4 = L_{f,1} + L_{f,2} - 1, \tag{28}$$

$$a_3 = 2\left[L_{f,1} + L_{f,2} + \left(1 - 1/\alpha\right)\left(L_{f,1} - 1\right)\right], \tag{29}$$

$$a_2 = L_{f,1} + L_{f,2} + (1-1/\alpha)\left[4L_{f,1} + (1-1/\alpha)(L_{f,1}-1)\right], \tag{30}$$

$$a_1 = 2L_{f,1}(1-1/\alpha)(2-1/\alpha), \tag{31}$$

$$a_0 = L_{f,1}(1-1/\alpha)^2. \tag{32}$$

Eq. (27) can be solved analytically by using one of the standard algorithms for quartic equations, for instance, Ferrari's method [88], Descartes–Euler method [89], or Neumark's method [90]. When $\alpha > 1$, $L_{f,1} > 0$, and $L_{f,2} > 0$, it has only one positive real root that must give the height of the first shock. Based on simulation study with ten million random combinations of $L_{f,1}$, $L_{f,2}$ and α, it has been demonstrated that the Ferrari's solution is computationally the most stable option for solving Eq. (27).

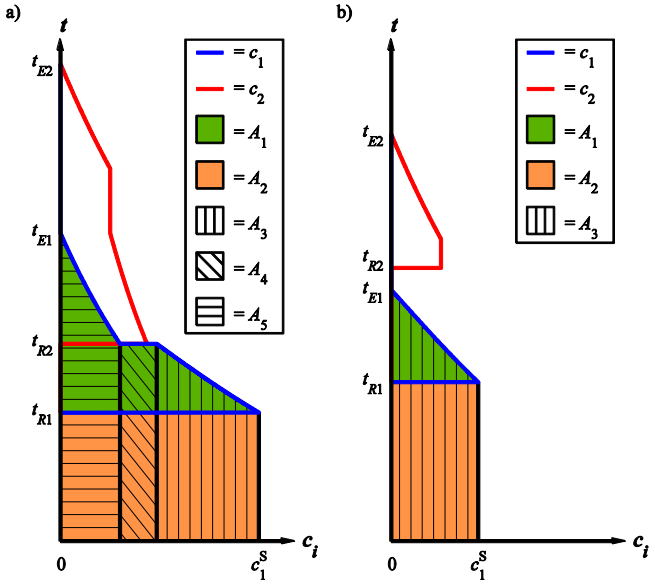

Fig. 8. Individual elution profiles of a rectangular injection pulse in the concentration–time coordinate system. A_1, the total amount of component 1; A_2, the difference between the sum of integral terms A_3–A_5 and the total amount of component 1 A_1; A_3–A_5, integral terms in Eqs. (25) and (26).

Once c_1^S is obtained, the retention time of the first shock can be calculated from Eq. (24) by setting $c_1 = c_1^S$. In addition, a novel simple parametric representation that gives the trajectory of the first shock in the distance–time diagram as a function of c_1^S is given in Paper II.

Finally, it is worth noting that explicit equations for the height and retention time of the first shock can be obtained also by using another approach. Rajendran and Mazzotti [60] have

derived a parametric representation of the trajectory of the first shock by using the ω-transform. Although not pursued by Rajendran and Mazzotti, it is straightforward to show that their equations also lead to a quartic when solved for characteristic parameter ω_1^S which corresponds to the shock height.

4.1.4 Hodograph representations of process configurations

Hodograph representation, shown in Fig. 9, is a convenient tool for visualizing the steady state operation of different chromatographic processes. In the case of classical batch chromatography (Figs. 1a and 9a), the composition of the column feed is equal to the fresh feed composition because nothing is recycled and solvent is not removed. The image of the chromatographic cycle on the hodograph plane depends on the duration of the feed pulse. When the feed pulse is large enough, the feed state as well as the two intermediate states, *P* and *Q*, prevail during elution (Fig. 7b), whereas for relatively low Δt_F values, one or more of the concentration plateaus erode completely (Fig. 9a). In the case of competitive Langmuir isotherm, however, the image of the rear part of the chromatographic cycle is always independent of the duration of the feed pulse.

For conventional SSR process without solvent removal (Figs. 1b and 9b), the steady state feed concentrations are lower than the fresh feed concentrations due to dilution of the recycle fraction. When SSR process is operated such that any of the pure products are not recycled, the cut points t_{A2} and t_{B1} are located on the Γ_+ characteristic that passes through the fresh feed, *FF*. As a result, also the volume-average composition of the recycle fraction *R*, and the steady state feed composition *F*, which is obtained by mixing *FF* and *R*, map to the same Γ_+ characteristic [1, 81]. On the other hand, when part of the pure first component fraction is recycled, the cut point t_{A2} is located on the pure first component plateau (state *Q* in Fig. 7) or on the pure first component wave, and when part of the second component fraction is recycled, the cut point t_{B1} may locate on the pure second component wave, *i.e.* Γ_- characteristic. In these cases, the steady state feed composition moves away from Γ_+ characteristic corresponding to the fresh feed. The Γ_- characteristic, in contrast, is independent of the recycling strategy, and thus remains unaltered when the duration of the feed pulse or the cut times changes.

When the solvent removal unit is operated such that the recovery yields of both components in the solvent removal unit are 100%, the relative composition of the concentrated solution is not changed in the unit. The operating line of the solvent removal unit on the hodograph plane is thus a straight line that passes through the origin and has a slope equal to c_1/c_2 of the treated solution. Solvent removal corresponds to moving upwards on that line.

In the case of classical batch chromatography with solvent removal from the feed mixture (Figs. 4a and 9c), the operating line of the solvent removal unit passes through the origin and the fresh feed *FF*. The resulting concentrated fresh feed composition is denoted as *FF*'. It is located on the Γ_+ characteristic which slope is smaller than the slope of the Γ_+ characteristic that corresponds to the non-concentrated fresh feed mixture *FF*.

In SSR–SR configuration I (Figs. 4b and 9d), solvent is removed from the fresh feed *FF*. Again, the operating line of the solvent removal unit passes through the origin and the point *FF*. The resulting composition maps onto point *FF*'. When the recycle fraction *R* and the concentrated fresh feed *FF*' are mixed together, the actual feed composition in the chromatographic column *F* is obtained. According to lever rule, point *F* is located on the line segment between *FF*' and *R*. When none of the pure component zones are recycled, the steady state feed composition *F* and the recycle point *R* lie on the Γ_+ characteristic that passes through the concentrated fresh feed *FF*'. The slope of this characteristic is denoted as $\tilde{\zeta}_+^F$. When part of the pure fractions are recycled, the slope of the Γ_+ characteristic corresponding to the steady state feed is greater than $\tilde{\zeta}_+^F$.

In SSR–SR option II (Figs. 4c and 9e), solvent is removed from the recycle fraction. In this case, the operating line of the solvent removal unit passes through the origin and the volume-average recycle fraction composition *R*. The resulting composition is denoted as *R*'. Mixing the concentrated recycle fraction *R*' with the fresh feed *FF*, the actual feed composition *F* is obtained. The steady state feed composition *F* is again located on the same Γ_+ characteristic as the steady state recycle fraction composition *R* when the pure component zones are not recycled.

In SSR–SR option III (Figs. 4d and 9f), the fresh feed *FF* and the recycle fraction *R* are mixed before solvent removal. The resulting mixture, denoted as *F*'', is located on the line segment between *FF* and *R*. The operating line of the solvent removal unit passes through the origin and *F*''. The resulting feed composition maps onto point *F*. Similarly to configurations I and II, the steady state feed *F* and the steady state recycle fraction *R* are located on the same Γ_+ characteristic as far as the pure component zones are not recycled.

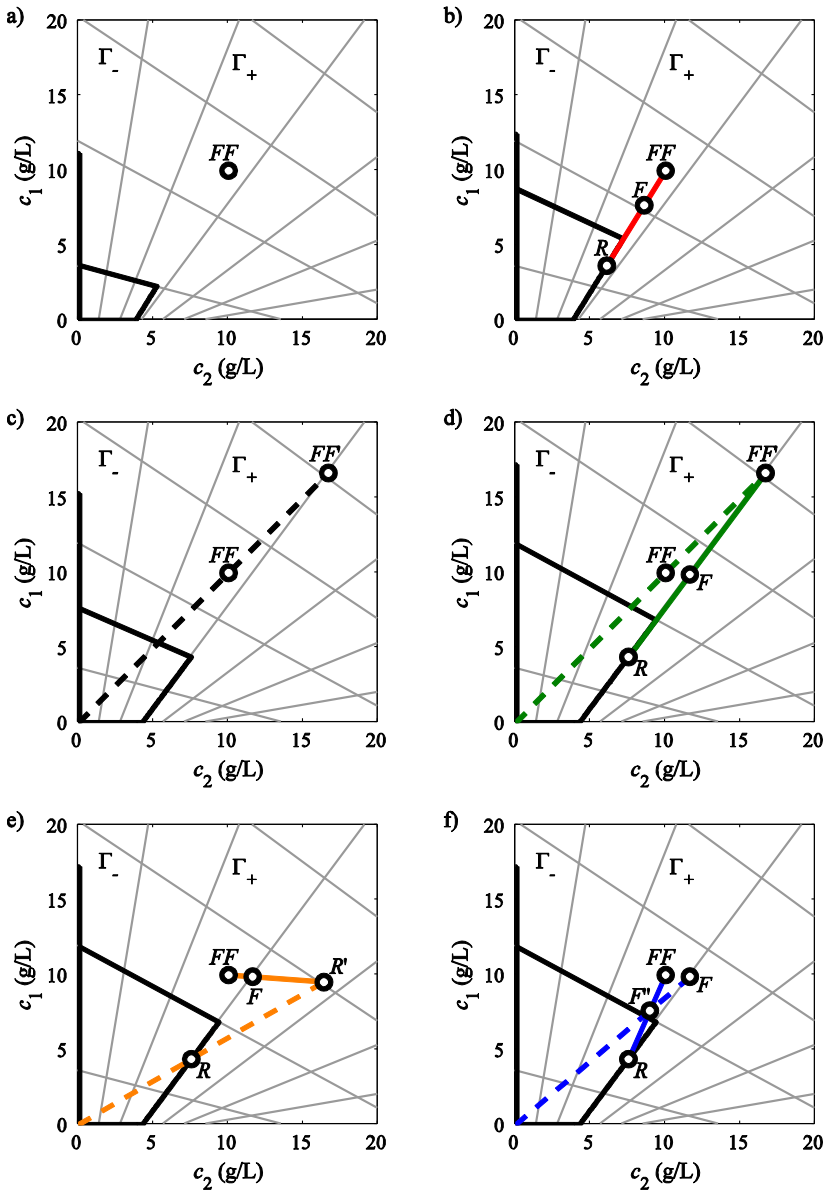

Fig. 9. Schematic representations of alternative process configurations on the hodograph plane. (a) batch chromatography, (b) SSR chromatography, (c) batch chromatography with solvent removal, (d) SSR–SR configuration I (solvent removal from fresh feed), (e) SSR–SR configuration II (solvent removal from recycle fraction), (f) SSR–SR configuration III (solvent removal from mixed fraction). Grey lines: Γ_- and Γ_+ characteristics.

4.2 Non-ideal process model

To validate the equilibrium theory-based design method and to study the influence of dispersive effects on the process design (Sections 6.1.2 and 6.2.2), a non-ideal process model is applied. The finite mass transfer rate and axial dispersion in the chromatographic column is described by using the transport-dispersive model with the solid film linear driving force approach. The mass balances of the components are given by

$$u_y^L \frac{\partial c_i}{\partial y} + \frac{\partial}{\partial t}\left(c_i + F q_i\right) = D_{ax} \frac{\partial^2 c_i}{\partial y^2}, \tag{33a}$$

$$\frac{\partial q_i}{\partial t} = k_i \left(q_i^{\mathrm{eq}} - q_i\right), \tag{33b}$$

where D_{ax} is the axial dispersion coefficient and k_i is the mass transfer coefficient of solute i. The initial and boundary conditions of Eq. (33) are given by Eqs. (4)–(6).

In the modelling of the solvent removal unit, it is assumed that the solvent is removed by using membrane filtration operated in feed and bleed mode. The transport of solvent and solutes through the membrane are described by solution–diffusion model. The concentration polarization effect is neglected. The solvent flux, J_S, and the solute flux, J_i, are given

$$J_S = B_S\left(\Delta P_{memb} - \Delta\pi\right), \tag{34}$$

$$J_i = B_i\left(c_i^{memb} - c_i^{perm}\right), \tag{35}$$

where B_S and B_i are the permeabilities of solvent and solute i, respectively, ΔP_{memb} is the transmembrane pressure, $\Delta\pi$ is the osmotic pressure, c_i^{memb} is the concentration of solute i in the membrane feed, and c_i^{perm} is the concentration of solute i in the permeate. The osmotic pressure is described by van't Hoff equation:

$$\Delta\pi = RT\sum\left(c_i^{memb} - c_i^{perm}\right), \tag{36}$$

where R is the gas constant and T is the temperature. The solvent removal rate and the permeate concentrations are given by

$$Q_{SR} = Q_{perm} = A_{memb} J_S, \tag{37}$$

$$c_i^{perm} = \frac{J_i}{J_S}, \tag{38}$$

where A_{memb} is the membrane surface area.

The flow rates into the membrane feed, Q_{memb}, the total retentate, $Q_{ret,tot}$, and the retentate that is fed from the membrane unit to the column feed tank, $Q_{ret,feed,}$ are calculated from the following volume balances:

$$Q_{memb} = Q_{mix} + Q_{ret,rec}, \tag{39}$$

$$Q_{ret,tot} = Q_{memb} - Q_{perm}, \tag{40}$$

$$Q_{ret,feed} = Q_{ret,tot} - Q_{ret,rec}, \tag{41}$$

where Q_{mix} is the flow rate from the intermediate mixing tank to the solvent removal unit, and $Q_{ret,rec}$ is the flow rate of the recycled retentate. The solute concentrations in the streams are given by

$$c_i^{memb} = \frac{c_i^{perm} Q_{perm} + c_i^{ret,tot} Q_{ret,tot}}{Q_{memb}}, \tag{42}$$

$$c_i^{ret,tot} = c_i^{ret,feed} = \frac{c_i^{mix} Q_{mix} - c_i^{perm} Q_{perm}}{Q_{ret,feed}}. \tag{43}$$

To model the eluent, column feed, and membrane feed reservoirs, perfect mixing is assumed. This yield to the following material balances:

$$\frac{dV^j}{dt} = \sum Q_{in}^j - \sum Q_{out}^j, \tag{44}$$

$$\frac{dn_i^j}{dt} = \frac{d\left(V^j c_i^j\right)}{dt} = \sum Q_{in}^j c_{i,in}^j - \sum Q_{out}^j c_{i,out}^j. \tag{45}$$

In the above equations, V^J, n_i^j, and c_i^j denote the volume of solution, the amount of solute *i*, and the concentration of solute *i* in the reservoir *j*, respectively.

The model equations are solved with finite difference methods by discretizing the time and the column axial coordinates. The transport-dispersive model of chromatography, Eq. (33), is integrated by using an explicit backward-forward scheme, where the axial dispersion term is approximated numerically by the step size in the spatial discretization. For the reservoirs mass balances, Eqs (44) and (45), the Euler method is applied.

5 DESIGN METHOD BASED ON THE IDEAL MODEL

5.1 Design specifications

In the following discussion, it is assumed that fresh feed concentrations and the dimensions of the chromatographic column are fixed and the isotherm parameters and the packing properties are known. A binary mixture is separated in isocratic mode either into one product and one waste fraction or into two products fractions with user-given purity and/or yield requirements. In the case of only one product fraction, either the more or the less retained solute is the target component. The purity and yield constraints are defined as follows:

$$p_1^A = \frac{n_1^A}{n_1^A + n_2^A} = \frac{p_1^{FF} Y_1}{p_1^{FF} Y_1 + (1 - Y_2)(1 - p_1^{FF})}, \tag{46}$$

$$p_2^B = \frac{n_2^B}{n_1^B + n_2^B} = \frac{(1 - p_1^{FF}) Y_2}{(1 - p_1^{FF}) Y_2 + (1 - Y_1) p_1^{FF}}, \tag{47}$$

$$Y_1 = \frac{n_1^A}{n_1^{FF}} = \frac{p_1^A}{p_1^{FF}} \frac{p_1^{FF} + p_2^B - 1}{p_1^A + p_2^B - 1}, \tag{48}$$

$$Y_2 = \frac{n_2^B}{n_2^{FF}} = \frac{p_2^B}{1 - p_1^{FF}} \frac{p_1^A - p_1^{FF}}{p_1^A + p_2^B - 1}, \tag{49}$$

where p_i^j is the purity of component $i = (1, 2)$ in the fraction $j = (A, B, FF)$, n_i^j is the amount of component $i = (1, 2)$ in the fraction $j = (A, B, FF)$, and Y_i is the recovery yield of component $i = (1, 2)$. The purity and yield requirements are interchangeable such that, when any two of the four constraints, Eqs. (46)–(49), are specified, the remaining two are also fixed [38].

For the fixed bed SSR–SR process, there exist the following freely adjustable operating parameters: (1) the duration of the feed pulse into the chromatographic column, Δt_F, (2) the four fractionation times t_{A1}, t_{A2}, t_{B1}, and t_{B2}, (3) the volumetric flow rate of the mobile phase in the column, Q_{col}, and (4) the volumetric flow rate of removed solvent, Q_{SR}. The operating parameters can be expressed in dimensionless form as follows:

$$m_1 = \frac{t_{B2} - \Delta t_F - t_0}{F t_0} = \frac{Q_{col}(t_{B2} - \Delta t_F) - \varepsilon V_{col}}{(1 - \varepsilon) V_{col}}, \tag{50}$$

$$m_2 = \frac{t_{B1} - \Delta t_F - t_0}{F t_0} = \frac{Q_{col}(t_{B1} - \Delta t_F) - \varepsilon V_{col}}{(1 - \varepsilon) V_{col}}, \tag{51}$$

$$m_3 = \frac{t_{A2} - t_0}{F t_0} = \frac{Q_{col} t_{A2} - \varepsilon V_{col}}{(1-\varepsilon) V_{col}}, \tag{52}$$

$$m_4 = \frac{t_{A1} - t_0}{F t_0} = \frac{Q_{col} t_{A1} - \varepsilon V_{col}}{(1-\varepsilon) V_{col}}, \tag{53}$$

$$m_R = \frac{t_{B1} - t_{A2}}{F t_0} = \frac{V_R}{(1-\varepsilon) V_{col}}, \tag{54}$$

$$K_{SR} = \frac{V_{SR}}{V_{FF}}. \tag{55}$$

Parameters m_1, m_2, m_3, and m_4 denote the dimensionless fractionation points, m_R is the volume of the recycle fraction with respect to the volume of the stationary phase, and K_{SR} is the amount of removed solvent with respect to the processed fresh feed. The beginning and end of the product fraction *A* (m_3 and m_4) are expressed in time relative to the beginning of the feed pulse, whereas the beginning and end of the product fraction *B* (m_1 and m_2) are given in time relative to the end of the feed pulse. For batch chromatography with or without solvent removal, $m_R = 0$, and for batch and SSR processes without solvent removal, $K_{SR} = 0$.

The above definitions allow expressing the range of the feasible cut points *A*2 and *B*1 on the dimensionless (m_2, m_3) plane that is formally analogous to the coordinate system that is widely applied for the design of counter-current multi-column SMB process. The dimensionless volume of fresh feed, m_{FF}, volume of feed pulse, m_F, volume of product *A*, m_A, and volume of product *B*, m_B, per cycle are given by

$$m_{FF} = \frac{V_{FF}}{(1-\varepsilon) V_{col}} = \frac{(m_3 - m_2)}{(1-K_{SR})}, \tag{56}$$

$$m_F = \frac{V_F}{(1-\varepsilon) V_{col}} = \frac{Q_{col} \Delta t_F}{(1-\varepsilon) V_{col}} = (m_3 - m_2 + m_R), \tag{57}$$

$$m_A = \frac{V_A}{(1-\varepsilon) V_{col}} = m_3 - m_4, \tag{58}$$

$$m_B = \frac{V_B}{(1-\varepsilon) V_{col}} = m_1 - m_2. \tag{59}$$

To ensure positive fresh feed flow, m_2 must be lower than m_3 when $K_{SR} < 1$ and larger than m_3 when $K_{SR} > 1$. In a special case when $K_{SR} = 1$, m_2 and m_3 must be equal, right hand side of Eq. (56) has no defined value, and m_{FF} must be chosen independently.

Under ideal conditions, the fluid flow rate in the column does not affect the operating boundaries of *m*-parameters. It can be selected independently, *e.g.* such that given pressure constraint is not exceeded. For a given fluid flow rate, the duration of the feed pulse, the four cut times, and the solvent removal rate are given by

$$\Delta t_F = Ft_0\left(m_3 - m_2 + m_R\right), \tag{60}$$

$$t_{A1} = t_0\left(Fm_4 + 1\right), \tag{61}$$

$$t_{A2} = t_0\left(Fm_3 + 1\right), \tag{62}$$

$$t_{B1} = t_0\left(Fm_2 + 1\right) + \Delta t_F, \tag{63}$$

$$t_{B2} = t_0\left(Fm_1 + 1\right) + \Delta t_F, \tag{64}$$

$$Q_{SR} = \frac{(1-\varepsilon)V_{\mathrm{col}}}{\Delta t_{cycle}} K_{SR} m_{FF}. \tag{65}$$

In the case of operation without waste fraction between cycles, the cycle time must be set as follows:

$$\Delta t_{cycle} = t_{B2} - t_{A1} = Ft_0\left(m_1 - m_2 + m_3 - m_4 + m_R\right). \tag{66}$$

The freely adjustable operating parameters for classical cross-current chromatography are the width of the feed section, the three fractionation points, and either the volumetric flow rate of the fluid phase in the *y*-direction or the volumetric flow rate of the solid phase in the *x*-direction. Degree of recycling and solvent removal provide two additional degree of freedom, namely the width of the recycle fraction and the rate of solvent removal. The operating parameters can be expressed in dimensionless form that is analogous to those of fixed bed schemes given by Eqs. (50)–(55). More details are given in Paper V.

The extent of solvent removal is often limited by various factors. The solvent removal constraints can be divided in the following two categories: (1) maximum concentration achievable in the solvent removal unit (*e.g.* solubility, osmotic pressure, or vapour pressure limit) and (2) maximum concentration of the solution fed into the column (*e.g.* solubility or viscosity limit). The following discussion is limited to continuous constraints that can be expressed in form

$$g_1\left(c_1^j, c_2^j\right) \le 0 \quad \text{for } j = \left(FF', R', F\right), \tag{67}$$

$$g_2\left(c_1^F, c_2^F\right) \le 0, \tag{68}$$

where the limit for the maximum concentration of the solution in the solvent removal unit is given by function g_1 and the limit for the maximum concentration of the column feed is given

by function g_2. By using the notation in Fig. 9 we have $j = FF$' for configuration I, $j = R$' for configuration II, and $j = F$ for configuration III.

The design task is to select the freely adjustable operating parameters such that user-given purity and/or yield constraints, Eqs. (46)–(49), as well as the solvent removal constraints, Eqs. (67) and (68), are satisfied. Next, a design method for predicting the feasible range of operating parameters for single-column batch, SSR, and SSR–SR processes developed in this work is summarized. The method is based on the equilibrium theory of chromatography and holds under ideal conditions for binary systems that follow competitive Langmuir adsorption isotherm model. The same approach can be used also for cross-current chromatographic systems by using the transform given by Eq. (15). Detail derivation of the design equations is given in Papers I–V.

At the beginning of the summary, a method to calculate the feasible range of dimensionless cut times that correspond to arbitrary purity constraints is described in Section 5.2. The feasible operating region on the (m_2, m_3) plane is identical for all process concepts as far as identical K_{SR} is used. The influence of solvent removal constraints on the selection of m_R and K_{SR} for different process configurations is then considered in Section 5.3. Finally, selection of optimal and robust operating parameters is discussed in Sections 5.4 and 5.5, respectively. In the optimization analysis, the process performance is assessed in terms of productivity and specific eluent consumption. The productivity is defined as the total amount of components in the desired product fractions obtained per time unit and column volume as follows:

$$PR = \frac{n_1^A + n_2^B}{\Delta t_{cycle} V_{col}} = \frac{\left(Y_1 c_1^{FF} + Y_2 c_2^{FF}\right) V_{FF}}{\Delta t_{cycle} V_{col}} = \frac{\left(Y_1 c_1^{FF} + Y_2 c_2^{FF}\right) m_{FF} Q_{col}}{\left(m_1 - m_2 + m_3 - m_4 + m_R\right) V_{col}}. \tag{69}$$

The specific eluent consumption is given by ratio between the amount of eluent, V_E, and the amount of products

$$EC = \frac{V_E}{n_1^A + n_2^B} = \frac{Q_{col}\Delta t_{cycle} - V_F}{\left(Y_1 c_1^{FF} + Y_2 c_2^{FF}\right) V_{FF}} = \frac{m_1 - m_4}{\left(Y_1 c_1^{FF} + Y_2 c_2^{FF}\right) m_{FF}}. \tag{70}$$

In practice, the removed solvent can be used as eluent to reduce the need of fresh eluent as mentioned in Section 3.3. In addition, also the solvent removal capacity affects the separation costs and could be considered as a third performance parameter. In this study, however, it is assumed that an equal solvent removal capacity is applied in all process configurations. If it is not possible to remove solvent from the recycle or feed fractions, the solvent is removed from the product fractions. The definition of *EC* used here is thus justified, and it allows showing that solvent removal may decrease the eluent consumption even when removed solvent is not reused as eluent.

5.2 Feasible range of dimensionless cut times

The set of boundaries for the dimensionless fractionation points can be expressed in the following general form:

$$m_{1,\min} \le m_1 , \tag{71}$$

$$m_{2,\min} \le m_2 \le m_{2,\max} , \tag{72}$$

$$m_{3,\min} \le m_3 \le m_{3,\max} , \tag{73}$$

$$m_4 \le m_{4,\max} . \tag{74}$$

In general case, all the lower and upper limits depend on the values of m_2, m_3, m_R, and K_{SR}, the adsorption isotherm parameters, and the fresh feed concentrations but not on m_1 and m_4 as far as they are selected such that the consecutive chromatograms do not overlap. In the case of competitive Langmuir isotherm and ideal conditions, however, the boundaries of m_1, m_2, and m_3 are independent of m_R because the shape of the rear part of the chromatogram is independent of the volume of the feed pulse. It has been shown in Paper I that all three SSR–SR configurations lead to exactly the same steady state when same operating are used. This means that the boundaries of m_1, m_2, m_3, m_4 for different SSR–SR schemes are identical when an equal solvent removal capacity is applied.

To ensure that the consecutive chromatograms do not overlap, the cut time t_{B2} must be chosen higher than or equal to the time of complete elution of the second component, t_{E2}. This means that m_1 must be higher than or equal to H_2.

The boundaries of m_2 and m_3 parameters are conveniently represented on the (m_2, m_3) and (m_2, m_{FF}) planes. Two examples with different K_{SR} values are shown in Fig. 10. When $K_{SR} < 1$, *i.e.* the amount of removed solvent is lower than the amount of processed fresh feed, the feasible operating region is located above the diagonal $m_3 = m_2$ (Figs. 10a and 10b). In the case of $K_{SR} > 1$, positive fresh feed flow is achieved with $m_2 > m_3$ (Figs. 10c and 10d). As will be demonstrated in Section 5.3, K_{SR} can be higher than unity when the solvent is removed from the recycle fraction (Fig. 4c) or from the column feed (Fig. 4d) but not when the solvent is removed from the fresh feed of batch (Fig. 4a) or SSR (Fig. 4b) processes. To ensure that the volume of the feed pulse is positive, m_R must be higher than or equal to the difference $m_2 - m_3$. In a special case of $K_{SR} = 1$, the operating region on the (m_2, m_3) plane shrinks to the diagonal. In that case, it is more convenient to use (m_2, m_{FF}) plane instead of (m_2, m_3) coordinates.

Different regions on the (m_2, m_3) plane corresponds to different product purity levels. The complete separation region, where the purities of both product fractions are 100%, is a triangle-like domain limited by three straight lines *ab*, *bw*, and *rw*, and a curve *ar*. Explicit equations to calculate the boundaries of the complete separation for batch and SSR processes have been derived in Paper V. Identical equations can be applied for SSR–SR process by replacing the value of a characteristic parameter ω_2 at fresh feed state by ω_2 that corresponds to the slope of Γ_+ characteristic passing through the steady state feed composition when no pure products are recycled. The slope of characteristic, denoted as $\tilde{\zeta}_+^F$, is related to the solvent removal capacity as follows:

$$\tilde{\zeta}_{+}^{F} = \frac{\eta + \sqrt{\eta^2 - 4K_1K_2H_1H_2c_1^{FF}c_2^{FF}}}{2K_1H_2c_2^{FF}}, \tag{75}$$

where η is an auxiliary parameter given by

$$\eta = (1 - K_{SR})(H_2 - H_1) + K_1H_2c_1^{FF} + K_2H_1c_2^{FF}. \tag{76}$$

Once $\tilde{\zeta}_{+}^{F}$ is known, the corresponding ω_2 value is calculated from Eq. (19).

When $K_{SR} = 0$, the complete separation regions of batch and SSR processes are identical to that of counter-current SMB process with same fresh feed concentrations and isotherm parameters. The influence of solvent removal on the shape of the operating region is similar to that observed in SMB process when the fresh feed is concentrated. This phenomenon is discussed more detailed in Section 5.5.

In batch process with or without solvent removal, the size of the feed pulse into the column is directly proportional to the difference ($m_3 - m_2$). The components are separated complete when the operating point on the (m_2, m_3) plane is located between the diagonal and the line that is parallel to the diagonal and passes through the point *w*. The curve *ar* stand for the case where the duration of the feed pulse is so small that the pure second component plateau is eroded completely during elution. The middle cut point t_{A2} (or t_{B1}) is equal to the beginning of the elution profile of the second component, t_{R2}. On the line *rw*, V_F is larger and the second component plateau prevails. The cut time t_{A2} is again equal to the front of the second band. The maximum duration of the feed pulse is achieved in the point *w*. This corresponds to the operation with touching bands where the time of complete elution of the first component, t_{E1}, matches to t_{R2}. Along the line *bw*, the middle cut point t_{A2} is equal to the end of the first component profile. The duration of the feed pulse decreases when the operating point is shifted towards the point *b*. The second component plateau is eroded or not depending on the size of the feed pulse, *i.e.* term $(m_3 - m_2)/(1 - K_{SR})$.

For conventional SSR process and different SSR–SR schemes, the line *ar* on the (m_2, m_3) plane corresponds to the condition where the cut point t_{A2} is set equal to the retention time of the second shock and t_{B1} is located on the pure second component wave. As a result, a part of the pure second component zone is recycled. Along the line *rw*, t_{A2} is again equal to t_{R2}, but t_{B1} lies on the pure second component plateau. The maximum amount of fresh feed can be processed in the point *w* where $t_{A2} = t_{R2}$ and $t_{B1} = t_{E1}$. In this case, no pure fractions are recycled. The line *bw* stand for the case where t_{B1} is equal to end of the first component zone. The cut point t_{A2} is located on the pure first component wave or on the pure first component plateau depending on m_R. A part of the pure first component fraction is thus recycled.

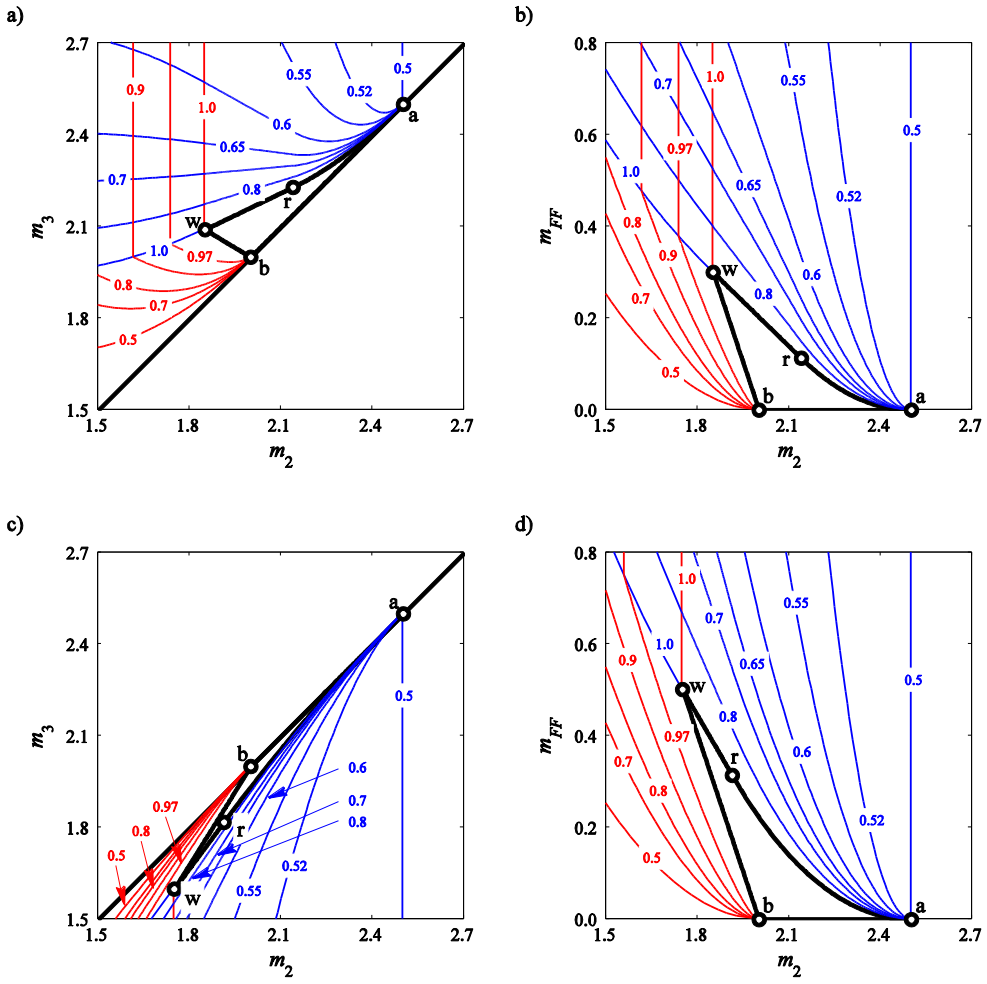

Fig. 10. Feasible separation regions in SSR–SR process on the (m_2, m_3) and (m_2, m_{FF}) planes. Blue and red lines show the contours of purities p_1^A and p_2^B, respectively. Fresh feed concentrations: $c_1^{FF} = c_2^{FF} = 5$ g/L. Isotherm parameters: $K_1 = 0.02$ L/g, $K_2 = 0.025$ L/g, $N_1 = N_2 = 100$ g/L. Solvent removal capacity: (a) and (b) $K_{SR} = 0.2$, (c) and (d) $K_{SR} = 1.3$.

When the operating point is shifted outside the complete separation region further away from the diagonal such that m_2 is kept constant but the difference between m_2 and m_3 increases, the product *B* remains pure, while the product *A* becomes contaminated by component 2. In the case of $K_{SR} < 1$, this corresponds to the operation above the line *arw* (Fig. 10a), and in the case of $K_{SR} > 1$, to the operation below the line *arw* (Fig. 10c). On the left hand side of the

line *bw*, on the other hand, the product *A* is pure, while the product *B* is contaminated by component 1. The region where both products are impure is located on the top left of the (m_2, m_3) plane when $K_{SR} < 1$ and on the bottom left when $K_{SR} > 1$. As seen in Figs. 10b and 10d, the amount of fresh feed that can be processed during each cycle is now larger. In practice, this means that relaxing the purity constraints enables to significantly increase the process productivity. Finally, the region on the right hand side of the point *a* corresponds to a condition where the products *A* and *B* are flooded with feed and eluent, respectively, while operation in the bottom left corner leads to the opposite behaviour. Explicit equations to calculate the dimensional cut points with which arbitrary product purities are matched exactly have been derived for batch chromatography in Paper III, for SSR chromatography by Sainio and Kaspereit in [81], and for SSR–SR schemes in Paper I. The dimensional cut times can be converted to dimensionless *m*-values by using Eqs. (50)–(54).

The upper bound of m_4 is equal to the beginning of the first component band, *i.e.* to the retention time of the pure first component shock, t_{R1}. The value depends on the volume of the feed pulse, *i.e.* m_2, m_3, and m_R, the isotherm parameters, and the feed concentrations into the column at steady state. For classical batch chromatography without solvent removal, the column feed concentrations are equal to the fresh feed concentrations. When solvent is removed from the batch feed, the concentrated feed composition is given by

$$c_i^F = \frac{c_i^{FF}}{1 - K_{SR}}. \tag{77}$$

A method to calculate the retention time of the pure first component shock has been described in Section 4.1.3. As already mentioned, t_{R1} is solved piecewise depending on whether the plateau on the top of the first component band is eroded or not. When the duration of the feed pulse is relatively high, the first component plateau prevails and t_{R1} is calculated with an equation derived by Golshan-Shirazi and Guiochon [58]. In that case, the upper limit of m_4 is equal to ω_1^F. In the case of relatively small feed pulse, the first plateau erodes completely, the height of the first shock decreases, and the propagation velocity of the shock slows down. The retention time of the shock and hence the upper limit of m_4 are obtained analytically by using the explicit equations derived in Paper II.

To solve the upper limit of m_4 for SSR and SSR–SR schemes, the steady state feed concentrations are needed. They depend on the values of m_2, m_3, and m_R, and can be solved from Eq. (7) by setting:

$$c_i^R = \frac{\int_{t_{A2}}^{t_{B1}} c_i(t)\,\mathrm{d}t}{t_{B1} - t_{A2}} \quad \text{for } i = (1, 2). \tag{78}$$

The individual elution profiles at the column outlet, $c_i(t)$, depend on the steady state feed concentrations and the duration of the feed pulse. They can be calculated by using the analytical solution of the equilibrium model [58].

When the purity constraint p_1^A is less than 100%, the cut point t_{A2} is located either on the mixed wave or on the feed plateau. For this case, explicit equations to calculate the steady state feed concentrations have been derived in Papers I and IV. In contrast, when p_1^A = 100%, the cut point t_{A2} is located on the pure first component plateau or on the pure first component wave. In this case, explicit solution of set of Eqs. (7) and (78) is very difficult if not impossible because a quartic equation may be needed to be solved in order to find the amount of component 1 in the recycle fraction. For this reason, numerical methods are recommended to find the steady state feed concentrations. For example, c_1^F and c_2^F can be searched by calculating the chromatograms analytically from cycle to cycle until the periodic steady state is reached. In every cycle, the recycle fraction composition can be computed by integrating the chromatogram numerically, for example, with trapezoidal rule. As an alternative, numerical multidimensional root-finding algorithms can be applied to find c_1^F and c_2^F.

Once the steady state feed composition is found, the retention time of the first component shock and thus the upper limit of m_4 for SSR and SSR–SR schemes can be solved by using the same procedure as in the case of batch chromatography described above. When p_1^A = 100%, p_2^B = 100%, and m_R is so large that the feed plateau prevails, the upper boundary of m_4 is identical to that of counter-current SMB processes reported in [64].

The upper limit of m_4 in SSR and SSR–SR processes increases with increasing m_R until it levels off as m_R becomes so high that the cut point t_{A2} is located either on the pure first component plateau (p_1^A = 100%) or on the feed plateau (p_1^A < 100%). It is always higher than or equal to that of batch scheme when the applied solvent removal capacities are identical. This is because the feed concentrations into the column decrease due to diluted recycle fraction. As a result, the propagation velocity of the first shock decreases, the retention time of the shock increases, and thus a higher value for t_{A1} can be chosen.

Since the complete separation regions on the (m_2, m_3) plane for batch, SSR, and multi-column SMB processes are identical, the maximum amounts of fresh feed that can be processed in these configurations during a chromatographic cycle or switch are equal. However, any conclusions about the productivities cannot be made because optimization of column length is not possible within the frame of the equilibrium theory. As to the specific eluent consumption, the SSR and SMB concepts outperform the batch chromatography because a higher value of m_4 can be selected.

The above comparison results hold also for the ideal plug-flow single-column SMB analogue because its operating boundaries are identical to those of the equivalent multi-column SMB setup [26]. The main difference between the mixed-recycle SSR chromatography and the single-column SMB analogue is that in the latter case also products and eluent are partially recycled, not only the unresolved part of the elution profile. In the plug-flow SMB analogue, in addition, the already achieved partial separation of the unresolved recycle fraction is preserved. The above findings imply that this kind of “closed-loop” recycling does not enable processing more fresh feed in a single chromatographic column during a chromatographic cycle under ideal conditions. Moreover, the fact that the recycling schemes provide lower

minimum eluent consumption than the batch process seems to be related to the recycling of the unresolved mixture, not to the recycling of pure products or eluent.

5.3 Feasible range of solvent removal capacity and volume of recycle fraction

The solvent removal capacity and the volume of the recycle fraction have a significant effect on the concentrations of different streams in SSR–SR process. They must be selected such that the concentration constraints, *e.g.* solubility, viscosity, osmotic pressure, or vapour pressure limits, given by Eqs. (67) and (68), are not violated. The region of feasible solvent removal capacity and volume of the recycle fraction is conveniently represented on the (K_{SR}, m_R) plane. In addition to the solvent removal limitations, the shape and size of the operating domain depend on the process configuration, the fresh feed concentrations, the isotherm parameters, and the purity constraints.

A method to calculate the operating boundaries corresponding to arbitrary solvent removal constraints for the three SSR–SR configurations as well as for the batch chromatography with an integrated solvent removal unit has been developed in Paper IV. The operating regions in the case of no solvent removal constraints derived in Paper I are obtained as a limiting value by setting $g_1 \leq \infty$. The approach gives the regions of feasible K_{SR} and m_R values within which the solvent removal constraints are not violated when m_1 and m_4 are selected such that the consecutive chromatograms do not overlap and m_2 and m_3 are selected such the user-given purity constraints are matched exactly. In the case of 100% purity requirements, it is assumed that the operating point on the (m_2, m_3) plane is located on the optimal operating point *w*. In the original works, the operation regions are represented on the dimensional (V_{FF}, V_F) plane, but also equations to calculate the corresponding solvent removal capacity and volume of recycle fraction have been provided.

In the following Sections 5.3.1 to 5.3.3, the operating regions of different process configurations in the case when the maximum concentration reachable in the solvent removal unit, Eq. (67), is the limiting factor are first considered. The case when the maximum concentration of the feed of the chromatographic column, Eq. (68) limits the operation as well as the case when both the constraints for the solvent removal unit and the column feed, Eqs. (67) and (68), affect the process operation are then discussed in Section 5.3.4.

5.3.1 SSR–SR configuration I and batch process with solvent removal

An example of the operating region for SSR–SR configuration I (solvent removal from the fresh feed) in the case when the maximum concentration achievable in the solvent removal unit, Eq. (67), limits the operation is displayed in Fig. 11a. The region is a half-open domain limited by the following three lines: (1) operating line of conventional SSR chromatography $K_{SR} = 0$ (limit *A*), (2) operating line of batch chromatography with solvent removal $m_R = 0$ (limit *B*), and (3) upper limit of K_{SR} that depends on the solvent removal constraint (limit *C*). For the volume of the recycle fraction, there is no upper limit. However, when m_R is relatively high, the cut point t_{A2} is located on the feed plateau. Part of the feed plateau is recycled, and the operation is suboptimal. The maximum m_R with which the feed plateau is not recycled is

denoted in Fig. 11a by violet dashed line (limit *G*). Above the limit, the steady state feed concentrations are independent of m_R. As to the hodograph plane (Fig. 11b), the limit corresponds to the minimum steady state feed composition of SSR–SR process. The upper limit of K_{SR} in the case of no solvent removal constraints, denoted by grey line, is shown as a reference.

The upper limit of K_{SR} is obtained when point *FF*' on the hodograph plane is located on the solvent removal constraint (Fig. 11b). To calculate the maximum K_{SR}, the intersection of the operating line of the solvent removal unit, $c_1 = (c_1^{FF} / c_2^{FF})c_2$, and the solvent removal constraint, Eq. (67), is first solved. The point will henceforth be denoted as $(c_{2,C}^{FF'}, c_{1,C}^{FF'})$. When the solvent removal constraint is linear, a simple analytic expression for the intersection is obtained. In general case, the point must be solved numerically. Once the point $(c_{2,C}^{FF'}, c_{1,C}^{FF'})$ is known, the corresponding solvent removal capacity is calculated from the mass balance around the solvent removal unit

$$K_{SR,C} = \frac{c_{i,C}^{FF'} - c_i^{FF}}{c_{i,C}^{FF'}}. \tag{79}$$

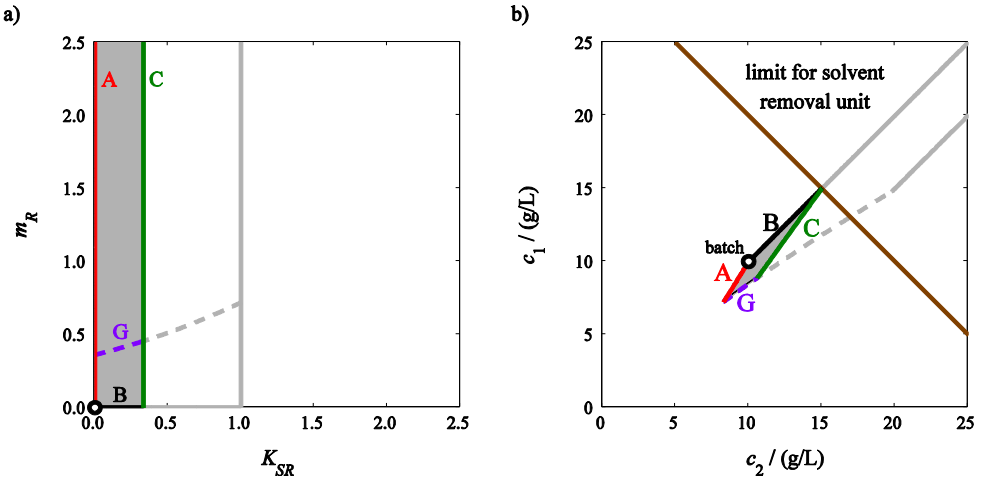

Fig. 11. (a) Regions of feasible operating parameters and (b) regions of feasible steady state feed compositions for SSR–SR configuration I (solvent removal from fresh feed) when the limit for solvent removal unit is $c_1^{FF'} + c_2^{FF'} \leq 30$ g/L. Grey lines: operating regions without solvent removal constraints. Fresh feed concentrations: $c_1^{FF} = c_2^{FF} = 10$ g/L. Isotherm parameters: $K_1 = 0.020$ L/g, $K_2 = 0.025$ L/g, $N_1 = N_2 = 100$ g/L. Phase ratio $F = 1/3$. Purity constraints: $p_1^A = p_2^B = 0.9$.

When the solvent removal constraints tends towards infinity, the maximum solvent removal capacity $K_{SR,C}$ tends towards 1 (grey line in Fig. 11a). In other words, when the solvent removal is not constrained by physical limits, the upper limit of K_{SR} is obtained with $V_{FF} = V_{SR}$. As to the hodograph plane, this means that the steady state feed composition cannot be located on such a characteristic Γ_+ that has a slope lower than c_1^{FF} / c_2^{FF}.

5.3.2 SSR–SR configuration II

For SSR–SR configuration II (solvent removal from the recycle fraction), the upper limit of K_{SR} is achieved when the composition of the concentrated recycle fraction R' is located on the solvent removal constraint. Two examples are displayed in Fig. 12. The composition of R' with different K_{SR} values is denoted by orange dashed line. Explicit equations to calculate R' as a function of K_{SR} and m_R are given in Paper IV. In principle, the upper limit of K_{SR} can be constructed on the (K_{SR}, m_R) plane by varying the point R' on the solvent removal constraint curve and by solving the corresponding K_{SR} and m_R values. The system of Eqs. $K_{SR} = f(c_2^{R'}, c_1^{R'})$ and $m_R = f(c_2^{R'}, c_1^{R'})$, however, remains implicit and it must be solved numerically. In this work, the limit is calculated by applying a numerical root-finding algorithm to find the value of K_{SR} for each m_R with which $g_1(c_2^{R'}(K_{SR}), c_1^{R'}(K_{SR})) = 0$.

The shape of the upper limit of K_{SR} depends on the maximum concentration achievable in the solvent removal unit, Eq. (67), with respect to the limits for the minimum and maximum recycle fraction composition in the case of SSR–SR process II without solvent removal constraints. The upper limit of R is equal to the minimum steady state feed composition (limit G in Figs. 12b and 12d). The lower limit of R (black dotted line in Figs. 12b and 12d) is obtained by calculating the recycle fraction composition by using the values of K_{SR} and m_R that corresponds to the upper limit of K_{SR} in the case of no solvent removal constraints, *i.e.* $K_{SR} = m_R/m_{FF}$ (grey line in Figs. 12a and 12c). The minimum, $R_{\min}^{\mathrm{SSR}}$, and maximum, $R_{\max}^{\mathrm{SSR}}$, recycle fraction compositions in the conventional SSR process are denoted in Figs. 12b and 12d by black triangle and black square, respectively.

Figs. 12a and 12b represent the case where the maximum concentration reachable in the solvent removal unit is higher than $R_{\max}^{\mathrm{SSR}}$. On the (K_{SR}, m_R) plane, the operating line is a half-open domain limited by the operating line of conventional SSR chromatography (limit A) and the upper boundary of K_{SR} (limit D). The upper limit of K_{SR} is larger than zero independent of m_R.

In Figs. 12c and 12d, the solvent removal constraint is located between $R_{\min}^{\mathrm{SSR}}$ and $R_{\max}^{\mathrm{SSR}}$. With relatively low m_R, the point R in SSR–SR process is located below the solvent removal constraint and removing solvent from the recycle fraction is feasible. When m_R increases, the volume-average composition of the recycle fraction becomes higher than the solvent removal limit. Operation of SSR–SR II is no longer possible. In the latter case, $g_1(c_2^{R'}(K_{SR}), c_1^{R'}(K_{SR})) > 0$ independent of K_{SR}, and the function g_1 has no root.

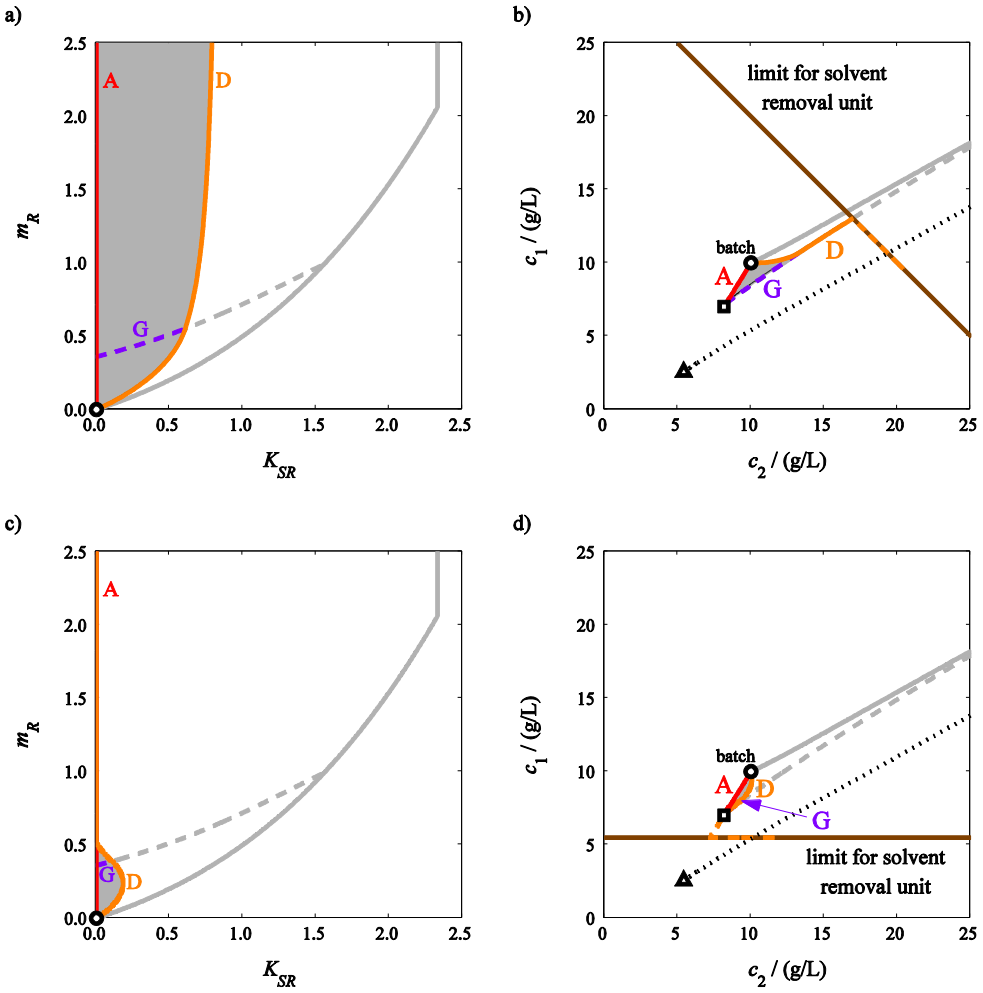

Fig. 12. (a) Regions of feasible operating parameters and (b) regions of feasible steady state feed compositions for SSR–SR configuration II (solvent removal from recycle fraction) when the limit for solvent removal unit is $c_1^{R'} + c_2^{R'} \leq 30$ g/L. (c) Regions of feasible operating parameters and (d) regions of feasible steady state feed compositions for SSR–SR configuration II when the limit for solvent removal unit is $c_1^{R'} \leq 6$ g/L. Grey lines: operating regions without solvent removal constraints. Black triangle: minimum R in SSR process. Black square: maximum R in SSR process. Black dotted line: lower limit of R in SSR–SR process II. Orange dashed line: R' corresponding to the upper limit of K_{SR} in SSR–SR process II without solvent removal constraints. Same fresh feed concentrations, isotherm parameters, phase ratio, and purity constraints as in Fig. 11.

In addition to the examples shown in Fig. 12, it is possible that the solvent removal constraint lies below the minimum recycle fraction composition $R_{\min}^{\mathrm{SSR}}$. In that case, the operation of SSR–SR configuration II is not feasible independent of the volume of the recycle fraction.

5.3.3 SSR–SR configuration III

In SSR–SR configuration III (solvent removal from the mixed fraction), the upper limit of K_{SR} is obtained when the steady state feed concentrations on the hodograph plane are located on the solvent removal constraint. To construct the limit into the (K_{SR}, m_R) plane, the steady state feed composition is varied along the solvent removal constraint, Eq. (67), and the corresponding K_{SR} and m_R values are solved by using the explicit equations derived in Paper IV.

Two examples of the operating boundaries for SSR–SR configuration III are displayed in Fig. 13. The shape of the operating region depends on the location of the limit for maximum concentration achievable in the solvent removal unit, Eq. (67), with respect to the region of feasible steady state feed concentrations for SSR–SR process III without solvent removal constraints denoted by grey lines in Fig. 13.

In the first case, illustrated in Figs. 13a and 13b, the fresh feed composition is lower than the concentration constraint for the solvent removal unit. On the hodograph plane (Fig. 13b), the solvent removal constraint intersects the upper (limit *B*) and the lower (limit *G*) limits of *F* but not the operating line of conventional SSR chromatography (limit *A*). As to the (K_{SR}, m_R) plane, the upper limit of K_{SR} (limit *E*) is larger than zero independent of m_R.

When m_R is relatively low, the steady state feed composition is located above the limit *G*, *i.e.* the cut point t_{A2} lies on the mixed wave. In that case, the point (c_2^F, c_1^F) on the hodograph plane uniquely fixes the values of K_{SR} and m_R. In contrast, when m_R is relatively high and the cut point t_{A2} is located on the feed plateau (limit *G*), the steady state feed composition is independent of m_R. On the (K_{SR}, m_R) plane, the upper limit of K_{SR} is thus a straight vertical line above the limit *G*. The corresponding steady state feed composition is located at the intersection of the solvent removal constraint and the limit *G* (Fig. 13b).

When the solvent removal constraint tends towards infinity, the maximum K_{SR} approaches a certain finite value as shown in Paper I. The value is independent of m_R, so the upper limit of K_{SR} is a straight vertical line (grey line in Figs. 13a and 13c).

In the second example (Figs. 13c and 13d), the solvent removal constraint intersects the operating line of conventional SSR process (limit *A*). When m_R is relatively small, the steady state composition of the mixed fraction is higher than the maximum concentration achievable in the solvent removal unit, and SSR–SR configuration III cannot be operated. For high m_R, the mixed fraction composition is located below the solvent removal limit and the operation is feasible.

In practice, it is also possible that the solvent removal constraint does not intersect the region of *F* in the case of SSR–SR process III without solvent removal constraints, *i.e.* the lower

limit for steady state feed composition (limit *G*) in the case of no solvent removal constraints is higher than the maximum concentration reachable in the solvent removal unit. In that case, the operation of SSR–SR configuration III is not feasible.

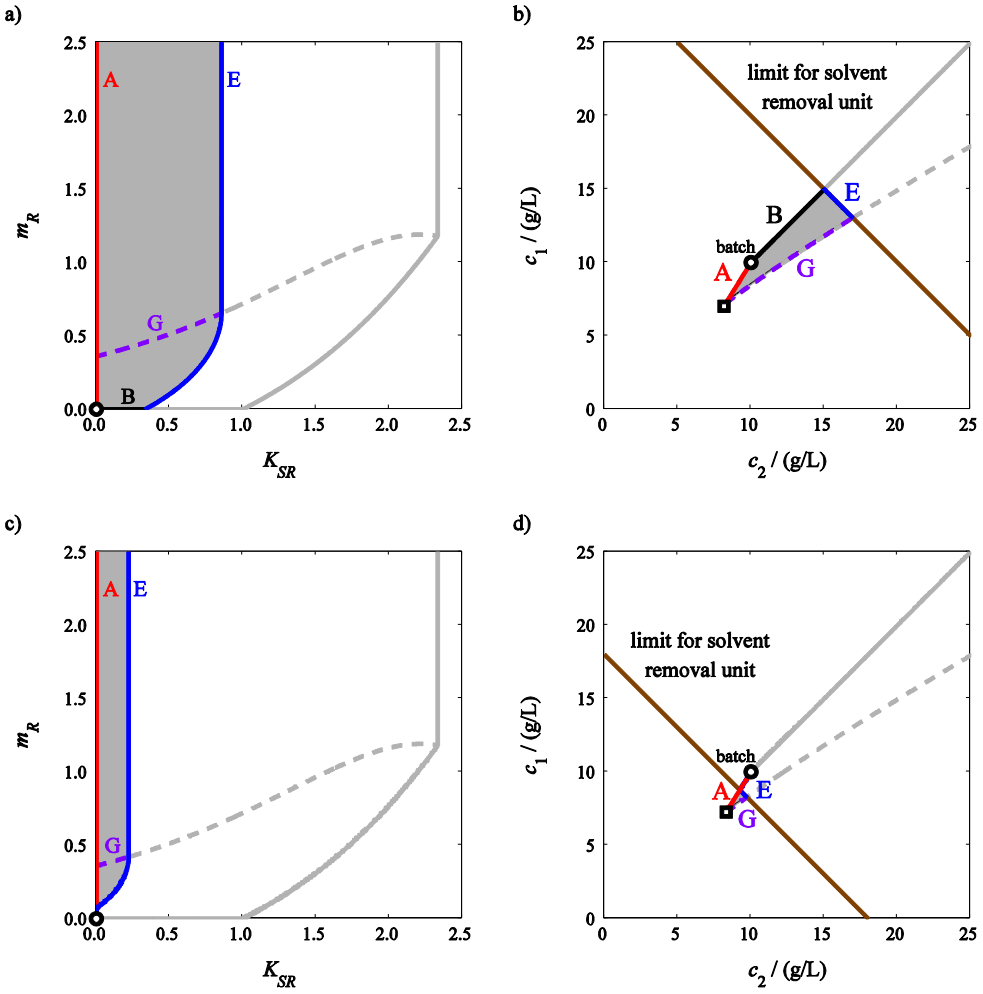

Fig. 13. (a) Regions of feasible operating parameters and (b) regions of feasible steady state feed compositions for SSR–SR configuration III (solvent removal from mixed fraction) when the limit for solvent removal unit is $c_1^F + c_2^F \leq 30$ g/L. (c) Regions of feasible operating parameters and (d) regions of feasible steady state feed compositions for SSR–SR configuration III when the limit for solvent removal unit is $c_1^F + c_2^F \leq 18$ g/L. Grey lines: operating regions without solvent removal constraints. Same fresh feed concentrations, isotherm parameters, phase ratio, and purity constraints as in Fig. 11.

5.3.4 Combination of operating limits

In Sections 5.3.1 to 5.3.3, the operating boundaries of SSR–SR configurations were discussed in the case when only the maximum concentration reachable in the solvent removal unit limits the operation. Next, the following two cases will be considered (1) the operation is limited by the constraint for maximum concentration of the solution fed into the chromatographic column and (2) the operation is limited by both the constraint for maximum concentration reachable in the solvent removal unit and the constraint for maximum concentration of the solution fed into the column. Examples of these two cases are displayed in Fig. 14.

Figs. 14a and 14b represent the case where the upper limit for total feed concentration into the column is 45 g/L. In SSR–SR configuration III, the composition of the outlet stream of the solvent removal unit is equal to the column feed. The operating region for SSR–SR process III is thus obtained by using the approach described in Section 5.3.3 by replacing the limit for solvent removal unit, Eq. (67), by limit for column feed, Eq. (68). The operating domain on the (K_{SR}, m_R) plane is a half-open region limited by lines *A*, *B* and *E* (Fig. 14a).

The operating regions of SSR–SR configurations I and II are intersections of the corresponding operating regions without solvent removal constraints (grey lines in Figs. 14a and 14b) and the operating region of SSR–SR configuration III. When m_R is relatively small, the operation of SSR–SR process I is limited by the maximum concentration of the column feed (limit *E* in Figs. 14a and 14b). For sufficiently large m_R, on the other hand, the steady state feed concentration reachable in the SSR–SR process I is smaller than the limit for column feed because large recycle fraction dilutes the feed solution. The upper limit of K_{SR} is equal to the corresponding limit without concentration constraints (limit *C* in Figs. 14a and 14b).

In the case of SSR–SR configuration II, relatively small values of m_R lead to steady state feed concentrations that are lower than the constraint for maximum column feed. The upper limit for K_{SR} is equal to the corresponding limit without concentration constraints (limit *D* in Figs. 14a and 14b). When the volume of the recycle fraction increases, the steady state feed concentrations on the limit *D* increase. For sufficiently large m_R, the operation is thus limited by the constraint for column feed (limit *E* in Figs. 14a and 14b).

Figs. 14c and 14d show the case when both the constraint for solvent removal unit ($g_1 = c_1^j + c_2^j \leq 45$ g/L) and the constraint for the column feed ($g_2 = c_1^F + c_2^F \leq 30$ g/L) limit the operation. The operation region for SSR–SR III is now achieved by using the approach described in Section 5.3.3 and the stricter of the two constraints g_1 and g_2. The operation domains of SSR–SR configurations I and II are, in turn, intersections of the corresponding operating regions when only the solvent removal constraint limits operation (grey lines in Figs. 14c and 14d) and the region when the operation is limited by the constraint for column feed. The behaviour is very similar as in the previous case. When m_R is relatively small the operation of SSR–SR process I is limited by the maximum feed concentration in the column (limit *E* in Figs. 14c and 14d), while for large m_R the constraint for solvent removal limits the operation (limit *C* in Figs. 14c and 14d). For SSR–SR configuration II, opposite behaviour is again observed.

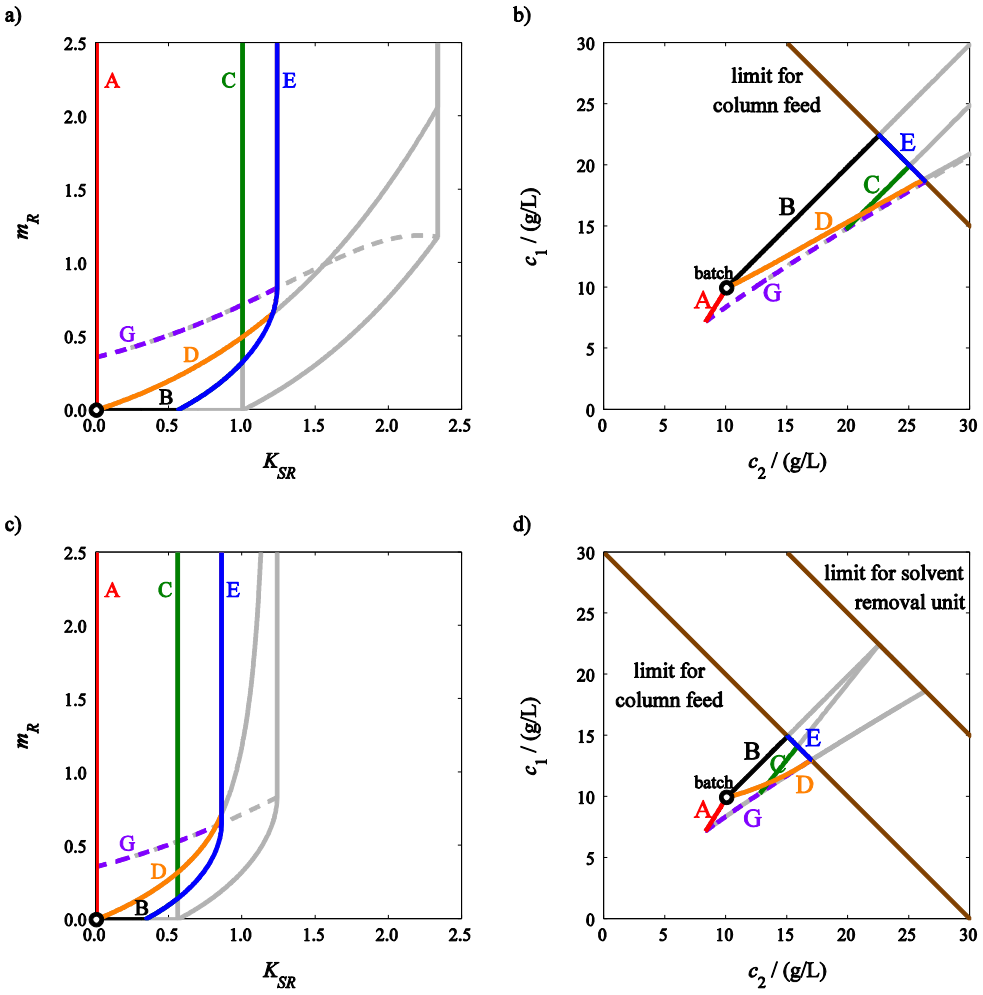

Fig. 14. (a) Regions of feasible operating parameters and (b) regions of feasible steady state feed compositions for different SSR–SR configurations when the limit for column feed is $c_1^F + c_2^F \leq 45$ g/L. (c) Regions of feasible operating parameters and (d) regions of feasible steady state feed compositions for different SSR–SR configurations when the limit for solvent removal unit is $c_1^j + c_2^j \leq 45$ g/L (j = *FF*', *R*', *F*) and the limit for column feed is $c_1^F + c_2^F \leq 30$ g/L. Same fresh feed concentrations, isotherm parameters, phase ratio, and purity constraints as in Fig. 11.

Finally, it should be noted that the SSR–SR configuration III has always the widest range of feasible K_{SR} and m_R values when there is no physical solvent removal limitations (grey lines in

Figs. 11–13). Moreover, the SSR–SR III process provides usually the widest operating region even when the solvent removal is constrained because the upper limit of solvent removal capacity increases when either the fresh feed or the recycle fraction composition is below the solvent removal constraint. An exception for this may be observed when the maximum concentration reachable in the solvent removal unit is lower than the fresh feed. In that case, it might be beneficial to remove solvent from the recycle stream as demonstrated by Hellstén et al. [51].

5.4 Optimal operating conditions

As usual in designing separation processes, it is important to find the operating parameters that lead to optimal process performance. Next, selection of the operating conditions to maximize the productivity, defined by Eq. (69), and to minimize the specific eluent consumption, Eq. (70), is discussed. The optimization of different SSR–SR configurations has been analysed in Papers I and IV. All the following conclusions are congruent with the findings reported by Golshan-Shirazi and Guiochon [78] for batch chromatography and by Sainio and Kaspereit [81] for conventional SSR chromatography.

For a given solvent removal capacity, the maximum productivity and the minimum specific eluent consumption are achieved when maximum amount of fresh feed is processed during a chromatographic cycle. This means that the difference between m_2 and m_3 values, *i.e.* the distance between the operating point and the diagonal of (m_2, m_3) plane, must be maximized. When the purity constraints are 100%, the optimal operating point on the (m_2, m_3) plane is located on the point w (see Fig. 10 in Section 5.2). As to the batch chromatography with or without solvent removal, this corresponds to the touching band operation where the front of the second component band is equal to the time of complete elution of the first component. In the cases of recycling concepts, only the unresolved middle zone between the pure component bands is recycled, not any pure component fractions. When the purity constraints are less than 100%, they must be matched exactly to achieve the maximum performance.

In all process configurations, the productivity increases and the specific eluent consumption decreases when m_1 decreases and m_4 increases due to decreased cycle time. The optimal values of m_1 and m_4 thus coincide with their lower and upper bounds, respectively. In practice, this corresponds to the operation with "stacked injections" such that no gap exists between the consecutive chromatographic cycles.

The volume of the recycle fraction does not affect the amount of fresh feed in the case of ideal conditions and competitive Langmuir isotherm. This is because the shape of the rear part of the chromatogram and thus the composition of the product fraction *B* remains unaltered when the volume of the feed pulse changes. On the other hand, the cycle time increases monotonically with increasing m_R. This means that m_R must be minimized to achieve maximum productivity. In the cases of classical chromatographic schemes without solvent removal, this corresponds to operation in batch mode [81]. When solvent is removed, the maximum productivity is obtained by using the lowest value of m_R with which the solvent removal constraints are not violated. As to the specific eluent consumption, it decreases with increasing m_R until it levels off as the volume of the feed pulse becomes sufficiently large.

The limit is obtained when a part of the feed plateau is recycled (limit *G* in Figs. 11–14). The selection of m_R is thus a trade-off between productivity and eluent consumption.

When the solvent removal capacity increases, the maximum amount of fresh feed that can be introduced into different process schemes increases. The maximum productivity and the minimum specific eluent consumption, however, are not always obtained with maximum K_{SR}. This behaviour originates from two different causes. Firstly, the steady state feed concentrations into the chromatographic column increase and thus the propagation velocity of the first shock becomes higher when K_{SR} increases. As a consequence, the upper limit of m_4 decreases leading to prolonged cycle time. Secondly, it is common that the value of m_R must be increased when the solvent removal capacity is increased in order to guarantee that the solvent removal constraints are not violated. Again, the cycle time increases.

The operating point on the (K_{SR}, m_R) plane that leads to maximum productivity is always located on the solvent removal constraint (limits *C*, *D*, and *E* in Figs. 11–14) because the productivity is maximized with minimum m_R. The minimum specific eluent consumption, in contrast, may be obtained by using the operating point inside the feasible region of K_{SR} and m_R. Influence of isotherm parameters on this phenomenon is discussed in more detailed in Sections 6.1.1 and 6.2.1 with two case studies. It will be demonstrated that a clear compromise between productivity and eluent consumption must be usually made also in the selection of K_{SR}.

Finally, it should be reminded that SSR–SR configuration III is usually the most flexible option with respect to the selection of K_{SR} and m_R parameters as discussed in Section 5.3.4. For this reason, it has most often the highest performance as well. A comparison of different process concepts will be shown in Section 6.

5.5 Robust operating conditions

In practical applications, it is important that the unit operations can tolerate at least to some extent fluctuations in the uncontrollable process variables and chemico-physical properties, *i.e.* the selected operating conditions must be robust. The optimal operating parameters discussed in Section 5.4 are inherently very sensitive to various kinds of disturbances because they are commonly located on the boundaries of the feasible operating regions. Firstly, perturbations in the column flow rate or in the cut points and uncertainties in the estimation of the column dimensions or the total void fraction of the bed may modify the dimensionless cut times, and the operating point may move outside the feasible region. Secondly, perturbations in the solvent removal capacity or in the fresh feed concentrations, inaccuracies in the estimation of isotherm parameters, and finite column efficiency alter the shape and size of the region of feasible cut times. The actual range of feasible operating points differs from the domain predicted by the design equations, and it may not include the selected operating point. In both cases, the purity constraints are not satisfied. On the other hand, fluctuations in the solvent removal capacity, in the fresh feed concentrations, or in the recycle fraction composition may lead to violation of the solvent removal constraints. As a consequence, the components may precipitate, osmotic pressure may become excessively high leading to

significant decrease in solvent removal capacity, or the viscosity of the feed solution into the column may increase too much leading to viscous fingering or too high pressure drop.

The robustness of classical batch and SSR processes can be improved by adjusting the cut times, whereas in the cases of different SSR–SR concepts and batch chromatography with solvent removal, one can also tune the solvent removal capacity. The effect of K_{SR} on the process robustness is demonstrated in Figs. 15 and 16. The examples stand for SSR–SR configuration III, but the observations are qualitatively valid also for other process options studied in this work.

It is seen in Figs. 15 and 16 that adjustment of the solvent removal capacity affects the process robustness in two different ways. Firstly, when K_{SR} decreases, the feed concentrations in the column decrease (Fig. 15). This means that the solvent removal constraints, such as solubility, viscosity, osmotic pressure, or vapour pressure limits, are not violated so easily. The upper limit of K_{SR} depends on the volume of the recycle fraction. When m_R is relatively low (below the dotted line in Fig. 15), the feed plateau is not recycled and the steady state feed concentrations decrease with increasing m_R due to dilution of recycle stream. At the same time, the upper limit of K_{SR} increases. When m_R is high and part of the feed plateau is recycled, the steady state feed concentrations as well as the upper limit of K_{SR} are independent of m_R.

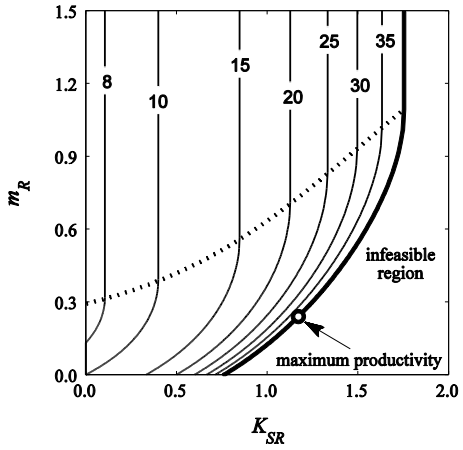

Fig. 15. Region of feasible K_{SR} and m_R values for SSR–SR process when the solvent removal constraint is $c_1^F + c_2^F \leq 40$ g/L . The contour lines show the total steady state feed concentration. The steady state feed concentrations are independent of m_R when the feed plateau is recycled (above the dotted line). Fresh feed concentrations: $c_1^{FF} = c_2^{FF} = 5$ g/L. Isotherm parameters: $K_1 = 0.020$ L/g, $K_2 = 0.025$ L/g, $N_1 = N_2 = 100$ g/L. Phase ratio $F = 1/3$. Purity constraints: $p_1^A = p_2^B = 0.9$.

Secondly, the solvent removal capacity has a significant effect on the shape of the region of feasible cut times (Fig. 16). When K_{SR} and the thus the column feed concentrations increase, competitive nature of phase equilibrium, *i.e*. non-linearity of the system, increases. As a consequence, the operation region on the (m_2, m_3) plane and the top of the region on the (m_2, m_{FF}) plane become narrower. This makes it more difficult to find robust cut times with which the distance from the operation boundaries is large enough. A similar trend is observed in a counter-current SMB unit when the feed concentrations are increased [64].

To select the robust cut times, the operating point on the (m_2, m_3) plane must be adjusted inside the triangle. At the same time, the amount of processed fresh feed with respect to the used eluent decreases. As a result, the recycle fraction becomes more dilute and the solvent removal constraints are not violated so easily when the dimensionless solvent removal capacity is kept constant. In practice, it is also beneficial for robustness to adjust the beginning of the product fraction *A*, m_4, and the end of the product fraction *B*, m_1, such that a small safety gap exists between the consecutive chromatograms.

The (m_2, m_3) plot helps to select the direction in which it is beneficial to shift the operating point to make the process more robust. The direction depends on the solvent removal capacity, the fresh feed concentrations, and the isotherm parameters. When the solvent removal capacity and the fresh feed concentrations are relatively low, m_2 must be increased and m_3 decreased. The increase in m_2 with respect to the decrease in m_3 must be the stronger the higher the steady state feed concentrations are. Under very strong non-linear conditions, both m_2 and m_3 must be increased. The minimum recommended distance between the operating point and the boundaries of the feasible separation region depends on the size of the expected perturbations.

When the solvent removal rate is decreased or the cut times on the (m_2, m_3) plane are adjusted towards the diagonal, the amount of processed fresh feed decreases. Moreover, adjustment of m_1 and m_4 values to obtain longer safety gap between the consecutive chromatograms increases the cycle time. In all cases, the process productivity decreases and the specific eluent consumption increases. The final choice of the operating parameters is thus a trade-off between different performance characteristics and robustness of the process.

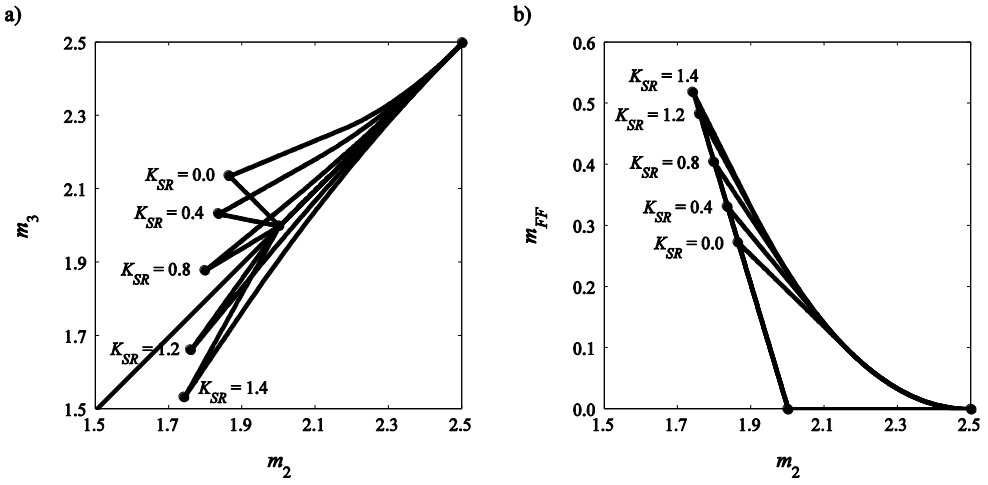

Fig. 16. Effect of solvent removal capacity on the shape of the complete separation region (a) on the (m_2, m_3) plane and (b) on the (m_2, m_{FF}) plane. Same fresh feed concentrations and isotherm parameters as in Fig. 15.

6 APPLICATION EXAMPLES

6.1 Case study: separation of EMD 53986 enantiomers

6.1.1 Performance evaluation under ideal conditions

The design method described in Section 5 has been applied to compare the performance of different fixed bed batch and SSR configurations with or without solvent removal under ideal conditions. Detailed results of the comparison study are found in Paper IV.

The adsorption equilibrium of EMD 53986 enantiomers in 100% ethanol on amylose-tris(3,5-dimethylphenylcarbamate) stationary phase is characterized by modified competitive Langmuir isotherm model [91]. One of the enantiomers can be used as a precursor for a pharmaceutical calcium sensitising agent whereas the other has no such activity. In this work, the modified Langmuir isotherms are approximated with competitive Langmuir model. The resulting isotherm parameters at 25 °C are $K_1 = 0.067$ L/g, $N_1 = 112.3$ g/L, $K_2 = 0.251$ L/g, and $N_2 = 72.8$ g/L. The separation factor is thus relatively large, $\alpha = 2.34$. The total void fraction of the bed is 0.72.

The maximum concentration achievable in the solvent removal unit and the maximum concentration of column feed are limited by the solubility of EMD 53986 enantiomers in ethanol. The solubility curve shown in Fig. 17 is interpolated from the solubility data reported by Ströhlein et al. [36]. The curve is symmetric with respect to line $c_1 = c_2$ and its shape is characteristic for enantiomer systems that form a racemic compound.

The feasible ranges of solvent removal capacity and volume of recycle fraction as well as the boundaries of feasible steady state feed concentrations for the studied process configurations are shown in Figs. 18 and 17, respectively. The fresh feed concentrations are $c_1^{FF} = c_2^{FF} = 1.0$ g/L and the purity constraints $p_1^A = p_2^B = 0.99$. Productivity and specific eluent consumption are displayed as contour lines that show the points with equal values of certain performance parameter. The dimensionless cut points m_1 and m_4 are selected such that the consecutive chromatograms do not overlap, but there is no gap between then either. The target purities are matched exactly by adjusting the cut points m_2 and m_3.

As seen in Fig. 18, SSR–SR configuration III (solvent removal form the column feed; boundaries *A*–*B*–*E*) has the widest range of feasible operating parameters. For SSR–SR configuration I (solvent removal from the fresh feed; boundaries: *A*–*B*–*C*), however, the upper limit of K_{SR} is only slightly lower than for SSR–SR III. This stems from relatively low fresh feed concentrations compared to those of recycle fraction. In the case of SSR–SR configuration II (solvent removal from the recycle fraction; boundaries: *A*–*D*), the volume of the recycle fraction is smaller than the required V^{SR} when m_R is relatively low. For sufficiently large m_R, the operation is possible.

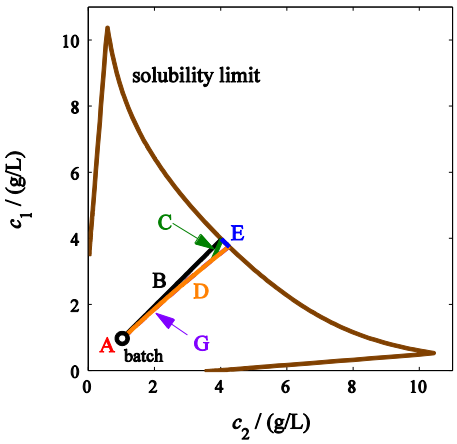

Fig. 17. Regions of feasible steady state feed compositions on the hodograph plane for separation of EMD 53986 enantiomers. Fresh feed concentrations: $c_1^{FF} = c_2^{FF} =$ 1.0 g/L. Purity constraints: $p_1^A = p_2^B = 0.99$.

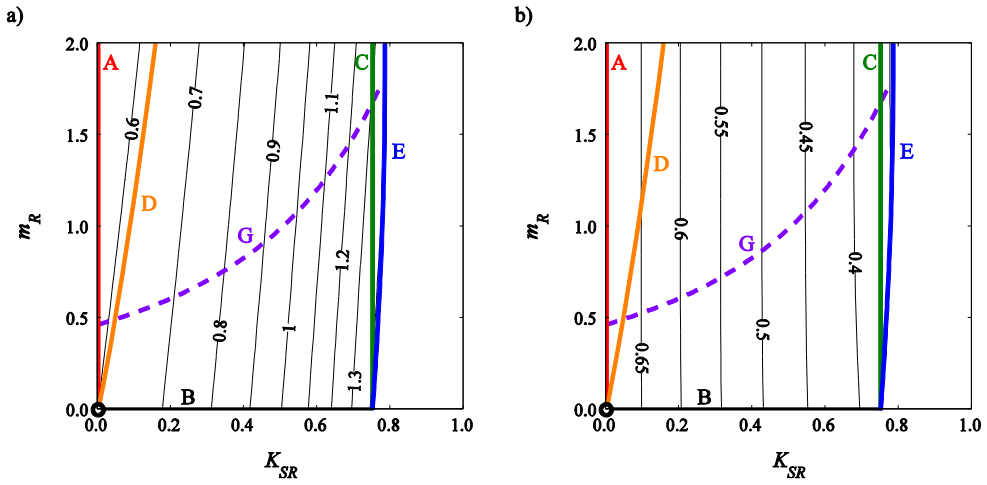

Fig. 18. Regions of feasible operating parameters for separation of EMD 53986 enantiomers with (a) productivity contour lines and (b) eluent consumption contour lines. Same fresh feed concentrations and purity constraints as in Fig. 17.

The images of the operating regions on the hodograph plane are very narrow (Fig. 17). This is because the pure second component plateau is relatively high due to low separation factor. As

a result, the recycle fraction composition is very close to the feed composition even when m_R is small. The limit of m_R corresponding to recycling the feed plateau is thus relatively low (limit *G* in Fig. 18), and the lower limit of steady state feed composition is relatively high (limit *G* in Fig. 17).

For a given solvent removal capacity, the productivity decreases when the volume of the recycle fraction increases. This is because the amount of processed fresh feed is independent of m_R under ideal conditions, whereas the cycle time increases with increasing m_R. In addition, increase in m_R decreases the steady state feed concentrations and slows down the propagation velocity of the first shock when the volume of the recycle fraction is relatively low (below limit *G* in Fig. 18). This means that the upper limit of m_4 can be increased, and the eluent consumption decreases until it levels off as the feed plateau is recycled (above limit *G* in Fig. 18). The behaviour is similar to that reported by Sainio and Kaspereit [81] for conventional SSR process without solvent removal. In the present case, however, the effect of m_R on the eluent consumption is very small. This is because both the separation factor and the absolute Henry constants are large. As a consequence, the relative effect of change in m_4 on the absolute amount of eluent needed per cycle, which is directly proportional to the difference $m_1 - m_4$, is small.

When the volume of the recycle fraction is constant, the amount of fresh feed increases with increasing solvent removal. The maximum productivities and the minimum specific eluent consumptions of all SSR–SR configurations are obtained when the operating point is located on the upper limit of K_{SR}.

The overall process performance consisting of productivity and eluent consumption is displayed by using Pareto frontiers in Fig. 19. The Pareto curves show the maximum productivity achievable with certain eluent consumption. The most efficient process configurations for the present case are SSR–SR III, SSR–SR I, and batch–SR. In all these cases, optimal steady state feed composition with respect to productivity lies on the solubility limit and relatively small feed pulse is beneficial. The maximum productivities of classical batch chromatography and conventional SSR process are about 60% lower and the minimum eluent consumptions about 80% higher than those for best SSR–SR option. This is due to low column feed concentrations in the conventional processes. The benefit of solvent removal would be much lower if the fresh feed concentrations were high. In the case of SSR–SR configuration II, the volume of the recycle fraction must be increased significantly to increase the volume of fresh feed per cycle. This leads to relatively low eluent consumption but also to low productivity due to prolonged cycle time.

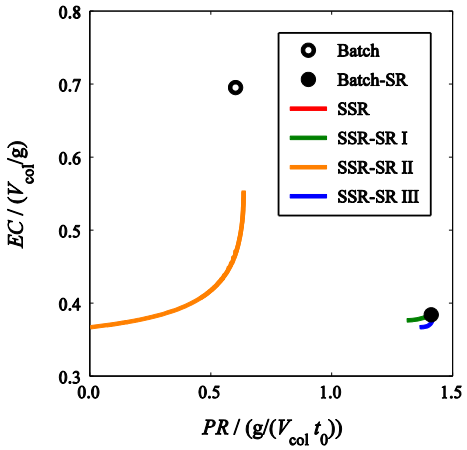

Fig. 19. Pareto frontiers of different process configurations for separation of EMD 53986 enantiomers. Same fresh feed concentrations and purity constraints as in Fig. 17.

6.1.2 Effect of finite column efficiency on process operation

The influence of dispersive effects, such as axial dispersion and mass transfer resistance, on the separation of EMD 53986 enantiomers has been analyzed in Paper VI by using the non-ideal process model described in Section 4.2. The simulation parameters are summarized in Table I.

The selection of m_2 and m_3 parameters was of special interest because it is the most critical step in the design procedure. For this reason, m_1 and m_4 were chosen with a sufficient safety margin that guarantees that the consecutive chromatograms did not overlap. For SSR and SSR–SR setups, the volume of the recycle fraction was selected such that the feed plateau prevailed. This provides minimum eluent consumption for a certain solvent removal capacity without significant decrease in productivity [82].

The number of theoretical plates of the column, *NTP*, was determined under linear conditions for the less strongly adsorbed component. The mass transfer coefficients were varied between 4.32–163.2 min^{-1} that corresponds to variation from 50 to 500 theoretical plates.

The dimensionless solvent removal capacity K_{SR} in SSR–SR process was kept constant at 0.625. The total steady state feed concentration increased to level of 6.2–6.4 g/L in the optimal operating point predicted by the equilibrium theory (point *w* in Fig. 10). The solute retention in the membrane filtration was assumed to be 0.98.

Table I Parameters for the model systems used in numerical simulation study in Sections 6.1.2 and 6.2.2.

parameter	EMD 53986	mandelic acid
fresh feed concentrations, c_i^{FF} (g/L)	1.5	4.5
column length, L_{col} (cm)	15.0	15.0
column diameter, D_{col} (cm)	1.0	1.0
axial dispersion coefficient, D_{ax} (cm^2/min)	0.036	0.006
mass transfer coefficients, k_i (min^{-1})	4.32–163.2	46.68–343.5
eluent flow rate, Q_{col} (mL/min)	1.8	1.8
membrane area, A_{memb} (cm^2)	4.37–84.6	3.67
solvent permeability, B_S (L/m^2 h bar)	0.5	1.5
solute permeability, B_i (L/(m^2 h))	0.1	0.3
effective pressure, $\Delta P_{memb} - \Delta\pi$ (bar)	10.0	10.0

The influence of limited column efficiency on the size, shape, and location of the feasible operating region on the (m_2, m_3) plane for batch, SSR, and SSR–SR III processes is illustrated in Figs. 20–22. As expected, the separation domain under non-ideal conditions approaches the ideal region predicted by the equilibrium theory when the column efficiency is high (Figs. 20a, 21a, and 22a). When the column efficiency decreases, the operating regions corresponding to given target purities shrink, and the deviations from the ideal case are higher.

It is seen in Figs. 20–22 that the dispersive effects have a most intense impact on the purities in the bottom left corner of the separation region. This is explained by the fact that the tail of first component band broadens easily due to dispersion, and pollutes the product *B*. The phenomenon is qualitatively similar to that reported earlier for SMB concept in [92]. In practice, this means that it is most beneficial to make the processes more robust by decreasing the amount of processed fresh feed m_{FF}, while keeping the value of m_3 near its upper limit.

When NTP = 50 and the processes are operated in their optimal operating points of the ideal complete separation regions (*i.e.* in the vertexes of the triangles shown in Figs. 5b, 6b, and 7b), the achieved product purities are in batch process p_1^A = 0.955, p_2^B = 0.945, in SSR process p_1^A = 0.966, p_2^B = 0.950, and in SSR–SR process p_1^A = 0.986, p_2^B = 0.950. The relatively high purities can be explained by large separation factor. It enables using large column loading even in batch process. This makes the separation less sensitive to dispersive effects. The highest product purities are achieved in SSR–SR scheme even though its complete separation region predicted by the equilibrium theory is the narrowest one. This is because the steady state feed concentrations increase when solvent is removed, and the thermodynamic effects become more predominant.

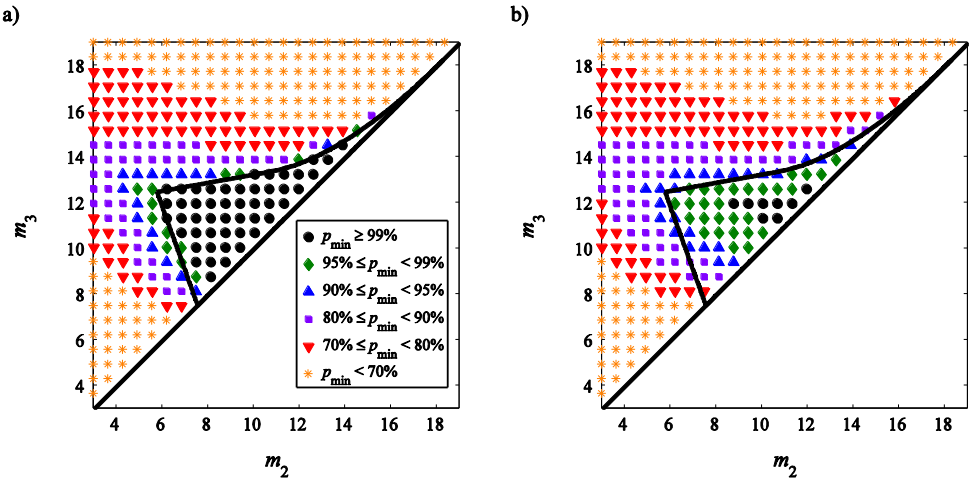

Fig. 20. Product purities for separation of EMD 53986 enantiomers in batch chromatography. Symbols: product purities under non-ideal conditions when (a) *NTP* = 500 and (b) *NTP* = 50. Solid line: complete separation region under ideal conditions. Simulation parameters are given in Table I.

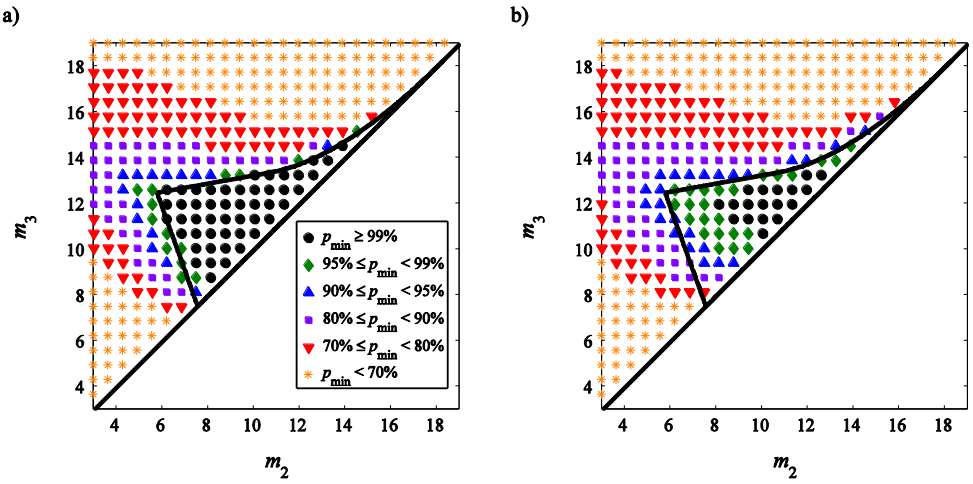

Fig. 21. Product purities for separation of EMD 53986 enantiomers in SSR chromatography. Symbols: product purities under non-ideal conditions when (a) *NTP* = 500 and (b) *NTP* = 50. Solid line: complete separation region under ideal conditions. Simulation parameters are given in Table I.

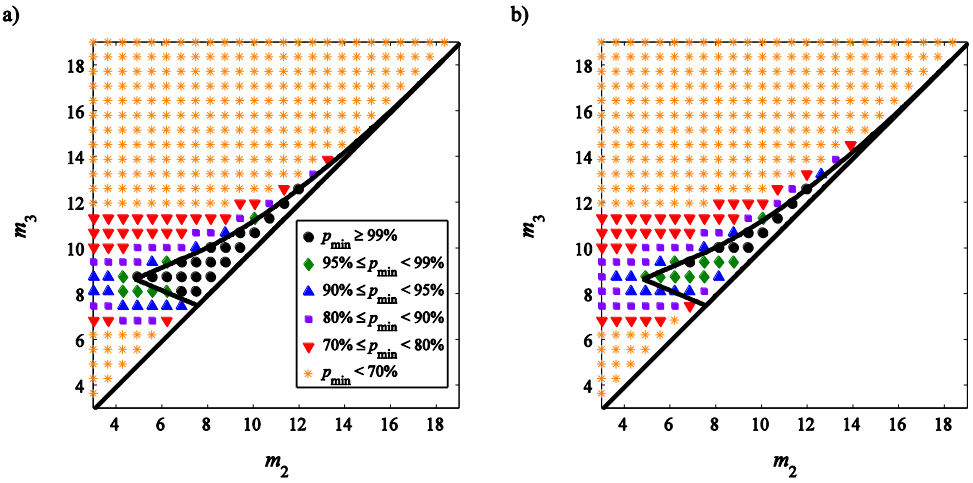

Fig. 22. Product purities for separation of EMD 53986 enantiomers in SSR–SR III process. Symbols: product purities under non-ideal conditions when (a) *NTP* = 500 and (b) *NTP* = 50. Solid line: complete separation region under ideal conditions. Simulation parameters are given in Table I.

6.2 Case study: separation of mandelic acid enantiomers

6.2.1 Performance evaluation under ideal conditions

The adsorption equilibrium of mandelic acid enantiomers in water–acetic acid–acetonitrile (86.4:9.1:4.5, v/v), 0.05 mol/L ammonium acetate (pH = 3.0) mobile phase on nucleodex β-OH stationary phase follows competitive Langmuir model [93]. The isotherm parameters at 20 °C for the less absorbed *S*(+)-enantiomer are K_1 = 0.1111 L/g and N_1 = 72.5 g/L and for the more absorbed *R*(−)-enantiomer K_2 = 0.1222 L/g and N_2 = 70.6 g/L. The separation factor, α = 1.07, is now much smaller compared to separation of EMD 53986 enantiomers. The overall void fraction of the bed is 0.756.

The solubility of the mandelic acid enantiomers in the considered mobile phase is relatively high (more than 50 g/L) [93]. The maximum total concentration of the column feed is limited by the fact that pH must be stabilized to avoid significant change of the adsorption equilibrium and decrease of selectivity [94]. For the given specific buffer concentration, pH starts to change when the total mandelic acid concentrations exceeds 10 g/L [93].

The operating boundaries for the separation of mandelic acid enantiomers in the case of $c_1^{FF} = c_2^{FF}$ = 1.0 g/L and $p_1^A = p_2^B$ = 0.99 are shown in Figs. 23 and 24. As expected, the SSR–SR configuration III has again the widest operating domain. Due to low separation factor and relatively non-linear conditions, the images of the operating regions on the hodograph plane are broad, and the differences in the upper limits of K_{SR} for different

configurations are significant. For example, the maximum K_{SR} in SSR–SR I process is more than 80% lower than that in SSR–SR configuration III. This is caused by the fact that for relatively high K_{SR} values the required V_{SR} is higher than V_{FF} and enough solvent cannot be removed from the fresh feed. As a consequence the amount of fresh feed that can be processed in SSR–SR configuration I is 59% smaller than that in SSR–SR III process.

When the solvent removal capacity is constant, productivity and eluent consumption decrease with increasing volume of recycle fraction until the eluent consumption levels off as the feed plateau is recycled (above limit *G* in Fig. 24). The behaviour is qualitatively similar to that observed in separation of EMD 53986 enantiomers.

When the volume of the recycle fraction is constant and the solvent removal capacity increases, the productivity increases monotonically due to increased amount of fresh feed. The specific eluent consumption, in contrast, goes through minimum. This is because the solvent removal increases the steady state feed concentrations and speeds up the propagation velocity of the first shock. This leads to increased absolute need of eluent which counterbalances the increase of the amount of fresh feed.

The Pareto frontiers for the separation of mandelic acid enantiomers are shown in Fig. 25. In the case of all SSR schemes with or without solvent removal, a compromise between productivity and eluent consumption is clearly needed. For example, when the SSR–SR process III is optimized with respect to maximum productivity, eluent consumption is 17.6% higher than achievable minimum eluent consumption.

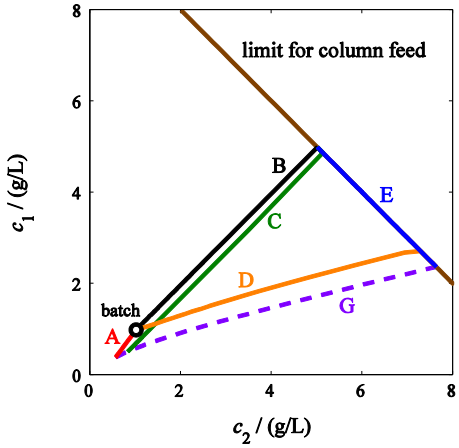

Fig. 23. Regions of feasible steady state feed compositions on the hodograph plane for separation of mandelic acid enantiomers. Fresh feed concentrations: $c_1^{FF} = c_2^{FF} =$ 1.0 g/L. Purity constraints: $p_1^A = p_2^B = 0.95$.

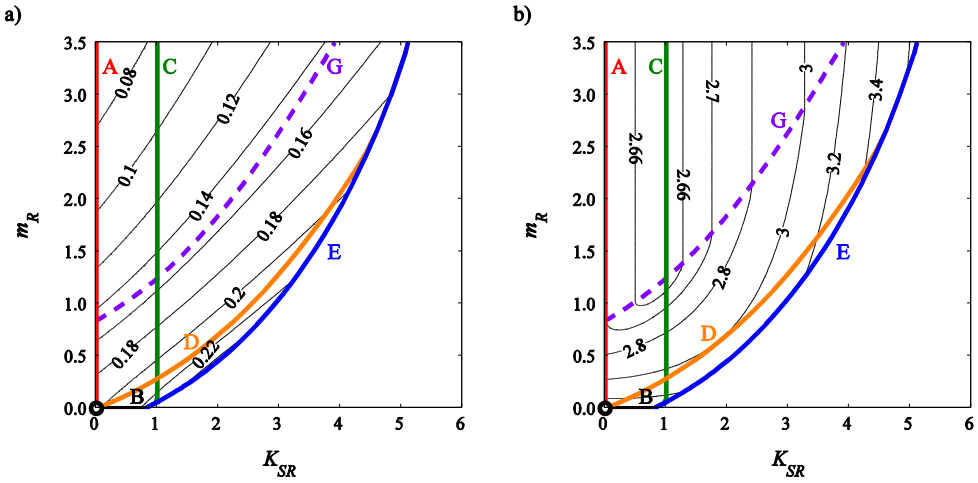

Fig. 24. Regions of feasible operating parameters for separation of mandelic acid enantiomers with (a) productivity contour lines and (b) eluent consumption contour lines. Same fresh feed concentrations and purity constraints as in Fig. 23.

As can be expected, SSR–SR configuration III is again the most efficient one due to largest operating region. It leads to 4.4% higher productivity with 5.7% lower eluent consumption than batch process with a similar solvent removal unit when the processes are optimized with respect to productivity. Due to ideal conditions, however, here the benefit is much smaller compared to those reported under strongly non-ideal conditions by Hellstén et al. [51] for separation of glucose and galactose and by Kaspereit and Sainio [82] for separation of two cycloketones. In simple terms, the performance of batch operation with or without solvent removal is much more strongly affected by dispersion than that of SSR mode. If SSR and batch processes were operated with the same fresh feed amount under non-ideal conditions, SSR operation would lead to higher product purities for two reasons. Firstly, in SSR process the overlapping parts of the chromatogram that were affected by dispersion are not collected into the product fractions but recycled, whereas in batch operation the purity constraints can be satisfied only by decreasing the amount of fresh feed. Secondly, SSR schemes are less sensitive to dispersive effects due to higher column overloading. As a result, the advantages of SSR operation are emphasized when the column efficiency is low.

As to the SSR–SR configuration I, it slightly outperforms batch–SR process in terms of maximum productivity. This is because the concentrations of the column feed instead of the operation of the solvent removal unit limit the amount of solvent removal. In the case of SSR–SR I, fresh feed can be concentrated over the pH stability limit and diluted with recycle fraction. The maximum productivity of SSR–SR configuration II is smaller than that of other SSR–SR processes because operation with relatively small recycle fraction volumes is not possible.

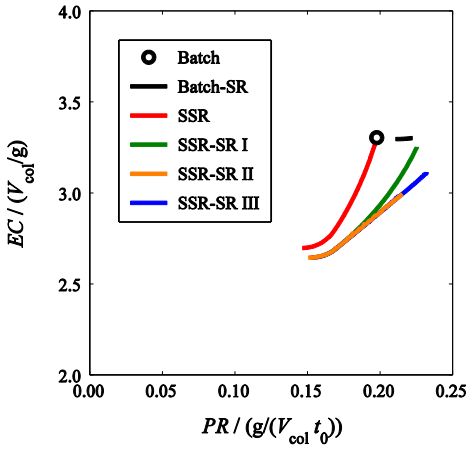

Fig. 25. Pareto frontiers of different process configurations for separation of mandelic acid enantiomers. Same fresh feed concentrations and purity constraints as in Fig. 23.

6.2.2 Effect of finite column efficiency on process operation

The parameters for the simulation study under non-ideal conditions for separation of mandelic acid enantiomers are listed in Table I. The column efficiency must now be higher than in separation of EMD 53986 enantiomers to achieve desired separation due to low separation factor. For this reason, the mass transfer coefficients were varied between 46.68–343.5 min^{-1} that correspond, in this case, to 500–2000 theoretical plates for the component 1. The dimensionless solvent removal capacity in SSR–SR III process was set equal to 10. The total steady state feed concentration was 1.2 g/L, while in the conventional SSR process it was 0.63 g/L due to dilution caused by the recycle fraction.

The effect of column efficiency on the product purities is demonstrated in Fig. 26. Again, the operating point on the (m_2, m_3) plane was set equal to the point *w* predicted by the equilibrium theory. The achieved product purities are now much lower than in separation of EMD 53986 enantiomers despite higher column efficiencies. This is caused by low separation factor that limits the column loading. As a consequence, the thermodynamic effects are less predominant. The product purities of batch process decrease most rapidly because in that case the volume of the feed pulse is the smallest one. Purity of the product fraction *A* is highest in SSR–SR process, whereas SSR setup outperforms SSR–SR schemes in terms of purity of the product *B*. The differences in the values of p_2^B, however, are relatively small, and it can be again concluded that the SSR–SR process tolerates dispersive effects at least to the same degree as SSR setup.

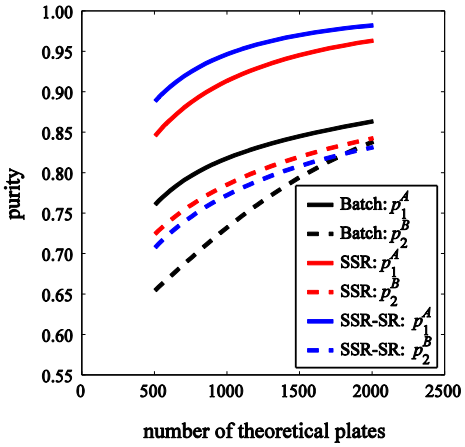

Fig. 26. Influence of column efficiency on the product purities for separation of mandelic acid enantiomers when the processes are operated in the optimal operating point of the ideal complete separation region on the (m_2, m_3) plane (point *w*). Simulation parameters are given in Table I.

7 SHORTCUT DESIGN UNDER NON-IDEAL CONDITIONS

7.1 Design approach

The design method discussed in Section 5 is based on the assumption of finite column efficiency and holds for chromatographic systems that follow competitive Langmuir adsorption isotherm. Next, a shortcut design approach to predict first estimates of m_2 and m_3 parameters under practically relevant non-ideal conditions with significant dispersive effects and for convex (favourable) or concave (unfavourable) adsorption isotherms in general is summarized. The method has been originally developed for stand-alone SSR process by Kaspereit and Sainio [82], and extended for batch process in this work in Paper III. The same approach can also be applied for the design of counter-current multi-column SMB units due to analogy between the dimensionless operating parameters of various chromatographic concepts as demonstrated in Paper V.

The shortcut design method is based on a simple procedure applied to a single conventional chromatogram. The design chromatogram can be an experimental chromatogram or, if a column model and parameters are available, a simulated one. It is generated for an injection of fresh feed with a relatively large volume of feed pulse. If an experimental chromatogram is used, it must be decomposed into the individual concentration profiles but no isotherm parameters or model is required. In the case of simulation, the approach is independent of the used model, *i.e.* whichever chromatographic model that takes dispersive effects into account (*e.g.* equilibrium-dispersive model, transport-dispersive model, or general rate model) can be applied.

In the case of convex isotherms (*e.g.* Langmuir isotherm), the shortcut design is based on the fact that the rear part of the chromatogram is nearly independent of the volume of the feed pulse over a wide range of injection widths. First estimates for m_2 and m_3 are predicted from the design chromatogram by using the following procedure. At first, the beginning of the product fraction *B* relative to end of the feed pulse, *i.e.* the value of m_2, is solved by integrating the design chromatogram backward until the purity constraint p_2^B, Eq. (47), is satisfied. Once m_2 has been solved, also the amount of component 2 in the product fraction *B*, n_2^B, is known from the backward integration. The amount of fresh feed is then calculated from the mass balance of the second component as follows:

$$m_{FF} = \frac{n_2^B}{Y_2 c_2^{FF} (1-\varepsilon) V_{col}} . \tag{80}$$

As a last step, the value of m_3 is obtained from Eq. (56) which yields

$$m_3 = m_2 + m_{FF} . \tag{81}$$

In the case of concave isotherms (*e.g.* anti-Langmuir isotherm) the front of the chromatogram is nearly independent of the volume of the feed pulse, and an analogous but opposite design approach compared to the case of convex isotherms is used. At first, the end of the product

fraction *A* relative to the beginning of the feed pulse, *i.e.* the value of m_3, is solved by integrating the front of the design chromatogram to find the point where the purity constraint p_1^A, Eq. (46), is satisfied. The amount of fresh feed is then solved from the mass balance of the first component which yields

$$m_{FF} = \frac{n_1^A}{Y_1 c_1^{FF} (1-\varepsilon) V_{col}} . \tag{82}$$

Finally, the value of m_2 is calculated as follows:

$$m_2 = m_3 - m_{FF} . \tag{83}$$

7.2 Evaluation of the shortcut method for designing batch chromatography

Applicability of the shortcut approach for design of batch chromatography under strongly non-ideal conditions has been evaluated by means of numerical simulation by using the transport-dispersive model with the solid film linear driving force approximation described in Section 4.2. The following three case studies have been investigated: (1) separation of Tröger's base enantiomers, Langmuir isotherm, (2) separation of cycloketones, bi-Langmuir isotherm, and (3) a generic example, anti-Langmuir isotherm. Detailed results are found in Paper III.

The shortcut design provides more accurate estimations for m_2 and m_3 parameters than the equilibrium theory since the effect of dispersion on the rear (convex isotherms) or on the front (concave isotherms) of the chromatogram is inherently taken into account during integration. Accuracies of the estimations depends strongly on the column efficiency, purity constraints, fresh feed concentrations, and isotherm parameters. The method works the better the more predominant thermodynamic effects are, *i.e.* the higher the column efficiency and the column loading are.

The shortcut approach predicts generally a too high value for m_{FF}. This is because the column loading corresponding to the design chromatogram is larger than that with which the target purities are matched exactly. As a consequence, the role of dispersive effects is underestimated. For the same reason, the prediction of m_2 is typically too low in the case of convex isotherms and the prediction of m_3 is too high in the case of concave isotherms.

In the case of convex isotherms, the purity of product *B* is typically matched better than the purity of product *A*. This is because the front of the chromatogram is strongly influenced by the accuracy of the predicted m_3. Especially in the case of high purity requirements, the centre cut point is positioned at the "root" of the mixed shock – a position which is very susceptible to the influence of dispersion. As a consequence, even a small inaccuracy in the prediction of m_3 leads to significant deviation of p_1^A from the target value. For concave isotherms, an opposite behaviour is observed.

7.3 Evaluation of the shortcut method for designing SMB process

As mentioned in Section 5.2, the complete separation regions on the (m_2, m_3) plane for fixed bed, cross-current, and counter-current processes are identical in the case of ideal conditions and competitive Langmuir adsorption isotherm. This observation provides the basis for estimating the feasible operating conditions for all mentioned process options by using the information obtained for one setup. Under non-ideal conditions, however, deviations between the process configurations are expected because the role of dispersive effects depends on the mutual direction of the solid and fluid flows and the column loading. In addition, the fluid flow rates and thus the column efficiencies in different configurations cannot be fully matched because four different flow rates are used in the four zones of the counter-current units, while the fluid flow rate is constant in the fixed bed and cross-current schemes.

Applicability of the single-column shortcut method for the design of counter-current SMB units has been demonstrated in Paper V. Feasible m_2 and m_3 parameters corresponding to given purity constraints were first estimated by using the approach described in Section 7.1, and the obtained parameters were then applied to simulate the steady state purities of SMB 1-1-1-1 and 1-2-2-1 configurations. The total bed length and the average fluid flow rates in sections 1 to 4 of the SMB unit were set equal to the column length and the fluid flow rate of single-column process, respectively. The total pressure drop in the SMB columns was thus equal to that of fixed bed mode. The values of m_1 and m_4 were selected such that they guaranteed complete regeneration of the solid and fluid phases, respectively, because the shortcut design method does not consider overlapping between the consecutive chromatograms. The parameters of the two generic model systems as well as the conditions of the shortcut design are summarized in Table II. The number of theoretical plates in fixed bed column was 200.

In addition to the results shown in Paper V, iso-purity contours on the (m_2, m_3) plane were simulated for the SMB units by using a square grid spaced by $\Delta m = 0.065$. In these calculations, the switch time was kept constant and the values of m_1 and m_4 was again selected such that the solid and fluid phase were regenerated completely in zones 1 and 4, respectively.

The results of the simulation study are shown in Table III and in Fig. 27. It is seen that the design approach works best when the target purities are low and the separation factor is large. This is because these conditions provide large column loading that makes the thermodynamic effects more predominant. In the case of model system 1, in fact, the column efficiency is so low that it is not even possible to achieve 0.98 product purities by using the SMB 1-1-1-1 configuration (Fig. 27a).

Table II Parameters for the model systems used in the evaluation of the applicability of the single-column shortcut method for the design of counter-current SMB units.

Parameter	System 1	System 2
fresh feed concentration of component 1, c_1^{FF} (g/L)	4.0	
fresh feed concentration of component 2, c_2^{FF} (g/L)	4.0	
total bed length, $N_{col,tot} L_{col}$ (cm)	84.0	
column diameter, D_{col} (cm)	2.5	
isotherm parameters (Langmuir isotherm):		
K_1 (L/g)	0.025	
H_1	2.5	
K_2 (L/g)	0.035	0.050
H_2	3.5	5.0
total void fraction of the bed, ε	0.7	
axial dispersion coefficient, D_{ax} (cm^2/min)	0.213	
mass transfer coefficient of component 1, k_1 (1/min)	6.0	
mass transfer coefficient of component 2, k_2 (1/min)	6.0	
fluid flow rate in the single-column processes, Q (mL/min)	12.5	
volume of the feed pulse in the shortcut design, V_F^{design} (mL)	600	

The deviations observed in the cases of high purity requirements can be explained by two different factors. Firstly, the single-column shortcut method provides systematically too optimistic estimations for m_{FF} and m_3 of batch and SSR processes as reported in Paper III and in [82], respectively. Consequently, the purity of the first eluting component is typically lower than the target. Secondly, identical m-parameters do not guarantee identical purities for all process configurations under non-ideal conditions because the units tolerate dispersive effects differently. The SMB configuration 1-2-2-1, in particular, is less sensitive to dispersive effects than the other schemes and leads to higher product purities when identical m-parameters are used. In that case, it might be possible to improve the accuracies of the predictions by using higher column efficiency in the generation of the design chromatogram, for example, by adjusting the flow rate or the column length.

An interesting finding is also that SSR and SMB 1-1-1-1 configurations provide almost equal product purities when identical m_2 and m_3 parameters are used (see Table III). This implies that the operating points on the (m_2, m_3) plane with which the target purities are matched exactly in these two process options are most probably very close to each other as well. This property is very useful when the feasible operating parameters for one of these schemes are known and the operating parameters for the other one are needed.

Table III Application of the single-column shortcut design for different process schemes and purity requirements. Simulation parameters are given in Table II.

Case:	System 1						System 2					
	A		B		C		A		B		C	
Target purities:	p_1^A	p_2^B	p_1^A	p_2^B	p_1^A	p_2^B	p_1^A	p_2^B	p_1^A	p_2^B	p_1^A	p_2^B
	0.98	0.98	0.90	0.90	0.80	0.80	0.98	0.98	0.90	0.90	0.80	0.80
Predicted *m*-parameters:												
m_1	5.050		5.050		5.050		6.840		6.840		6.840	
m_2	2.842		2.280		1.870		2.337		1.784		1.283	
m_3	3.141		3.001		3.095		3.959		4.088		4.479	
m_4	1.300		1.300		1.300		1.310		1.310		1.310	
Achieved purities:	p_1^A	p_2^B	p_1^A	p_2^B	p_1^A	p_2^B	p_1^A	p_2^B	p_1^A	p_2^B	p_1^A	p_2^B
Batch	0.781	0.962	0.822	0.879	0.783	0.792	0.936	0.977	0.891	0.898	0.800	0.800
SSR	0.813	0.985	0.843	0.902	0.787	0.801	0.944	0.980	0.893	0.901	0.799	0.800
SMB 1-1-1-1	0.841	0.983	0.867	0.913	0.797	0.809	0.948	0.971	0.896	0.895	0.802	0.798
SMB 1-2-2-1	0.885	1.000	0.887	0.977	0.800	0.842	0.987	0.998	0.901	0.923	0.801	0.801

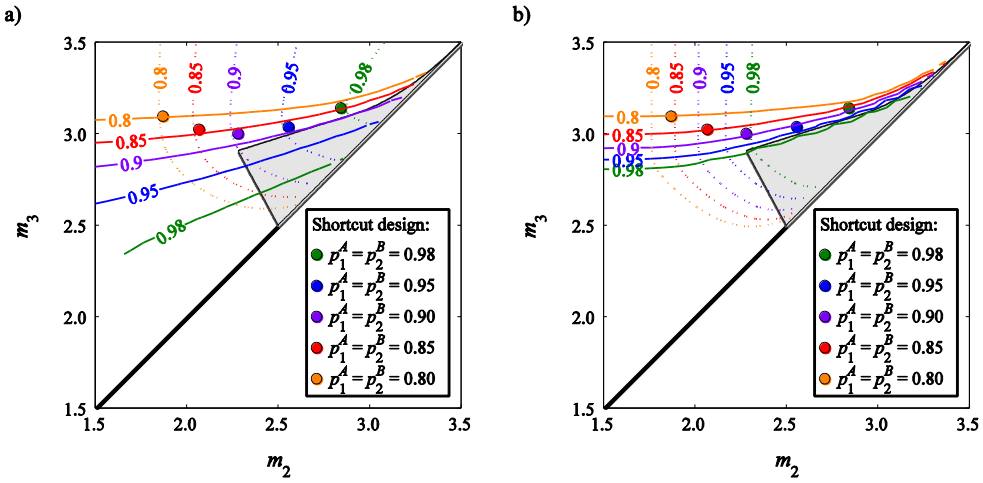

Fig. 27 Applicability of the single-column shortcut method for the design of (a) SMB 1-1-1-1 unit and (b) SMB 1-2-2-1 unit. Solid and dotted lines: contours of p_1^A and p_2^B, respectively. Symbols: operating points predicted by using the shortcut approach. Switch time: (a) t^* = 13.5 min, (b) t^* = 9.0 min. Other simulation parameters are given in Table II (system 1).

8 CONCLUSIONS

In this thesis, two methods were developed for the design of chromatographic separation processes. The first one is based on the equilibrium theory of chromatography and is applicable for the design of fixed bed batch chromatography with or without an integrated solvent removal unit, fixed bed mixed-recycle SSR chromatography with or without solvent removal, and corresponding cross-current processes. It was shown that the design criteria can be set in general, dimensionless form that is formally analogous to that applied earlier in the triangle theory of counter-current multi-column SMB processes. The design approach allows predicting the range of feasible operating parameters as well as selecting the optimal and robust operating conditions for binary separations such that user-given purity and/or yield requirements are satisfied.

Analytical design equations were derived for systems that follow competitive Langmuir adsorption isotherm model. In addition, explicit equations for the height and retention time of the pure first component shock in the case of a small feed pulse were presented. The height of the first shock is obtained as an only positive root of a quartic equation. Hence, it was shown that for binary Langmuir systems the individual concentration profiles at the column outlet can be expressed entirely in closed-form.

The developed design method was utilized to analyse the possibility to improve the performance of SSR chromatography by partial solvent removal. The following three SSR–SR process configurations were compared: (1) solvent is removed from the fresh feed, (2) solvent is removed from the recycle fraction, and (3) solvent is removed from the actual feed solution into the chromatographic unit that is obtained by mixing the fresh feed and the recycle fraction.

The theoretical analysis revealed that solvent removal makes possible to treat more fresh feed during each chromatographic cycle and thus increase the performance of conventional SSR process. The need of solvent removal capacity, however, increases rapidly when the amount of fresh feed increases. All three SSR–SR configurations have identical performance when the same operating parameters are used. In contrast, the maximum solvent removal capacity as well as the range of feasible volume of recycle fraction depends strongly on solvent removal constraints, such as solubility, viscosity, or osmotic pressure limit, and is not identical for all SSR–SR schemes. The configuration where solvent is removed from the mixed fraction is typically the most flexible one with respect to the range of feasible operating parameters and provides the highest performance.

Applicability of the equilibrium design for practically relevant separation problems with finite column efficiency was evaluated with two case studies. The separation of EMD 53986 enantiomers and the separation of mandelic acid enantiomers were used as model systems. As expected, the method is most applicable for high performance systems where thermodynamic effects are predominant, while some conclusions may not be valid for systems of moderate or low efficiency.

The second design method is a shortcut approach that is applicable under non-ideal conditions with significant dispersive effects for convex and concave isotherms in general. The method

is based on a single pulse injection to a batch column and can be applied without knowledge of adsorption isotherm parameters. It was demonstrated that the approach allows designing batch and counter-current SMB processes with good accuracy, especially for relatively low purity requirements.

The main limitation of the proposed design methods is that they do not allow optimization of the eluent flow rate or the column dimensions. For this reason, the methods are mainly recommended for qualitative early-stage comparison of process alternatives and for prediction of the preliminary operating parameters that can be later fine-tuned by detailed simulations.

REFERENCES

1 Bailly, M. and Tondeur, D., Recycle optimization in non-linear productive chromatography—I Mixing recycle with fresh feed. *Chem. Eng. Sci.*, 37(1982), 1199–1212.

2 Grill, C.M., Closed-loop recycling with periodic intra-profile injection: a new binary preparative chromatographic technique. *J. Chromatogr. A*, 796(1998), 101–113.

3 Charton, F., *Optimisation des coupes et recyclages en chromatographie preparative industrielle*. PhD thesis, Institut National Polytechnique de Lorraine, Nancy, France, 1995.

4 Charton, F., Bailly, M., and Guiochon, G., Recycling in preparative liquid chromatography. *J. Chromatogr. A*, 687(1994), 12–31.

5 Adam, P., Nicoud, R.-M., Bailly, M., and Ludemann-Hombourger, O., US Patent 6,136,198 A, 2000.

6 Ludemann-Hombourger, O., Nicoud, R.-M., and Bailly, M., The "VARICOL" process: a new multicolumn continuous chromatographic process. *Sep. Sci. Technol.*, 35(2000), 1829–1862.

7 Kearney, M.M. and Hieb, K.L., US Patent 5,102,553 A, 1992.

8 Tanimura, M., Tamura, M., Teshima, T., Japanese Patent 07-046097B, 1995.

9 Kloppenburg, E. and Gilles, E.D., A new concept for operating simulated moving-bed processes. *Chem. Eng. Technol.*, 22(1999) 813–817.

10 Zang, Y. and Wankat, P.C., SMB operation strategy-partial feed. *Ind. Eng. Chem. Res.*, 41(2002) 2504–2511.

11 Zhang, Z., Mazzotti, M., and Morbidelli, M., PowerFeed operation of simulated moving bed units: changing flow-rates during the switching interval. *J. Chromatogr. A*, 1006(2003) 87–99.

12 Bae, Y.-S. and Lee, C.-H., Partial-discard strategy for obtaining high purity products using simulated moving bed chromatography. *J. Chromatogr. A*, 1122(2006) 161–173.

13 Schramm, H., Kaspereit, M., Kienle, A., and Seidel-Morgenstern, A., Improving simulated moving bed processes by cyclic modulation of the feed concentration. *Chem. Eng. Technol.*, 25(2002), 1151–1155.

14 Schramm, H., Kienle, A., Kaspereit, M., and Seidel-Morgenstern, A., Improved operation of simulated moving bed processes through cyclic modulation of feed flow and feed concentration. *Chem. Eng. Sci.*, 58(2003), 5217–5227.

15 Jensen, T.B., Reijns, T.G.P., Billiet, H.A.H., and van der Wielen, L.A.M., Novel simulated moving-bed method for reduced solvent consumption. *J. Chromatogr. A*, 873(2000), 149–162.

16 Migliorini, C., Wendlinger, M., Mazzotti, M., and Morbidelli, M., Temperature gradient operation of a simulated moving bed unit. *Ind. Eng. Chem. Res.*, 40(2001), 2606–2617.

17 Antos, D. and Seidel-Morgenstern, A., Application of gradients in the simulated moving bed process. *Chem. Eng. Sci.*, 56(2001), 6667–6682.

18 Nicolaos, A., Muhr, L., Gotteland, P., Nicoud, R.-M., and Bailly, M., Application of equilibrium theory to ternary moving bed configurations (four+four, five+four, eight and nine zones) I. Linear case. *J. Chromatogr. A*, 908(2001) 71–86.

19 Nicolaos, A., Muhr, L., Gotteland, P., Nicoud, R.-M., and Bailly, M., Application of the equilibrium theory to ternary moving bed configurations (4+4, 5+4, 8 and 9 zones) II. Langmuir case. *J. Chromatogr. A*, 908(2001) 87–109.

20 Lee, K., Two-section simulated moving-bed process. *Sep. Sci. Technol.*, 35(2000), 519–534.

21 Zang, Y. and Wankat, P.C., Three-zone simulated moving bed with partial feed and selective withdrawal. *Ind. Eng. Chem. Res.*, 41(2002), 5283-5289.

22 Jin, W., Wankat, P.C., Two-zone SMB process for binary separation. *Ind. Eng. Chem. Res.*, 44(2005), 1565–1575.

23 Rodrigues, R.C.R., Canhoto, T.J.S.B., Araújo, J.M.M., and Mota J.P.B., Two-column simulated moving-bed process for binary separation. *J. Chromatogr. A*, 1180(2008), 42–52.

24 Abunasser, N., Wankat, P.C., Kim, Y.-S., and Koo, Y.-M., One-column chromatograph with recycle analogous to a four-zone simulated moving bed., *Ind. Eng. Chem. Res.*, 42(2003), 5268–5279.

25 Abunasser, N. and Wankat, P.C., One-column chromatograph with recycle analogous to simulated moving bed adsorbers: Analysis and applications. *Ind. Eng. Chem. Res.*, 43(2004), 5291–5299.

26 Mota, J.P.B. and Araújo, J.M.M., Single-column simulated-moving-bed process with recycle lag. *AIChE J.*, 51(2005), 1641–1653.

27 Bubnik, Z., Pour, V., Gruberova, A., Starhova, H., Hinkova, A., and Kadlec, P., Application of continuous chromatographic separation in sugar processing. *J. Food Eng.*, 61(2004), 509–513.

28 Ruthven, D.M. and Ching, C.B., Counter-current and simulated counter-current adsorption separation processes. *Chem. Eng. Sci.*, 44(1989), 1011–1038.

29 Rajendran, A., Paredes, G., and Mazzotti, M., Simulated moving bed chromatography for the separation of enantiomers. *J. Chromatogr. A*, 1216(2009), 709–738.

30 Huckman, M.E., Latheef, I.M., and Anthony, R.G., Designing a commercial ion-exchange carousel to treat DOE wastes using CST granules. *AIChE J.*, 47(2001), 1425–1431.

31 Virolainen, S., Suppula, I., and Sainio, T., Continuous ion exchange for hydrometallurgy: Purification of Ag(I)–NaCl from divalent metals with aminomethylphosphonic resin using counter-current and cross-current operation. *Hydrometallurgy*, 142(2014), 84–93.

32 Antos, D., *Gradient Techniques in Preparative Chromatography: Modeling and Experimental Realization*. Lambert Academic Publishing, Saarbrücken, Germany, 2009.

33 Guiochon, G., Felinger, A., Shirazi, D.G., and Katti, A.M., *Fundamentals of Preparative and Nonlinear Chromatography*. 2nd ed., Academic Press, Amsterdam, Netherlands, 2006.

34 Lim, B.-G., Ching, C.-B., Tan, R.B., and Ng, S.-C., Recovery of (−)-praziquantel from racemic mixtures by continuous chromatography and crystallization. *Chem. Eng. Sci.*, 50(1995), 2289–2298.

35 Lorenz, H., Sheehan, P., and Seidel-Morgenstern, A., Coupling of simulated moving bed chromatography and fractional crystallisation for efficient enantioseparation. *J. Chromatogr. A*, 908(2001), 201–214.

36 Ströhlein, G., Schulte, M., and Strube, J., Hybrid processes: design method for optimal coupling of chromatography and crystallization units. *Sep. Sci. Technol.*, 38(2003), 3353–3383.

37 Fung, K.Y., Ng, K.M., and Wibowo, C., Synthesis of chromatography-crystallization hybrid separation processes. *Ind. Eng. Chem. Res.*, 44(2005), 910–921.

38 Kaspereit, M., Gedicke, K., Zahn, V., Mahoney, A.W., and Seidel-Morgenstern, A., Shortcut method for evaluation and design of a hybrid process for enantioseparations. *J. Chromatogr. A*, 1092(2005), 43–54.

39 Kaspereit, M., *Separation of enantiomers by a process combination of chromatography and crystallization*. PhD thesis, Otto von Guericke University, Magdeburg, Shaker Verlag, Aachen, Germany, 2006.

40 Amanullah, M. and Mazzotti, M., Optimization of a hybrid chromatography-crystallization process for the separation of Tröger's base enantiomers. *J. Chromatogr. A*, 1107(2006), 36–45.

41 Kaemmerer, H., Horvath, Z., Lee, J.W., Kaspereit, M., Arnell, R., Hedberg, M., Herschend, B., Jones, M.J., Larson, K., Lorenz, H., and Seidel-Morgensten, A., Separation of racemic bicalutamide by an optimized combination of continuous chromatography and selective crystallization. *Org. Process Res. Dev.*, 16(2012), 331–342.

42 Swernath, S., Kaspereit, M., and Kienle, A., Dynamics and control of coupled continuous chromatography and crystallization processes for the production of pure enantiomers. *Chem. Eng. Technol.*, 36(2013) 1417–1429.

43 Bechtold, M., Makart, S., Heinemann, M., and Panke, S., Integrated operation of continuous chromatography and biotransformations for the generic high yield production of fine chemicals. *J. Biotechnol.*, 124(2006), 146–162.

44 Wagner, N., Fuereder, M., Bosshart, A., Panke, S., and Bechtold, M., Practical aspects of integrated operation of biotransformation and SMB separation for fine chemical synthesis. *Org. Process Res. Dev.*, 16(2012), 323–330.

45 Nimmig, S. and Kaspereit, M., Continuous production of single enantiomers at high yields by coupling single column chromatography, racemization, and nanofiltration. *Chem. Eng. Process.*, 67(2013), 89–98.

46 Swernath, S., Kaspereit, M., and Kienle, A., Dynamics and control of coupled continuous chromatography and racemization processes for the production of pure enantiomers. *Chem. Eng. Technol.*, 37(2014) 643–651.

47 Hashimoto, K., Adachi, S., Noujima, H., and Ueda, Y., A new process combining adsorption and enzyme reaction for producing higher-fructose syrup. *Biotechnol. Bioeng.*, 25(1983), 2371–2393.

48 Kaspereit, M., García Palacios, J., Meixús Fernández, T., and Kienle, A., Systematic design of production processes for enantiomers with integration of chromatography and racemisation reactions. *Comput. Aided Chem. Eng.*, 25(2008), 97–102.

49 García Palacios, J., Kaspereit, M., and Kienle, A., Integrated simulated moving bed processes for production of single enantiomers. *Chem. Eng. Technol.*, 34(2011), 688–698.

50 García Palacios, J., Kramer, B., Kienle, A., and Kaspereit, M., Experimental validation of a new integrated simulated moving bed process for the production of single enantiomers. *J. Chromatogr. A*, 1218(2011), 2232–2239.

51 Hellstén, S., Siitonen, J., Mänttäri, M., and Sainio, T., Steady state recycling chromatography with an integrated solvent removal unit – Separation of glucose and galactose. *J. Chromatogr. A*, 1251(2012), 122–133.

52 Abdelmoumen, S., Muhr, L., Bailly, M., and Ludemann-Hombourger, O., The M3C process: a new multicolumn chromatographic process integrating a concentration step. I—the equilibrium model. *Sep. Sci. Technol.*, 41(2006), 2639–2663.

53 Paredes, G., Rhee, H.-K., and Mazzotti, M., Design of simulated-moving-bed chromatography with enriched extract operation (EE-SMB): Langmuir isotherms. *Ind. Eng. Chem. Res.*, 45(2006), 6289–6301.

54 Perrin, S.R., Hauck, W., Ndzie, E., Blehaut, J., Ludemann-Hombouger, O., Nicoud, R.-M., and Pirkle, W.H., Purification of difluoromethylornithine by global process optimization: coupling of chemistry and chromatography with enantioselective crystallization. *Org. Process Res. Dev.*, 11(2007), 817–824.

55 von Langermann, J., Kaspereit, M., Shakeri, M., Lorenz, H., Hedberg, M., Jones, M.J., Larson, K., Herschend, B., Arnell, R., Temmel, E., Bäckvall, J.-E., Kienle, A., and Seidel-Morgenstern, A., Design of an integrated process of chromatography, crystallization and racemization for the resolution of 2',6'-pipecoloxylidide (PPX). *Org. Process Res. Dev.*, 16(2012), 343−352.

56 Rhee, H.-K., Aris, R., and Amundson, N.R., *First-Order Partial Differential Equations. Theory and Application of Single Equations, Volume I*. Dover Publications, New York, USA, 2001.

57 Rhee, H.-K., Aris, R., and Amundson, N.R., *First-Order Partial Differential Equations. Theory and Application of Hyperbolic Systems of Quasilinear Equations, Volume II*. Dover Publications, New York, USA, 2001.

58 Golshan-Shirazi, S. and Guiochon, G., Analytical solution for the ideal model of chromatography in the case of a pulse of a binary mixture with competitive Langmuir isotherm. *J. Phys. Chem.*, 93(1989), 4143–4157.

59 Mazzotti, M., Local equilibrium theory for the binary chromatography of species subject to a generalized Langmuir isotherm. *Ind. Eng. Chem. Res.*, 45(2006), 5332–5350.

60 Rajendran, A. and Mazzotti, M., Local equilibrium theory for the binary chromatography of species subject to a generalized Langmuir isotherm. 2. Wave interactions and chromatographic cycle. *Ind. Eng. Chem. Res.*, 50(2011), 352–377.

61 Storti, G., Mazzotti, M., Morbidelli, M., and Carrà, S., Robust design of binary countercurrent adsorption separation processes. *AIChE J.*, 39(1993), 471–492.

62 Mazzotti, M., Storti, G., and Morbidelli, M., Robust design of countercurrent adsorption separation processes: 2. Multicomponent systems. *AIChe J.*, 40(1994), 1825–1842.

63 Mazzotti, M., Storti, G., and Morbidelli, M., Robust design of countercurrent adsorption separation: 3. Nonstoichiometric systems. AIChe J., 42(1996), 2784–2796.

64 Mazzotti, M., Storti, G., and Morbidelli, M., Optimal operation of simulated moving bed units for nonlinear chromatographic separations. *J. Chromatogr. A*, 769(1997), 3–24.

65 Mazzotti, M., Storti, G., and Morbidelli, M., Robust design of countercurrent adsorption separation processes: 4. Desorbent in the feed. *AIChe J.*, 43(1997), 64–72.

66 Gentilini, A., Migliorini, C., Mazzotti, M., and Morbidelli, M., Optimal operation of simulated moving-bed units for non-linear chromatographic separations II. Bi-Langmuir isotherm. *J. Chromatogr. A*, 805(1998), 37–44.

67 Migliorini, C., Mazzotti, M., and Morbidelli, M., Robust design of countercurrent adsorption separation processes: 5. Nonconstant selectivity. *AIChe J.*, 46(2000), 1384–1399.

68 Mazzotti, M., Design of simulated moving bed separations: generalized Langmuir isotherm. *Ind. Eng. Chem. Res.*, 45(2006), 6311–6324.

69 Mazzotti, M., Equilibrium theory based design of simulated moving bed processes for a generalized Langmuir isotherm. *J. Chromatogr. A*, 1126(2006), 311–322.

70 Kaspereit, M., Seidel-Morgenstern, A., and Kienle, A., Design of simulated moving bed processes under reduced purity requirements. *J. Chromatogr. A*, 1162(2007), 2–13.

71 Rajendran, A., Equilibrium theory-based design of simulated moving bed processes under reduced purity requirements Linear isotherms. *J. Chromatogr. A*, 1185(2008), 216–222.

72 Mazzotti, M., Storti, G., and Morbidelli, M., Supercritical fluid simulated moving bed chromatography. *J. Chromatogr. A*, 786(1997), 309–320.

73 Abel, S., Mazzotti, M., and Morbidelli, M., Solvent gradient operation of simulated moving beds I. Linear isotherms. *J. Chromatogr. A*, 944(2002), 23–39.

74 Abel, S., Mazzotti, M., and Morbidelli, M., Solvent gradient operation of simulated moving beds 2. Langmuir isotherms. *J. Chromatogr. A*, 1026(2004), 47–55.

75 Paredes, G., Abel, S., Mazzotti, M., Morbidelli, M., and Standler, J., Analysis of a simulated moving bed operation for three-fraction separations (3F-SMB). *Ind. Eng. Chem. Res.*, 43(2004), 6157–6167.

76 Katsuo, S. and Mazzotti, M., Intermittent simulated moving bed chromatography: 1. Design criteria and cyclic steady-state. *J. Chromatogr. A*, 1217(2010) 1354–1361.

77 Silva, R.J.S., Rodrigues, R.C.R, and Mota, J.P.B, Relay simulated moving bed chromatography: Concept and design criteria. *J. Chromatogr. A*, 1260(2012) 132–142.

78 Golshan-Shirazi, S. and Guiochon, G., Theory of optimization of the experimental conditions of preparative elution using the ideal model of liquid chromatography. *Anal. Chem.*, 61(1989), 1276–1287.

79 Knox, J.H. and Pyper, H.M., Framework for maximizing throughput in preparative liquid chromatography. *J. Chromatogr.*, 363(1986), 1–30.

80 Golshan-Shirazi, S. and Guiochon, G., Theory of optimization of the experimental conditions of preparative elution chromatography: optimization of the column efficiency. *Anal. Chem.*, 61(1989), 1368–1382.

81 Sainio, T. and Kaspereit, M., Analysis of steady state recycling chromatography using equilibrium theory. *Sep. Purif. Technol.*, 66(2009), 9–18.

82 Kaspereit, M. and Sainio, T., Simplified design of steady-state recycling chromatography under ideal and nonideal conditions. *Chem. Eng. Sci.*, 66(2011), 5428–5438.

83 Giddings, J.C., Theoretical basis for a continuous, large-capacity gas chromatographic apparatus. *Anal. Chem.*, 34(1962), 37–39.

84 Wankat, P.C., The relationship between one-dimensional and two-dimensional separation processes. *AlChE J.*, 23(1977), 859–867.

85 Goto, M. and Goto, S., Continuous separation using an annular chromatograph with rotating inlet and outlet. *J. Chem. Eng. Jpn.*, 20(1987), 598–603.

86 Thiele, A., Falk, T., Tobiska, L., and Seidel-Morgenstern, A., Prediction of elution profiles in annular chromatography. *Comput. Chem. Eng.*, 25(2001), 1089–1101.

87 Siitonen, J., Sainio, T., Rajendran, A., Bypass chromatography – design and analysis of an improved strategy for operating batch chromatography processes. *J. Chromatogr.* A, 1230(2012), 77–92.

88 Beyer, W.H. (Ed.), *CRC Standard Mathematical Tables*. CRC Press, Boca Raton, Florida, USA, 2000.

89 Burington, R.S., *Handbook of Mathematical Tables and Formulas*. 5th ed., McGraw-Hill, New York, USA, 1973.

90 Neumark, S., *Solution of Cubic and Quartic Equations*. Pergamon Press, Oxford, UK, 1965.

91 Jupke, A., Epping, A., and Schmidt-Traub, H., Optimal design of batch and simulated moving bed chromatographic separation processes. J. Chromatogr. A, 944(2002), 93–117.

92 Migliorini, C., Gentilini, A., Mazzotti, M., and Morbidelli, M., Design of simulated moving bed units under nonideal conditions. *Ind. Eng. Chem. Res.*, 38(1999), 2400–2410.

93 Kaspereit, M., Jandera, P., Škavrada, M., and Seidel-Morgenstern, A., Impact of adsorption isotherm parameters on the performance of enantioseparation using simulated moving bed chromatography. *J. Chromatogr. A*, 944(2002), 249–262.

94 Jandera, P., Škavrada, M., Klemmová, K., Bačkovská, V., and Guiochon, G., Effect of the mobile phase on the retention behaviour of optical isomers of carboxylic acids and amino acids in liquid chromatography on bonded Teicoplanin columns. *J. Chromatogr. A*, 917(2001), 123–133.

Article I

Separation and Purification Technology 78 (2011) 21–32

Contents lists available at ScienceDirect

Separation and Purification Technology

journal homepage: www.elsevier.com/locate/seppur

Theoretical analysis of steady state recycling chromatography with solvent removal

Jani Siitonen [a], Tuomo Sainio [a,*], Malte Kaspereit [b]

[a] Lappeenranta University of Technology, Skinnarilankatu 34, FI-53850 Lappeenranta, Finland
[b] Max Planck Institute for Dynamics of Complex Technical Systems, Sandtorstrasse 1, D-39106 Magdeburg, Germany

ARTICLE INFO

Article history:
Received 17 June 2010
Received in revised form 11 January 2011
Accepted 12 January 2011

Keywords:
Chromatography
Recycling
Solvent removal
Equilibrium theory
Process design

ABSTRACT

The possibility to enhance the process performance of steady state recycling (SSR) chromatography by removing solvent was investigated in the framework of the equilibrium theory. A method was developed to choose *a priori* the relevant cut times corresponding to arbitrary purity constraints and to predict the steady state of the process without performing dynamic simulations. The amount of fresh feed introduced per cycle and the injection width were identified as the only free operating parameters. A relationship was derived between the amount of fresh feed and the solvent removal capacity required to achieve the chosen purities.

The performance of three different process configurations was analyzed: solvent removal applied to (I) the fresh feed, (II) the recycle fraction, and (III) their mixture. It was found that solvent removal facilitates treating more fresh feed per cycle than is possible in a conventional SSR process. In addition, it was shown that the three SSR-SR configurations have identical performance with the same operating parameters. In contrast, the configurations differ with respect to the maximum amount of fresh feed that can be processed per cycle, as well as to the range of feasible injection widths.

It was shown that SSR with solvent removal can yield higher productivity and lower eluent consumption than an optimized batch chromatography process that employs solvent removal.

1. Introduction

Preparative chromatography is a highly developed technique in the pharmaceutical and fine chemical industries and is used for the separation and purification of a wide range of substances. Single-column batch chromatography and multi-column simulated moving bed (SMB) chromatography are the most common process schemes. The batch mode usually suffers from high eluent consumption and low productivity but is versatile, provides multiple product fractions, and allows rapid method development. As to the SMB, high productivity and low eluent consumption are counterbalanced by high investment costs and a high degree of complexity. For these reasons, there is room for simple, compact, yet efficient chromatographic processes.

The idea of enhancing the separation by recycling the chromatogram partially or as a whole is not new, but has recently received considerable attention. Many recycling methods have been suggested, such as closed loop recycling [1–3], peak shaving [2], and steady state recycling (SSR) chromatography [4–15]. In an SSR process, the pure leading and trailing sections of the chromatogram are collected, while the unresolved remainder is recycled back to the inlet of the column. In addition, a constant amount of fresh feed is added to the recycled fraction, which eventually causes the process to attain a periodic steady state. The process can be operated in different modes depending on the injection method. In the closed-loop mode (CL-SSR) [4–9], the recycle fraction and the fresh feed are introduced separately in order to preserve the already achieved partial separation. In the mixed-recycle mode (MR-SSR) [10–15], the recycle fraction is mixed with fresh feed before injection.

The optimal design of SSR chromatography is challenging due the dynamic character of the process. The limiting case of complete separation under ideal conditions was studied by Bailly and Tondeur [10–12] and Charton [13] for binary Langmuir systems by using the equilibrium theory. Sainio and Kaspereit [15] extended this approach to the case of arbitrary purity requirements, and provided a detailed analysis of MR-SSR. In addition, Sainio and Kaspereit developed a method for the *a priori* calculation of fractionation times that guarantee the fulfillment of arbitrary purity or yield constraints at the steady state. The method requires the isotherm parameters only and does not employ dynamic simulations.

In an SSR process, the recycle fraction is typically more dilute than the fresh feed. It seems plausible that process perfor-

* Corresponding author. Tel.: +358 40 3578683.
E-mail address: tuomo.sainio@lut.fi (T. Sainio).

1383-5866/$ – see front matter © 2011 Elsevier B.V. All rights reserved.
doi:10.1016/j.seppur.2011.01.013

mance could be enhanced by concentrating the recycle fraction by removing some of the solvent. In the case of multi-column chromatography systems, this kind of solvent removal from the internal process stream has been used successfully. In SMB operation, a portion of the extract stream can be concentrated and re-injected at the same point of the unit [16]. Under certain circumstances, a high concentration of the more retained compound intensifies the displacement effect on the less retained compound and improves the process performance. This technique is called M3C [17] or enriched extract SMB (EE-SMB) [16,18]. However, solvent removal from the recycle fraction in SSR has not been theoretically investigated before, and no analysis or design principles of such a process concept have been presented.

The objective of the present work is to investigate the possibility to enhance the mixed-recycle SSR performance by introducing a solvent removal unit into the chromatographic separation process. The process concept will henceforth be abbreviated as SSR-SR. Solvent removal could be applied to (I) the fresh feed, (II) the recycle fraction, or (III) the actual feed solution (which is obtained by mixing the fresh feed and the recycle fraction). A theoretical framework will be provided for the analysis of the characteristic features of these process configurations and for the optimal design of SSR-SR chromatography. The approach will be based on the so-called equilibrium theory, where mass-transfer resistance and axial dispersion are neglected, and will be limited to binary systems that follow the competitive Langmuir adsorption isotherm model. This means that the proposed theory will be most applicable for systems of high efficiency. It should be also noted that, in practice, the extent of solvent removal would be limited by for example the solubility of the components or the viscosity of the solution. Here we focus on developing the theoretical background of steady state recycling chromatography with solvent removal, and such limitations are beyond the scope of this work.

A short summary of the analysis and design of the conventional MR-SSR process developed by Sainio and Kaspereit [15] will be presented. After that, the theoretical framework concerning the SSR-SR process will be developed, and a method to predict the steady state of the SSR-SR process will be provided. The method allows choosing the operating parameters such that, in the steady state, arbitrary purity and yield constraints will be satisfied. It will be shown that different SSR-SR process configurations will lead to exactly the same steady state and thus have identical performance when the operation parameters (*i.e.* the injection volume and the volume of fresh feed processed during each cycle) as well as purity constraints are same. However, the range of feasible injection volumes and the maximum amount of fresh feed that can be processed per cycle are not identical. Finally, the method will be used to investigate the performance of different SSR-SR process configurations.

2. Theory of SSR chromatography

The analysis and design of SSR with solvent removal requires understanding of the corresponding principles of a conventional SSR process. For this reason, the basic theory and the design method for the mixed-recycle SSR chromatography developed by Sainio and Kaspereit [15] are briefly described in the following sections (Sections 2.1–2.3).

The design method, based on the equilibrium theory, allows for the direct prediction of the steady state for systems with competitive Langmuir adsorption isotherms. The steady state can be obtained on the basis of adsorption isotherm parameters only without performing dynamic simulations. The operating parameters (in this case, the cut times t_{A1}, t_{A2}, t_{B1} and t_{B2} shown in Fig. 1 and the injection volume V_{inj}) can be chosen such that, in the steady state, arbitrary purity and yield constraints are satisfied. With respect to Fig. 1b, the purities are defined as follows:

$$p^A = \frac{m_1^A}{m_1^A + m_2^A} = \frac{\int_{t_{A1}}^{t_{A2}} c_1\, dt}{\int_{t_{A1}}^{t_{A2}} (c_1 + c_2)\, dt} \tag{1}$$

$$p^B = \frac{m_2^B}{m_1^B + m_2^B} = \frac{\int_{t_{B1}}^{t_{B2}} c_2\, dt}{\int_{t_{B1}}^{t_{B2}} (c_1 + c_2)\, dt} \tag{2}$$

where m_i^j denotes the mass of component $i = (1, 2)$ in the product fraction $j = (A, B)$. It is assumed that component 1 is the less adsorbed one and is the target compound in product fraction A.

As an alternative to the specifications of the desired purities, the yields of the components can be given. However, since the SSR (and SSR-SR) process represents a binary separation without a waste stream, the purity and yield constraints are interchangeable [19]:

$$Y_1 = \frac{m_1^A}{m_1^{FF}} = \frac{p^A}{p^{FF}} \frac{p^{FF} + p^B - 1}{p^A + p^B - 1} \tag{3}$$

$$Y_2 = \frac{m_2^B}{m_2^{FF}} = \frac{p^B}{1 - p^{FF}} \frac{p^A - p^{FF}}{p^A + p^B - 1} \tag{4}$$

where p^{FF} is defined as the purity of component 1 in fresh feed: $p^{FF} = c_1^{FF}/(c_1^{FF} + c_2^{FF})$. In other words, by specifying any two of the four quantities, the remaining two are also determined.

2.1. Equilibrium theory for binary Langmuir adsorption isotherm system

In the ideal model, column efficiency is assumed to be infinite. The material balance, which can be written in matrix form as follows in Eqs. (5) and (6), governs the propagation of the concentration states in the column.

$$\mathbf{A}\frac{\partial \mathbf{c}}{\partial t} + u\frac{\partial \mathbf{c}}{\partial x} = 0, \tag{5}$$

where

$$\mathbf{A} = \begin{bmatrix} 1 + F(\partial q_1/\partial c_1) & F(\partial q_1/\partial c_2) \\ F(\partial q_2/\partial c_1) & 1 + F(\partial q_2/\partial c_2) \end{bmatrix}, \qquad \mathbf{c} = \begin{bmatrix} c_1 \\ c_2 \end{bmatrix} \tag{6}$$

and q is the stationary phase concentration, F is the phase ratio, x is the space coordinate, t is time, and u is the interstitial velocity. According to the competitive Langmuir adsorption isotherm, the stationary phase concentration is given by

$$q_i = \frac{q_{m,i} b_i c_i}{1 + b_1 c_1 + b_2 c_2} \quad (\text{for} \quad i = 1, 2) \tag{7}$$

where $q_{m,i}$ is the saturation capacity of the adsorbent for species i, and b_i is its Langmuir parameter.

Because of the competitive behavior of the phase equilibrium, the model forms a coupled system of two partial differential equations which has no analytical solution when the space coordinate x and time t are the independent variables. However, using the concentrations c_1 and c_2 as the independent variables, Eq. (5) can be solved analytically with the method of characteristics. This is the basis of the so-called equilibrium theory, which is described extensively in the literature [20,21]. Here, only its most relevant aspects will be explained.

When a rectangular pulse of a mixture of two components is injected at the inlet of a clean column, two simple wave transitions and two shock transitions are composed. The solution of Eq. (5) consists of describing the movement of these waves and their interactions along the column. The solution at the column outlet can be constructed in the so-called hodograph plane. An example of hodograph representation and corresponding chromatograms

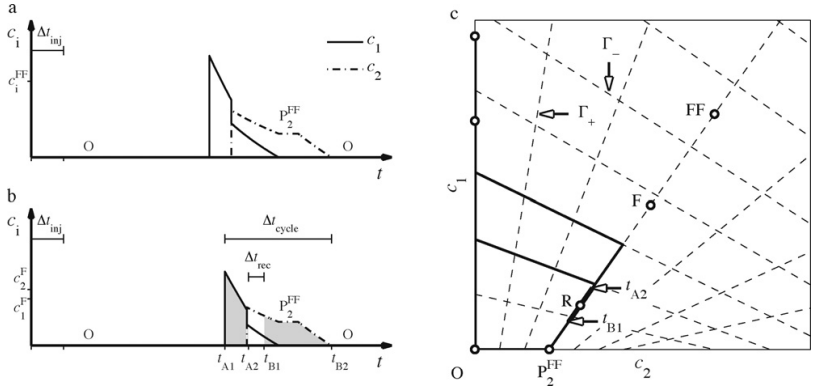

Fig. 1. Steady state recycling chromatography in the mixed-recycle mode. (a) Chromatogram for the first injection (injection of fresh feed with concentrations c_i^{FF}). (b) Chromatogram at the steady state (injection with concentrations c_i^F). (c) Corresponding hodograph representations.

are given in Fig. 1. In the case of Langmuir isotherms, simple waves correspond on the hodograph plane to segments on straight lines, which are called characteristics. The characteristics with a positive slope dc_1/dc_2 are referred to as Γ_+ characteristics and those with a negative slope as Γ_- characteristics. The slopes can be calculated explicitly from the right eigenvectors of the coefficient matrix **A** in Eq. (6), and therefore depend on the isotherm parameters only. The propagation velocities of simple waves can be obtained from the eigenvalues of **A**.

For Langmuir isotherms, the images of shock transitions (called Σ_+ and Σ_- shocks) also fall into the characteristics. The propagation velocities of shock waves are given by the mass balance across the discontinuity. In addition, if the injection is wide enough, the chromatographic profile includes concentration plateaus between simple and shock waves. On these plateaus, c_1 and c_2 are constant. Consequently, these regions are represented on the hodograph plane by single points.

2.2. Determination of cut times and steady state feed composition

In the conventional SSR process, the steady state feed composition F in the hodograph plot is always located in the Γ_+ characteristic that passes through the fresh feed composition FF [15]. In addition, as long as the SSR process is operated such that the purity constraints are fulfilled, the rear of the elution profile remains unaltered even if the feed plateau or the first component plateau erodes during elution. For this reason, we can first determine the cut times t_{B1} and t_{B2}. Obviously, the cut time t_{B2} should be chosen such that it matches the time of the complete elution of the injection. For the Langmuir system, t_{B2} is given by the following equation:

$$t_{B2} = \Delta t_{inj} + t_0(1 + F\, q_{m,2} b_2) \tag{8}$$

The injection time Δt_{inj} refers to the width of the pulse that is fed into the column after mixing the recycle fraction and the fresh feed, and t_0 is the elution time of a non-retained component.

Next, the cut time t_{B1} is chosen so that the purity constraints of product fraction B are fulfilled. An explicit expression for t_{B1} can be obtained, but it is rather complex. A more convenient option is to exploit the numerical technique and use some type of search algorithm to find the lower integration limit that satisfies Eq. (2). The required analytical expressions for $c_i(t)$ given by Guiochon et al. [20] are presented in Appendix A.

Once t_{B1} and t_{B2} are obtained, the volume of fresh feed that can be processed per cycle V^{FF} and the cut time t_{A2} can be solved with given purity constraints as follows [15]:

$$V^{FF} = \frac{\int_{t_{B1}}^{t_{B2}} c_2\, dt}{c_2^{FF} Y_2}\dot{V} = \frac{p^A + p^B - 1}{(c_1^{FF} + c_2^{FF})(p^A - p^{FF})p^B}\int_{t_{B1}}^{t_{B2}} c_2\, dt\dot{V} \tag{9}$$

$$t_{A2} = t_{B1} - \Delta t_{inj} + \frac{V^{FF}}{\dot{V}} \tag{10}$$

where $\dot{V}$ is the volume flow rate. Consequently, the steady state feed composition can be solved from the mass balance around the feed node

$$c_i^F = \frac{\int_{t_{A2}}^{t_{B1}} c_i dt + (c_i^{FF} V^{FF}/\dot{V})}{\Delta t_{inj}} \quad (\text{for} \quad i = 1, 2) \tag{11}$$

As the last step, the remaining cut time t_{A1} should be equal to the elution time of the pure component 1 shock that corresponds to the steady state feed concentration. In the case of a large injection width, the plateau P_1^F in the front of the elution profile is not eroded during elution, and the analytical solution for the cut time t_{A1} is given by:

$$t_{A1} = t_0\left(1 + F\frac{q_1\left(c_1^{PF}, 0\right)}{c_1^{PF}}\right) \tag{12}$$

where the height of the plateau P_1^F is obtained from the intersection of the c_1 axis and the Γ_- characteristic passing though the steady state feed on the hodograph plane. In contrast, for sufficiently small injections, the pure component 1 plateau erodes completely, and a numerical approach to solve t_{A1} is needed. Several methods have been presented in the literature for solving this problem, for example by Guiochon et al. [20] and by Rhee et al. [21].

2.3. Performance of mixed-recycle SSR chromatography

In addition to developing the design method, Sainio and Kaspereit [15] have analyzed the performance of mixed-recycle SSR chromatography. The results can be summarized as follows:

1. The amount of fresh feed introduced to the process per cycle is independent of the total injection width (obtained by mixing the fresh feed and the recycle fraction).

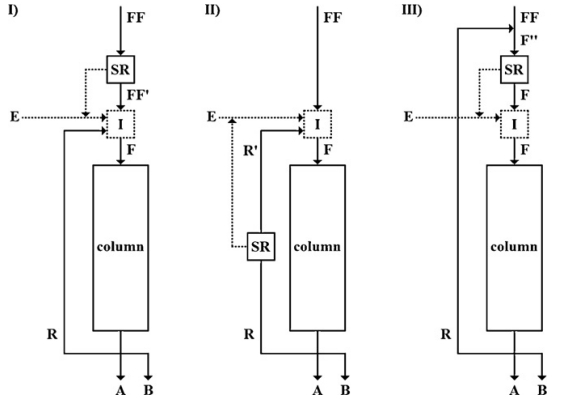

Fig. 2. Schematic representations of alternative SSR-SR configurations. (I) Solvent removal from fresh feed. (II) Solvent removal from recycle fraction. (III) Solvent removal from mixed fraction. *FF*, fresh feed; *FF′*, concentrated fresh feed; *R*, recycle fraction, *R′*, concentrated recycle fraction; *F″*, mixed fraction; *F*, column feed; *E*, eluent; *SR*, solvent removal unit; *I*, injection port; *A*, product fraction *A* (weaker adsorbing component 1); *B*, product fraction *B* (strong adsorbing component 2).

2. The cycle time always increases as the injection width increases.
3. The productivity of SSR decreases with the increasing injection width and is always lower than that of a batch process which is optimized so that no gap exists between successive chromatographic cycles.
4. The eluent consumption decreases with an increasing injection width for small injections, but is independent of the injection width for large injections. In terms of eluent consumption, SSR chromatography always outperforms batch chromatography.
5. The concentration of product fraction *A* increases with the injection width for small injections, but is independent of the injection width for large injections. With respect to the concentration of the product fraction *A*, an SSR process always outperforms an optimized batch process.
6. The concentration of the product fraction *B* is independent of the injection width and always the same as in batch chromatography.

As will be seen later, these findings can also be exploited to some extent in investigating the characteristic features of SSR-SR chromatography.

3. Theory of SSR chromatography with solvent removal

As mentioned in Section 1, there are basically three alternative configurations for applying solvent removal in a steady state recycling chromatography process. These are illustrated in Fig. 2. Either the fresh feed (option I) or the recycle fraction (option II) can be concentrated before they are mixed together and introduced to the column. Alternatively, solvent can be removed from their mixture (option III). The removed solvent can be used as eluent and thus reduce the consumption of fresh eluent.

Similarly to a conventional MR-SSR chromatography process (Fig. 1), the steady state operation of these three process options is conveniently presented in the hodograph plane as shown in Fig. 3. The relative composition of a solution is not changed in an ideal solvent removal unit. Therefore, the *operating line of the solvent removal unit* is a straight line on the hodograph plane, and solvent removal corresponds to moving upwards on it. As seen in Fig. 3, the operating line passes through the origin and has a slope equal to c_1/c_2 of the solution treated.

In process option I (Fig. 3I), solvent removal is applied to the fresh feed *FF*. The operating line thus passes through the origin and *FF*, and the resulting composition maps onto point *FF′*. On every cycle, a recycle fraction is collected between cut times t_{A2} and t_{B1}. The volume-average composition of the recycle fraction is presented on the hodograph plane as *R*. When the recycle fraction *R* is mixed with the concentrated fresh feed *FF′*, the actual feed composition *F* is obtained. When the SSR process operates at the steady state, the feed point *F*, and thus also the recycle point *R*, must be located on the Γ_+ characteristic that passes through the concentrated fresh feed *FF′*. It will be shown below that the steady state of the process is uniquely determined by specifying (in addition to the purity/yield constraints) the injection volume and one of the following: (1) the amount of fresh feed introduced per cycle, (2) the amount of solvent removed per cycle, or (3) the relative volumes of fresh feed and removed solvent.

In process option II (Fig. 3II), solvent removal is applied to the recycle fraction *R* instead of the fresh feed *F*. In that case, the operating line of the solvent removal unit passes through the origin and the recycle fraction *R*. The resulting composition maps onto point *R′*. Mixing the concentrated recycle fraction *R′* and the fresh feed *FF* together, the actual feed composition *F* is obtained. According to the lever rule, *F* must be located on the line segment between *FF* and *R′*. At steady state, the feed point *F* does not move on the hodograph plane from cycle to cycle, and is located on the same Γ_+ characteristic as the steady state recycle fraction composition *R*. It will be shown below that the performance of option II is identical to option I within certain limits.

In process option III (Fig. 3III), the fresh feed *FF* and the recycle fraction *R* are mixed before solvent removal. The mixture, referred to as *F″*, is located on the line segment between *FF* and *R*. Since solvent is removed from the mixture, the operating line passes through the origin and *F″*. The resulting feed composition maps onto point *F*. Similarly to configurations I and II, the steady state feed composition *F* and the steady state recycle fraction *R* are located on the same Γ_+ characteristic. It will be shown below that option III is the most versatile with respect to the amount of fresh feed that can be processed or the amount of solvent that can be removed per cycle.

The aim of solvent removal is to enhance process performance through increasing the volume of fresh feed that can be fed to the column in each cycle. The question arises, which of these SSR-SR process concepts yields the best process performance? In the following sections, we will investigate the operation of different options. At first, in sections 3.1 and 3.2, the dependency between the volume of fresh feed, the volume of removed solvent and the composition of the steady state feed are considered generally. In section 3.3, a method is presented for predicting the steady state of an SSR-SR process without performing dynamic simulations. At the same time, it will be shown that all SSR-SR options have equal performance when the injection width as well as the volume of fresh feed introduced to the column during each cycle are the same. Finally, in section 3.4, the operation limits of different configurations are compared.

3.1. Dependency between V^{FF} and steady state feed composition

In conventional SSR chromatography, the steady state feed composition and the fresh feed composition are located on the same Γ_+ characteristic on the hodograph plane [15]. Consequently, specifying the purity requirements determines the volume of fresh feed V^{FF} that can be processed per cycle. When solvent removal is applied, the steady state feed composition is no longer located on the same Γ_+ characteristic as the fresh feed (see Fig. 3). The following questions arise: (1) is the volume of fresh feed per cycle in this case fixed by specifying the purities, or is it an independent variable, and (2)

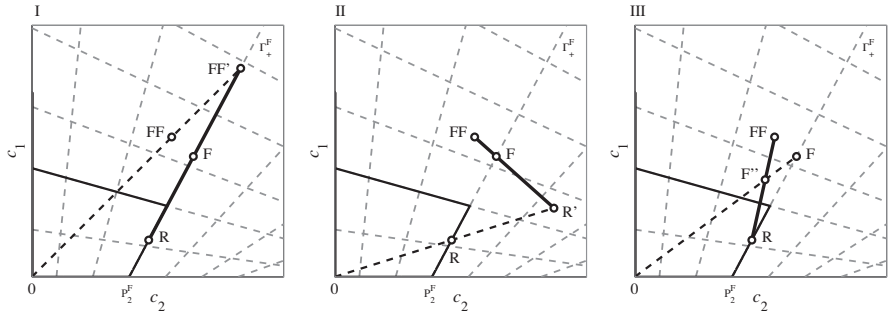

Fig. 3. Schematic representations of alternative SSR-SR configurations in the hodograph plane. (I) Solvent removal from fresh feed. (II) Solvent removal from recycle fraction. (III) Solvent removal from mixed fraction.

if V^{FF} is not fixed, how do it and the location of the steady state feed composition on the hodograph plane depend on each other?

As opposed to the conventional SSR process, the volume of fresh feed is *not* fixed when solvent is removed. This can be shown by considering the amounts of components 1 and 2 in the product fraction B. Evidently, the specification of the fresh feed composition, the volume of fresh feed per cycle and purity requirements fixes the masses m_1^B and m_2^B. On the other hand, those masses can be obtained by integrating the rear part of the steady state chromatogram from the cut time τ_{B1} to τ_{B2} [15]:

$$m_1^B = \frac{(1-p^B)(p^A-p^{FF})}{p^{FF}(p^A+p^B-1)} c_1^{FF} V^{FF} = \left(\int_{\tau_{B1}}^{\tau_{B2}} c_1 \, dt \right) \dot{V} \tag{13}$$

$$m_2^B = \frac{p^B(p^A-p^{FF})}{(1-p^{FF})(p^A+p^B-1)} c_2^{FF} V^{FF} = \left(\int_{\tau_{B1}}^{\tau_{B2}} c_2 \, dt \right) \dot{V} \tag{14}$$

Time here is presented relative to the end of the injection ($\tau = t - \Delta t_{inj}$) in order to emphasize that the obtained results are independent of the injection width. Explicit expressions for the integral terms are given in Appendix A. Their values depend on the integration limits (τ_{B1}, τ_{B2}) as well as on which Γ_+ characteristic the point F is located. Let us denote the characteristic in question by, its slope by Γ_+^F, and the intersection between the characteristic and the c_2 axis by c_2^{PF}. Physically, c_2^{PF} corresponds to the height of the pure component 2 plateau in the tail of the chromatogram. The relationship between ξ_+^F and c_2^{PF} is given by [20]:

$$\xi_+^F = \frac{\alpha - 1 - b_2 c_2^{PF}}{\alpha b_1 c_2^{PF}} \tag{15}$$

When the cut time τ_{B2} is set equal to the time of complete elution of component 2, its value is obtained directly from the adsorption isotherm parameters (see Eq. (8)). Hence, the composition of the product fraction B depends on the cut time τ_{B1} and the concentration c_2^{PF} only. These values can be solved from the pair of Eqs. (13) and (14), which has at most one solution (see Appendix B for uniqueness of solution). This means that for every V^{FF} there can be only one characteristic Γ_+^F on which the steady state feed composition can be located. Accordingly, since Γ_+^F is not fixed in the SSR-SR process, neither can V^{FF}. Moreover, if an SSR-SR process is designed by specifying the volume of fresh feed (in addition to purity requirements), the steady state feed composition F will always map onto a certain characteristic Γ_+^F irrespective of the injection width.

Let us next investigate how Γ_+^F changes with the amount of fresh feed. As seen in Eq. (B.9), the higher c_2^{PF} is, the shorter τ_{B1} has to be in order to fulfill the purity requirements. In addition, when τ_{B1} is constant, m_2^B increases with the increasing c_2^{PF} (Eq. (B.2)) and, when c_2^{PF} is constant, m_2^B increases with the decreasing τ_{B1} (Eq. (B.5)). This means that m_2^B, and thus the volume of fresh feed, must increase with the increasing c_2^{PF} with the given purity requirements

$$\left.\frac{\partial V^{FF}}{\partial c_2^{PF}}\right|_{p^B} > 0 \Leftrightarrow \left.\frac{\partial c_2^{PF}}{\partial V^{FF}}\right|_{p^B} > 0 \tag{16}$$

By applying the chain rule to Eqs. (B.9) and (16), it is observed that the cut time τ_{B1} decreases as V^{FF} increases:

$$\left.\frac{\partial \tau_{B1}}{\partial V^{FF}}\right|_{p^B} = \left.\frac{\partial \tau_{B1}}{\partial c_2^{PF}}\right|_{p^B} \left.\frac{\partial c_2^{PF}}{\partial V^{FF}}\right|_{p^B} < 0 \tag{17}$$

In practice, this means that the larger the amount of fresh feed that is introduced to the column during each cycle, the higher a c_2^{PF} and the shorter a τ_{B1} are needed to fulfill the purity requirements. We shall use this information in Section 3.4 to derive operation limits for the various SSR-SR configurations.

3.2. Dependency between V^{FF} and V^{SR}

Let us next analyze how the volume of fresh feed V^{FF} and the volume of removed solvent V^{SR} depend on each other. For all configurations shown in Fig. 3 (in other words, regardless of the position of the solvent removal unit), the following equation holds for the injection width:

$$V_{inj} = V^{FF} + V^R - V^{SR} \tag{18}$$

Because solvent removal does not affect the amounts of components 1 and 2 in the treated fraction (*i.e.* the fraction to which the solvent removal is applied), the two mass balances around the feed node are given by

$$V_{inj} c_1^F = V^{FF} c_1^{FF} + V^R c_1^R \tag{19a}$$

$$V_{inj} c_2^F = V^{FF} c_2^{FF} + V^R c_2^R \tag{19b}$$

In addition, since the steady state feed composition F and the steady state recycle fraction composition R are located on the same Γ_+ characteristic on the hodograph plane, we can write

$$c_1^F = \xi_+^F (c_2^F - c_2^{PF}) \tag{20a}$$

$$c_1^R = \xi_+^F (c_2^R - c_2^{PF}) \tag{20b}$$

and solve the injection volume by eliminating the steady state feed composition from Eqs. (19a), (19b) and (20a):

$$V_{inj} = \frac{\xi_+^F (V^{FF} c_2^{FF} + V^R c_2^R) - (V^{FF} c_1^{FF} + V^R c_1^R)}{\xi_+^F c_2^{PF}} \tag{21}$$

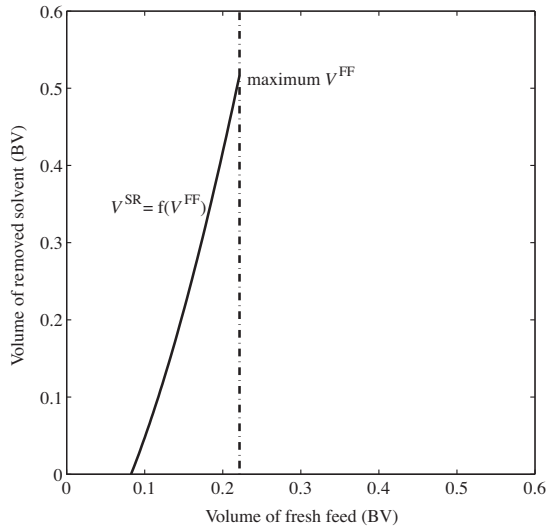

Fig. 4. Effect of fresh feed volume on the required solvent removal capacity as bed volumes in a mixed-recycle SSR-SR process. The calculation method used is described in Section 3.3. Parameters: $c_1^{FF} = c_2^{FF} = 10$ g/L; $F = 1/3$; $q_{m,1} = q_{m,2} = 100$ g/L; $b_1 = 0.02$ L/g; $b_2 = 0.025$ L/g. Purity constraints $p^A = p^B = 0.9$. The dash-dotted line shows the upper limit of V^{FF} that can be achieved (see Section 3.4).

The volume of solvent removed per cycle can now be solved by combining Eqs. (18), (20b) and (21):

$$V^{SR} = V^{FF}\left(1 + \frac{c_1^{FF}}{\xi_+^F c_2^{PF}} - \frac{c_2^{FF}}{c_2^{PF}}\right) \tag{22}$$

As seen in the equation, the volume of the solvent removed during each cycle is independent of the injection width. This means that specifying the volume of fresh feed uniquely fixes the amount of removed solvent.

In addition, it is interesting to note that V^{SR} increases with an increasing V^{FF}. This can be observed by substituting ξ_+^F from Eq. (15) into Eq. (22) and differentiating the resulting equation with respect to c_2^{PF}:

$$\frac{\partial(V^{SR}/V^{FF})}{\partial c_2^{PF}} = \frac{c_1^{FF}\alpha b_1 b_2}{(\alpha - 1 - b_2 c_2^{PF})^2} + \frac{c_2^{FF}}{(c_2^{PF})^2} > 0 \tag{23}$$

By applying the chain rule to Eqs. (16) and (23), we can note that the ratio V^{SR}/V^{FF} must increase with an increasing V^{FF}

$$\frac{\partial(V^{SR}/V^{FF})}{\partial V^{FF}} = \frac{\partial(V^{SR}/V^{FF})}{\partial c_2^{PF}} \frac{\partial c_2^{PF}}{\partial V^{FF}} > 0 \tag{24}$$

and, thus also V^{SR} must increase with an increasing V^{FF}

$$\frac{\partial V^{SR}}{\partial V^{FF}} > 0 \tag{25}$$

Eq. (25) means that the dependency between V^{FF} and V^{SR} is single-valued also the other way around: specifying V^{SR} uniquely fixes V^{FF} with which the desired purity requirements can be satisfied. Moreover, if the process is designed by specifying the ratio V^{FF}/V^{SR}, both parameters are fixed, as can be seen from Eq. (24).

An example of the dependency between the volume of fresh feed and the volume of removed solvent is shown in Fig. 4. As seen in the figure, the more fresh feed is introduced to the column per cycle, the more solvent must be removed. The trend is the same as predicted in Eq. (25). In addition, the curve is convex downward. This means that the solvent removal capacity that is required to operate an SSR-SR process increases faster than the amount of fresh feed that can be processed per cycle (see Eq. (24)).

Using the findings above, it can also be observed that the volume of the recycle fraction must increase linearly with an increasing injection width. Since both V^{FF} and V^{SR} are independent of V_{inj}, we can differentiate Eq. (18) with respect to the injection width and obtain

$$\left.\frac{\partial V^R}{\partial V_{inj}}\right|_{V^{FF}} = 1 \tag{26}$$

Finally, it should be emphasized that these results are also valid when $V^{SR} = 0$, which of course corresponds to the conventional MR-SSR process. By setting $V^{SR} = 0$ in Eq. (22), it is observed that the steady state feed composition must be located on the Γ_+ characteristic passing through the fresh feed composition. This is congruent with the findings by Sainio and Kaspereit [15].

3.3. Method for predicting the steady state of SSR-SR

The previous analysis of dependency between the volume of fresh feed, the volume of removed solvent and the steady state feed composition provides the basis for designing the SSR-SR process. Next, the method by Sainio and Kaspereit [15] to predict the steady state of the conventional SSR process without performing dynamic simulations will be extended to SSR chromatography with solvent removal. The goal is to find the cut times (t_{A1}, t_{A2}, t_{B1} and t_{B2}) such that, in the steady state, arbitrary purity constraints are satisfied.

The main difference between designing SSR processes with and without solvent removal is that there is one more independent variable in the latter case. In the conventional SSR process, the injection width is the only freely chosen operating parameter [15] when the fresh feed composition and the purity requirements are given. In the case of SSR-SR, however, one of the following can be chosen in addition to V_{inj}: (1) the volume of fresh feed per cycle V^{FF}, (2) the volume of solvent removed per cycle V^{SR}, or (3) the ratio V^{SR}/V^{FF} (see Section 3.2). As will be shown below, this choice affects the method for the prediction of the steady state.

Since the fresh feed and the steady state feed compositions are not located on the same Γ_+ characteristic on the hodograph plane, the first step in designing an SSR-SR process is to determine the Γ_+ characteristic passing through the steady state feed composition. The method for determining Γ_+^F depends on the parameter used as the design criterion. The simplest alternative is to select the ratio between V^{SR} and V^{FF} as a starting point. In that case, the slope ξ_+^F of Γ_+^F is obtained analytically from Eq. (22). The resulting equation is a second order polynomial with respect to ξ_+^F and has only one positive root. When V^{FF} or V^{SR} is used as a design parameter, determining Γ_+^F is somewhat more complicated. c_2^{PF} is solved form the pair of Eqs. (13) and (14) when V^{FF} is specified, and from the set of Eqs. (13), (14) and (22) when V^{SR} is specified. As seen in those equations, an analytic solution is no longer practical (even if possible). The most convenient way is to use a numerical technique for root finding.

When the desired Γ_+^F characteristic has been obtained, the rear part of the chromatogram is known and the cut times (t_{A1}, t_{A2}, t_{B1} and t_{B2}) as well as the steady state feed composition can be solved. The procedure is very similar to the conventional SSR process. At first, the cut time t_{B2} can be obtained from Eq. (8) and t_{B1} should be chosen such that the purity constraints of product fraction B are fulfilled. When calculating the cut time t_{A2}, the volume of the removed solvent V^{SR} has to be taken into account:

$$t_{A2} = t_{B1} - \Delta t_{inj} + \frac{V^{FF} - V^{SR}}{\dot{V}} \tag{27}$$

If V^{FF} or V^{SR} are not used as a design criterion, their values must be solved from Eqs. (9) and (22), respectively, before applying Eq.

(27). It is worth noting that, similarly to conventional MR-SSR, t_{A2} is independent of V_{inj} (since $\tau_{B1} = t_{B1} - \Delta t_{inj}$ is independent of V_{inj}).

The steady state feed composition can be solved from the mass balance around the feed node, Eq. (11). As in the case of conventional MR-SSR, it is independent of the injection width when t_{A2} is located on the injection plateau (*i.e.* for large injection volumes). This can be observed by rewriting Eq. (11) as

$$c_i^F = \frac{\int_{\tau_P}^{\tau_{B1}} c_i d\tau + c_i^{FF}(t_{A2} - \tau_{B1} + (V^{SR}/\dot{V}))}{t_{A2} - \tau_P} \quad (28)$$

where τ_P denotes the elution time of the end of the injection plateau relative to the end of the injection and thus depends on c_i^F and isotherm parameters only.

Finally, the remaining cut time t_A should be equal to the elution time of the pure component 1 shock for minimizing the cycle time. The solution is analogous to that outlined in Section 2.2 for the conventional SSR process.

It is important to note that the previous approach is independent of the process configuration (I–III) concerned. This means that all process options with the same injection width and fresh feed volume per cycle must lead to exactly the same steady state. Consequently, the process performance with the same operating parameters is also identical.

3.4. Feasible range of operation parameters for different SSR-SR configurations

The conclusion above concerning the identical performance of various SSR-SR configurations requires that the same operating parameters can be used for all options. However, this is not always possible. As will be shown shortly, the configurations differ with respect to the amounts of fresh feed that can be processed per cycle, as well as the range of feasible injection widths. Especially the limits for the maximum fresh feed volume and the minimum injection width are not identical. The minimum fresh feed volume, however, is the same for all configurations. In addition, there is no upper limit for the injection volume since the volume of the recycle fraction can be increased without any limits. The limits for different configurations are illustrated in Fig. 5 and can be derived as follows.

Let us first consider the lower limit for the fresh feed volume. As mentioned before, the volume of fresh feed always increases with an increasing volume of removed solvent. This means that the minimum V^{FF} for all three configurations is achieved when $V^{SR} = 0$. Obviously, this corresponds to the operation of the *conventional SSR process*. Since V^{FF} is independent of the injection volume for a certain V^{SR}, the limit is a straight vertical line in Fig. 5 (limit A). The corresponding V^{FF} can be obtained from Eq. (9).

3.4.1. Specific limits for configuration I

In configuration I (solvent removal from fresh feed), the minimum injection volume for a certain V^{FF} is achieved when $V^R = 0$ (limit B in Fig. 5). This can be observed by considering that V_{inj} always increases with an increasing V^R (see Eq. (26)). The condition corresponds to *batch chromatography with solvent removal*. The limit can be constructed in Fig. 5 by giving the ratio V^{SR}/V^{FF} goes upward from 0 (more exactly from 0 to 1, as will be shown shortly) and solving the corresponding V^{FF} and V^{SR} values with the design method described in Section 3.3. The desired V_{inj} values are then obtained from Eq. (18) by setting V^R to 0, which yields $V_{inj,I} = V_I^{FF} - V_I^{SR}$.

The upper limit for the fresh feed volume originates from the fact that V^{SR} can never be larger than the fraction to which the solvent removal is applied. In the case of configuration I, this means that the volume of solvent removed has to be less than the volume of fresh feed:

$$V_I^{SR} < V_I^{FF} \quad (29)$$

Hence, the maximum is achieved when $V_I^{SR} = V_I^{FF}$ (*i.e.* $V_I^{SR}/V_I^{FF} = 1$). On the hodograph plane, this corresponds to the situation where the *operating line of the solvent removal unit is parallel to* Γ_+^F. As for Fig. 5, the limit is a vertical line (limit C), the V^{FF} coordinate of which can be obtained by setting $V_I^{SR}/V_I^{FF} = 1$ to Eq. (22), solving the corresponding c_2^{PF}, and finally calculating V^{FF} from Eq. (9).

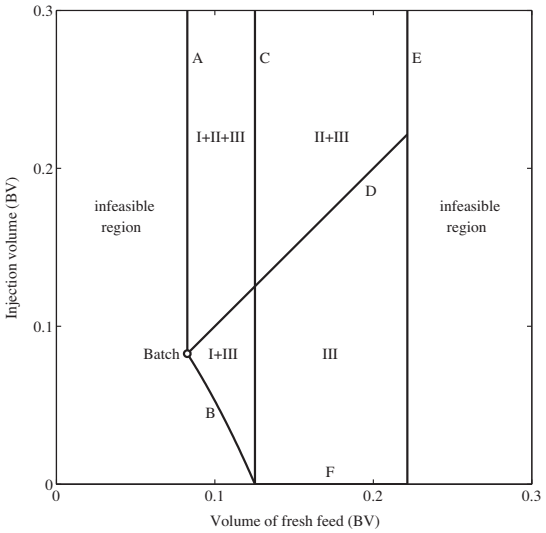

Fig. 5. Regions of feasible operating parameters for different SSR-SR configurations. Limit A: $V^{SR} = 0$ (conventional SSR chromatography), limit B: $V^R = 0$ (batch chromatography with solvent removal), limit C: $V^{SR} = V^{FF}$, limit D: $V^{SR} = V^R$, limit E: $t_{A2} = t_0$, limit F: $V_{inj} = 0$. Feed concentrations, isotherm parameters and purity constraints are the same as in Fig. 4.

3.4.2. Specific limits for configuration II

Let us next consider the case of solvent removal from the recycle fraction (option II in Fig. 3). The volume of removed solvent must be less than the volume of the recycle fraction:

$$V_{II}^{SR} < V_{II}^{R} \quad (30)$$

In addition, V^R increases linearly with an increasing V_{inj}, as mentioned before. This means that the lower limit for the injection width is achieved when $V_{II}^{SR} = V_{II}^{R}$. Obviously, this corresponds to $V_{inj} = V^{FF}$, and hence in Fig. 5 the limit is a straight line with slope 1 (limit D).

Since solvent removal does not constrain V_{II}^{FF} but V_{II}^{SR} (compare Eqs. (29) and (30)), the volume of fresh feed in option II can be larger than in option I. Of course, this requires that the injection volume is large enough. On the hodograph plane, this means that the steady state feed composition F can be located on a characteristic Γ_+, the slope of which is smaller than c_1^{FF}/c_2^{FF}. However, there is an upper limit for V^{FF} also in option II. This condition is obtained by considering that the cut time t_{A2} must be larger than the elution time of a non-retained component t_0

$$t_{A2} = \tau_{B1} + \frac{V^{FF} - V^{SR}}{\dot{V}} > t_0 \quad (31)$$

It can be shown that the left hand side of the inequality decreases monotonically with an increasing c_2^{PF} and approaches minus infinity when c_2^{PF} approaches its maximum value, the so-called watershed point. This means that there has to be a maximum

V^{FF}, which does not fulfill the condition above (limit E in Fig. 5). The value can be solved numerically by searching for a V^{FF} with which t_{A2} corresponds to t_0.

3.4.3. Specific limits for configuration III

In process option III (solvent removal from the mixed fraction before injection), the volume of the mixed fraction $V^{F'}$ must be larger than the volume of removed solvent V^{SR}

$$V_{\mathrm{III}}^{SR} < V_{\mathrm{III}}^{F'} = V_{\mathrm{III}}^{FF} + V_{\mathrm{III}}^{R} \tag{32}$$

In practice, this means that the injection volume must always be positive $V_{inj} > 0$ (limit F in Fig. 5). However, the volume of the recycle fraction cannot be negative in this case, either. For this reason, when $V^{SR}/V^{FF} < 1$ the lower limit of V_{inj} for configuration III is the same as for configuration I (limit B).

As to the upper limit of V^{FF}, configuration III is equal to configuration II (limit E). This means that configuration III is the most flexible one with respect to the injection width and the volume of fresh feed. As can been seen from Fig. 5, there exists no combination of operating parameters V_{inj} and V^{FF} that allows the operation of configuration I or II but not configuration III.

4. Performance evaluation of SSR-SR process

As usual in designing separation processes, it is important to find the operating parameters that lead to optimal process performance. In the present case, the most interesting performance parameters are (1) specific productivity, (2) specific eluent consumption, and (3) the average product concentrations. The productivity and the eluent consumption are here defined for component 1 (and analogously for component 2) as follows:

$$PR_1 = \frac{m_1^A}{\Delta t_{cycle}} = \frac{Y_1 c_1^{FF} V^{FF}}{\Delta t_{cycle}} \tag{33}$$

$$EC_1 = \frac{\dot{V}\Delta t_{cycle} - V_{inj} - V^{SR}}{Y_1 c_1^{FF} V^{FF}} \tag{34}$$

As seen in the latter equation, it is assumed that the removed solvent can be used as eluent in the process. Evidently, this reduces the need for fresh eluent. The average concentration of product fraction *A* is defined with respect to component 1 and the average concentration of product fraction *B* with respect to component 2:

$$\bar{c}_1^A = \frac{m_1^A}{(t_{A2} - t_{A1})\dot{V}} = \frac{1}{t_{A2} - t_{A1}} \int_{t_{A1}}^{t_{A2}} c_1 dt \tag{35}$$

$$\bar{c}_2^B = \frac{m_2^B}{(t_{B2} - t_{B1})\dot{V}} = \frac{1}{t_{B2} - t_{B1}} \int_{t_{B1}}^{t_{B2}} c_2 dt \tag{36}$$

To predict the optimum performance of different SSR-SR configurations, the system is assumed to operate in "stacked injections" mode. This means that injection times are chosen so that no gaps exist between fraction B and fraction A of the following cycle. Hence, the cycle time is

$$\Delta t_{cycle} = t_{B2} - t_{A1} = \Delta t_{inj} + \tau_{B2} - t_{A1} \tag{37}$$

Since τ_{B2} is always independent of the injection width, the effect of V^{FF} on the cycle time depends only on the behavior of t_{A1}. According to our understanding, the derivative $\partial t_{A1}/\partial \Delta t_{inj}$ is always non-negative but less than unity, which yields

$$0 < \left.\frac{\partial \Delta t_{cycle}}{\partial \Delta t_{inj}}\right|_{V^{FF}} = 1 - \left.\frac{\partial t_{A1}}{\partial \Delta t_{inj}}\right|_{V^{FF}} \leq 1 \tag{38}$$

The behavior is similar to the case of conventional SSR. The equality sign refers to large injections with witch the pure component 1 plateau is not eroded and the cut time t_{A2} is located on the injection plateau. This can be seen considering that in this case the steady state feed composition and thus also the cut time t_{A1} are independent of the injection width. On the other hand, when small injection volumes are applied, no closed form expression for derivative $\partial t_{A1}/\partial \Delta t_{inj}$ can be given. However, a parametric analysis using the approach by Guiochon et al. [20] for the calculation of t_{A1} and applying small and large separation factors, low and high purities as well as weakly and strongly non-linear adsorption isotherms implied that the inequality above is valid also when solvent removal is applied.

4.1. Effect of injection volume on performance parameters

When evaluating the performance of the SSR-SR process, the valuable findings concerning conventional SSR chromatography can be exploited (see Section 2.3). Obviously, the SSR-SR configuration I is equivalent to a conventional SSR chromatography process (no solvent removal) if the feed concentration of the latter is

$$c_{\mathrm{SSR}}^{FF} = \frac{V_{\mathrm{I}}^{FF}}{V_{\mathrm{I}}^{FF} - V_{\mathrm{I}}^{SR}} c_{\mathrm{SSR\text{-}SR}}^{FF} \tag{39}$$

In addition, in Section 3.3 it was shown that all three SSR-SR options have identical performance when the same operating parameters are used. This means that the results obtained by Sainio and Kaspereit [15] are valid for all SSR-SR configurations as far as they are operated in region which is feasible for configuration I (see Fig. 5). Consequently, for a certain solvent removal capacity (*i.e.* also for a certain V^{FF}) productivity always decreases with an increasing injection volume. Moreover, eluent consumption decreases and average concentrations in product fraction *A* increase with an increasing injection width until they level off as the injection volume becomes sufficiently large. The limit is achieved when t_{A2} is located on the injection plateau. Average concentrations in product fraction *B* are, in contrast, always independent of the injection width. Comparing the SSR-SR process with optimized batch chromatography with the same V^{SR} (*i.e.* $c_{batch}^{FF} = c_{\mathrm{SSR}}^{FF}$ from Eq. (39)), the recycling scheme is always better in terms of the specific eluent consumption and concentration of the first product fraction. As to the specific productivity, batch chromatography is better.

The results above concerning the operation area of configuration I can be easily extended also to other regions. By differentiating Eqs. (33)–(36) with respect to the injection volume and accepting the empirical inequality in Eq. (38), the following expressions are obtained:

$$\left.\frac{\partial PR_1}{\partial \Delta t_{inj}}\right|_{V^{FF}} = -\frac{Y_1 c_1^{FF} V^{FF}}{(\Delta t_{cycle})^2} \left.\frac{\partial \Delta t_{cycle}}{\partial \Delta t_{inj}}\right|_{V^{FF}} < 0, \tag{40}$$

$$\left.\frac{\partial EC_1}{\partial \Delta t_{inj}}\right|_{V^{FF}} = \frac{\dot{V}}{Y_1 c_1^{FF} V^{FF}} \left(\left.\frac{\partial t_{cycle}}{\partial \Delta t_{inj}}\right|_{V^{FF}} - 1 \right) \leq 0, \tag{41}$$

$$\left.\frac{\partial \bar{c}_1^A}{\partial \Delta t_{inj}}\right|_{V^{FF}} = \left.\frac{\partial}{\partial \Delta t_{inj}} \left(\frac{Y_1 c_1^{FF} V^{FF}}{(t_{A2} - t_{A1})\dot{V}} \right)\right|_{V^{FF}} = \frac{Y_1 c_1^{FF} V^{FF}}{(t_{A2} - t_{A1})^2 \dot{V}} \left.\frac{\partial t_{A1}}{\partial \Delta t_{inj}}\right|_{V^{FF}} \geq 0, \tag{42}$$

$$\left.\frac{\partial \bar{c}_2^B}{\partial \Delta t_{inj}}\right|_{V^{FF}} = \left.\frac{\partial}{\partial \Delta t_{inj}} \left(\frac{Y_2 c_2^{FF} V^{FF}}{(t_{B2} - t_{B1})\dot{V}} \right)\right|_{V^{FF}} = 0 \tag{43}$$

As can be seen, these are equivalent with the findings above. In addition, the same results for productivity and eluent consumption are obtained if the analysis is carried out for component 2.

Regions for optimal operation conditions concerning different performance parameters are presented in Fig. 6. The curve line G

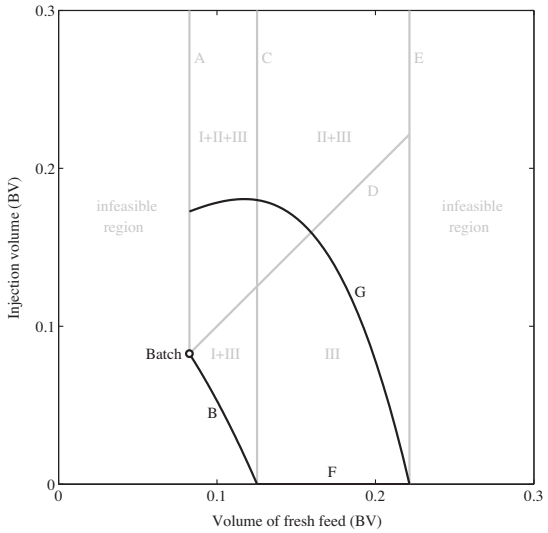

Fig. 6. Limits of optimal operating parameters for the SSR-SR process. For a certain V^{FF}, maximum productivity is obtained at the limits B and F. Minimum eluent consumption and maximum product concentrations in fraction A are obtained at the limit G and above it. Gray background: regions of feasible operating parameters for different SSR-SR configurations (see Fig. 5). Feed concentrations, isotherm parameters and purity constraints are the same as in Fig. 4.

corresponds to the maximum injection width with which the injection plateau is not recycled. As can be seen in Eqs. (41) and (42), the minimum eluent consumption and maximum product concentrations of fraction *A* for a certain V^{FF} are obtained at this limit and above it. In contrast, as to the productivity, the optimum is always achieved with the smallest possible injection width (see Eq. (40)). In Fig. 6, this corresponds on limits *B* and *F*.

As seen from Fig. 6, for a certain V^{FF} the process option I can be operated both at the point of maximum productivity and in the region of the minimum eluent consumption. However, the maximum fresh feed volume that can be obtained is lower than in other cases, as mentioned already in Section 3.4. In configuration II, the value chosen for V^{FF} can be more flexible, but the maximum productivity is never achieved. All this means that the optimum operating point, which is naturally a trade-off between different performance parameters as well as the required solvent removal capacity, may be located in a region where only the process scheme III can be operated. Such calculations are beyond the scope of this work, however.

4.2. Simulation of process performance with a generic example

The design method presented above can be used to compare the performance of different SSR-SR process configurations. In particular, the effect of the operating parameters V^{FF} and V_{inj} on the specific productivity, the specific eluent consumption, and the average product concentrations were of interest here. The simulations were carried out with a generic model system. The feed concentrations

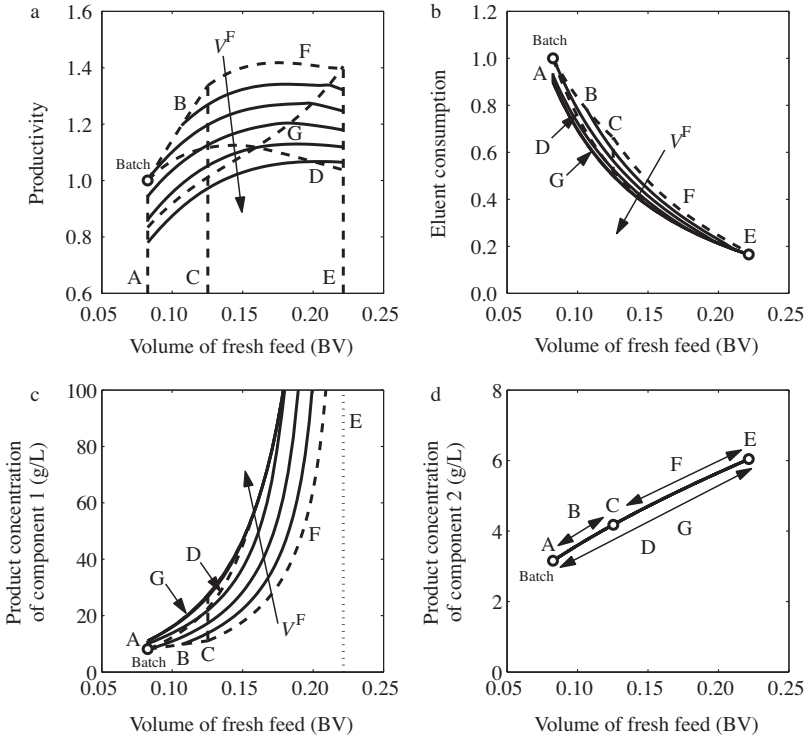

Fig. 7. Effect of volume of fresh feed and injection volume on the performance of mixed-recycle SSR chromatography with solvent removal. The direction of increasing injection volume (0.04, 0.08, 0.12, 0.16 and 0.20 BV) is indicated with an arrow. Feed concentrations and isotherm parameters are given in the text. Circles: batch chromatography without solvent removal; dashed lines: operation limits of SSR-SR configurations (limits A–G in Figs. 5 and 6).

were $c_1^{FF} = c_2^{FF} = 10$ g/L, the phase ratio $F = 1/3$, and the parameters of Langmuir isotherms, Eq. (7), $q_{m,1} = q_{m,2} = 100$ g/L, $b_1 = 0.02$ L/g and $b_2 = 0.025$ L/g. The purity constrains of both product fractions were set equal to 0.9.

The dependence of the performance parameters on the volume of fresh feed and the injection volume is displayed in Fig. 7. Because the same feed concentrations and purity requirements were used for both components, the productivities and eluent consumptions behave identically. The white circles in the subfigures represent the performance of batch chromatography without solvent removal and the dashed lines the operation limits of various SSR-SR configurations (limits A–G in Figs. 5 and 6).

It is observed in Fig. 7a that productivity increases with an increasing V^{FF}. It is interesting to note that an SSR-SR process can achieve a higher productivity than an optimized batch chromatography process that also employs solvent removal (line B in Fig. 7a). In this respect, SSR-SR is fundamentally different from conventional SSR. However, this condition requires that the volume of removed solvent is larger than the volume of fresh feed (see also Fig. 5, limit C). In other words, the SSR-SR must operate in an area that is not feasible for batch chromatography with solvent removal or for the SSR-SR configuration I. Considering that the solvent removal capacity required to operate SSR-SR increases rapidly with V^{FF} (see Fig. 4), the economic optimum might not be where the productivity is the highest. As mentioned before, such calculations are beyond the scope of this work, however.

It can also be observed from Fig. 7a that productivity decreases with an increasing V_{inj} (direction of the arrows). This effect is the same as predicted in Eq. (40) and can be explained in a similar way as in the case of a conventional SSR process [15]. When the volume of fresh feed is constant, the volume of the recycle fraction increases rapidly with the increasing injection volume. Hence, less fresh feed is introduced compared to the size of the recycle fraction, and the operation is less efficient. This means that when the ratio V^{SR}/V^{FF} is less than 1 (Fig. 5, limit C), batch chromatography with solvent removal always outperforms SSR-SR chromatography in terms of productivity. When the ratio V^{SR}/V^{FF} is at least 1, the optimum injection volume (with respect to productivity) is zero.

In Fig. 7b, it is seen that the eluent consumption decreases with an increasing volume of fresh feed. The trend originates from two different causes. Firstly, the amounts of components in the product fractions increase as V^{FF} increases. This means that the denominator in Eq. (34) increases, and thus the specific eluent consumption decreases. Secondly, the more fresh feed is introduced into the column, the more solvent has to be removed. As mentioned before, the removed solvent can be used as eluent, and less fresh eluent is needed.

The effect of the injection volume on the eluent consumption is congruent with Eq. (41) and the findings by Sainio and Kaspereit [15]. The eluent consumption decreases with an increasing injection volume until it levels off as the injection volume becomes sufficiently large. The limit is achieved when the injection plateau is recycled.

Using a larger volume of fresh feed also results in higher concentrations of components 1 and 2 in product fractions *A* and *B*, respectively (Fig. 7c and d). It is interesting to note that when the volume of fresh feed approaches its maximum value (limit E), the product concentrations in fraction *A* approach infinity. However, the concentrations in fraction *B* remain finite. Similarly to conventional SSR, the injection volume has no effect on the average concentrations in the product fraction *B*, as predicted in Eq. (43). Moreover, the average concentrations in the product fraction *A* become independent of the injection volume when t_{A2} is located on the injection plateau (see Eq. (42)).

5. Conclusions

Operation and performance of mixed-recycle SSR chromatography with solvent removal was analyzed theoretically in the framework of the equilibrium theory. A method was developed to choose *a priori* the cut times for fractionating the outlet stream of the chromatography column so that the user-given purity and/or yield specifications are fulfilled. With this approach, the steady state is obtained on the basis of adsorption isotherm parameters only, without performing dynamic simulations. The amount of fresh feed introduced per cycle and the injection width were identified as the only free operating parameters. A relationship was derived between the amount of fresh feed and the solvent removal capacity required to achieve the chosen purities.

The following three process configurations were investigated: (I) solvent removal is applied to the fresh feed, (II) solvent removal is applied to the recycle fraction, and (III) solvent removal is applied after mixing the recycle fraction and the fresh feed. It was shown that, due to solvent removal, it is possible to treat more fresh feed in each cycle in an SSR-SR process than in the conventional SSR concept. In addition, it was demonstrated that specifying the volume of fresh feed (together with the purity requirements) fixes the volume of solvent that has to be removed. The solvent removal capacity was shown to increase rapidly with the amount of fresh feed introduced to the column per cycle.

The theoretical analysis also revealed that all three SSR-SR configurations have identical performance when the same operating parameters, *i.e.* injection volume and fresh feed volume, are used. However, the maximum amounts of fresh feed that can be processed per cycle, as well as the range of feasible injection widths, are not identical. With respect to the considered process performance parameters, the configuration where solvent removal is applied after mixing the recycle fraction with the fresh feed is the most flexible one and can provide the highest performance.

SSR-SR chromatography was shown to have a lower eluent consumption and higher concentration of the first product fraction compared to batch chromatography with the same solvent removal capacity. As to the productivity, the optimized batch operation with solvent removal outperforms SSR-SR when solvent is removed from the fresh feed. However, when the solvent removal in SSR-SR is applied to the mixed fraction, higher productivity can be achieved than in the optimized batch operation.

Finally, it should be reminded that the theory presented in this work is based on the equilibrium theory of chromatography with assumption of infinite column efficiency. For this reason, the approach is most applicable for high performance systems, while some conclusions may not be valid for systems of moderate or low efficiency. However, we believe that the proposed approach can be used in many real industrial applications to predict the preliminary operating parameters which can be later optimized by detailed simulations. In practice, solvent removal in a chromatographic process has also some limitations that were not considered here. The solubility of the solutes or the viscosity of the concentrated solution may limit the amount of solvent that can be removed.

Nomenclature

A	coefficient matrix in Eq. (5)
a	coefficient of the Langmuir isotherm
b	Langmuir parameter (L/mol or L/g)
c	concentration (mol/L or g/L)
$\bar{c}$	average concentration in a product fraction (mol/L or g/L)
F	phase ratio

EC	eluent consumption
m	mass (g)
p^j	purity of fraction j with respect to a target component
P_i	pure component plateau in a chromatogram with constant concentration of i
PR	productivity
q	stationary phase concentration (mol/L or g/L)
q_m	saturation capacity of the adsorbent (mol/L or g/L)
t	time relative to beginning of cycle (min)
t_0	elution time of a non-retained component (min)
u	interstitial velocity (m/min)
V	volume (L or BV)
$\dot{V}$	volume flow rate (L/min)
x	space coordinate (m)
Y	yield with respect to a target component

Greek symbols

α	separation factor
Γ	characteristic of a simple wave
γ	auxiliary parameter in Eqs. (A.1)–(A.5)
ξ	slope of the characteristic in the hodograph plane
Σ	shock wave
τ	time relative to the end of injection (min)
τ_R^0	retention time at infinite dilution relative to the end of injection (min)

Subscripts

1, 2	components to be separated
I, II, III	type of SSR-SR process configuration
$A1$	beginning of product fraction A
$A2$	end of product fraction A
$B1$	beginning of product fraction B
$B2$	end of product fraction B
cycle	cycle of an SSR process
$E1$	end of mixed zone
$E2$	end of elution profile
I	end of pure component 2 plateau
inj	injection
P	end of injection plateau
+	faster wave or shock
–	slower wave or shock

Superscripts

A	product fraction A
B	product fraction B
F	steady state feed
F'	steady state feed before solvent removal
FF	fresh feed before solvent removal
FF'	fresh feed after solvent removal
P	pure component plateau
R	recycle fraction before solvent removal
R'	recycle fraction after solvent removal
SR	solvent removal

Appendix A. Integral terms in Eqs. (13) and (14)

In this appendix, analytical expressions for the integral terms in Eqs. (13) and (14) are given. The elution profiles of components 1 and 2 as a function of time are given by Guiochon et al. [20] for the mixed wave as in Eqs. (A.1) and (A.2):

$$c_1 = \frac{1}{b_1 + b_2/(\alpha\xi_+^F)}\left[\sqrt{\frac{\gamma}{\alpha}\frac{\tau_{R,1}^0 - t_0}{\tau - t_0}} - 1\right] \tag{A.1}$$

$$c_2 = \frac{1}{b_2 + \alpha b_1 \xi_+^F}\left[\sqrt{\gamma\frac{\tau_{R,2}^0 - t_0}{\tau - t_0}} - 1\right] \tag{A.2}$$

and for the pure component 2 wave as in Eq. (A.3):

$$c_2 = \frac{1}{b_2}\left[\sqrt{\gamma\frac{\tau_{R,2}^0 - t_0}{\tau - t_0}} - 1\right] \tag{A.3}$$

The following parameters are used in Eqs. (A.1)–(A.3). The initial slope of the Langmuir isotherm is $a_i = b_i q_{m,i}$, the separation factor $\alpha = a_2/a_1$, the retention time at infinite dilution $\tau_{R,i}^0 = t_0(1 + Fa_i)$, and an auxiliary parameter $\gamma = \alpha/(1 + b_2 c_2^{PF})$.

The integration limits are the end time of the mixed zone, Eq. (A.4), the end time of the pure component 2 concentration plateau, Eq. (A.5), and the end time of the elution profile, Eq. (A.6).

$$\tau_{E1} = t_0\left(1 + \frac{\gamma Fa_1}{\alpha}\right) \tag{A.4}$$

$$\tau_I = t_0\left[1 + Fa_2\left(\frac{\gamma}{\alpha}\right)^2\right] \tag{A.5}$$

$$\tau_{E2} = t_0(1 + Fa_2) \tag{A.6}$$

By employing these equations, the integral term in Eq. (13) can be integrated analytically to give

$$\int_{\tau_{B1}}^{\tau_{B2}} c_1 dt = \int_{\tau_{B1}}^{\tau_{E1}} c_1 dt = \frac{\alpha - 1 - b_2 c_2^{PF}}{b_1(\alpha - 1)}\left[\tau_{B1} + t_0\left(\frac{Fa_1}{1 + b_2 c_2^{PF}} - 1\right) - 2\sqrt{\frac{t_0 Fa_1}{1 + b_2 c_2^{PF}}(\tau_{B1} - t_0)}\right] \tag{A.7}$$

and the integral term in Eq. (14) to give

$$\begin{aligned}\int_{\tau_{B1}}^{\tau_{B2}} c_2 dt = \int_{\tau_{B1}}^{\tau_{E1}} c_2 dt + \int_{\tau_{E1}}^{\tau_I} c_2 dt + \int_{\tau_I}^{\tau_{E2}} c_2 dt = \frac{c_2^{PF}}{(\alpha - 1)}\Bigg[\tau_{B1} &+ t_0\left(\frac{(2\alpha - 1)Fa_1}{1 + b_2 c_2^{PF}} - 1\right) - 2\alpha\sqrt{\frac{t_0 Fa_1}{1 + b_2 c_2^{PF}}(\tau_{B1} - t_0)} \\ &+ t_0 Fa_1 c_2^{PF}\left[\frac{\alpha}{(1 + b_2 c_2^{PF})^2} - \frac{1}{1 + b_2 c_2^{PF}}\right] \\ &+ \frac{t_0 Fa_2}{b_2}\left(1 - \frac{1}{1 + b_2 c_2^{PF}}\right)^2\end{aligned} \tag{A.8}$$

Appendix B. Uniqueness of solution to pair of Eqs. (13) and (14)

An essential intermediate result in the analysis of SSR-SR is the fact that specifying V^{FF} (in addition to purity or yield requirements) determines the characteristic Γ_+^F onto which F will map in the steady state. This characteristic is independent of the injection width. This holds true if the pair of Eqs. (13) and (14) has a unique solution, which can be shown as follows.

If we determine the cut time τ_{B1} as a function of c_2^{PF} so that the purity p^B matches a design constraint, we get a strictly decreasing curve. The same applies if we determine τ_{B1} as a function of c_2^{PF} so that the mass m_1^B, given on the left in Eq. (13), is correct. In contrast, when we determine τ_{B1} so that m_2^B is correct, a strictly increasing curve is obtained. This can be observed as follows.

When the cut time τ_{B1} is held at a fixed value but c_2^{PF} is increased (*i.e.* the height of the pure component 2 plateau increases), the amount m_1^B decreases (due to enhanced displacement) and m_2^B increases:

$$\left.\frac{\partial m_1^B}{\partial c_2^{PF}}\right|_{\tau_{B1}} < 0 \tag{B.1}$$

$$\left.\frac{\partial m_2^B}{\partial c_2^{PF}}\right|_{\tau_{B1}} > 0 \tag{B.2}$$

Thus, the purity of the product fraction B must also increase with an increasing c_2^{PF}:

$$\left.\frac{\partial p^B}{\partial c_2^{PF}}\right|_{\tau_{B1}} > 0 \tag{B.3}$$

In addition, for a constant c_2^{PF} but a decreasing τ_{B1} (*i.e.* the increasing length of product fraction B along a chosen Γ_+ characteristic), m_1^B and m_2^B both increase, whereas p^B decreases.

$$\left.\frac{\partial m_1^B}{\partial \tau_{B1}}\right|_{c_2^{PF}} < 0 \tag{B.4}$$

$$\left.\frac{\partial m_2^B}{\partial \tau_{B1}}\right|_{c_2^{PF}} < 0 \tag{B.5}$$

$$\left.\frac{\partial p^B}{\partial \tau_{B1}}\right|_{c_2^{PF}} > 0 \tag{B.6}$$

By applying the triple product rule to Eqs. (B.1) and (B.4), to Eqs. (B.2) and (B.5) and to Eqs. (B.3) and (B.6), we can determine the sign of the partial derivatives of τ_{B1} with respect to c_2^{PF} in the case of a constant m_1^B, m_2^B, and p^B, as shown in Eqs. (B.7)–(B.9). These are equivalent to our statements above:

$$\left.\frac{\partial \tau_{B1}}{\partial c_2^{PF}}\right|_{m_1^B} < 0 \tag{B.7}$$

$$\left.\frac{\partial \tau_{B1}}{\partial c_2^{PF}}\right|_{m_2^B} > 0 \tag{B.8}$$

$$\left.\frac{\partial \tau_{B1}}{\partial c_2^{PF}}\right|_{p^B} < 0 \tag{B.9}$$

Evidently, the solution of the equation pair (13) and (14) can be found from the intersection of the curves $\tau_{B1} = f(c_2^{PF})_{m_1^B}$, $\tau_{B1} = f(c_2^{PF})_{p_2^B}$ and $\tau_{B1} = f(c_2^{PF})_{p^B}$. Because strictly increasing and strictly decreasing curves can have only one intersection, also the pair of Eqs. (13) and (14) has only one solution.

References

[1] K.J. Bombaugh, W.A. Dark, R.F. Levangie, High-resolution steric chromatography, J. Chromatogr. Sci. 7 (1969) 42–47.
[2] A. Seidel-Morgenstern, G. Guiochon, Theoretical study of recycling in preparative chromatography, AIChE J. 39 (1993) 809–819.
[3] C. Heuer, A. Seidel-Morgenstern, P. Hugo, Experimental investigation and modeling of closed-loop recycling in preparative chromatography, Chem. Eng. Sci. 50 (1995) 1115–1127.
[4] C.M. Grill, Closed-loop recycling with periodic intra-profile injection: a new binary preparative chromatographic technique, J. Chromatogr. A 796 (1998) 101–113.
[5] C.M. Grill, L. Miller, Separation of a racemic pharmaceutical intermediate using closed-loop steady state recycling, J. Chromatogr. A 827 (1998) 359–371.
[6] C.M. Grill, L. Miller, T.Q. Yan, Resolution of a racemic pharmaceutical intermediate. A comparison of preparative HPLC, steady state recycling, and simulated moving bed, J. Chromatogr. A 1026 (2004) 101–108.
[7] J. Kennedy, M. Belvo, V. Sharp, J. Williams, Comparison of separation efficiency of early phase active pharmaceutical intermediates by steady state recycle and batch chromatographic techniques, J. Chromatogr. A 1046 (2004) 55–60.
[8] T.Q. Yan, C. Orihuela, Rapid and high throughput separation technologies-Steady state recycling and supercritical fluid chromatography for chiral resolution of pharmaceutical intermediates, J. Chromatogr. A 1156 (2007) 220–227.
[9] J.W. Lee, P.C. Wankat, Comparison of recycle chromatography and simulated moving bed for pseudobinary separations, Ind. Eng. Chem. Res. 48 (2009) 7724–7732.
[10] M. Bailly, D. Tondeur, Recycle optimization in nonlinear productive chromatography. I. Mixing recycle with fresh feed, Chem. Eng. Sci. 37 (1982) 1199–1212.
[11] M. Bailly, D. Tondeur, Reversibility and performances in productive chromatography, Chem. Eng. Process. 18 (1984) 293–302.
[12] D. Tondeur, M. Bailly, in: P. Barker, G. Ganetsos (Eds.), Preparative and Production-scale Chromatography, Chromatographic Science Series, vol. 61, Marcel-Dekker, New York, 1993, pp. 79–109.
[13] F. Charton, Optimisation des coupes et recyclages en chromatographie preparative industrielle, PhD thesis, Institut National Polytechnique de Lorraine, Nancy, 1995.
[14] F. Charton, M. Bailly, G. Guiochon, Recycling in preparative liquid chromatography, J. Chromatogr. A 687 (1994) 13–31.
[15] T. Sainio, M. Kaspereit, Analysis of steady state recycling chromatography using equilibrium theory, Sep. Purif. Technol. 66 (2009) 9–18.
[16] M. Bailly, R.-M. Nicoud, A. Philippe, O. Ludemann-Hombourger, Method and device for chromatography comprising a concentration step, U.S. Patent Application No. WO204039468, 2004.
[17] S. Abdelmoumen, L. Muhr, M. Bailly, O. Ludemann-Hombourger, The M3C process: a new multicolumn chromatographic process integrating a concentration step. I—the equilibrium model, Sep. Sci. Technol. 41 (2006) 2639–2663.
[18] G. Paredes, H.-K. Rhee, M. Mazzotti, Design of simulated-moving-bed chromatography with enriched extract operation (EE-SMB): Langmuir isotherms, Ind. Eng. Chem. Res. 45 (2006) 6289–6301.
[19] M. Kaspereit, K. Gedicke, V. Zahn, A.W. Mahoney, A. Seidel-Morgenstern, Shortcut method for evaluation and design of a hybrid process for enantioseparations, J. Chromatogr. A 1092 (2005) 43–54.
[20] G. Guiochon, D.G. Shirazi, A. Felinger, A.M. Katti, Fundamentals of Preparative and Nonlinear Chromatography, Academic Press, Boston, 2006.
[21] H.-K. Rhee, R. Aris, N.R. Amundson, First-order Partial Differential Equations Theory and Applications of Hyperbolic Systems of Quasilinear Equations, vol. II, Dover Publications, Mineola, N.Y., 2001.

Article II

Journal of Chromatography A, 1218 (2011) 6379–6387

Contents lists available at ScienceDirect

Journal of Chromatography A

journal homepage: www.elsevier.com/locate/chroma

Explicit equations for the height and position of the first component shock for binary mixtures with competitive Langmuir isotherms under ideal conditions

Jani Siitonen, Tuomo Sainio*

Lappeenranta University of Technology, Skinnarilankatu 34, FIN-53850 Lappeenranta, Finland

ARTICLE INFO

Article history:
Received 14 April 2011
Received in revised form 24 June 2011
Accepted 1 July 2011
Available online 8 July 2011

Keywords:
Equilibrium theory
Ideal model
First component shock
Langmuir isotherm

ABSTRACT

Explicit equations for the height c_1^S and retention time $t_{R,1}$ of the pure first component shock in the case of a narrow rectangular injection pulse of a binary mixture with competitive Langmuir isotherms were derived within the frame of the equilibrium theory. The height of the first shock is obtained as an only positive root of a quartic equation. Hence, it was shown that, for binary Langmuir systems, the individual concentration profiles at the column outlet can be expressed entirely in closed-form. In addition, a novel, simple parametric representation that gives the trajectory of the first shock in the distance–time diagram as a function of c_1^S was derived. The practical relevance of the new equations was demonstrated by utilizing them for optimization of batch chromatography. It was shown that c_1^S increases and $t_{R,1}$ decreases with increasing duration of injection for given feed concentrations when the pure first component plateau is eroded during elution. The derivative of the cycle time with respect to the duration of injection is always more than unity. For this reason, the maximum productivity of more retained component is obtained when the duration of injection is selected so that the purity constraint can be fulfilled by having 100% yield. For the less retained component, an implicit expression for the maximum productivity was derived. When the injected loadings are constant, $t_{R,1}$ decreases with increasing feed concentrations while c_1^S and the cycle time are independent of them. In addition, the productivities of both components always increase with increasing feed concentrations.

1. Introduction

Preparative chromatography is a highly developed technique for many difficult separations in the pharmaceutical, fine chemical and food industries. Within these applications, chromatography is typically operated at overloaded conditions, for which nonlinear competitive adsorption behavior is characteristic. Under these conditions, the solute propagation in the column is essentially controlled by the thermodynamics of phase equilibria, while kinetic properties have a secondary, albeit not negligible, effect on the system dynamics [1].

For decades, different chromatographic systems have been described by using so called equilibrium theory of chromatography [1–9]. Within the frame of the theory, the propagation of the concentration states in the column are described by considering convection and phase equilibrium only, while mass transfer resistance and axial dispersion are neglected. The theory provides an understanding of the main features of the column dynamics, such as formation and propagation of concentration shocks, dispersive waves and their interactions for single, binary as well as multi-component systems. It has been used widely for the analysis and design of both single-column [10–13] and multi-column chromatographic processes [14,15].

The equilibrium model consists of hyperbolic first-order partial differential equations. In the case of classical competitive Langmuir isotherms and piecewise constant boundary condition, the solution of the model equations can be given mostly in explicit form, also in the case of multi-component systems. First comprehensive analyses of the problem have been presented already in the 1940s by Devault [2] and by Glueckauf [3]. They both discussed the mathematical theory of the two-component problem and showed, for example, the existence of two discontinuities, one in front of each band. Later, Helfferich and Klein [1] and Rhee et al. [4] calculated the composition trajectories in the distance–time plane by exploiting two different approaches: so-called h-transform and the method of characteristics, respectively. Based on these approaches, Golshan-Shirazi and Guiochon [5,6] have presented an exact, analytical solution for almost the entire chromatographic cycle at column outlet in the case of a binary Langmuir system. However, in the case of small injection, they have been unable to derive a closed-form solution for the height of the pure first component shock c_1^S and for the retention time of the shock $t_{R,1}$. Recently, Rajendran and Mazzotti [9] have presented the trajectory of the first shock in the distance–time diagram in parametric form by using ω-transform,

* Corresponding author. Tel.: +358 5 62111; fax: +358 5 62199.
E-mail address: tuomo.sainio@lut.fi (T. Sainio).

0021-9673/$ – see front matter © 2011 Elsevier B.V. All rights reserved.
doi:10.1016/j.chroma.2011.07.004

but they have not discussed the solution at the column outlet. Closed-form equations for the height and position of the first shock have not been reported.

Lack of explicit equations for c_1^S and $t_{R,1}$ significantly complicates the analysis and design of chromatographic systems, especially the evaluation of the key performance parameters such as productivity and eluent consumption [10–13]. This is because the most useful definition of the cycle time allows "stacked injections" where the front of each injection profile touches (but does not overlap with) the tail of the preceding one. In absence of the complete closed-form solution of the chromatogram, the cycle time has even been defined excessively large in some optimization studies [10,11], which limits the practical relevance of the results. In addition, equations for the retention times of the shock fronts are needed to estimate adsorption isotherm parameters in a recently introduced experimental method [16].

The main objective of the present work is to derive a closed-form expression for the height and retention time of the pure first component shock in the case of a narrow rectangular injection pulse of a binary mixture with competitive Langmuir isotherm. The approach is based on the equilibrium theory of chromatography and it can be considered as a complement to the work of Golshan-Shirazi and Guiochon [5].

At the beginning of this contribution, the fundamentals of the equilibrium theory will be summarized. After that, analytic solutions for c_1^S and $t_{R,1}$ are derived. It will be shown that, for binary Langmuir systems, the individual concentration profiles at column outlet can be expressed entirely in closed-form. The obtained results are applied to derive a simple parametric representation for the trajectory of the first shock in the distance–time diagram. The location of the first shock in physical plane is given as a function of c_1^S. Finally, the practical relevance of the novel equations will be demonstrated by deriving differentials of c_1^S and $t_{R,1}$ with respect to typical operating parameters that can be varied in practical applications and by using them for optimization of batch chromatography.

2. Background

Within the frame of the equilibrium theory, the mass balance for an individual component i is written as

$$\frac{\partial}{\partial t}(c_i + Fq_i) + u\frac{\partial c_i}{\partial x} = 0 \quad (i = 1, 2) \tag{1}$$

where c_i and q_i are the mobile and the stationary phase concentrations of solute i, F is the phase ratio, t is time, x is the space coordinate, and u is the interstitial velocity. For binary systems that follow the competitive Langmuir adsorption isotherm model the equilibrium relationship is given by

$$q_i = \frac{q_{m,i} b_i c_i}{1 + b_1 c_1 + b_2 c_2} \quad (i = 1, 2) \tag{2}$$

where $q_{m,i}$ and b_i are the saturation capacity of the stationary phase and the Langmuir parameter of solute i, respectively. In the following discussion, it is assumed that component 1 is the less strongly adsorbed one. This means that $a_2 > a_1$, where $a_i = b_i q_{m,i}$ is the Henry constant of component i.

Eqs. (1) and (2) form a coupled system of two first-order partial differential equations. The system can be solved by the method of characteristics when Riemann boundary conditions are used. Typically, the task is to describe the solute propagation in the column when a rectangular pulse of binary mixture with known duration, Δt_{inj}, is first injected to an initially clean column and then eluted. In this case, the initial and boundary conditions of Eq. (1) are

$$c_i(x, t = 0) = 0 \quad \text{for} \quad 0 \le x \le L \tag{3}$$

$$c_i(x = 0, t) = c_i^F \quad \text{for} \quad 0 \le t \le \Delta t_{inj} \tag{4}$$

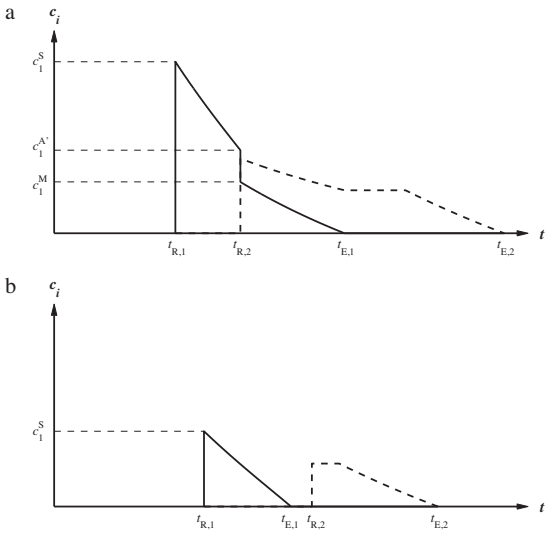

Fig. 1. Individual elution profiles of a rectangular injection pulse at the column outlet. (a) Incomplete separation. Conditions: $c_1^F = c_2^F = 10$ g/L; $q_{m,1} = q_{m,2} = 100$ g/L; $b_1 = 0.02$ L/g; $b_2 = 0.025$ L/g; $F = 1/3$; $V_{inj} = 0.1$ bed volumes. (b) Complete separation. Same conditions as for (a) except $V_{inj} = 0.03$ bed volumes.

$$c_i(x = 0, t) = 0 \quad \text{for} \quad t > \Delta t_{inj} \tag{5}$$

where L is the column length and c_i^F is the concentration of component i in feed.

If the injection is wide enough, the pure component 1 plateau in the front of the elution profile is not eroded during elution, and the individual concentration profiles at the column outlet can expressed entirely in closed form [5]. However, for sufficiently small injections, the plateau erodes completely, and the height of the front shock decreases while it propagates through the column. For such a case, no closed-form expression has been presented for the height or retention time of the first pure component shock. The distance from the column inlet, where the pure first component plateau is eroded completely, is given by

$$x_E = \frac{u(1 + b_1 c_1^A)^2 \Delta t_{inj}}{F a_1 b_1 c_1^A}\left[1 - \frac{\beta b_2 c_2^F}{\alpha(\beta + b_1 c_1^A)^2}\right] \tag{6}$$

where $\alpha = a_2/a_1$ is the separation factor, $\beta = 1 - 1/\alpha$ is an auxiliary parameter, $c_1^A = c_1^F[1 + b_2/(\alpha b_1 \xi_+)]$ is the height of the first shock before erosion, and ξ_+ is the slope of Γ_+ characteristic corresponding the feed composition whose value can be calculated explicitly from adsorption isotherm parameters [8].

Typical elution profiles in the case of a narrow injection pulse are illustrated in Fig. 1. Depending on the resolution between the bands there are two possibilities. Fig. 1a represents the case where the components are not separated completely. The concentration profiles at column outlet consist of three zones. A zone of pure first component elutes between times $t_{R,1}$ and $t_{R,2}$, a mixed zone between $t_{R,2}$ and $t_{E,1}$, and a zone of pure second component between $t_{E,1}$ and $t_{E,2}$. In the case of complete separation, illustrated in Fig. 1b, there is no mixed zone left. The main features of the solution are a concentration shock in the front of both bands, a pure diffuse boundary for both components and a possible second component concentration plateau.

If the components are not separated completely (Fig. 1a), the retention time of the second shock $t_{R,2}$ and the end of elution profile

of the first component $t_{E,1}$ are given by [5]

$$t_{R,2} = \Delta t_{inj} + t_0 \left[1 + Fa_2\gamma\left(1 - \sqrt{L'_f}\right)^2\right] \quad (7)$$

$$t_{E,1} = \Delta t_{inj} + t_0\left(1 + \frac{\gamma Fa_1}{\alpha}\right) \quad (8)$$

In the above equations, t_0 is the elution time of a non-retained component, $L_{f,2} = (b_2 c_2^F \Delta t_{inj})/(Fa_2 t_0)$ is the loading factor of the second component, and $L'_f = (1 + \xi_+ b_1/b_2)L_{f,2}$ and $\gamma = (\alpha b_1\xi_+ + b_2)/(b_1\xi_+ + b_2)$ are auxiliary parameters.

The concentration profile of the first component in mixed zone (between $t_{R,2}$ and $t_{E,1}$) is given by

$$c_1 = \frac{1}{b_1 + b_2/(\alpha\xi_+)}\left[\sqrt{\frac{\gamma}{\alpha}\frac{t_0 Fa_1}{t - \Delta t_{inj} - t_0}} - 1\right] \quad (9)$$

and in the pure first component zone (between $t_{R,1}$ and $t_{R,2}$) by

$$t = \Delta t_{inj} + t_0 + t_0 Fa_1\left[\frac{1}{(1 + b_1c_1)^2} - L_{f,2}\frac{\beta}{(\beta + b_1c_1)^2}\right] \quad (10)$$

It should be noted that the latter equation gives elution time as a function of c_1, while there is no closed-form solution giving the relationship the other way around. This is the very reason that has complicated the derivation of a complete analytic solution for the ideal model of chromatography. The first component concentration at the rear of the second shock c_1^M (see Fig. 1a) is obtained from Eq. (9) by setting $t = t_{R,2}$

$$c_1^M = \frac{\alpha\xi_+}{b_2 + \alpha b_1\xi_+}\frac{\sqrt{L'_f} - \beta}{1 - \sqrt{L'_f}} \quad (11)$$

and at the front of the second shock $c_1^{A'}$ from Eq. (10)

$$c_1^{A'} = \frac{\sqrt{L'_f} - \beta}{b_1\left(1 - \sqrt{L'_f}\right)} \quad (12)$$

For the retention time of the first shock $t_{R,1}$, there has not been a closed-form solution so far. For solving this problem Golshan-Shirazi and Guiochon [5] have provided a numerical approach. Alternatively, $t_{R,1}$ can be solved from the parametric representation given by Rajendran and Mazzotti [9].

In the case of complete separation (Fig. 1b), the mixed zone has disappeared and the rear diffuse profile of the first component can be calculated entirely by Eq. (10). The end time of the profile is given by

$$t_{E,1} = \Delta t_{inj} + t_0 + t_0 Fa_1\left(1 - \frac{L_{f,2}}{\beta}\right) \quad (13)$$

As in the case of incomplete separation, there has been no method for solving the height or the retention time of the front shock in closed-form, but the above mentioned numerical approaches can be applied.

3. Closed-form equations for the height and retention time of the first shock

A closed-form solution for the height and retention time of the first component shock is derived as follows. As in the numerical method by Golshan-Shirazi and Guiochon [5], the idea is to utilize mass balance of the first component to calculate first c_1^S and then $t_{R,1}$.

Although the elution profile of the pure first component (Eq. (10)) cannot be presented in closed-form such that it gives c_1 as a function of time, the mass of the first component eluted from the column can be calculated as a function of c_1^S. This is obtained by integrating the elution profile piecewise with respect to c_1 from 0 to c_1^S and by subtracting $c_1^S t_{R,1}$ from the value of the integral. The calculation principle is presented in Fig. 2. The areas of hatched regions A_3–A_5 correspond to the values of the integral terms, the area of dark grey region A_1 to the amount of component 1, and the area of light grey region A_2 to the difference between these values.

In the case of incomplete separation (Fig. 2a), the mass balance can be written as

$$\begin{aligned} c_1^F\Delta t_{inj} = A_1 = A_5 + A_4 + A_3 - A_2 &= \int_0^{c_1^M} t\,dc_1 + \int_{c_1^M}^{c_1^{A'}} t\,dc_1 \\ &+ \int_{c_1^{A'}}^{c_1^S} t\,dc_1 - c_1^S t_{R,1} = \frac{t_0 Fa_1}{b_1}\left(\frac{b_1c_1^S}{1 + b_1c_1^S}\right)^2 \\ &- \left\{\frac{\alpha b_2 c_2^F}{b_1}\left[\frac{b_1c_1^S}{\alpha(1 + b_1c_1^S) - 1}\right]^2\right\}\Delta t_{inj} \end{aligned} \quad (14)$$

and in the case of complete separation (Fig. 2b) as

$$\begin{aligned} c_1^F\Delta t_{inj} = A_1 = A_3 - A_2 &= \int_0^{c_1^S} t\,dc_1 - c_1^S t_{R,1} \\ &= \frac{t_0 Fa_1}{b_1}\left(\frac{b_1c_1^S}{1 + b_1c_1^S}\right)^2 \\ &- \left\{\frac{\alpha b_2 c_2^F}{b_1}\left[\frac{b_1c_1^S}{\alpha(1 + b_1c_1^S) - 1}\right]^2\right\}\Delta t_{inj} \end{aligned} \quad (15)$$

It is interesting to note that both cases lead to exactly the same result. By dividing the both sides of Eq. (14) or Eq. (15) by $c_1^F\Delta t_{inj}$ and by simplifying the resulting equation, the following implicit expression for c_1^S is obtained:

$$L_{f,1}\left(1 + \frac{1}{b_1c_1^S}\right)^2 + L_{f,2}\left(1 + \frac{1}{\alpha(1 + b_1c_1^S) - 1}\right)^2 = 1 \quad (16)$$

As seen in Eq. (16), the height of first component shock depends only on the loading factors, the separation factor and the Langmuir parameter of the first component. The concentration c_1^S can be solved by re-arranging the above equation to give

$$A(b_1c_1^S)^4 + B(b_1c_1^S)^3 + C(b_1c_1^S)^2 + Db_1c_1^S + E = 0 \quad (17)$$

where

$$A = L_{f,1} + L_{f,2} - 1 \quad (18)$$

$$B = 2[L_{f,1} + L_{f,2} + \beta(L_{f,1} - 1)] \quad (19)$$

$$C = L_{f,1} + L_{f,2} + \beta[4L_{f,1} + \beta(L_{f,1} - 1)] \quad (20)$$

$$D = 2L_{f,1}\beta(\beta + 1) \quad (21)$$

$$E = L_{f,1}\beta^2 \quad (22)$$

Eq. (17) is a quartic equation with respect to $b_1c_1^S$. It can be solved analytically, for example by using Ferrari's method [17], Descartes–Euler method [18] or Neumark's method [19]. In Appendix A, it is shown that, when $\alpha > 1$, $L_{f,1} > 0$, and $L_{f,2} > 0$, Eq. (17) has only one positive real root. This root must give the height of the first shock. Applicability of different algorithms for solving Eq. (17) is discussed in the next section.

Once c_1^S is obtained, the retention time of the first shock can be calculated from Eq. (10) by setting $c_1 = c_1^S$. An alternative form,

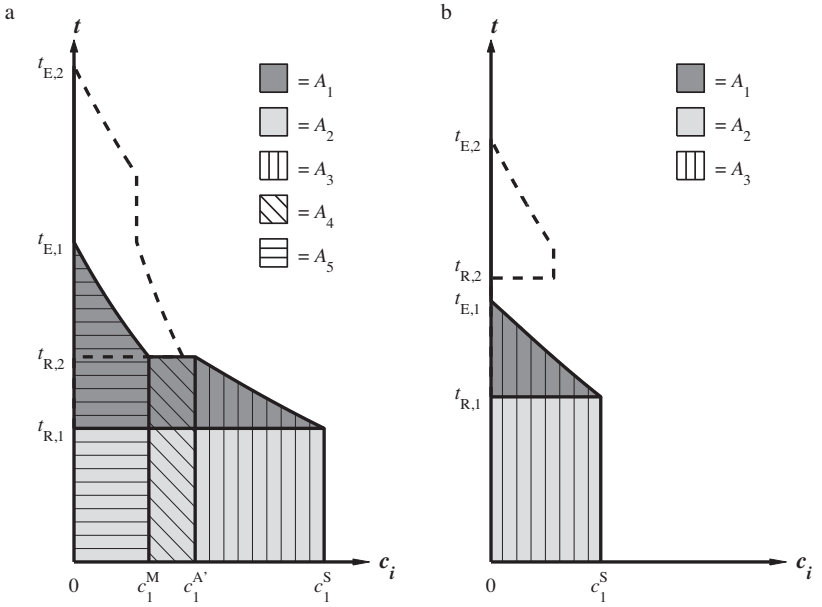

Fig. 2. Individual elution profiles of a rectangular injection pulse presented in the concentration–time coordinate system. A_1, the total amount of component 1. A_2, the difference between the sum of integral terms A_3–A_5 and the total amount of component 1 A_1. A_3–A_5, integral terms in Eqs. (14) and (15). Same conditions as in Fig. 1.

where $t_{R,1}$ is expressed as a function of $L_{f,1}$, is obtained by combining Eqs. (10) and (16)

$$t_{R,1} = \Delta t_{inj} + t_0 + t_0 Fa_1 \left[\frac{1}{\alpha(1 + b_1 c_1^S)^2} + L_{f,1} \frac{\beta}{(b_1 c_1^S)^2} \right] \quad (23)$$

Finally, it should be noted that closed-form equations for the height and retention time of the first shock can be obtained also by using another approach. Rajendran and Mazzotti [9] have recently derived a parametric representation of the trajectory of the first shock by using the ω-transform. Although not pursued by Rajendran and Mazzotti, it is straightforward to show that their equations also lead to a quartic when solved for characteristic parameter ω_1^S which corresponds to the shock height. Unfortunately, the solution is more complex than the one presented here. A somewhat simpler form is obtained by substituting loading factors into the parametric representation of Rajendran and Mazzotti, but this will not be discussed here.

4. Solution of the quartic equation

Several analytic algorithms have been published to solve quartic equations [17–19]. However, as to the computational implementation, none of them is unconditionally stable with arbitrary parameters. The methods have different properties with regard to overflow and round-off errors. Physical constraints pose the following limits for the coefficients of Eq. (17): $-1 < A < 0$, $-2 < B < 2$, $-1 < C < 5$, $0 < D < 4$, $0 < E < 1$. The question arises, which algorithm is best suited for solving this quartic equation?

A Matlab code was developed to compare the following four algorithms: (1) Ferrari's solution [17], (2) Descartes–Euler solution [18], (3) Neumark's solution [19], and (4) the solution given by Matlab's Symbolic Math Toolbox. Ten million random combinations of parameters $L_{f,1}$, $L_{f,2}$, and α, were examined with all algorithms. The accuracy of each solution was checked by substituting the obtained positive root c_1^{S*} back into the left hand side of Eq. (16) and by calculating the relative residual defined as

$$res = \left| \frac{1 - f(c_1^{S*})}{1} \right| \quad (24)$$

According to the simulations, the most applicable option for solving Eq. (17) is the Ferrari's solution. With this algorithm, the relative residual was always less than 32×10^{-12}. However, also the Descartes–Euler solution and the Neumark's solution were observed to be relatively stable. The maximum relative residual with the Descartes–Euler solution was 0.45×10^{-6} and with the Neumark's solution 0.24×10^{-3}.

In contrast to the other methods, the Matlab's symbolic solution was not completely stable. The maximum residual was 0.80, and in 1413 cases out of ten million the relative residual was more than 1%. In addition, in 616 cases a root was not obtained at all, because the round-off errors led to an indeterminate form 0/0. For example, with parameters $L_{f,1} = 0.028$, $L_{f,2} = 0.067$ and $\alpha = 1.4$ the relative residual was 4.3% and with parameters $L_{f,1} = 0.031$, $L_{f,2} = 0.243$ and $\alpha = 2.0$ no root was obtained. In the former case, the retention time of the first shock calculated by Eq. (10) was 0.85% too large, when $\Delta t_{inj}/t_0 = 0.1$ and $Fa_1 = 4.5$. In addition, the Matlab solution was about one hundred times slower than the other ones. This is not a major factor, however, since the calculation time of one root was always less than 5 ms on a standard desktop computer.

The recommended Ferrari's algorithm is given in Table 1. The idea is to first solve one root of a particular cubic equation (I.1), the coefficients of which are obtained from those of the original quartic equation. This root is then used to factorize the quartic into two quadratics that can be solved.

In Eqs. (I.4) and (I.5) $\sqrt{}$ and $\sqrt[3]{}$ stand for any determination of the square or cubic root. However, it was observed that the algorithm is most stable when the principal cubic root is used. In addition, it is recommended to select the sign of Q opposite to the sign of m.

As mentioned in Section 3, Eq. (17) has only one positive real root. In addition, it is shown in Appendix A that Eq. (17) does not

Table 1
Ferrari's algorithm for solving a quartic equation [17].

The subsidiary cubic equation

$$y^3 + ky + m = 0 \quad \text{(I.1)}$$

$$k = \frac{BD}{A^2} - \frac{C^2}{3A^2} - \frac{4E}{A} \quad \text{(I.2)}$$

$$m = \frac{BCD}{3A^3} - \frac{2C^3}{27A^3} - \frac{D^2}{A^2} - \frac{B^2E}{A^3} + \frac{8CE}{3A^2} \quad \text{(I.3)}$$

A root of the cubic equation

$$y = \frac{\sqrt[3]{Q - 108m}}{6} - \frac{2k}{\sqrt[3]{Q - 108m}} \quad \text{(I.4)}$$

$$Q = 12\sqrt{12k^3 + 81m^2} \quad \text{(I.5)}$$

The four roots of the original quartic equation (17)

$$(b_1c_1^S)_1 = -\frac{B}{4A} + \frac{R}{2} + \frac{\sqrt{S + T/R}}{2} \quad \text{(I.6)}$$

$$(b_1c_1^S)_2 = -\frac{B}{4A} + \frac{R}{2} - \frac{\sqrt{S + T/R}}{2} \quad \text{(I.7)}$$

$$(b_1c_1^S)_3 = -\frac{B}{4A} - \frac{R}{2} + \frac{\sqrt{S - T/R}}{2} \quad \text{(I.8)}$$

$$(b_1c_1^S)_4 = -\frac{B}{4A} - \frac{R}{2} - \frac{\sqrt{S - T/R}}{2} \quad \text{(I.9)}$$

$$R = \sqrt{\frac{B^2}{4A^2} - \frac{2C}{3A} + y} \quad \text{(I.10)}$$

$$S = \frac{B^2}{2A^2} - \frac{4C}{3A} - y \quad \text{(I.11)}$$

$$T = \frac{BC}{A^2} - \frac{B^3}{4A^3} - \frac{2D}{A} \quad \text{(I.12)}$$

have any complex root with positive real part. For these reasons, the right root is always the one having the largest real part. The right solution is given by Eq. (I.6), if

$$\mathrm{Re}(2R) > \mathrm{Re}\left(\sqrt{S - \frac{T}{R}} - \sqrt{S + \frac{T}{R}}\right) \quad (25)$$

and otherwise by Eq. (I.8). It was observed in the numerical tests performed that the above inequality held true for every set of parameters when the principal cubic root was used in Eq. (I.4), and the correct root was always obtained from Eq. (I.6).

5. Construction of the distance–time diagram

The solute movement in a chromatography column is conveniently presented in a distance–time diagram. In such a diagram, composition variables are shown as contour lines in a two-dimensional coordinate system with distance from the column inlet x as one coordinate and time t as the other. An example of the distance–time diagram is shown in Fig. 3.

The moment, when the pure first component plateau is eroded completely, is indicated in Fig. 3 by point E. Beyond this point, the height of first shock decreases and the velocity of the shock decelerates. Graphically this means that the trajectory of the first shock S_1 is no longer a straight line but is curved upwards.

It is obvious that, since the retention time of the first shock at column outlet can be expressed explicitly as described in Section 3, also the location of the first component shock in the distance–time diagram can be obtained in closed form. This is observed by considering that the column length can be varied and the corresponding time calculated by Eq. (10). However, because the analytic solution for $t_{R,1}$ is relatively complicated, a more convenient method to create the trajectory of the first shock on the distance–time diagram in parametric form as a function of c_1^S was derived. The method is a simpler alternative to the methods by Rhee et al. [8] and by Rajendran and Mazzotti [9].

At the point E, the height of first component shock has not yet decreased, and c_1^S is given by $c_1^S = c_1^A$. As the distance and time increase, c_1^S decreases and approaches zero when x and t approach

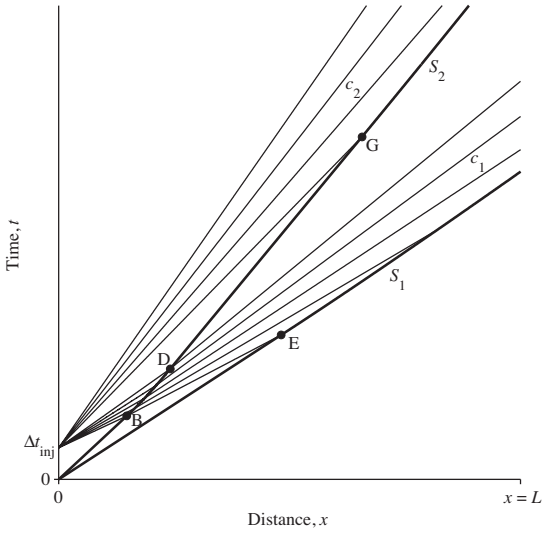

Fig. 3. Propagation of concentration states in the distance–time diagram for an arbitrary system. B, feed plateau is eroded; D, components are separated completely; E, pure first component plateau is eroded; G, pure second component plateau is eroded; S_1, first shock; S_2, second shock.

infinity. The distance x, where a given c_1^S is found in the column, can be calculated by using the global mass balance of the first component

$$\frac{x}{L} = L_{f,1}\left(1 + \frac{1}{b_1c_1^S}\right)^2 + L_{f,2}\left(1 + \frac{1}{\alpha(1 + b_1c_1^S) - 1}\right)^2 \quad (26)$$

It should be noted that Eq. (26) is equal to Eq. (16) at the column outlet where $x = L$.

The corresponding time $t_{R,1}$ can be solved by applying Eq. (10):

$$t_{R,1} = \left\{1 - \frac{(\alpha - 1)b_2c_2^F}{[\alpha(1 + b_1c_1^S) - 1]^2}\right\}\Delta t_{inj} + \frac{x}{L}\left[1 + \frac{Fa_1}{(1 + b_1c_1^S)^2}\right]t_0 \quad (27)$$

Eq. (27) gives time $t_{R,1}$ as a function of c_1^S and x. The latter parameter can be eliminated by substituting Eq. (26) to Eq. (27) which yields

$$t_{R,1} = \left\{1 + \frac{b_1c_1^F}{(b_1c_1^S)^2}\left[1 + \frac{(1 + b_1c_1^S)^2}{Fa_1}\right] + \frac{b_2c_2^F}{[\alpha(1 + b_1c_1^S) - 1]^2}\left[1 + \frac{\alpha^2(1 + b_1c_1^S)^2}{Fa_2}\right]\right\}\Delta t_{inj} \quad (28)$$

Hence, the trajectory of the first shock S_1 can be constructed by giving c_1^S values from c_1^A to 0 and calculating the corresponding x and t from Eqs. (26) and (28).

6. Demonstration of the practical relevance of the novel equations

The novel analytic equations, derived in Section 3, can be used to calculate differentials of c_1^S and $t_{R,1}$ with respect to typical operating parameters that can be varied in practical applications. Next, such derivatives will be derived and utilized in optimization of batch chromatography in two different cases. First, the effect of the duration of injection on c_1^S, $t_{R,1}$, and the main process performance parameters is investigated when the feed concentrations c_1^F and c_2^F

are constant. Secondly, the total feed concentration will be varied while keeping the injected loadings $L_{f,1}$ and $L_{f,2}$ constant. The purpose is to demonstrate that the novel analytic equations have also practical relevance. It should be noted that the following discussion is limited to the case where the shock is eroded during elution, *i.e.* narrow injections, because the height of the shock, and hence its propagation velocity, is constant for sufficiently large injections.

6.1. Purification strategy

In this work, it is assumed that one or other of the components of a binary mixture is purified to a given purity constraint. The first component is the target constituent in the product fraction A, and the second component in the product fraction B. The purities of the product fractions are given by

$$p^{\mathrm{A}} = \frac{m_1^{\mathrm{A}}}{m_1^{\mathrm{A}} + m_2^{\mathrm{A}}} = \frac{\int_{t_{\mathrm{R},1}}^{t_{\mathrm{cut}}} c_1 \,\mathrm{d}t}{\int_{t_{\mathrm{R},1}}^{t_{\mathrm{cut}}} (c_1 + c_2)\mathrm{d}t} \tag{29}$$

$$p^{\mathrm{B}} = \frac{m_2^{\mathrm{B}}}{m_1^{\mathrm{B}} + m_2^{\mathrm{B}}} = \frac{\int_{t_{\mathrm{cut}}}^{t_{\mathrm{E},2}} c_2 \,\mathrm{d}t}{\int_{t_{\mathrm{cut}}}^{t_{\mathrm{E},2}} (c_1 + c_2)\mathrm{d}t} \tag{30}$$

where t_{cut} is the cut time at which the collection of the first fraction ends and the collection of second fraction begins.

The most common performance parameters of chromatographic processes are productivity *PR*, specific eluent consumption *EC*, and recovery yield *Y*. The focus of this work is on the productivity and the specific eluent consumption. This is because the complete analytic solution of the elution profiles allows using more a realistic definition of the cycle time than in previous studies. However, also the yield is discussed briefly, because it has an influence on the total separation costs. The performance parameters are here defined for component 1 (and analogously for component 2) as follows:

$$Y_1 = \frac{m_1^{\mathrm{A}}}{m_1^{\mathrm{F}}} = \frac{\int_{t_{\mathrm{R},1}}^{t_{\mathrm{cut}}} c_1 \,\mathrm{d}t}{m_1^{\mathrm{F}}} \tag{31}$$

$$PR_1 = \frac{m_1^{\mathrm{A}}}{\Delta t_{\mathrm{cycle}}} \tag{32}$$

$$EC_1 = \frac{V_{\mathrm{eluent}}}{m_1^{\mathrm{A}}} = \frac{(\Delta t_{\mathrm{cycle}} - \Delta t_{\mathrm{inj}})\dot{V}}{m_1^{\mathrm{A}}} \tag{33}$$

where $\Delta t_{\mathrm{cycle}}$ is the cycle time and V_{eluent} is the amount of eluent used in a chromatographic cycle.

The cycle time is here defined by assuming that no gap exists between consecutive chromatographic cycles. This means that the first component of the $(n+1)$th injection begins to elute just after the second component of the nth injection has left the column:

$$\Delta t_{\mathrm{cycle}} = t_{\mathrm{E},2} - t_{\mathrm{R},1} \tag{34}$$

The definition is different from the one used in many earlier optimization studies, where the effect of $t_{\mathrm{R},1}$ on the cycle time has not been taken account. For example, Golshan-Shirazi and Guiochon [10,11] have calculated the cycle time as the corrected analytical retention time of the second component $\Delta t_{\mathrm{cycle}} = t_{\mathrm{E},2}^0 - t_0$, where $t_{\mathrm{E},2}^0$ is the retention time of the second component at infinite dilution. In practice, the definition used in this work is more relevant, because it gives the minimum cycle time required for consecutive, isocratic injections. As will be shown shortly, the definition of the cycle time affects significantly the optimization results.

6.2. Effect of the duration of injection on c_1^S, $t_{R,1}$ and Δt_{cycle}

One of the most typical practical problems with regard to batch chromatography is to find the duration of injection that leads to optimal process performance, *i.e.* to minimum separation costs. Next, the effect of Δt_{inj} on c_1^{S}, $t_{\mathrm{R},1}$, $\Delta t_{\mathrm{cycle}}$, and the process performance will be analyzed in the case of constant feed concentrations.

The derivative of c_1^{S} is obtained by differentiating Eq. (16) implicitly with respect to Δt_{inj}

$$\left.\frac{\partial c_1^{\mathrm{S}}}{\partial \Delta t_{\mathrm{inj}}}\right|_{c_1^{\mathrm{F}}, c_2^{\mathrm{F}}} = \left\{ 2b_1(1 + b_1 c_1^{\mathrm{S}}) \left[\frac{L_{f,1}}{(b_1 c_1^{\mathrm{S}})^3} + \frac{L_{f,2}}{\alpha(\beta + b_1 c_1^{\mathrm{S}})^3} \right] \Delta t_{\mathrm{inj}} \right\}^{-1} > 0 \tag{35}$$

As seen in the above equation, the height of the first shock at column outlet always increases with increasing Δt_{inj}. This is reasonable, because the larger the injection is, the later the first shock begins to erode as seen in Eq. (6). In addition, when Δt_{inj} increases, the height of the first shock must increase at every point of the column beyond the beginning of the shock erosion x_{E} (see Fig. 3). This is because Eq. (35) is valid for every column length $L > x_{\mathrm{E}}$.

The corresponding derivative of the retention time $t_{\mathrm{R},1}$ is obtained by differentiating Eq. (10) with respect to Δt_{inj}, setting $c_1 = c_1^{\mathrm{S}}$, and by substituting Eq. (35) to the resulting equation

$$\left.\frac{\partial t_{\mathrm{R},1}}{\partial \Delta t_{\mathrm{inj}}}\right|_{c_1^{\mathrm{F}}, c_2^{\mathrm{F}}} = 1 - \frac{t_0 Fa_1}{\Delta t_{\mathrm{inj}}} \left\{ \frac{(1/(1 + b_1 c_1^{\mathrm{S}})^3) - (\beta L_{f,2}/(\beta + b_1 c_1^{\mathrm{S}})^3)}{\left[(L_{f,1}/(b_1 c_1^{\mathrm{S}})^3) + (L_{f,2}/\alpha(\beta + b_1 c_1^{\mathrm{S}})^3) \right] (1 + b_1 c_1^{\mathrm{S}})} + \frac{\beta L_{f,2}}{(\beta + b_1 c_1^{\mathrm{S}})^2} \right\} \tag{36}$$

On the basis of the right hand side of Eq. (36), it is not possible to say anything about the sign of the above derivative. However, the sign can be deduced by examining the shock height. As mentioned earlier, the shock height is independent of the duration of injection before the beginning of the shock erosion, x_{E}, and is the higher the larger the injection is beyond x_{E}. In addition, it is well known that the shock propagates the faster the higher it is. For these reasons, the first shock must reach the column outlet the earlier the larger the injection is, and the above derivative must therefore always be negative.

The derivative of the cycle time is obtained by differentiating Eq. (34). It is well known that the derivative of $t_{\mathrm{E},2}$ with respect to Δt_{inj} is always unity [12]. For this reason, the derivative of the cycle time must always be greater than unity

$$\left.\frac{\partial t_{\mathrm{cycle}}}{\partial \Delta t_{\mathrm{inj}}}\right|_{c_1^{\mathrm{F}}, c_2^{\mathrm{F}}} = 1 - \frac{\partial t_{\mathrm{R},1}}{\partial \Delta t_{\mathrm{inj}}} > 1 \tag{37}$$

6.3. Effect of the duration of injection on the process performance

The optimum values of the operating parameters depend much on whether one is interested in purifying the first or the second eluted component [10]. When the second component is the target, the mass of the product fraction m_2^{B} is independent of Δt_{inj}, provided that the injection is large enough for matching the purity requirement without collecting the pure first component to the product fraction B [10]. This means that the productivity always decreases when the duration of injection increases due to increasing cycle time:

$$\frac{\partial PR_2}{\partial \Delta t_{\mathrm{inj}}} = -\frac{m_2^{\mathrm{B}}}{(\Delta t_{\mathrm{cycle}})^2} \frac{\partial \Delta t_{\mathrm{cycle}}}{\partial \Delta t_{\mathrm{inj}}} < 0 \tag{38}$$

The specific eluent consumption increases, when Δt_{inj} increases. This is observed by differentiating Eq. (33), where the subscripts have been changed for component 2, which yields

$$\frac{\partial EC_2}{\partial \Delta t_{\mathrm{inj}}} = \frac{\dot{V}}{m_2^{\mathrm{B}}} \left(\frac{\partial \Delta t_{\mathrm{cycle}}}{\partial \Delta t_{\mathrm{inj}}} - 1 \right) > 0 \tag{39}$$

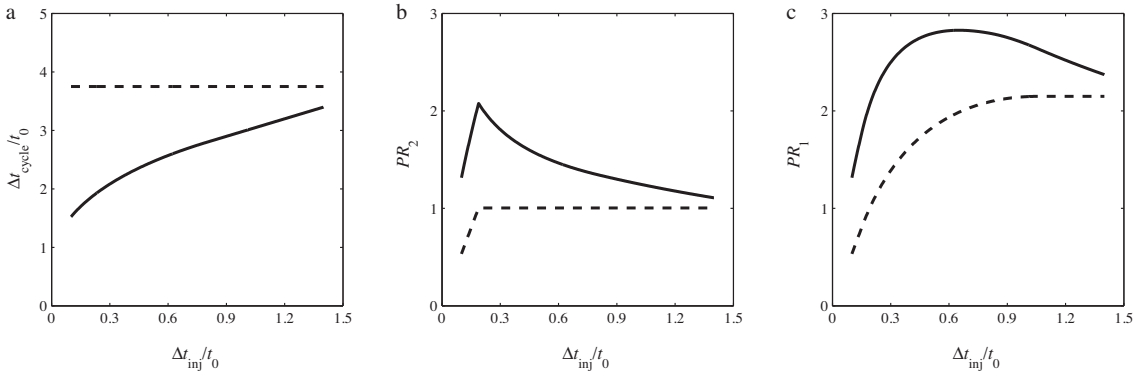

Fig. 4. Effect of the definition of the cycle time on the productivity. Solid lines: the cycle time is defined as $\Delta t_{cycle} = t_{E,2} - t_{R,1}$. Dotted lines: the cycle time is defined as $\Delta t_{cycle} = t^0_{E,2} - t_0$. Conditions: $c^F_1 = c^F_2 = 20$ g/L; $q_{m,1} = q_{m,2} = 100$ g/L; $b_1 = 0.02$ L/g; $b_2 = 0.025$ L/g; $F = 1/3$; $p^A = p^B = 0.98$.

In addition, it has been shown that the yield of the component 2 decreases when Δt_{inj} increases [10]. This means that the optimum duration of injection is always such that the yield of the second component is 100% and the cut time is equal to the retention time of the second shock.

For the first component, the amount of the product m^A_1 increases when Δt_{inj} increases [10]. This means that both the numerator and the denominator of Eq. (32) increase simultaneously. Hence, the analysis of the productivity of the first component is not as straightforward as for the second component. However, it can be shown that the productivity of the first component always goes through a maximum when Δt_{inj} increases. The maximum is achieved when the derivative of the productivity with respect to the Δt_{inj} is zero. An implicit expression for the zero point of the derivative is presented in Appendix B.

Because the derivative of the cycle time is greater than unity (see Eq. (37)), V_{eluent} increases with increasing Δt_{inj}. The minimum specific eluent consumption of the first component can be calculated by using a similar approach than for the maximum productivity. In addition, the yield decreases rapidly with Δt_{inj} [10]. For these reasons, the economic optimum might not be where the productivity is highest. Such calculations are beyond the scope of this work, however.

The influence of the definition of the cycle time on the productivity is illustrated in Fig. 4. The solid lines represent the definition used in this work, Eq. (34). The dashed lines are calculated by defining the cycle time as the corrected analytical retention time of the second component, as suggested by Golshan-Shirazi and Guiochon [10,11]. As seen in Fig. 4a, the definition used in this work gives significantly shorter cycle times than the other alternative and therefore higher productivities (Figs. 4b and c).

It is observed in Fig. 4b that the productivity of the second component first increases with increasing Δt_{inj} regardless the definition of the cycle time. In this region, the resolution between bands is so high that a portion of the pure first component fraction has to be collected in the product fraction B to fulfill the purity constraint. After the yield begins to fall below 100%, PR_2 levels off, if the cycle time is defined as the corrected analytical retention time of the second component. In contrast, with the definition of the cycle time used in this work, the larger the injection, the longer the cycle time is. The productivity of the second component thus decreases for large injections.

For the first component, both the maximum productivity and Δt_{inj} with which it is obtained differ significantly (Fig. 4c). In fact, when the cycle time is defined as the corrected analytical retention time of the second component, the productivity always increases with Δt_{inj} until it levels off as the injection becomes so large that t_{cut} is located on the feed plateau. This gives a misleading impression that excessively large injections should be preferred.

6.4. Effect of the total feed concentration on c^S_1, $t_{R,1}$ and Δt_{cycle}

In many practical applications, also the total feed concentration can be easily modified, for example by evaporating some of the solvent from the feed solution. The total feed concentration increases while the feed composition c^F_1/c^F_2 remains constant. In this case, an important practical problem is, whether a large volume of dilute sample or a small volume of concentrated sample, should be injected into the chromatography process to minimize the separation costs?

When the injected loading is held constant and the total feed concentration increased, the duration of injection decreases. The derivative of c^S_1 with respect to Δt_{inj} for given loading factors can be obtained from Eq. (16). The height of the first shock depends on the loading factors and the adsorption isotherm parameters only. It is interesting to note that c^S_1 is independent of Δt_{inj}, and thus also on the total feed concentration, at constant loading factors:

$$\left.\frac{\partial c^S_1}{\partial \Delta t_{inj}}\right|_{L_{f,1}, L_{f,2}} = 0 \tag{40}$$

The derivative of $t_{R,1}$ with respect to Δt_{inj} is obtained by differentiating Eq. (10), where $t = t_{R,1}$ and $c_1 = c^S_1$

$$\left.\frac{\partial t_{R,1}}{\partial \Delta t_{inj}}\right|_{L_{f,1}, L_{f,2}} = 1 \tag{41}$$

Although c^S_1 is independent of the duration of injection, $t_{R,1}$ increases linearly with it. This is because, in the case of constant loading factors, a larger injection volume means a lower feed concentration, which in turn means that the first shock travels at a lower velocity before the beginning of the shock erosion x_E.

By differentiating Eq. (34) it is observed that the cycle time is independent of the duration of injection for given loading. This is because both the derivative of $t_{E,2}$ and the derivative of $t_{R,1}$ with respect to Δt_{inj} are unity

$$\left.\frac{\partial t_{cycle}}{\partial \Delta t_{inj}}\right|_{L_{f,1}, L_{f,2}} = 0 \tag{42}$$

6.5. Effect of the total feed concentration on the process performance

When the loading factors are constant and the duration of injection decreases, the amount of the product increases due to enhanced displacement effect. This has been proven analytically for the second component [20] and can be shown analogically for the first component. Because the cycle time is independent of Δt_{inj}, the productivity of both the first and the second component must decrease as the duration of injection increases. At the same time, the yield of the target component decreases since less product is obtained with same loading. This means that both the maximum productivity and the maximum yield are always achieved when the duration of injection is as small as possible and the total feed concentration is as high as possible. In practice, this usually means that the process is operated at the solubility limit. The results are congruent with the observations that in most cases the concentration overloading is a more economic approach than the volume overloading [12].

In some cases, the improvement in the productivity and yield gained by removing solvent from the feed is counter-balanced by increase in the specific eluent consumption. This is because V_{eluent} increases when the feed concentrations increase as seen by differentiating the numerator of Eq. (33). According to numerical simulations, the specific eluent consumptions go through minimum or tend towards minimum when the feed concentrations tend towards infinity. However, although the cycle time is independent of Δt_{inj}, it is not straightforward to derive a closed form equation for the zero points of derivatives $\partial EC_i/\partial \Delta t_{inj}$. This is because the slope of the Γ_+ characteristic corresponding feed state and so the rear part of the chromatogram changes when the feed concentrations change. Implicit expressions are obtained by calculating $\partial EC_i/\partial \Delta t_{inj}$ as a function of Δt_{inj}.

7. Conclusions

For decades, there has been available an exact analytic solution of the ideal model of chromatography for binary Langmuir systems that allows analytic calculation of individual elution profiles, except for the height and retention time of the first shock in the case of a narrow injection pulse. In this work, the existing solution was completed by deriving the missing closed-form equations for the height and retention time of the first shock. It was thus shown that, for binary Langmuir systems, the individual concentration profiles at column outlet can be expressed entirely in closed-form.

The height of the first shock is obtained as a root of a quartic equation, which has only one positive root. Four algorithms were compared for solving the quartic. The Ferrari's algorithm was observed to be the most stabile one.

The trajectory of the first shock in distance–time plane was discussed briefly. It was shown that the time coordinate of the first shock in the physical plane can be expressed analytically as a function of the distance from the column inlet. In addition, a novel, simple parametric representation, which gives the trajectory of the first shock as a function of shock height c_1^S, was derived.

The practical relevance of the analytic equations giving c_1^S and $t_{R,1}$ was demonstrated by using them for optimization of batch chromatography process. It was shown that c_1^S increases and $t_{R,1}$ decreases with increasing duration of injection when the feed concentrations are constant. In addition, the derivative of the cycle time with respect to Δt_{inj} is always more than unity. For this reason, the maximum productivity of component 2 is achieved when the duration of injection is selected so that the purity constraint can be fulfilled by having 100% yield. For the first component, productivity goes through a maximum, for which an implicit expression was derived.

When the injected loadings are constant, $t_{R,1}$ decreases with increasing feed concentrations. In contrast, c_1^S and Δt_{cycle} are independent of them. The maximum productivities of the components are always obtained with maximum feed concentrations, which are usually limited by viscosity or solubility.

Nomenclature

a	Henry constant
A	coefficient of the quartic term in Eq. (17)
b	Langmuir parameter, L/mol or L/g
B	coefficient of the cubic term in Eq. (17)
c	mobile phase concentration, mol/L or g/L
c_1^A	concentration of the first component at the first component plateau, mol/L or g/L
$c_1^{A'}$	concentration of the first component at the front of the second component shock, mol/L or g/L
c_i^F	concentration of component i in feed, mol/L or g/L
c_1^M	concentration of the first component at the rear of the second component shock, mol/L or g/L
c_1^S	concentration of the first component at the top of the first component shock, mol/L or g/L
C	coefficient of the quadratic term in Eq. (17)
D	coefficient of the linear term in Eq. (17)
E	constant term in Eq. (17)
EC	specific eluent consumption, L/mol or L/g
F	phase ratio
k	coefficient of the linear term in Eq. (I.1)
L	column length, m
L_f	loading factor
L_f'	auxiliary parameter, $(1+\xi_+ b_1/b_2)L_{f,2}$
m	constant term in Eq. (I.1)
p^j	purity of fraction j with respect to a target component
Q	auxiliary parameter defined by Eq. (I.5)
q	stationary phase concentration, mol/L or g/L
q_m	saturation capacity of the adsorbent, mol/L or g/L
PR	productivity, mol/s or g/s
R	auxiliary parameter defined by Eq. (I.10)
res	relative residual
S	auxiliary parameter defined by Eq. (I.11)
T	auxiliary parameter defined by Eq. (I.12)
u	interstitial velocity, m/s
t	time, s
t_0	elution time of a non-retained component, s
t_{cut}	cut time, ending of the collection of the first fraction and beginning of the collection of the second fraction, s
$t_{E,1}$	retention time of the end of elution profile of the first component, s
$t_{E,2}$	retention time of the end of elution profile of the second component, s
$t_{R,1}$	retention time of the front shock of the first component, s
$t_{R,2}$	retention time of the front shock of the second component, s
V	volume, L
$\dot{V}$	flow rate, L/s
V_{eluent}	amount of eluent used in a chromatographic cycle, L
x	axial coordinate, m
Y	recovery yield
y	a root of Eq. (I.1)

Greek symbols

α	separation factor
β	auxiliary parameter, $\beta = 1 - 1/\alpha$
Γ	characteristic of a simple wave
γ	auxiliary parameter, $\gamma = (\alpha b_1 \xi_+ + b_2)/(b_1 \xi_+ + b_2)$

Δt_{cycle} cycle time, s
Δt_{inj} duration of a rectangular injection pulse, s
η auxiliary parameter defined by Eq. (B.6)
κ auxiliary parameter defined by Eq. (B.4)
λ auxiliary parameter defined by Eq. (B.5)
ξ_+ slope of Γ_+ characteristic corresponding feed state

Subscripts
1, 2 components to be separated

Appendix A.

In this appendix, it is shown that Eq. (16), and thus Eq. (17), has at most one positive real root and does not have any complex root with positive real part. For this purpose, Eq. (16) is rewritten as

$$f = L_{f,1}\left(1+\frac{1}{b_1 c_1^S}\right)^2 + L_{f,2}\left(1+\frac{1}{\alpha(1+b_1c_1^S)-1}\right)^2 - 1 = 0 \quad (A.1)$$

and f is differentiated with respect to c_1^S

$$\frac{\partial f}{\partial c_1^S} = -2b_1(1+b_1c_1^S)\left[\frac{L_{f,1}}{(b_1c_1^S)^3} + \frac{L_{f,2}}{\alpha(1-1/\alpha+b_1c_1^S)^3}\right] < 0 \quad (A.2)$$

The above derivative is always negative when $b_1 > 0$, $\alpha > 1$, $L_{f,1} > 0$, $L_{f,2} > 0$, and $c_1^S > 0$. This means that the left hand side of Eq. (16) is strictly decreasing when $c_1^S > 0$, and thus Eq. (16) has at most one positive real root.

The fact that Eq. (16) does not have any complex root with positive real part can be shown by setting $c_1^S = \mathrm{Re}(c_1^S) + \mathrm{Im}(c_1^S)$ in Eq. (16). When the terms of the resulting equation are arranged to real and imaginary parts, it is seen that the imaginary part is always unequal to zero when $\mathrm{Re}(c_1^S)$ is positive. This implies that the above statement is true and the right root of Eq. (16) is always the one having the largest real part.

Appendix B. Calculation of the maximum productivity of the first component

In this appendix, it is shown how to calculate the duration of injection that leads to the maximum productivity of the first component, providing that Δt_{inj} is located on the region where the first component plateau is eroded. The discussion is limited to case where the feed concentrations are fixed.

PR_1 tends towards zero, when Δt_{inj} tends towards zero or infinity. For this reason, the maximum productivity is always achieved when the derivative of the productivity with respect Δt_{inj} equals zero

$$\frac{\partial PR_1}{\partial \Delta t_{inj}} = \frac{\Delta t_{cycle}(\partial m_1^A/\partial \Delta t_{inj}) - m_1^A(\partial \Delta t_{cycle}/\partial \Delta t_{inj})}{(\Delta t_{cycle})^2} = 0 \quad (B.1)$$

The above derivative can be calculated explicitly as a function of c_1^S. The cycle time is given by

$$\Delta t_{cycle} = t_0 F a_1\left[\alpha - \frac{1}{(1+b_1c_1^S)^2}\right] + \frac{\beta a_1 c_2^F}{q_{m,2}(\beta+b_1c_1^S)^2}\Delta t_{inj} \quad (B.2)$$

and the mass of the first component in the product fraction A by

$$m_1^A = c_1^F \Delta t_{inj} - \lambda\left(\sqrt{\kappa+\eta\Delta t_{inj}}\right)^2 \quad (B.3)$$

with

$$\kappa = \frac{(1-p^A)}{p^A}\alpha\xi_+ \quad (B.4)$$

$$\lambda = \frac{F(\gamma-1)(a_2-a_1)}{b_1(1-\kappa)^2} \quad (B.5)$$

$$\eta = \frac{\alpha b_2(1-\kappa)(((1-p^A)/p^A)c_1^F - c_2^F)}{F(a_2-a_1)(\gamma-1)} \quad (B.6)$$

For the duration of injection, the following expression is obtained from Eq. (16)

$$\Delta t_{inj} = \frac{t_0 F}{(c_1^F/q_{m,1})(1+(1/b_1c_1^S))^2 + (c_2^F/q_{m,2})((1+b_1c_1^S)/(\beta+b_1c_1^S))^2} \quad (B.7)$$

The derivate of the cycle time is obtained by differentiating Eq. (B.2)

$$\frac{\partial \Delta t_{cycle}}{\partial \Delta t_{inj}} = \frac{(t_0Fa_1/\Delta t_{inj})[(t_0F/\Delta t_{inj}(1+b_1c_1^S)^3) - (\beta c_2^F/q_{m,2}(\beta+b_1c_1^S)^3)]}{(1+b_1c_1^S)[(c_1^F/q_{m,1}(b_1c_1^S)^3) + (c_2^F/q_{m,2}\alpha(\beta+b_1c_1^S)^3)]} + \frac{\beta a_1 c_2^F}{q_{m,2}(\beta+b_1c_1^S)^2} \quad (B.8)$$

and the derivative of m_1^A by differentiating Eq. (B.3)

$$\frac{\partial m_1^A}{\partial \Delta t_{inj}} = c_1^F - \lambda\left(\eta - \frac{\eta}{\sqrt{\kappa+\eta\Delta t_{inj}}}\right) \quad (B.9)$$

Eq. (B.1) remains implicit with respect to c_1^S and must be solved numerically. Once c_1^S is obtained, the corresponding Δt_{inj} is calculated from Eq. (B.7). If Eq. (B.1) has no roots between 0 and c_1^A, the maximum productivity lies on the region where the first component plateau is not eroded.

Appendix C. Supplementary data

A Matlab code that calculates individual concentration profiles at column outlet analytically, to be used for non-commercial purposes, can be obtained from the publisher's website. Use command `ideal_model_binary_Langmuir(help);` to display instructions. The code requires Matlab version 7.5 (Matlab R2007b) or newer to run.

Supplementary data associated with this article can be found, in the online version, at doi:10.1016/j.chroma.2011.07.004.

References

[1] F. Helfferich, G. Klein, Multicomponent Chromatography. Theory of Interference , Marcel Dekker, New York, 1970.
[2] D. Devault, J. Am. Chem. Soc. 65 (1943) 532.
[3] E. Glueckauf, Discuss. Faraday Soc. 7 (1949) 12.
[4] H.-K. Rhee, R. Aris, N.R. Amundson, Philos. Trans. R. Soc. Lond. Ser. A 267 (1970) 419.
[5] S. Golshan-Shirazi, G. Guiochon, J. Phys. Chem. 93 (1989) 4143.
[6] S. Golshan-Shirazi, G. Guiochon, J. Chromatogr. 484 (1989) 125.
[7] H.-K. Rhee, R. Aris, N.R. Amundson, First-Order Partial Differential Equations. Theory and Application of Single Equations, vol. I, Dover Publications, New York, 2001.
[8] H.-K. Rhee, R. Aris, N.R. Amundson, First-Order Partial Differential Equations. Theory and Application of Hyperbolic Systems of Quasilinear Equations, vol. II, Dover Publications, New York, 2001.
[9] A. Rajendran, M. Mazzotti, Ind. Eng. Chem. Res. 50 (2011) 352.
[10] S. Golshan-Shirazi, G. Guiochon, Anal. Chem. 61 (1989) 1276.
[11] S. Golshan-Shirazi, G. Guiochon, Anal. Chem. 61 (1989) 1368.
[12] G. Guiochon, A. Felinger, D.G. Shirazi, A.M. Katti, Fundamentals of Preparative and Nonlinear Chromatography , 2nd ed., Academic Press, Amsterdam, 2006.
[13] T. Sainio, M. Kaspereit, Sep. Purif. Technol. 66 (2009) 9.
[14] G. Storti, M. Mazzotti, M. Morbidelli, S. Carra, AIChE J. 39 (1993) 471.
[15] M. Kaspereit, A. Seidel-Morgenstern, A. Kienle, J. Chromatogr. A 1162 (2007) 2.
[16] A. Rajendran, W. Chen, Sep. Purif. Technol. 67 (2009) 344.
[17] W.H. Beyer (Ed.), CRC Standard Mathematical Tables, CRC Press, Boca Raton, Florida, 2000.
[18] R.S. Burington, Handbook of Mathematical Tables and Formulas , 5th ed., McGraw-Hill, New York, 1973.
[19] S. Neumark, Solution of Cubic and Quartic Equations , Pergamon Press, Oxford, 1965.
[20] J. Siitonen, T. Sainio, M. Kaspereit, Sep. Purif. Technol. 78 (2011) 21.

Article III

Journal of Chromatography A, 1286 (2013) 55–68

Contents lists available at SciVerse ScienceDirect

Journal of Chromatography A

journal homepage: www.elsevier.com/locate/chroma

Design of batch chromatography for separation of binary mixtures under reduced purity requirements

Jani Siitonen [a], Tuomo Sainio [a,*], Arvind Rajendran [b]

[a] Lappeenranta University of Technology, Skinnarilankatu 34, FI-53850 Lappeenranta, Finland
[b] University of Alberta, Department of Chemical and Materials Engineering, 9107 - 116 Street, Edmonton, Alberta, Canada T6G 2V4

ARTICLE INFO

Article history:
Received 15 July 2012
Received in revised form 28 January 2013
Accepted 18 February 2013
Available online 26 February 2013

Keywords:
Batch chromatography
Binary separation
Equilibrium theory
Process design
Reduced purity

ABSTRACT

Two methods are presented for designing separation of binary mixtures in a batch chromatography column under reduced purity requirements such that no waste or recycle fractions are generated. The first one is based on the equilibrium theory of chromatography and requires adsorption isotherm parameters. The second one is a shortcut method that uses a single experimental or simulated design chromatogram as input and is recommended under strongly non-ideal conditions with significant dispersive effects. Both approaches allow prediction of the injection volume and the cut position that lead to given target purities. In principle, they apply for all systems with convex or concave isotherms. The applicability of the design methods is evaluated by using numerical simulations. Both design methods work the better the higher the column efficiency and the lower the purity constraints are.

1. Introduction

Preparative liquid chromatography is a highly developed technique applied successfully to numerous difficult separation tasks in the pharmaceutical, fine chemical and food industries. Typical examples are production of enantiomers, other isomers, sugars and proteins either into intermediate or final products [1].

For separation of a binary mixture into two products with given purities by batch chromatography, there exist two fundamentally different operation and fraction collection strategies. The first option (strategy I) aims at high productivity or low eluent consumption by using high column overloading. The two product fractions are collected from the front and the rear parts of the chromatogram such that their purity requirements are satisfied. The mixed band, eluting between them, is either wasted or recycled. In the second option (strategy II), generation of waste or recycle fraction is not allowed. The column overload is limited such that the effluent can be fractionated by a single cut into two product fractions whose purity requirements are satisfied.

The task in process design is to find the injection volume and cut times that yield the desired separation. Most of the design and optimization methods developed for batch chromatography apply for the cutting strategy I [2,3]. This is understandable because, when no yield constraints are set, strategy I often provides higher productivity than strategy II (see *e.g.* [4]). However, when high recovery yield is desired, the strategy II is preferred. Moreover, when the performance of conventional batch chromatography is compared with those of different recycling and simulated moving bed (SMB) schemes, that do not generate waste streams, it is necessary that disposal of a waste fraction is not allowed in batch mode either. It is also necessary that the purity constraints are matched exactly in such comparative studies in order to avoid misleading conclusions [5].

In the case of the purification strategy II, the available design approaches are limited to complete separations, *i.e.* operation with touching bands [6,7]. In contrast, for separation problems where two product fractions with reduced purities are required without waste streams, no straightforward design methods have been presented.

In this work, design methods are developed for chromatographic separation of a binary mixture into two products with given target purities in a batch column without generation of waste or recycle streams. Moreover, the same methods are applicable when only one product fraction with given purity and yield constraints is target. Both the limiting case of ideal conditions and the more practical case of non-ideal conditions are discussed. The approaches employed here allow prediction of the injection volume and the cut time for arbitrary purity requirements, and are applicable for all systems that follow convex or concave isotherm models. The

* Corresponding author. Tel.: +358 40 3578683.
E-mail address: tuomo.sainio@lut.fi (T. Sainio).

0021-9673/$ – see front matter © 2013 Elsevier B.V. All rights reserved.
http://dx.doi.org/10.1016/j.chroma.2013.02.051

predictions are exact under ideal conditions and approximate in the general case.

This contribution is organized as follows. After a short summary of basic theoretical fundamentals, the equilibrium theory of chromatography is applied to derive a design method under ideal conditions. Analytical design equations are provided for systems that follow Langmuir or anti-Langmuir isotherm models. Thereafter, the scope of the approach is extended to more realistic systems with significant dispersive effects. In that case, estimates for the injection volume and the cut time that lead to given target purities are obtained by applying a simple procedure to a single conventional chromatogram. Finally, the applicability of the methods is demonstrated by using numerical simulation with three case studies.

2. Theoretical background

2.1. Purification strategy

In the following discussion, it is assumed that a rectangular pulse of a binary mixture is injected to an initially clean column and then eluted in isocratic mode. The pulse is separated into two product fractions by one cut so that no waste or recycle streams are generated. The design task is to choose the injection volume, V_{inj}, and relevant cut time, t_{cut}, such that user-given purity requirements are fulfilled (see Fig. 1). The desired purities are used as design constrains and are defined as follows

$$p_1^A = \frac{m_1^A}{m_1^A + m_2^A} = \frac{\int_{t_{R1}}^{t_{cut}} c_1\,dt}{\int_{t_{R1}}^{t_{cut}} (c_1 + c_2)\,dt} \tag{1}$$

$$p_2^B = \frac{m_2^B}{m_1^B + m_2^B} = \frac{\int_{t_{cut}}^{t_{E2}} c_2\,dt}{\int_{t_{cut}}^{t_{E2}} (c_1 + c_2)\,dt} \tag{2}$$

where m_i^j is the amount of component $i = (1, 2)$ in the product fraction $j = (\mathrm{A}, \mathrm{B})$, t_{R1} is the beginning of the elution profile of the first component, t_{cut} is the cut time, and t_{E2} is the end of the elution profile of the second component.

As an alternative to employing purities as a design constraint, the yields of the components in the target fractions can be specified. Because no waste streams are allowed, the purity and yield requirements are interchangeable [8]

$$Y_1 = \frac{m_1^A}{m_1^F} = \frac{p_1^A}{p_1^F}\frac{p_1^F + p_2^B - 1}{p_1^A + p_2^B - 1} \tag{3}$$

$$Y_2 = \frac{m_2^B}{m_2^F} = \frac{p_2^B}{1 - p_1^F}\frac{p_1^A - p_1^F}{p_1^A + p_2^B - 1} \tag{4}$$

where p_1^F is defined as the purity of component 1 in feed: $p_1^F = c_1^F/(c_1^F + c_2^F)$. In other words, by specifying any two of the four constraints in Eqs. (1)–(4), the remaining two are also fixed. This means that the design methods developed below are applicable also when there is only one target component (either the more or the less strongly absorbed one) whose purity and yield requirements are given.

2.2. Modeling of chromatographic column

In this work, the following two chromatography models are considered: the equilibrium model and the transport-dispersive model. The first one holds under ideal conditions and is applied to derive the design method for infinite efficiency systems (Section 3.1). The second model is employed only for evaluation of the design approaches (Sections 3.2.2 and 4). It is not required for application of the methods.

2.2.1. Equilibrium theory of chromatography

The equilibrium model follows by neglecting any dispersive effects and by assuming local adsorption equilibrium. The mass balances for individual components are given by

$$\frac{\partial c_i}{\partial t} + u\frac{\partial c_i}{\partial x} + \phi\frac{\partial q_i^{eq}}{\partial t} = 0 \quad (i = 1, 2) \tag{5}$$

where c_i is the fluid phase concentration of solute i, q_i^{eq} is the stationary phase concentration that is in equilibrium with the fluid phase, $\phi = (1 - \varepsilon)/\varepsilon$ is the phase ratio, with ε being the total void fraction of the bed, u is the interstitial velocity, t is the time, and x is the column axial coordinate.

The design principles derived in the following sections are not limited to a specific adsorption isotherm type, but are valid for all convex (favorable) and concave (unfavorable) isotherms for which no inflection points or selectivity reversal exist. Analytic design equations under ideal conditions are derived for competitive Langmuir and anti-Langmuir isotherms

$$q_i^{eq} = \frac{N_i K_i c_i}{1 + p_1 K_1 c_1 + p_2 K_2 c_2} \tag{6}$$

where $p_1 = p_2 = 1$ for Langmuir isotherm and $p_1 = p_2 = -1$ for anti-Langmuir isotherm. N_i and K_i are the saturation capacity and the equilibrium parameter of solute i, respectively. In the following discussion, it is assumed that component 1 is the less strongly adsorbed one. This means that $H_2 > H_1$, where $H_i = N_i K_i$ is the Henry constant of component i. Moreover, only the compositions yielding to a finite positive stationary phase concentration are physically meaningful. The (c_1, c_2) domain of interest is thus defined by $c_1 \geq 0$, $c_2 \geq 0$, and $1 + p_1 K_1 c_1 + p_2 K_2 c_2 > 0$.

To solve the model Eqs. (5) and (6), proper initial and boundary conditions are needed. In this work, it is assumed that a rectangular pulse of binary mixture with known duration, Δt_{inj}, is first injected to an initially clean column and then eluted. In this case, the initial and boundary conditions of Eq. (5) are

$$c_i(x, t = 0) = 0 \quad \text{for} \quad 0 \leq x \leq L \tag{7}$$

$$c_i(x = 0, t) = c_i^F \quad \text{for} \quad 0 \leq t \leq \Delta t_{inj} \tag{8}$$

$$c_i(x = 0, t) = 0 \quad \text{for} \quad t > \Delta t_{inj} \tag{9}$$

where L is the column length and c_i^F is the concentration of component i in feed.

The model represents a system of two homogeneous quasi-linear partial differential equations. When Riemann boundary conditions are used, the model can be solved analytically by the method of characteristics. The fundamentals of the solution are described extensively in literature [9–13]. The most relevant aspects needed in this work are summarized in Appendix A. Examples of the solution at column outlet are given in Fig. 1.

2.2.2. Transport-dispersive model

The solid film linear driving force model (LDF) is employed in the transport-dispersive model to describe the effect of finite mass transfer rate. The component mass balances are given by

$$\frac{\partial c_i}{\partial t} + u\frac{\partial c_i}{\partial x} + \phi\frac{\partial q_i}{\partial t} = D_{ax}\frac{\partial^2 c_i}{\partial x^2} \tag{10a}$$

$$\frac{\partial q_i}{\partial t} = k_i(q_i^{eq} - q_i) \tag{10b}$$

where D_{ax} is the axial dispersion coefficient and k_i is the mass transfer coefficient of component i. The initial condition of Eq. (10) is again given by Eq. (7). In addition, the following Danckwerts boundary conditions are used

$$\left.\frac{\partial c_i}{\partial x}\right|_{x=0} = \frac{u(c_i - c_i^0)}{D_{ax}} \tag{11}$$

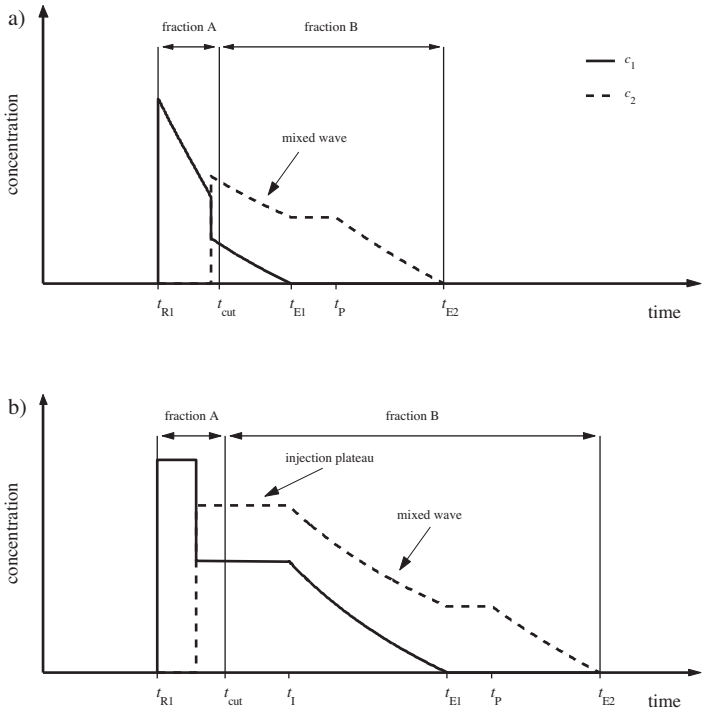

Fig. 1. Individual elution profiles under ideal conditions for an arbitrary system that follows Langmuir isotherm and fraction collection in conventional batch chromatography (strategy II): (a) small injection; (b) large injection.

$$\left.\frac{\partial c_i}{\partial x}\right|_{x=L} = 0 \tag{12}$$

where $c_i^0 = c_i^F$ for $0 \le t \le \Delta t_{inj}$ and $c_i^0 = 0$ for $t > \Delta t_{inj}$.

In addition to Langmuir and anti-Langmuir isotherms, Eq. (6), the competitive bi-Langmuir model is applied to demonstrate the validity of the design approaches. It assumes two energetically different interaction sites *I* and *II* of the Langmuir-type

$$q_i^{eq} = \frac{N_i^I K_i^I c_i}{1 + K_1^I c_1 + K_2^I c_2} + \frac{N_i^{II} K_i^{II} c_i}{1 + K_1^{II} c_1 + K_2^{II} c_2} \quad (i = 1, 2) \tag{13}$$

The model equations were implemented in Matlab and solved by using Matlab's ODE solver. The axial dispersion term was approximated numerically by the step size in the spatial discretization.

3. Design of batch chromatography

In this section, two design methods for finding relevant V_{inj} and t_{cut} that lead to given target purities are derived. The first one is based on the equilibrium theory of chromatography and holds under ideal conditions without dispersive effects. It is similar to that used by Golshan-Shirazi and Guiochon [2] for systems with Langmuir isotherm in a special case where only the second component is the target. A similar method was also used by Sainio and Kaspereit [14] to design mixed-recycle steady state recycling chromatography (MR-SSR), by Siitonen et al. [16] to design MR-SSR with an integrated solvent removal unit, and by Siitonen et al. [17] to design bypass chromatography. In this work, however, the approach is applied to batch separations where two product fractions without generation of waste or recycle fractions are desired. In addition, the method presented below is applicable for cases where only one component with given purity and yield constraints is target. The focus is on a demonstrative derivation of the method that is generally valid for all systems that follow convex or concave adsorption isotherm models. Moreover, as opposed to previous works, the complete sets of design equations are provided both for Langmuir isotherm (Table 1) and for anti-Langmuir isotherm (Table 2). Detailed derivations of these equations are given in Appendices B and C, respectively.

The second approach applies to more realistic conditions with finite column efficiency. It uses a single chromatogram as input and can be considered as an extension of the method developed by Kaspereit and Sainio [15] to obtain approximate injection volumes and cut times for MR-SSR under non-ideal conditions.

3.1. Design under ideal conditions

3.1.1. Design method for convex isotherms

It is commonly known that for systems with convex isotherms, *e.g.* competitive Langmuir isotherm, the shape of the rear part of the chromatogram remains basically unaltered when the injection width changes [12,14]. It is only linearly shifted in time by the duration of the injection, Δt_{inj}, as displayed in Fig. 2a. This observation provides the basis for starting the design by determining the cut point such that the purity constraint of the second fraction is fulfilled. For this purpose, Eq. (2) is rewritten in terms of the elution time relative to end of the injection, $\tau = t - \Delta t_{inj}$, as follows

$$p_2^B = \frac{\int_{\tau_{cut}}^{\tau_{E2}} c_2 \, d\tau}{\int_{\tau_{cut}}^{\tau_{E2}} (c_1 + c_2) \, d\tau} \tag{14}$$

Table 1
Design equations of batch chromatography for competitive Langmuir isotherm model.

Purity of the second fraction when the cut point is located at the end of the feed plateau

$$p_{2,limit}^{B} = \left(1 + \frac{p_1^F}{1-p_1^F}\frac{H_1-\omega_1^F}{H_2-\omega_1^F}\right)^{-1} \quad (I.1)$$

The cut point is located on the mixed wave, $p_2^B > p_{2,limit}^B$

$$\lambda = \sqrt{\frac{1-p_2^B}{p_2^B}\frac{K_1H_1(H_2-\omega_2^F)}{K_2H_2(\omega_2^F-H_1)}} \quad (I.2)$$

$$\omega_1^{cut} = \frac{H_1-H_2\lambda}{1-\lambda} \quad (I.3)$$

$$\tau_{cut} = \left[1 + \frac{\phi(\omega_1^{cut})^2\omega_2^F}{H_1H_2}\right]t_0 \quad (I.4)$$

$$V_{inj} = \frac{(1-\varepsilon)(H_2-\omega_2^F)(H_2-\omega_1^{cut})^2}{K_2H_2(H_2-H_1)c_2^FY_2}V_{col} \quad (I.5)$$

The cut point is located on the feed plateau, $p_2^B \le p_{2,limit}^B$

$$\tau_I = \left[1 + \frac{\phi(\omega_1^F)^2\omega_2^F}{H_1H_2}\right]t_0 \quad (I.6)$$

$$m_1^{tail} = \frac{(1-\varepsilon)(\omega_2^F-H_1)(H_1-\omega_1^F)^2}{K_1H_1(H_2-H_1)}V_{col} \quad (I.7)$$

$$m_2^{tail} = \frac{(1-\varepsilon)(H_2-\omega_2^F)(H_2-\omega_1^F)^2}{K_2H_2(H_2-H_1)}V_{col} \quad (I.8)$$

$$\tau_{cut} = \tau_I - \frac{m_2^{tail} - [p_2^B/(1-p_2^B)]m_1^{tail}}{[p_2^B/(1-p_2^B)]c_2^F - c_1^F}\frac{1}{Q} \quad (I.9)$$

$$V_{inj} = \frac{(\tau_I-\tau_{cut})c_2^FQ + m_2^{tail}}{c_2^FY_2} \quad (I.10)$$

The fractionation time, τ_{cut}, that satisfies the purity constraints is obtained by finding the lower integration limit that satisfies Eq. (14). Depending on the purity constraint of the product fraction B, there exist two possibilities for the location of the cut point. When p_2^B is high, the cut point is located on the mixed wave (Fig. 1a) but for sufficiently low p_2^B it lies on the injection plateau (Fig. 1b). The limit for these two cases, $p_{2,limit}^B$, is obtained from Eq. (14) by setting

Table 2
Design equations of batch chromatography for competitive anti-Langmuir isotherm model.

Purity of the first fraction when the cut point is located at the front of the feed plateau

$$p_{1,limit}^{A} = \left(1 + \frac{1-p_1^F}{p_1^F}\frac{(\omega_2^F-H_2)}{(\omega_2^F-H_1)}\right)^{-1} \quad (II.1)$$

The cut point is located on the mixed wave, $p_1^A > p_{1,limit}^A$

$$\kappa = \sqrt{\frac{1-p_1^A}{p_1^A}\frac{K_2H_2(\omega_1^F-H_1)}{K_1H_1(H_2-\omega_1^F)}} \quad (II.2)$$

$$\omega_2^{cut} = \frac{H_2-H_1K}{1-K} \quad (II.3)$$

$$t_{cut} = \left[1 + \frac{\phi\omega_1^F(\omega_2^{cut})^2}{H_1H_2}\right]t_0 \quad (II.4)$$

$$V_{inj} = \frac{(1-\varepsilon)(\omega_1^F-H_1)(\omega_2^{cut}-H_1)^2}{K_1H_1(H_2-H_1)c_1^FY_1}V_{col} \quad (II.5)$$

The cut point is located on the feed plateau, $p_1^A \le p_{1,limit}^A$

$$t_I = \left(1 + \frac{\phi\omega_1^F(\omega_2^F)^2}{H_1H_2}\right)t_0 \quad (II.6)$$

$$m_1^{front} = \frac{(1-\varepsilon)(\omega_1^F-H_1)(\omega_2^F-H_1)^2}{K_1H_1(H_2-H_1)}V_{col} \quad (II.7)$$

$$m_2^{front} = \frac{(1-\varepsilon)(H_2-\omega_1^F)(\omega_2^F-H_2)^2}{K_2H_2(H_2-H_1)}V_{col} \quad (II.8)$$

$$t_{cut} = t_I + \frac{m_1^{front} - [p_1^A/(1-p_1^A)]m_2^{front}}{[p_1^A/(1-p_1^A)]c_2^F - c_1^F}\frac{1}{Q} \quad (II.9)$$

$$V_{inj} = \frac{(t_{cut}-t_I)c_1^FQ + m_1^{front}}{c_1^FY_1} \quad (II.10)$$

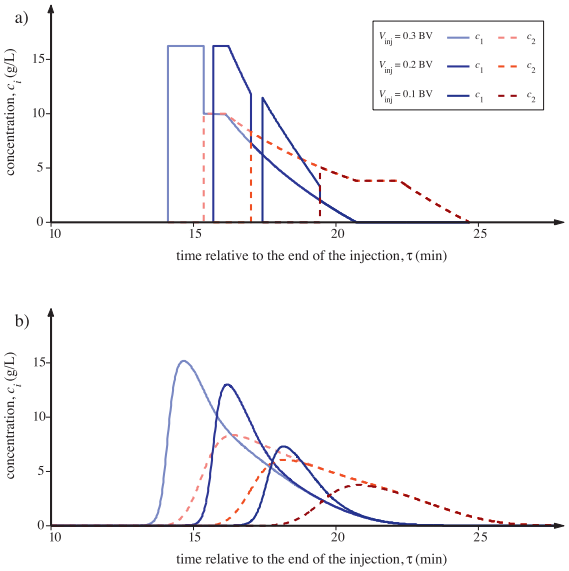

Fig. 2. Effect of injection volume on the elution profiles of a system that follows Langmuir isotherm model. *Isotherm parameters*: K_1 = 0.020 L/g, K_2 = 0.025 L/g, $N_1 = N_2$ = 100 g/L. *Feed concentrations*: $c_1^F = c_2^F$ = 10 g/L. Void fraction, ε = 0.63. Retention time of a non-retained component, t_0 = 10 min: (a) ideal conditions; (b) non-ideal conditions, *NTP* = 500.

$\tau_{cut} = \tau_I$ with τ_I being the end of the injection plateau. In the case of Langmuir isotherm, the design is based on Eqs. (I.4) and (I.5) when $p_2^B > p_{2,limit}^B$, otherwise Eqs. (I.9) and (I.10) are used.

Once the cut time τ_{cut} is obtained, also the amount of the product fraction B is known from the backward integration. The injection volume is solved from the global mass balance of the second component. Because no waste streams are allowed, the resulting expression for V_{inj} is

$$V_{inj} = \Delta t_{inj}Q = \frac{Q\int_{\tau_{cut}}^{\tau_{E2}} c_2\,d\tau}{c_2^FY_2} \quad (15)$$

where Q is the volumetric flow rate. Y_2 can be calculated from the purity constraints as shown in Eq. (4).

As a last step, the cut time in terms of elution time relative to the beginning of the injection is calculated as follows

$$t_{cut} = \tau_{cut} + \Delta t_{inj} = \tau_{cut} + \frac{V_{inj}}{Q} \quad (16)$$

3.1.2. Design method for concave isotherms

In the case of concave isotherms, *e.g.* anti-Langmuir isotherm, the front of the chromatogram is independent of the injection width (Fig. 3a). It is not even shifted in time but the fronts of the elution profiles are identical in terms of time relative to the beginning of the injection. Consequently, for concave isotherms, an analogous but opposite design approach compared to the case of convex isotherms is used.

At first, the cut time is solved by searching the point where the purity constraint of the product fraction A is fulfilled, *i.e.* the upper integration limit that satisfies Eq. (1). Again, there exist two possibilities for the location of the cut point. When p_1^A is sufficiently high, the cut point is located on the mixed wave. In the case of anti-Langmuir isotherm, the design is based on Eqs. (II.4) and (II.5). For low p_1^A, on the other hand, the cut point lies on the injection plateau, and Eqs. (II.9) and (II.10) are used. The limit for these cases

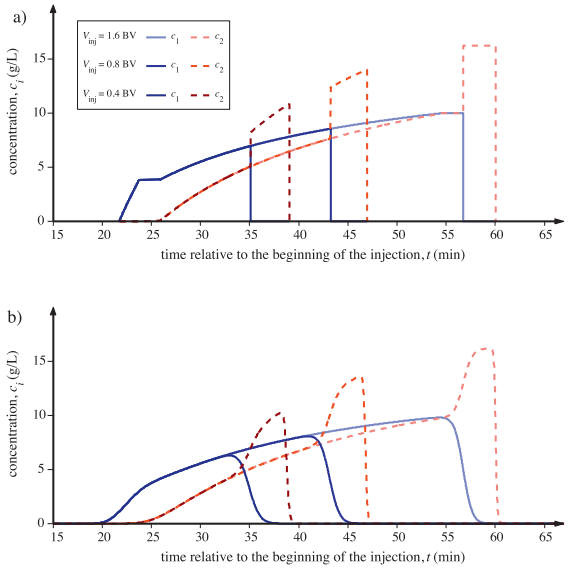

Fig. 3. Effect of injection volume on the elution profiles of a system that follows anti-Langmuir isotherm model. Isotherm parameters: K_1 = 0.020 L/g, K_2 = 0.025 L/g, $N_1 = N_2$ = 100 g/L. *Feed concentrations*: $c_1^F = c_2^F$ = 10 g/L. Void fraction, ε = 0.63. Retention time of a non-retained component, t_0 = 10 min: (a) ideal conditions; (b) non-ideal conditions, *NTP* = 500.

is obtained by integrating the front of the chromatogram from the beginning of the elution profile of the first component, t_{R1}, to the beginning of the injection plateau, t_I

$$p_{1,limit}^A = \frac{\int_{t_{R1}}^{t_I} c_1\, d\tau}{\int_{t_{R1}}^{t_I} (c_1 + c_2)\, d\tau} \tag{17}$$

As a second step, the injection volume is solved from the global mass balance of the first component. The resulting expression is given by

$$V_{inj} = \Delta t_{inj} Q = \frac{Q \int_{t_{R1}}^{t_{cut}} c_1\, d\tau}{c_1^F Y_1} \tag{18}$$

where Y_1 is obtained from Eq. (3).

3.1.3. Validation of the design equations

The validity of the explicit design equations derived for the Langmuir isotherm was verified with the software described in Ref. [13], which calculates the entire chromatogram using explicit equations. Verification of the design equations for the anti-Langmuir isotherm was done by using the analytical solutions described in Ref. [12]. The validation was carried out by applying various purity constraints (0.6–1.0) and separation factors $\alpha = H_2/H_1$ (1.1–3.0) such that both the cases where the cut point is located on the mixed wave and those where it lies on the injection plateau were covered.

For each set of isotherm parameters and purity constraints, relevant V_{inj} and t_{cut} were first calculated by using the design equations given in Tables 1 and 2. The analytic solution of the ideal model was then applied to construct the individual elution profiles with obtained V_{inj}. Finally, the purities of the product fractions were calculated by integrating the chromatogram numerically with trapezoidal rule.

In all simulations, the injection volume and the cut time predicted with the design equations were observed to lead to the target purities. The deviation between achieved p_1^A and p_2^B values and the purity constraints, caused by numerical integration of the profile by trapezoidal rule, was always less than 10^{-6} confirming the validity of the design method.

3.2. Design under non-ideal conditions

3.2.1. Design principle

In principle, the equilibrium design method presented above can be employed also in the non-ideal case to obtain rough estimates for the injection volume and cut time. The accuracy of the estimates depends on the amount of dispersion, isotherm type, and concentration levels. This is because under non-ideal conditions the rear part of the chromatogram in the case of convex isotherms and the front of the chromatogram in the case of concave isotherms are not fully independent of the injection volume. However, the variation is often relatively small over a wide range of injection widths as seen in Figs. 2b and 3b.

Based on the above observation, V_{inj} and t_{cut} can be estimated by measuring or simulating a single "design chromatogram" with a relative large injection volume (the choice of V_{inj} for the design chromatogram is discussed in Section 3.2.2). If an experimental chromatogram is used, it must be decomposed into the individual concentration profiles but no isotherm parameters or model is required. In the case of simulation, the approach is independent of the used model, *i.e.* whichever chromatographic model that takes account dispersive effects (*e.g.* equilibrium-dispersive model, transport-dispersive model, general rate model) can be applied. The design chromatogram is applicable for a given column efficiency. A new chromatogram must be generated when the column efficiency changes significantly due to a change in the flow rate or the column dimensions.

Estimates for V_{inj} and t_{cut} are obtained from the design chromatogram by using a similar approach as in the ideal case. In the case of convex isotherms, the cut time relative to the end of the injection is first solved by integrating the chromatogram backwards to find the lower integration limit that satisfies Eq. (14). The procedure is independent of whether the injection point is located on the mixed wave or on the injection plateau, *i.e.* the value of p_2^B. Once the cut point is solved, also the amount of the product fraction B is known from the backward integration. The relevant injection volume is then calculated from the mass balance of the second component, Eq. (15). For concave isotherms, an analogous but opposite approach is again applied as described in Section 3.1.2.

3.2.2. Choice of the injection volume for the design chromatogram

The task of selecting the injection volume for the design chromatogram, V_{inj}^{design}, was investigated by performing numerical simulations. Separation of Tröger's base enantiomers, whose phase equilibrium can be described by competitive Langmuir isotherm model [18], was used as a model case. The isotherm and kinetic parameters of the system are given in Table 3 (system 1).

In the simulation study, several design chromatograms were simulated with different injection volumes by using the transport-dispersive model. From each design chromatogram, estimations for the injection volume and the cut time, V_{inj}^{est} and t_{cut}^{est}, were predicted by the method described in Section 3.2.1. The correct values of the injection volume and the cut time, V_{inj}^* and t_{cut}^*, were calculated as references by using Matlab's *fzero* function to search V_{inj} and t_{cut} that lead to given target purities. The accuracies of the predictions were assessed as relative errors defined as

$$\delta V_{inj} = \frac{V_{inj}^{est} - V_{inj}^*}{V_{inj}^*} 100\% \tag{19}$$

Table 3
Parameters for the model systems.

Parameter	System 1	System 2	System 3
Column length, L (cm)	25	25	25
Column diameter, D_{col} (cm)	1.0	1.0	1.0
Total void fraction of the bed, ε	0.63	0.63	0.63
Volumetric flow rate, Q (mL/min)	0.7	0.7	0.7
Axial dispersion coefficient, D_{ax} (cm^2/min)	0.012	0.012	0.012
Mass transfer coefficients, $k_1 = k_2$ (min^{-1})	2.988–86.70	1.152–33.48	2.928–84.86
Number of theoretical stages for component 1, NTP	100–1000	100–1000	100–1000
Isotherm model	Langmuir	Bi-Langmuir	Anti-Langmuir
Isotherm parameters			
K_1 or K_1^I (L/g)	0.065[a]	0.0247[b]	0.025
K_2 or K_2^I (L/g)	0.39[a]	0.0421[b]	0.074
N_1 or N_1^I (g/L)	33.54[a]	272.5[b]	100
N_2 or N_2^I (g/L)	16.54[a]	318.0[b]	100
K_1^{II} (L/g)	–	0.3429[b]	–
K_2^{II} (L/g)	–	1.1159[b]	–
N_1^{II} (g/L)	–	22.10[b]	–
N_2^{II} (g/L)	–	25.78[b]	–

[a] Value from [18]
[b] Value from [15].

$$\delta t_{cut} = \frac{t_{cut}^{est} - t_{cut}^{*}}{t_{cut}^{*}} 100\% \quad (20)$$

The choice of the injection volume for the design chromatogram is demonstrated in Fig. 4. When V_{inj}^{design} is relatively small, the injection volume predicted by the design method increases with increasing injection volume. In this region, the amount of component 2 that is injected into the column is less than what could be collected to fraction B by using V_{inj}^{*}. For this reason, the design method predicts too low values for the injection volume, and the purities of the components are higher than required.

When V_{inj}^{design} is larger than or equal to V_{inj}^{*} (point where $\delta V_{inj} = 0$), the predicted injection volume and cut time are almost independent of V_{inj}^{design}. This is because the shape of the rear part of chromatogram, and hence the composition of the fraction B remains nearly constant when the injection volume varies. This means that relatively large injection volume should be preferred as V_{inj}^{design}. The only exception is observed when the column efficiency is very low ($NTP_1 = 100$) and the purity constraints are high ($p_1^A = p_2^B = 0.99$). In this case, the dispersive effects are so strong and the correct injection volume is so small that the assumption of invariant shape of the rear of the chromatogram is not valid. The predicted injection volume is thus systematically too large (see also Tables 4–6 in Section 4).

It is also observed that the injection volume predicted by the ideal model (circles in Fig. 4) is always slightly larger than V_{inj}^{*} because dispersive effects are neglected. For this reason, the equilibrium based design method provides a very useful guess for V_{inj}^{design}.

In summary, when the isotherm parameters are known and the system follows Langmuir or anti-Langmuir adsorption model (for which explicit solutions of the ideal model are available) it is recommended to use the equilibrium theory based design method to calculate a suitable injection volume for the design chromatogram. In other cases, large injection volume for which the injection plateau prevails is preferred.

4. Evaluation of the design methods

To evaluate the applicability of the design methods for designing real chromatographic separations, that involve dispersive effects due to mass-transfer resistances, axial dispersion, *etc.*, numerical simulations were carried out by using the solid film linear driving force model. The following three case studies were investigated: (1) separation of Tröger's base enantiomers, Langmuir isotherm, (2) separation of cycloketones, bi-Langmuir isotherm, and (3) a

Table 4
Application of the short cut design methods for the separation of Tröger's base enantiomers (Langmuir isotherm). Isotherm and kinetic parameters are given in Table 3 Feed concentrations: $c_1^F = c_2^F = 6$ g/L. Top part: purity constraints and correct values of V_{inj} and t_{cut} that lead to them. Middle: relative errors of V_{inj} and t_{cut} obtained by using the design method under ideal conditions and resulting product purities. Bottom: relative errors of V_{inj} and t_{cut} obtained by using the design method under non-ideal conditions and resulting product purities.

			$NTP = 100$			$NTP = 500$			$NTP = 1000$					
Correct values	p_1^A	[%]	99	99	90	90	99	99	90	90	99	99	90	90
	p_2^B	[%]	99	90	99	90	99	90	99	90	99	90	99	90
	V_{inj}^{*}	[mL]	5.06	7.79	6.49	9.66	7.00	9.15	7.82	10.12	7.20	9.23	8.02	10.17
	t_{cut}^{*}	[min]	41.46	36.74	41.56	37.94	38.30	36.14	39.41	37.48	37.97	36.07	39.13	37.41
Design under ideal conditions	p_1^A	[%]	98.33	97.98	91.38	91.20	99.48	99.48	90.46	90.58	99.42	99.53	90.29	90.39
	p_2^B	[%]	93.07	84.34	94.63	86.59	97.57	88.58	97.70	88.94	98.18	89.22	98.21	89.28
	δV_{inj}	[%]	47.28	27.79	27.82	18.67	6.53	3.56	4.35	3.31	3.55	1.88	2.38	1.86
	δt_{cut}	[%]	−9.47	−6.27	−6.46	−5.37	−2.01	−1.32	−1.46	−1.23	−1.17	−0.79	−0.87	−0.74
Design under non-ideal conditions	p_1^A	[%]	97.43	97.06	90.16	90.06	98.97	98.90	90.06	90.06	99.05	99.04	90.05	90.05
	p_2^B	[%]	98.54	88.28	98.95	89.80	98.99	89.96	99.03	90.11	99.01	90.06	99.02	90.08
	δV_{inj}	[%]	15.87	14.01	9.62	5.77	0.11	0.18	0.03	−0.07	−0.11	−0.13	−0.16	−0.17
	δt_{cut}	[%]	−2.31	−1.44	−1.02	−0.81	−0.01	0.01	0.02	0.01	0.00	0.00	0.01	0.00

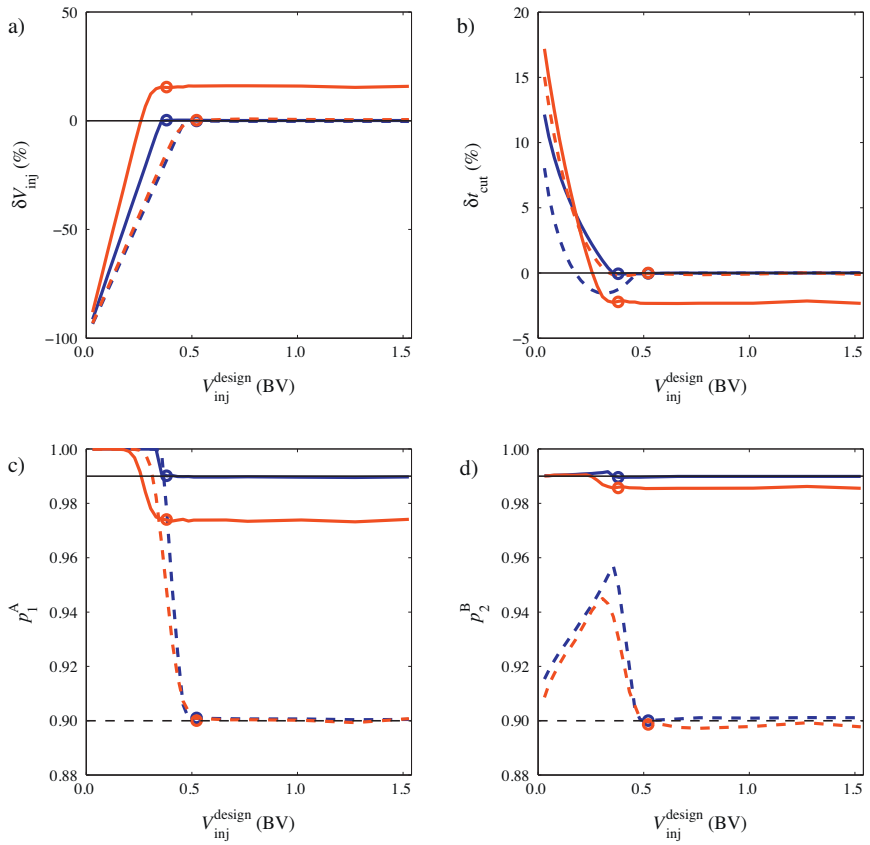

Fig. 4. (a–d) Effect of injection volume of the design chromatogram on the applicability of the design method for non-ideal conditions in the separation of Tröger's base enantiomers. Blue solid line: $NTP = 500$, $p_1^A = p_2^B = 0.99$; blue dashed line: $NTP = 500$, $p_1^A = p_2^B = 0.90$; red solid line: $NTP = 100$, $p_1^A = p_2^B = 0.99$; red dashed line: $NTP = 100$, $p_1^A = p_2^B = 0.90$. Circles: the volume of design chromatogram is equal to the injection volume predicted by the design method based on ideal conditions (Eq. (15)). Isotherm and kinetic parameters are given in Table 3. *Feed concentrations*: $c_1^F = c_2^F = 6$ g/L. (For interpretation of color in the artwork, the reader is referred to the web version of the article.)

generic example, anti-Langmuir isotherm. The isotherm and kinetic parameters of the systems are given in Table 3.

In the simulation study, the effects of column efficiency, purity constraints, and feed concentrations on the accuracy of the design methods were considered. The column efficiency as number of theoretical plates, *NTP*, was determined under linear conditions for the less strongly adsorbed component. The injection volumes of the design chromatograms were selected such that in each case the injection plateau prevails.

4.1. Case 1: Langmuir isotherm

To study the effect of the column efficiency on the applicability of the design methods for the Langmuir isotherm system, the mass transfer coefficients, k_1 and k_2, were varied between 2.988–86.70 min^{-1}. In terms of *NTP*, this corresponds to variation from 100 to 1000 theoretical plates. The simulations were carried out by using the following two feed compositions: (1) $c_1^F = c_2^F = 6$ g/L (strongly non-linear conditions) and (2) $c_1^F = c_2^F = 0.1$ g/L

Table 5
Application of the short cut design methods for separation of cyclopentanone and cyclohexanone (bi-Langmuir isotherm). Isotherm and kinetic parameters are given in Table 3 Feed concentrations: $c_1^F = 20$ g/L, $c_2^F = 20$ g/L. Top part: purity constraints and correct values of V_{inj} and t_{cut} that lead to them. Bottom: relative errors of V_{inj} and t_{cut} obtained by using the design method under non-ideal conditions and resulting product purities.

			NTP = 100				*NTP* = 500				*NTP* = 1000			
Correct values	p_1^A	[%]	99	99	90	90	99	99	90	90	99	99	90	90
	p_2^B	[%]	99	90	99	90	99	90	99	90	99	90	99	90
	V_{inj}^*	[mL]	14.53	22.09	17.84	27.92	19.58	27.01	21.84	29.87	20.18	27.35	22.46	30.12
	t_{cut}^*	[min]	118.44	96.24	118.46	99.31	105.55	92.48	108.67	96.43	103.96	91.98	107.21	95.94
Design under non-ideal conditions	p_1^A	[%]	97.15	96.01	89.83	89.52	98.98	98.88	90.05	90.07	99.04	99.04	90.04	90.05
	p_2^B	[%]	98.75	88.78	98.96	89.73	99.00	89.93	99.02	89.99	99.01	90.00	99.01	90.00
	δV_{inj}	[%]	11.29	14.92	10.52	6.59	0.01	0.23	0.10	0.03	−0.10	−0.06	−0.08	−0.07
	δt_{cut}	[%]	−2.36	−1.70	−1.13	−0.90	0.01	0.01	0.02	0.01	0.02	0.00	0.00	0.00

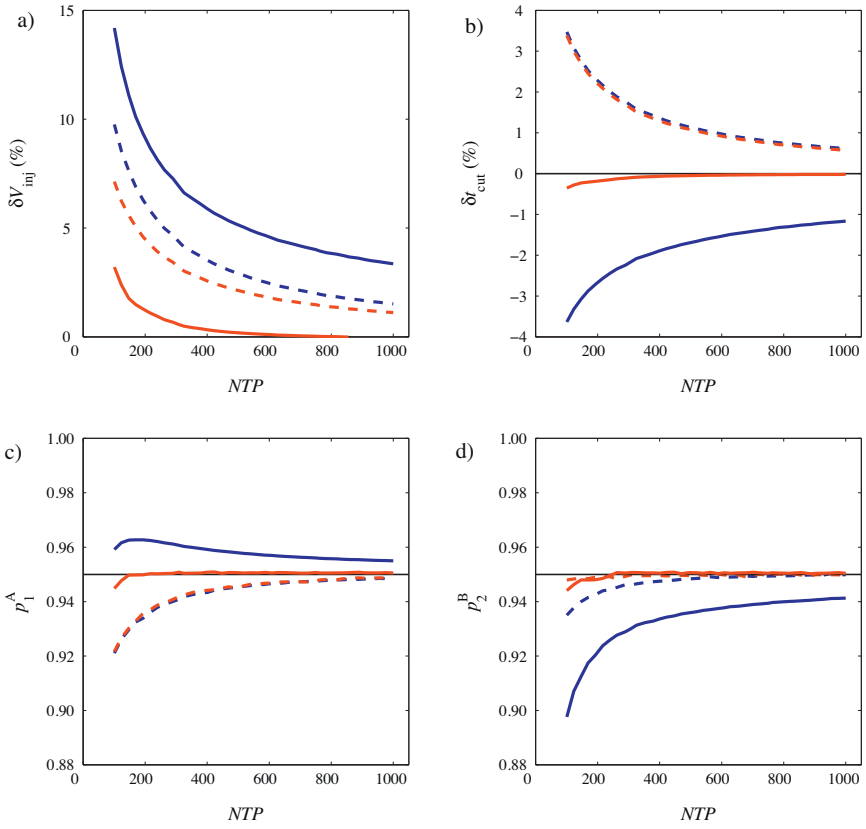

Fig. 5. (a–d) Effect of column efficiency on the applicability of the design methods in the separation of Tröger's base enantiomers. Blue solid line: design method based on ideal conditions, $c_1^F = c_2^F = 6$ g/L. Red solid line: design method for non-ideal conditions, $c_1^F = c_2^F = 6$ g/L. Blue dashed line: design method based on ideal conditions, $c_1^F = c_2^F = 0.1$ g/L. Red dashed line: design method for non-ideal conditions, $c_1^F = c_2^F = 0.1$ g/L. Isotherm and kinetic parameters are given in Table 3. Purity constraints: $p_1^A = p_2^B = 0.95$. (For interpretation of color in the artwork, the reader is referred to the web version of the article.)

(weakly non-linear conditions). The purities of the product fractions were set equal to 0.95.

As seen in Fig. 5, the equilibrium based design method works the better the more efficient the column is. With column efficiencies higher than 800 theoretical plates, the relative error of the injection volume is less than 4% and both purity constraints are fulfilled with an accuracy of 1 percentage unit. In contrast, when *NTP* is 100, $\delta V_{inj} = 14.2\%$, $p_1^A = 0.959$, and $p_2^B = 0.898$ for high feed concentrations ($c_i^F = 6$ g/L) and $\delta V_{inj} = 9.8\%$, $p_1^A = 0.921$, and $p_2^B = 0.935$ for low feed concentrations ($c_i^F = 0.1$ g/L).

The injection volumes predicted by the ideal model are systematically too large (Fig. 5a). This stems from neglecting the dispersive

Table 6
Application of the short cut design methods for system that follows anti-Langmuir isotherm model. Isotherm and kinetic parameters are given in Table 3 Feed concentrations: $c_1^F = 4$ g/L, $c_2^F = 6$ g/L. Top part: purity constraints and correct values of V_{inj} and t_{cut} that lead to them. Middle: relative errors of V_{inj} and t_{cut} obtained by using the design method under ideal conditions and resulting product purities. Bottom: relative errors of V_{inj} and t_{cut} obtained by using the design method under non-ideal conditions and resulting product purities.

			NTP = 100			*NTP* = 500			*NTP* = 1000					
Correct values	p_1^A	[%]	99	99	90	90	99	99	90	90	99	99	90	90
	p_2^B	[%]	99	90	99	90	99	90	99	90	99	90	99	90
	V_{inj}^*	[mL]	27.60	35.25	45.94	55.76	34.48	39.88	51.11	58.30	35.43	40.67	51.70	58.69
	t_{cut}^*	[min]	97.41	98.68	127.27	129.03	105.44	105.56	132.65	132.81	106.72	106.74	133.36	133.39
Design under ideal conditions	p_1^A	[%]	96.52	96.68	87.66	87.96	98.16	98.18	89.24	89.29	98.44	98.44	89.50	89.51
	p_2^B	[%]	97.28	90.03	97.73	90.06	98.71	90.02	98.84	90.02	98.95	90.01	99.00	90.01
	δV_{inj}	[%]	33.95	25.40	19.72	14.15	7.25	6.64	4.76	3.75	4.36	4.23	2.96	2.39
	δt_{cut}	[%]	12.16	11.43	8.87	7.43	3.62	3.56	2.66	2.28	2.38	2.37	1.76	1.52
Design under non-ideal conditions	p_1^A	[%]	98.96	99.03	89.84	90.09	99.01	99.02	90.04	90.08	99.02	99.02	90.05	90.06
	p_2^B	[%]	96.79	89.91	97.47	89.97	98.56	89.95	98.71	89.96	98.84	89.96	98.89	89.97
	δV_{inj}	[%]	11.27	4.17	5.51	3.02	0.87	0.30	0.35	0.14	0.13	0.01	0.00	−0.05
	δt_{cut}	[%]	1.12	0.46	0.79	0.47	−0.01	−0.06	−0.05	−0.09	−0.07	−0.08	−0.08	−0.09

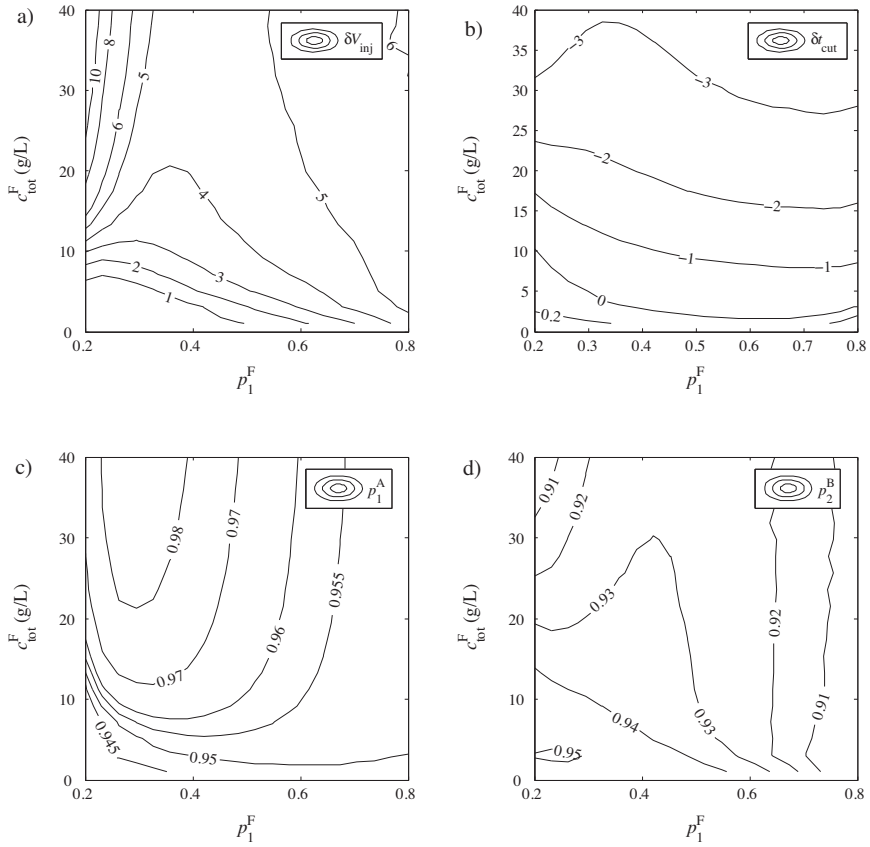

Fig. 6. (a–d) Effect of feed concentrations on the applicability of the design method based on ideal conditions in the separation of Tröger's base enantiomers. Isotherm and kinetic parameters are given in Table 3. Column efficiency: $NTP = 300$. Purity constraints: $p_1^A = p_2^B = 0.95$.

effects that limit the resolution between the bands. For this reason, the integration step in the design method predicts a too low value for the cut point in terms of the elution time relative to the end of the injection. At the same time, the amount of product fraction B, and thus the injection volume, is overestimated. As a result, the purity obtained for the fraction B is lower than required (Fig. 5d).

The deviation of the cut time relative to the beginning of the injection (Fig. 5b) stems from two causes. As already mentioned, due to neglecting the dispersive effects a too low value for the cut point relative to the end of the injection is predicted. In contrast, estimate for V_{inj}, and thus for Δt_{inj}, is too high, which partly eliminates the error. When the feed concentrations are high ($c_i^F = 6$ g/L), the effect of the first mentioned phenomenon on δt_{cut} is stronger and the deviation is negative. In the case of low feed concentrations ($c_i^F = 0.1$ g/L), the second phenomenon is dominating and a too high value for t_{cut} is obtained.

It is worth noting that the purity of fraction B resulting from the equilibrium based design is lower but the purity of fraction A higher than required when the feed concentrations are high. It is thus possible to improve the purity of fraction B such that p_1^A is still satisfied by chancing the cut time only. To fulfill the both purity constraints exactly the injection volume must be corrected too.

As expected, the shortcut method for non-ideal systems provides better estimates for V_{inj} and t_{cut} than the method for ideal systems. Although the predicted injection volumes are too large and the predicted cut times too small, the deviations from the correct values are significantly smaller than with the equilibrium theory method. This is because the effect of dispersion on the rear of the chromatogram is inherently taken into account during the integration.

In addition to the column efficiency, the influence of purity constrains on the accuracy of the design methods was investigated. The results are summarized in Table 4. It is observed that the design methods work best at when low purities are required. This is due to increased injection volume with low purities, for which reason the tail of the design chromatogram obtained with V_{inj}^* deviates less from that of the design chromatogram. In the case of non-ideal design method, the purity of fraction B is matched better than the purity of fraction A. This is because the front of the chromatogram is strongly influenced by the accuracy of the predicted injection volume. Especially in the case of high purity constraints (and low injection volume), the cut is positioned at the "root" of the mixed shock – a position which is very susceptible to the influence of dispersion. It is interesting also to note that the design methods are more accurate when p_1^A is low and p_2^B is high than in the opposite case, especially when the column efficiency is low. This also stems from the fact that for high p_1^A values the cut point falls on the steep shock layer in front of the second component's profile, and hence the influence of the cut time on the product purities is strong.

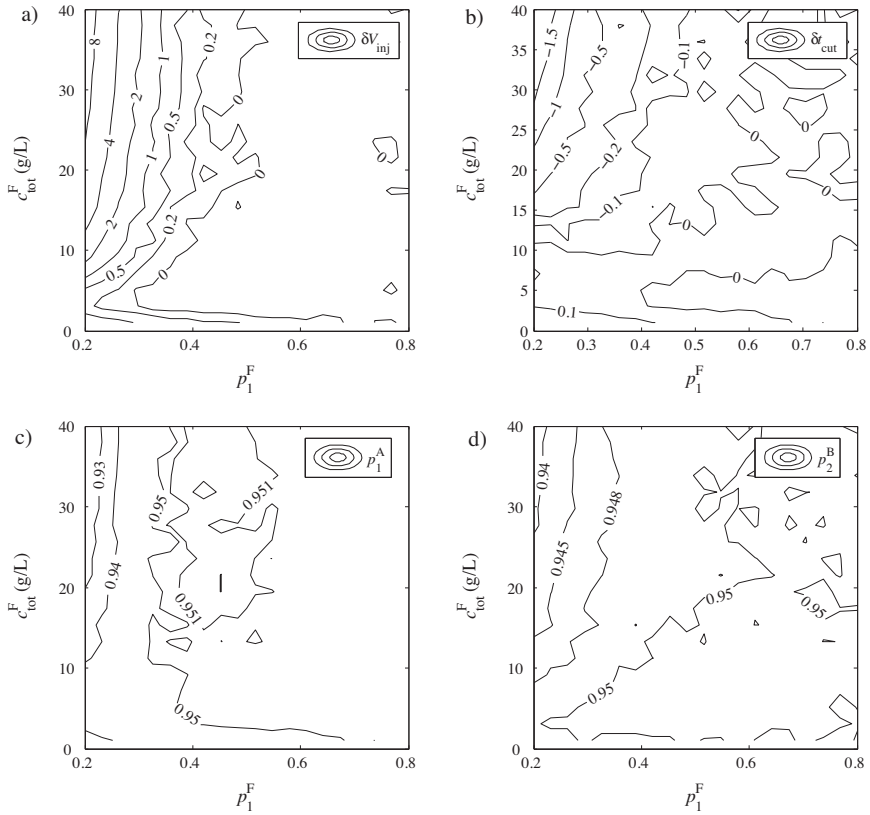

Fig. 7. (a–d) Effect of feed concentrations on the applicability of the design method for non-ideal conditions in the separation of Tröger's base enantiomers. Isotherm and kinetic parameters are given in Table 3. Column efficiency: $NTP = 300$. Purity constraints: $p_1^A = p_2^B = 0.95$.

To examine the effect of the feed concentrations on the feasibility of the design methods the total feed concentration, $c_{tot}^F = c_1^F + c_2^F$, was varied from 1 to 40 g/L and the ratio of feed concentrations, c_1^F/c_2^F, from 1:4 to 4:1. The column efficiency was kept constant at $NTP = 300$ and the purity constraints were set equal to 0.95. In reality, the solubility of Tröger's base enantiomers in ethanol is about 18 g/L [19] so all the values beyond that are hypothetical. The simulation results are displayed in contour maps (Figs. 6 and 7) where the contour lines show the points with same particular function value (δV_{inj}, δt_{inj}, p_1^A, or p_2^B).

As seen in Figs. 6a and 7a, the predictions for the injection volume are too large on the whole feed concentration region. In addition, neither of the design methods is very accurate when the total feed concentration and the excess of component 2 over component 1 are high. This stems from strong displacement effect that yields a high but narrow pure first component zone that is significantly affected by dispersive effects. The injection volume for which both purity constraints are satisfied is thus relatively small, and it deviates a lot from the injection volume of the design chromatogram.

An interesting finding is also that both the design methods are applicable in the case of low feed concentrations that correspond to the weakly non-linear region of the isotherm where kinetic effects influence strongly on band shapes. This can be explained by the fact that under weakly non-linear conditions the injection volume that leads to given target purities is larger compared to the strongly non-linear conditions. This decreases the sensitivity of non-ideal effects on the shape of the tail of the chromatogram.

As already mentioned, the cut times predicted by the equilibrium based design method are too small when the total feed concentration is relatively high. In this case, the limit is 2–10 g/L depending on the feed composition. With low feed concentrations a too high value for t_{cut} is estimated. In the case of the design method for non-ideal conditions, similar behavior is observed when the purity of the first component in feed is low. For high p_1^F values $|\delta t_{cut}|$ is lower than 0.1% on the whole total feed concentration region.

When the equilibrium based design method is applied, p_2^B is always lower than required while the behavior of p_1^A depends on the feed concentrations. With relative high c_{tot}^F values (the limit is 3–13 g/L in this case) purity of fraction A is higher but with low c_{tot}^F values lower than required. In the case of the design method for non-ideal conditions, the resulting purities of both product fractions are lower than or equal to the desired ones. The target constraints are matched the better the higher the purity of the first component in feed is.

4.2. Case 2: bi-Langmuir isotherm

Analogous simulations as in the case of Langmuir isotherms were performed for bi-Langmuir system. However, only the design method for non-ideal conditions was applied since explicit equations for the equilibrium based design are not available. The results are shown in Table 5.

Since both Langmuir and bi-Langmuir isotherms stand for convex isotherm type, the results obtained in these two cases show very similar trends. Again, the design method works best when the column efficiency is high and the purity constraints low. In addition, the relative errors of the injection volumes and the cut times as well as the product purities are of the same order as in the Langmuir case.

4.3. Case 3: anti-Langmuir isotherm

The effects of column efficiency and purity constrains on the applicability of the design methods in case of anti-Langmuir system are shown in Table 6. As in previous cases, both the design methods work best when the column efficiency is high and the target purities low. As expected, the design method for non-ideal systems provides better estimates for V_{inj} and t_{cut} than the method based on ideal conditions. For example, when the column efficiency is 100 theoretical plates and the target purities 0.9, the design method for non-ideal conditions predicts correct V_{inj} with an accuracy of 3% and both the purity constrains are satisfied with an accuracy of 0.1 percentage unit. In the case of the equilibrium based design, $\delta V_{inj} = 14.15\%$, $p_1^A = 87.96$, and $p_2^B = 90.06$.

The main difference compared to the previous cases is that the isotherm type is now concave. The purity constraints are thus matched better when p_1^A is high and p_2^B is low than in the opposite case. This is because the cut point is now located on the deep shock front when p_2^B is high. As expected, this is opposite to the behavior observed in the case of the competitive Langmuir isotherm.

5. Conclusions

Two design methods were developed for separation of binary mixtures in a batch chromatography. The first one holds under ideal conditions and is based on the equilibrium theory of chromatography. It allows direct prediction of the injection volume and the cut time that lead to given target purities without generation of a waste stream. These parameters provide the basis for further estimation of the process performance parameters such as productivity and eluent consumption. The approach is generally valid for all systems that follow convex or concave isotherm models. Explicit analytical design equations were derived for competitive Langmuir and anti-Langmuir isotherms.

The second approach is applicable for more realistic finite efficiency systems. Estimates for the injection volume and the cut time corresponding to arbitrary purity requirements are obtained by applying a simple procedure for a single conventional chromatogram. The choice of the injection volume for the design chromatogram was discussed briefly. When the isotherm parameters are known and the system follows Langmuir or anti-Langmuir isotherm model, it is recommended to use the ideal model to calculate proper injection volume. In other case, large injection volume for which the injection plateau prevails is preferred.

The applicability of the design methods was evaluated by numerical simulations. Three case studies with Langmuir, bi-Langmuir, and anti-Langmuir isotherms were considered. Both the design methods are most applicable for high performance systems. In contrast, when the column efficiency is low and the purity constrains are high, a systematic error in the predicted operating parameters is observed and the purity constraints are not fully satisfied. While in the end, any shortcut design needs some fine-tuning, we believe that the proposed approaches can be used in many practical applications to predict the preliminary injection volume and cut time.

Appendix A. Summary of equilibrium theory

The fundamentals of the local equilibrium theory of chromatography are summarized below. For details, the interested reader is referred to more comprehensive works [9–13].

When a rectangular pulse of a mixture of two components is injected at the inlet of a clean column, two simple wave transitions (Γ_1, Γ_2) and two shock transitions (Σ_1, Σ_2) are formed. The solution of the model consists of describing the movement of these waves and their interactions along the column. The design method derived in this work is, however, based on the properties of Γ_1 and Γ_2 transitions only. For this reason, the interactions between waves are not discussed here.

The image of the chromatographic cycle is conveniently constructed in the so-called hodograph (c_1, c_2) and characteristic (ω_1, ω_2) planes. Examples of these representations and corresponding chromatograms are given in Fig. A.1. In the figure, F and O denote the feed and initial states, respectively, while P and Q stand for two intermediate states. The images of the solution paths are given by

$$\text{Langmuir}: \quad \mathrm{O} \overset{\Gamma_2}{\rightarrow} \mathrm{P} \overset{\Gamma_1}{\rightarrow} \mathrm{F} \overset{\Sigma_2}{\rightarrow} \mathrm{Q} \overset{\Sigma_1}{\rightarrow} \mathrm{O} \tag{A.1}$$

$$\text{anti-Langmuir}: \quad \mathrm{O} \overset{\Sigma_2}{\rightarrow} \mathrm{P} \overset{\Sigma_1}{\rightarrow} \mathrm{F} \overset{\Gamma_2}{\rightarrow} \mathrm{Q} \overset{\Gamma_1}{\rightarrow} \mathrm{O} \tag{A.2}$$

For Langmuir and anti-Langmuir isotherms, simple waves correspond on the hodograph plane to segments on straight lines, called characteristics. The slopes of the characteristics, dc_1/dc_2, are obtained from the right eigenvectors of the matrix $A = [\delta_{ij} + \phi q_{ij}]$, where δ_{ij} is the Kronecker delta, defined as 1 if $i = j$ and 0 if $i \neq j$, and $q_{ij} = \partial q_i / \partial c_j$ is the partial derivative of the adsorption isotherm, Eq. (6). Explicit expressions for the slopes are given by

$$\xi_1 = \frac{-\eta + \sqrt{\eta^2 + 4p_1p_2K_1K_2H_1H_2c_1c_2}}{2p_1K_1H_2c_2} \tag{A.3}$$

$$\xi_2 = \frac{-\eta - \sqrt{\eta^2 + 4p_1p_2K_1K_2H_1H_2c_1c_2}}{2p_1K_1H_2c_2} \tag{A.4}$$

with $\eta = H_1(1 + p_2K_2c_2) - H_2(1 + p_1K_1c_1)$.

A convenient way to study the above Riemann problems is to perform a variable transform by introducing pair of characteristic parameters (ω_1, ω_2) defined as

$$\omega_1 = \frac{p_1p_2K_2H_1 + K_1H_2\xi_2}{p_1p_2K_2 + K_1\xi_2} \tag{A.5}$$

$$\omega_2 = \frac{p_1p_2K_2H_1 + K_1H_2\xi_1}{p_1p_2K_2 + K_1\xi_1} \tag{A.6}$$

It has been shown that there exists a one-to-one correspondence between the concentrations (c_1, c_2) and the two characteristics parameters (ω_1, ω_2) [11]. In addition, the parameter ω_1 is constant along the Γ_1 characteristic while ω_2 is constant along the Γ_2 characteristic. The limits for these two parameters are given by

$$\text{Langmuir}: \quad 0 < \omega_1 \leq H_1 \leq \omega_2 \leq H_2 \tag{A.7}$$

$$\text{anti-Langmuir}: \quad H_1 \leq \omega_1 \leq H_2 \leq \omega_2 < \infty \tag{A.8}$$

The propagation velocities of the simple waves are obtained from the eigenvalues of **A**. In the case of Langmuir and anti-Langmuir isotherms, the resulting expressions are given by

$$\Gamma_1: \quad \frac{dx}{dt} = \left(1 + \frac{\phi\omega_1^2\omega_2}{H_1H_2}\right)^{-1} u \tag{A.9}$$

$$\Gamma_2: \quad \frac{dx}{dt} = \left(1 + \frac{\phi\omega_1\omega_2^2}{H_1H_2}\right)^{-1} u \tag{A.10}$$

Since the characteristics on the hodograph plane are straight lines, the images of shock transitions Σ_1 and Σ_2 coincide with the

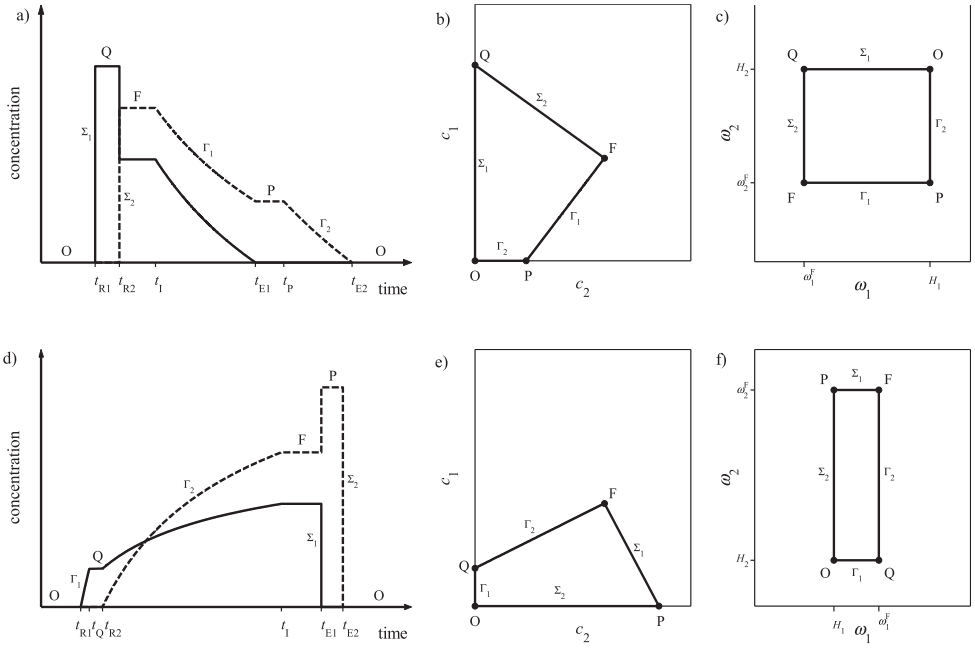

Fig. A.1. Chromatographic cycles under ideal conditions for arbitrary systems that follow Langmuir and anti-Langmuir isotherm models: (a) chromatograms, Langmuir isotherm; (b) hodograph plane, Langmuir isotherm; (c) characteristic plane, Langmuir isotherm; (d) chromatograms, anti-Langmuir isotherm; (e) hodograph plane, anti-Langmuir isotherm; (f) characteristic plane, anti-Langmuir isotherm.

characteristics Γ_1 and Γ_2, respectively. The propagation velocities of the shock waves are given by the mass balance across the discontinuity as follows

$$\Sigma_1: \quad \frac{dx}{dt} = \left(1 + \frac{\phi\omega_1^L\omega_1^R\omega_2}{H_1H_2}\right)^{-1} u \tag{A.11}$$

$$\Sigma_2: \quad \frac{dx}{dt} = \left(1 + \frac{\phi\omega_1\omega_2^L\omega_2^R}{H_1H_2}\right)^{-1} u \tag{A.12}$$

where the superscripts L and R refer to the states on the left and right sides of the shock wave.

Appendix B. Derivation of the design equations for Langmuir isotherm

In this appendix, a detail derivation of the equilibrium theory based design equations for systems that follow competitive Langmuir isotherm model is given. All the required equations for $\omega_i(t)$, used in this appendix as well as in Appendix C, are provided by Rajendran and Mazzotti [12].

To solve the cut time, explicit equations for the amounts of components 1 and 2 that elutes from column after an arbitrary cut point locating on the mixed wave are first derived. For this purpose, the rear parts of the individual elution profiles are integrated by employing ω-transform. The amount of component 1 is obtained by integrating the mixed wave, *i.e.* Γ_1 characteristic, from the cut point to the end of the elution profile of component 1, τ_{E1}. Because ω_2 parameter remains constant along the Γ_1 characteristic, we use substitution $t = f(\omega_1)$, which yieldsto the following expression

$$m_1^B(\tau_{cut}) = Q\int_{\tau_{cut}}^{\tau_{E1}} c_1(\tau)\,d\tau = Q\int_{\omega_1(\tau_{cut})}^{\omega_1(\tau_{cut})} c_1(\tau(\omega_1))\tau'(\omega_1)\,d\omega_1$$
$$= \frac{(1-\varepsilon)(\omega_2^F - H_1)(H_1 - \omega_1^{cut})^2}{K_1H_1(H_2 - H_1)}V_{col} \tag{B.1}$$

where ω_1^{cut} is ω_1-value at the cut point.

To calculate the amount of component 2, the elution profile must be integrated piecewise. In the mixed wave, ω_2 parameter remains constant and the integral is again calculated using substitution $t = f(\omega_1)$. In the pure second component plateau, c_2 is constant, and the integral term is replaced by $c_2(\tau_P)(\tau_P - \tau_{E1})$, where $c_2(\tau_P)$ is the concentration of component 2 at the pure second component plateau, τ_P is the end of the pure second component plateau, and τ_{E1} is the beginning of the pure second component plateau (equal to the end of the elution profile of component 1). Along the pure second component wave, *i.e.* Γ_2 characteristic, ω_1 parameter remains constant, and the substitution $t = f(\omega_2)$ is used. The resulting expression for $m_2^B(\tau_{cut})$ is

$$m_2^B(\tau_{cut}) = Q\int_{\tau_{cut}}^{\tau_{E1}} c_2(\tau)\,d\tau + Q\int_{\tau_{E1}}^{\tau_P} c_2(\tau)\,d\tau + Q\int_{\tau_P}^{\tau_{E2}} c_2(\tau)\,d\tau$$
$$= Q\int_{\omega_1(\tau_{cut})}^{\omega_1(\tau_{E1})} c_2(\tau(\omega_1))\tau'(\omega_1)\,d\omega_1 + Qc_2(\tau_P)(\tau_P - \tau_{E1})$$
$$+ Q\int_{\omega_2(\tau_P)}^{\omega_2(\tau_{E2})} c_2(\tau(\omega_2))\tau'(\omega_2)\,d\omega_2$$
$$= \frac{(1-\varepsilon)(H_2 - \omega_2^F)(H_2 - \omega_1^{cut})^2}{K_2H_2(H_2 - H_1)}V_{col} \tag{B.2}$$

The limit whether the cut point is located on the mixed wave or on the injection plateau, *i.e.* $p^B_{2,limit}$, is solved by setting $\omega_1^{cut} = \omega_1^F$ into Eqs. (B.1) and (B.2), and by substituting the resulting equations into definition of p_2^B, Eq. (2). Some rearrangement gives

$$p^B_{2,limit} = \left(1 + \frac{p_1^F}{1-p_1^F}\frac{H_1 - \omega_1^F}{H_2 - \omega_1^F}\right)^{-1} \tag{B.3}$$

When $p_2^B \geq p^B_{2,limit}$, the cut point is located on the mixed wave. An explicit expression for ω_1^{cut} is obtained by eliminating m_1^B and m_2^B from system of Eqs. (B.1), (B.2), and (2) which yields

$$\omega_1^{cut} = \frac{H_1 - H_2\lambda}{1-\lambda} \tag{B.4}$$

with λ being an auxiliary parameter given by

$$\lambda = \sqrt{\frac{1-p_2^B}{p_2^B}\frac{K_1H_1(H_2-\omega_2^F)}{K_2H_2(\omega_2^F - H_1)}} \tag{B.5}$$

The cut time relative to the end of the injection is now calculated from the propagation velocity of the mixed wave, Eq. (A.9)

$$\tau_{cut} = \left[1 + \frac{\phi(\omega_1^{cut})^2\omega_2^F}{H_1H_2}\right]t_0 \tag{B.6}$$

Finally, the injection volume is solved by substituting Eq. (B.2) into Eq. (15)

$$V_{inj} = \frac{(1-\varepsilon)(H_2-\omega_2^F)(H_2-\omega_1^{cut})^2}{K_2H_2(H_2-H_1)c_2^FY_2}V_{col} \tag{B.7}$$

When the cut point is located on the injection plateau, *i.e.* $p_2^B < p^B_{2,limit}$, the amounts of components 1 and 2 that are collected to fraction B are given by

$$m_1^B(\tau_{cut}) = (\tau_I - \tau_{cut})c_1^FQ + m_1^{tail} \tag{B.8}$$

$$m_2^B(\tau_{cut}) = (\tau_I - \tau_{cut})c_2^FQ + m_2^{tail} \tag{B.9}$$

where τ_I is the end of the injection plateau

$$\tau_I = \left[1 + \frac{\phi(\omega_1^F)^2\omega_2^F}{H_1H_2}\right]t_0 \tag{B.10}$$

and m_i^{tail} is the mass of component i that elutes from column after τ_I. Equations for m_i^{tail} are obtained from Eqs. (B.1) and (B.2) by substituting $\omega_1^{cut} = \omega_1^F$, which yields

$$m_1^{tail} = \frac{(1-\varepsilon)(\omega_2^F - H_1)(H_1-\omega_1^F)^2}{K_1H_1(H_2-H_1)}V_{col} \tag{B.11}$$

$$m_2^{tail} = \frac{(1-\varepsilon)(H_2-\omega_2^F)(H_2-\omega_1^F)^2}{K_2H_2(H_2-H_1)}V_{col} \tag{B.12}$$

To solve the cut time, m_1^B and m_2^B are eliminated from system of Eqs. (B.8), (B.9), and (2)

$$\tau_{cut} = \tau_I - \frac{m_2^{tail} - [p_2^B/(1-p_2^B)]m_1^{tail}}{[p_2^B/(1-p_2^B)]c_1^F - c_2^F}\frac{1}{Q} \tag{B.13}$$

The injection volume is again obtained by substituting the expression of m_2^B, Eq. (B.9), into Eq. (15)

$$V_{inj} = \frac{(\tau_I - \tau_{cut})c_2^FQ + m_2^{tail}}{c_2^FY_2} \tag{B.14}$$

Appendix C. Derivation of the design equations for anti-Langmuir isotherm

In this appendix, a detail derivation of the design equations for systems that follow competitive anti-Langmuir isotherm model is given. The approach is completely analogous but opposite to the case of Langmuir isotherm discussed in Appendix B.

The amount of component 1 that elutes before an arbitrary cut point locating on the mixed wave is calculated by integrating the elution profile piecewise from t_{R1} to t_{cut}. By employing substitution $t = f(\omega_1)$ to solve the integral term corresponding to the pure first component wave, *i.e.* Γ_1 characteristic, and substitution $t = f(\omega_2)$ to solve the integral term corresponding to the mixed wave, *i.e.* Γ_2 characteristic, the following expression for $m_1^A(t_{cut})$ is obtained

$$\begin{aligned} m_1^A(t_{cut}) &= Q\int_{t_{R1}}^{t_Q} c_1(t)\,dt + Q\int_{t_Q}^{t_{R2}} c_1(t)\,dt + Q\int_{t_{R2}}^{t_{cut}} c_1(t)\,dt \\ &= Q\int_{\omega_1(t_{R1})}^{\omega_1(t_Q)} c_1(t(\omega_1))t'(\omega_1)\,d\omega_1 + Qc_1(t_Q)(t_{R2}-t_Q) \\ &\quad + Q\int_{\omega_2(t_{R2})}^{\omega_2(t_{cut})} c_1(t(\omega_2))t'(\omega_2)\,d\omega_2 \\ &= \frac{(1-\varepsilon)(\omega_1^F - H_1)(\omega_2^{cut} - H_1)^2}{K_1H_1(H_2-H_1)}V_{col} \end{aligned} \tag{C.1}$$

where t_Q is the beginning of the pure first component plateau, t_{R2} is the end of the pure first component plateau (equal to the beginning of the elution profile of component 2), and ω_2^{cut} is ω_2-value at the cut point.

Component 2 starts to elute in the beginning of the mixed wave. Again, substitution $t = f(\omega_2)$ is used, which yields

$$\begin{aligned} m_2^A(t_{cut}) &= Q\int_{t_{R2}}^{t_{cut}} c_2(t)\,dt = Q\int_{\omega_2(t_{R2})}^{\omega_2(t_{cut})} c_2(t(\omega_2))t'(\omega_2)\,d\omega_2 \\ &= \frac{(1-\varepsilon)(H_2 - \omega_1^F)(\omega_2^{cut} - H_2)^2}{K_2H_2(H_2-H_1)}V_{col} \end{aligned} \tag{C.2}$$

To calculate the limit whether the cut point is located on the mixed wave or on the injection plateau, $\omega_2^{cut} = \omega_2^F$ is set into Eqs. (C.1) and (C.2), and the resulting equations are substituted into definition of p_1^A, Eq. (1). The following expression is obtained for $p^A_{1,limit}$

$$p^A_{1,limit} = \left(1 + \frac{1-p_1^F}{p_1^F}\frac{(\omega_2^F - H_2)}{(\omega_2^F - H_1)}\right)^{-1} \tag{C.3}$$

When $p_1^A \geq p^A_{1,limit}$, the cut point lies on the mixed wave. Elimination of m_1^A and m_1^B from system of Eqs. (C.1), (C.2), and (1) yields

$$\omega_2^{cut} = \frac{H_2 - H_1K}{1-K} \tag{C.4}$$

with

$$\kappa = \sqrt{\frac{1-p_1^A}{p_1^A}\frac{K_2H_2(\omega_1^F - H_1)}{K_1H_1(H_2-\omega_1^F)}} \tag{C.5}$$

The cut time is calculated from the propagation velocity of the mixed wave, Eq. (A.10)

$$t_{cut} = \left[1 + \frac{\phi\omega_1^F(\omega_2^{cut})^2}{H_1H_2}\right]t_0 \tag{C.6}$$

Finally, Eq. (C.1) is substituted into Eq. (18), which yields to the following expression for the injection volume

$$V_{inj} = \frac{(1-\varepsilon)(\omega_1^F - H_1)(\omega_2^{cut} - H_1)^2}{K_1 H_1 (H_2 - H_1) c_1^F Y_1} V_{col} \tag{C.7}$$

When the cut point is located on the injection plateau, *i.e.* $p_1^A < p_{1,limit}^A$, the amounts of components 1 and 2 eluting before the cut point are given by

$$m_1^A(t_{cut}) = (t_{cut} - t_I) c_1^F Q + m_1^{front} \tag{C.8}$$

$$m_2^A(t_{cut}) = (t_{cut} - t_I) c_2^F Q + m_2^{front} \tag{C.9}$$

where t_I is the beginning of the injection plateau

$$t_I = \left(1 + \frac{\phi \omega_1^F (\omega_2^F)^2}{H_1 H_2}\right) t_0 \tag{C.10}$$

and m_i^{front} is the amount of component i that elutes from the column before t_I obtained from Eqs. (C.1) and (C.2) by substituting $\omega_2^{cut} = \omega_2^F$, which yields

$$m_1^{front} = \frac{(1-\varepsilon)(\omega_1^F - H_1)(\omega_2^F - H_1)^2}{K_1 H_1 (H_2 - H_1)} V_{col} \tag{C.11}$$

$$m_2^{ftont} = \frac{(1-\varepsilon)(H_2 - \omega_1^F)(\omega_2^F - H_2)^2}{K_2 H_2 (H_2 - H_1)} V_{col} \tag{C.12}$$

To solve the cut time m_1^A and m_1^B are eliminated from system of Eqs. (C.8), (C.9), and (1)

$$t_{cut} = t_I + \frac{m_1^{front} - [p_1^A/(1-p_1^A)] m_2^{front}}{[p_1^A/(1-p_1^A)] c_2^F - c_1^F} \frac{1}{Q} \tag{C.13}$$

As a last step, an explicit expression for the injection volume is solved by substituting Eq. (C.8) into Eq. (18)

$$V_{inj} = \frac{(t_{cut} - t_I) c_1^F Q + m_1^{front}}{c_1^F Y_1} \tag{C.14}$$

References

[1] G. Guiochon, A. Felinger, D.G. Shirazi, A.M. Katti, Fundamentals of Preparative and Nonlinear Chromatography, 2nd ed., Academic Press, Amsterdam, 2006.
[2] S. Golshan-Shirazi, G. Guiochon, Anal. Chem. 61 (1989) 1276.
[3] S. Golshan-Shirazi, G. Guiochon, Anal. Chem. 61 (1989) 1368.
[4] A. Jupke, A. Epping, H. Schmidt-Traub, J. Chromatogr. A 944 (2002) 93.
[5] D. Schlinge, P. Scherpian, G. Schembecker, Chem. Eng. Sci. 65 (2010) 5373.
[6] J.H. Knox, H.M. Pyper, J. Chromatogr. 363 (1986) 1.
[7] S. Golshan-Shirazi, G. Guiochon, J. Chromatogr. 517 (1990) 229.
[8] M. Kaspereit, K. Gedicke, V. Zahn, A.W. Mahoney, A. Seidel-Morgenstern, J. Chromatogr. A 1092 (2005) 43.
[9] H.-K. Rhee, R. Aris, N.R. Amundson, First-Order Partial Differential Equations. Theory and Application of Single Equations, vol. I, Dover Publications, New York, 2001.
[10] H.-K. Rhee, R. Aris, N.R. Amundson, First-Order Partial Differential Equations. Theory and Application of Hyperbolic Systems of Quasilinear Equations, vol. II, Dover Publications, New York, 2001.
[11] M. Mazzotti, Ind. Eng. Chem. Res. 45 (2006) 5332.
[12] A. Rajendran, M. Mazzotti, Ind. Eng. Chem. Res. 50 (2011) 352.
[13] J. Siitonen, T. Sainio, J. Chromatogr. A 1218 (2011) 6379.
[14] T. Sainio, M. Kaspereit, Sep. Purif. Technol. 66 (2009) 9.
[15] M. Kaspereit, T. Sainio, Chem. Eng. Sci. 66 (2011) 5428.
[16] J. Siitonen, T. Sainio, M. Kaspereit, Sep. Purif. Technol. 78 (2011) 21.
[17] J. Siitonen, T. Sainio, A. Rajendran, J. Chromatogr. A 1230 (2012) 77.
[18] M. Amanullah, M. Mazzotti, J. Chromatogr. A 1107 (2006) 36.
[19] J. Worlitschek, M. Bosco, M. Huber, V. Gramlich, M. Mazzotti, Helv. Chim. Acta 87 (2004) 279.

Article IV

Journal of Chromatography A, 1341 (2014) 15–30

Contents lists available at ScienceDirect

Journal of Chromatography A

journal homepage: www.elsevier.com/locate/chroma

Steady state recycling chromatography with solvent removal—Effect of solvent removal constraints on process operation under ideal conditions

Jani Siitonen, Tuomo Sainio*

Lappeenranta University of Technology, Skinnarilankatu 34, FI-53850 Lappeenranta, Finland

ARTICLE INFO

Article history:
Received 29 December 2013
Received in revised form 4 March 2014
Accepted 11 March 2014
Available online 18 March 2014

Keywords:
Steady state recycling chromatography
Solvent removal
Equilibrium theory
Process design
Process integration

ABSTRACT

Steady state recycling chromatography (SSR) offers a means to reduce eluent consumption and increase productivity in preparative and production scale chromatographic separations. Even better performance is obtained with an integrated process by coupling solvent removal unit to the chromatographic separation unit. Here a design method for SSR with an integrated solvent removal unit (SSR–SR) is presented. The method is more practical than previous work as the effect of physical constraints, such as solubility or viscosity, imposed on the amount of solvent removed is included. The method holds under ideal conditions for binary systems with competitive Langmuir isotherm model. The design equations allow calculation of the regions of feasible operating parameters when either the maximum concentrations in the solvent removal unit or of the solution fed into the chromatographic column is restricted. The method was applied to analyze the performance of different SSR–SR configurations in two case studies: the separation of mandelic acid enantiomers and the separation of EMD 53986 enantiomers. The benefits of SSR–SR are relatively small under ideal conditions but the design method developed here can give a good starting point for designing SSR–SR processes under non-ideal conditions.

1. Introduction

Preparative liquid chromatography is one of the most selective separation techniques in the pharmaceutical, fine chemical and food industries. It is applied successfully for the separation and purification of a wide range of substances such as enantiomers, other isomers, sugars and proteins. The most common process schemes are single-column batch chromatography and multi-column simulated moving bed (SMB) chromatography. The batch mode is versatile and provides multiple product fractions, but usually suffers from low productivity, high eluent consumption and/or low recovery yield. As to the SMB, high productivity, low eluent consumption, and high yield are counterbalanced by high investment costs and a high degree of complexity.

Many single column recycling techniques are known to enhance the performance of classical batch chromatography with significantly lower investment costs than SMB processes [1–3]. The most promising concepts are steady state recycling schemes where the sufficiently pure leading and trailing sections of the elution profile are collected as product while the unresolved middle part is recycled into the column. A constant amount of fresh feed is added to the recycle fraction, which causes the process to attain a periodic steady state. The process can be operated in different injection modes. In the mixed-recycle scheme [4], the recycle fraction is mixed with the fresh feed before re-injection. In the closed-loop mode [5], the recycle fraction and the fresh feed are introduced separately in order to preserve the already achieved partial separation.

An advanced process concept, SSR–SR, where the performance of conventional steady-state recycling process is improved by integrating it with a solvent removal unit, *e.g.* membrane filtration or evaporation unit, has recently been introduced [1]. A similar approach for concentrating internal process streams has been proposed also for SMB chromatography [6,7]. In addition, various hybrid process concepts where either single column [8] or SMB [9,10] chromatography is combined with an enzymatic racemization and membrane filtration for solvent removal have received increased attention.

The solvent removal unit can be placed in different positions of the SSR–SR process. Solvent can be removed from: (I) the fresh feed, (II) the recycle fraction, and (III) the stream that is fed into the column (obtained by mixing the fresh feed and the recycle fraction). Siitonen et al. [1] investigated various SSR–SR configurations by

* Corresponding author. Tel.: +358 403578683.
E-mail address: tuomo.sainio@lut.fi (T. Sainio).

http://dx.doi.org/10.1016/j.chroma.2014.03.039
0021-9673/

using the equilibrium theory of chromatography and created the theoretical background for analysing and designing the process. A method was developed to choose *a priori* the relevant cut times for fractionating the outlet stream of the chromatography column and the capacity of the membrane filtration unit such that arbitrary purity constraints are satisfied. In addition, it was shown that the three SSR–SR configurations have identical performance with the same operating parameters. In contrast, the configurations differ with respect to the maximum amount of fresh feed as well as the range of feasible volumes of feed pulse into the column.

In practice, the extent of solvent removal is often limited by various factors. Firstly, the maximum concentration achievable in the solvent removal unit may be limited by solubility of the components since precipitation is not acceptable. On the other hand, if the solubility is high, osmotic pressure in membrane filtration or vapour pressure in evaporation may limit the operation. Secondly, the maximum concentration introduced into the chromatographic column may be limited by solubility, viscosity, or pressure drop.

Recently, Hellstén et al. [11] studied the effect of solvent removal constraints on the performance of SSR–SR process under non-ideal conditions by numerical simulations. Separation of glucose and galactose was used as a model case for a large scale biorefinery application of steady-state recycling chromatography. It was found that an optimized SSR–SR process yields always higher productivity than a conventional SSR chromatography or a batch process that employs a similar solvent removal unit. The most advantageous SSR–SR configuration depends on the fresh feed concentrations and the solvent removal constraint.

In this work, the theory of SSR–SR chromatography developed by Siitonen et al. [1] is extended to the case when practical solvent removal constraints affect the SSR–SR operation. A design method is developed for calculation regions of feasible volume of feed pulse into the column and volume of fresh feed. The approach is based on the equilibrium theory of chromatography and is applicable for binary systems that follow competitive Langmuir adsorption isotherm model. The performance of the three SSR–SR configurations is compared with the performance of (1) classical batch chromatography, (2) batch process with solvent removal, and (3) conventional SSR process without solvent removal with two case studies.

2. Background

2.1. Equilibrium theory of chromatography

Within the frame of the equilibrium theory of chromatography, it is assumed that the mass transfer resistance and the dispersive effects are negligible, the fluid velocity is constant, and the packing properties are homogeneous along the column. Under these conditions, the mass balance for an individual component i is given by

$$\frac{\partial c_i}{\partial t} + u\frac{\partial c_i}{\partial x} + \phi\frac{\partial q_i^{eq}}{\partial t} = 0 \quad i = (1,2) \tag{1}$$

where c_i is the fluid phase concentration of solute i, q_i^{eq} is the stationary phase concentration that is in equilibrium with the fluid phase, ϕ is the phase ratio ($\phi = (1-\varepsilon)/\varepsilon$ with ε being the total void fraction of the bed), u is the interstitial velocity ($u = L/t_0$ with L being the column length and t_0 being the retention time of a non-retained component), t is the time, and x is the column axial coordinate. For binary systems that follow the competitive Langmuir adsorption isotherm model the equilibrium relationship is given by

$$q_i^{eq} = \frac{N_i K_i c_i}{1 + K_1 c_1 + K_2 c_2} \tag{2}$$

where N_i and K_i are the saturation capacity and the equilibrium parameter of solute i, respectively. In the following discussion, it is assumed that the component 1 is the less strongly retained one. This means that $H_2 > H_1$, where $H_i = N_i K_i$ is the Henry constant of component i.

To solve the model Eqs. (1) and (2), proper initial and boundary conditions are needed. In this work, it is assumed that a rectangular pulse of binary mixture with known duration, Δt^F, is first fed to an initially clean column and then eluted in isocratic mode. In this case, the initial and boundary conditions of Eq. (1) are

$$c_i(x, t=0) = 0 \quad \text{for} \quad 0 \le x \le L \tag{3}$$

$$c_i(x=0, t) = c_i^F \quad \text{for} \quad 0 \le t \le \Delta t^F \tag{4}$$

$$c_i(x=0, t) = 0 \quad \text{for} \quad t > \Delta t^F \tag{5}$$

where c_i^F is the concentration of component i in column feed.

The model forms a system of two homogeneous quasilinear partial differential equations. It can be solved analytically by the method of characteristics. The fundamentals of the solution are described extensively in the literature [12–15].

2.2. Principle of SSR–SR process

Various single column chromatographic processes are presented schematically in Fig. 1. The classical mixed-recycle steady state recycling chromatography process (Fig. 1a) is started by introducing a certain amount of feed mixture from the feed tank into an initially clean column. The feed pulse is then eluted isocratically with eluent E. The initial state of the feed reservoir can be, for example, a fresh feed mixture, a diluted fresh feed mixture, or a solution whose composition corresponds to the steady state feed.

An example of the concentration profiles at the SSR column outlet is shown in Fig. 2. The actual SSR cycle starts at time t_{A1}, when the first component breaks through. The column effluent is directed to product fraction A to collect the leading section of the chromatogram containing an excess of the less adsorbed component 1. Between times t_{A2} and t_{B1} the unresolved fraction is collected and recycled. In the mixed-recycle mode, the whole recycle fraction is collected in the feed reservoir, mixed with fresh feed and then introduced back into the column. After time t_{B1}, the product fraction B containing an excess of the more retained component 2 is collected until the chromatogram is eluted completely at time t_{B2}.

The above procedure is repeated while keeping the time intervals between the fractionation valve switching events constant. This forces the process into a periodic steady state in which the elution profiles and the average product compositions do not vary from cycle to cycle.

In an SSR–SR process, the performance of MR–SSR chromatography is improved by integrating it with a solvent removal unit, *e.g.* a membrane filtration unit or an evaporation unit. As already mentioned, there are several options to position the solvent removal unit. In this work, the design and performance of the following three configurations are discussed: (I) solvent is removed from the fresh feed (Fig. 1b), (II) solvent is removed from the recycle fraction (Fig. 1c), and (III) solvent is removed from the actual feed solution entering the column (*i.e.*, solution obtained by mixing the fresh feed and the recycle fraction) (Fig. 1d).

The steady state operation of SSR chromatography and the three SSR–SR process options are conveniently presented on the hodograph plane as shown in Fig. 3. In this work, it is assumed that the solvent removal unit works ideally such that the relative composition of the solution is not changed in the unit. The operating line of the solvent removal unit is thus a straight line on the hodograph plane, and solvent removal corresponds to moving upwards on that line.

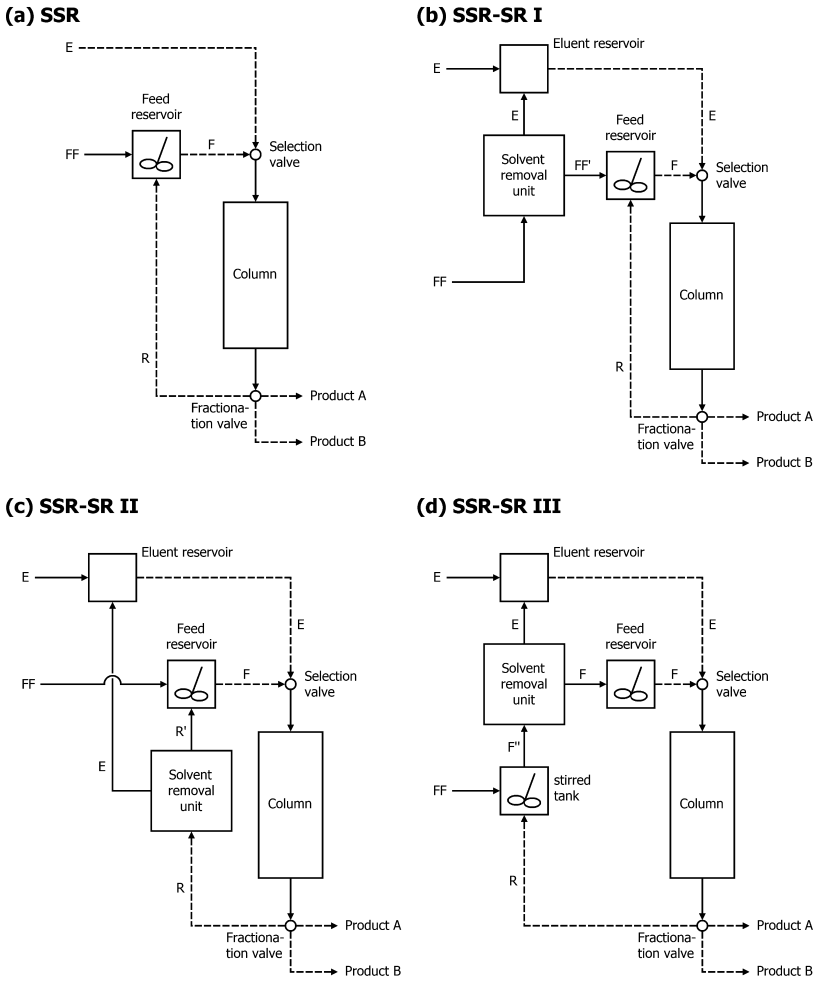

Fig. 1. Schematic setup of (a) conventional SSR chromatography, (b) SSR–SR configuration I (solvent is removed from fresh feed), (c) SSR–SR configuration II (solvent is removed from recycle fraction), (d) SSR–SR configuration III (solvent is removed from mixed fraction). *FF*, fresh feed; *FF′*, concentrated fresh feed; *R*, recycle fraction, *R′*, concentrated recycle fraction; *F″*, mixed fraction; *F*, column feed; *E*, eluent.

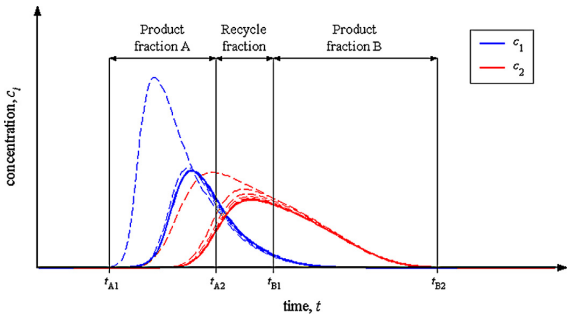

Fig. 2. Example of fraction collection and start-up behaviour of SSR chromatography in mixed-recycle mode. The diagram shows an overlay of the concentration profiles at column outlet for cycles from 1 to 30. Thick lines: concentration profiles at steady state (cycle 30).

In the case of conventional MR–SSR process (Figs. 1a and 3a), the feed composition cannot move away from the Γ_+ characteristic that passes through the fresh feed composition *FF* [16]. When the process operates at steady state, the feed point *F* and the volume-average composition of the recycle fraction *R* must locate on the same Γ_+ characteristic as the fresh feed *FF*. In addition, the image of the rear part of the chromatogram on the hodograph plane remains unaltered.

In SSR–SR configuration I (Figs. 1b and 3b), solvent is removed from the fresh feed *FF*. The operating line of the solvent removal unit thus passes through the origin and *FF*. The resulting composition maps onto point *FF′* in Fig. 3b. When the recycle fraction *R* and the concentrated fresh feed *FF′* are mixed together, the actual feed composition *F* is obtained. According to the lever rule, *F* must locate on the line segment between *FF′* and *R*. At the steady state, the feed point *F*, and thus also the recycle point *R*, lie on the Γ_+ characteristic that passes through the concentrated fresh feed *FF′*.

In process option II (Figs. 1c and 3c), the solvent is removed from the recycle fraction. In this case, the operating line passes through the origin and the recycle fraction *R*. The resulting

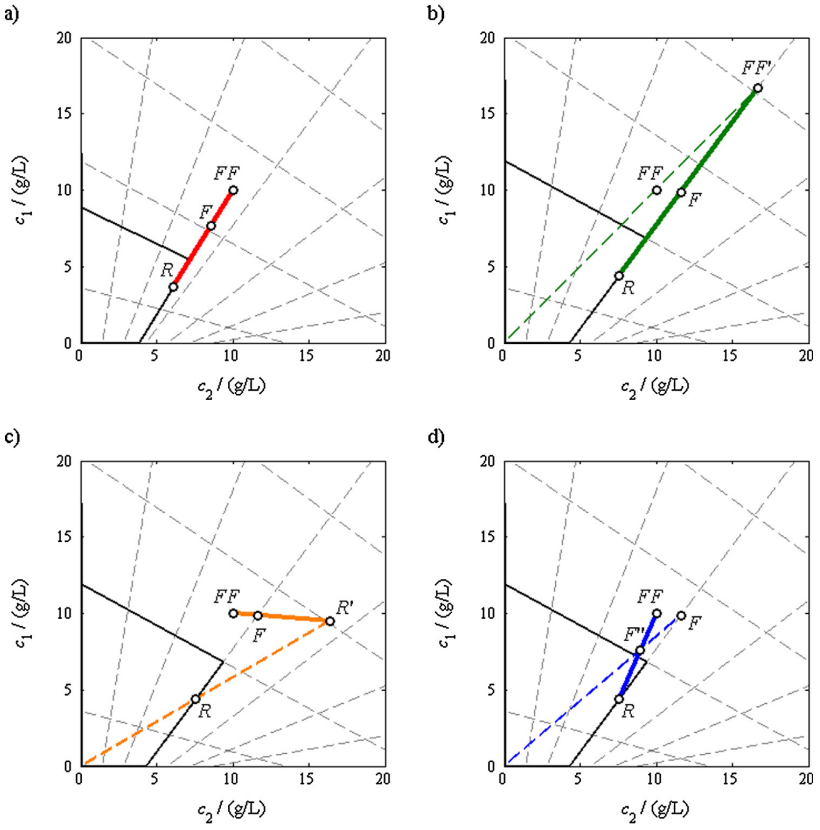

Fig. 3. Schematic representations of alternative process configurations on the hodograph plane. (a) Conventional SSR chromatography. (b) SSR–SR configuration I (solvent removal from fresh feed). (c) SSR–SR configuration II (solvent removal from recycle fraction). (d) SSR–SR configuration III (solvent removal from mixed fraction). Dashed lines: Γ_+ and Γ_- characteristics. Fresh feed concentrations: $c_1^{FF} = c_2^{FF} = 10$ g/L. Isotherm parameters: $K_1 = 0.02$ L/g, $K_2 = 0.025$ L/g, $N_1 = N_2 = 100$ g/L. Phase ratio $\varphi = 1/3$. Purity constraints: $p_1^A = p_2^B = 0.90$. Volume of feed pulse: 0.13 bed volumes. Solvent removal capacity in (b)–(d): $K = 0.4$.

composition maps onto point R'. Mixing the concentrated recycle fraction R' with the fresh feed FF, the actual feed composition F is obtained. The steady state feed composition F is again located on the same Γ_+ characteristic as the steady state recycle fraction composition R.

In process option III (Figs. 1d and 3d), the recycle fraction R and the fresh feed FF are mixed before solvent removal. The resulting mixture, referred to as F'', locates on the line segment between FF and R and the operating line of solvent removal unit passes through the origin and F''. The resulting feed composition maps onto point F. Similarly to configurations I and II, the steady state feed F and the steady state recycle fraction R are located on the same Γ_+ characteristic.

2.3. Design constraints

In the following discussion, it is assumed that the desired purities of the product fractions with respect to their target components and/or the recovery yields of the components are chosen as design constraints. These are defined as follows

$$p_1^A = \frac{m_1^A}{m_1^A + m_2^A} = \frac{\int_{t_{A1}}^{t_{A2}} c_1 dt}{\int_{t_{A1}}^{t_{A2}} (c_1 + c_2) dt} = \frac{p_1^{FF} Y_1}{p_1^{FF} Y_1 + (1 - Y_2)(1 - p_1^{FF})} \quad (6)$$

$$p_2^B = \frac{m_2^B}{m_1^B + m_2^B} = \frac{\int_{t_{B1}}^{t_{B2}} c_2 dt}{\int_{t_{B1}}^{t_{B2}} (c_1 + c_2) dt} = \frac{(1 - p_1^{FF}) Y_2}{(1 - p_1^{FF}) Y_2 + (1 - Y_1) p_1^{FF}} \quad (7)$$

$$Y_1 = \frac{m_1^A}{m_1^{FF}} = \frac{p_1^A}{p_1^{FF}} \frac{p_1^{FF} + p_2^B - 1}{p_1^A + p_2^B - 1} \quad (8)$$

$$Y_2 = \frac{m_2^B}{m_2^{FF}} = \frac{p_2^B}{1 - p_1^{FF}} \frac{p_1^A - p_1^{FF}}{p_1^A + p_2^B - 1} \quad (9)$$

where p_i^j is the purity of component $i = (1, 2)$ in the product fraction $j = (A, B)$, m_i^j is the amount of component $i = (1, 2)$ in the fraction $j = (A, B, FF)$, Y_i is the recovery yield of component $i = (1, 2)$, and $p_1^{FF} = c_1^{FF}/(c_1^{FF} + c_2^{FF})$ is the purity of component 1 in fresh feed.

Since the SSR–SR process represents a binary separation without a waste stream, the purity and yield constraints are interchangeable [17]. In other words, by specifying any two of the four constraints in Eqs. (6)–(9), the remaining two are also fixed. This means that the design approach developed below is applicable also when there is only one target component (either the more or the less strongly retained one) whose purity and yield requirements are given.

2.4. Design of SSR–SR process

In SSR–SR process, there exist two adjustable operating parameters for given column dimensions and volumetric flow rate [1]. One can choose freely the volume of feed introduced into the column, V^F, and one of the following parameters: (1) the volume of fresh feed treated per cycle, V^{FF}, (2) the volume of solvent removed per cycle, V^{SR}, or (3) the solvent removal capacity, $K = V^{SR}/V^{FF}$. The design task is to find the four cut times (t_{A1}, t_{A2}, t_{B1}, t_{B2}) for a given combination of free operating parameters such that user-given purity requirements on the two product fractions are satisfied exactly at the periodic steady state. In the case of 100% purity requirements, the following approach predicts the operating parameters that lead to the target purities without recycling pure component fractions, *i.e.* maximum amounts of products are obtained.

In this section, the basic theory and design method of SSR–SR process developed by Siitonen et al. [1] is briefly summarized since it provides the basis for understanding the effects of solvent removal constraints on process operation. Detail derivation of the explicit design equations is given in Appendix A. The derivation is based on a variable transform from concentrations (c_1, c_2) to characteristic parameters (ω_1, ω_2) which yields more simple expressions than originally given in [1].

The design approach allows to choose *a priori* the relevant cut times corresponding to arbitrary purity or yield constraints and to predict the steady state of the process without performing dynamic simulations in the case of binary system with Langmuir isotherm and ideal conditions. The three SSR–SR configurations lead to exactly the same steady state when the same operating parameters are used [1]. The design method is thus independent of the position of the solvent removal unit. The limits for the feasible adjustable variables are discussed in Section 3.

The first step in the design of SSR–SR process is to solve the slope of the Γ_+^F characteristic on the hodograph plane that passes through the steady state feed composition, ξ_+^F. It is shown that specifying any of the design variables V^{FF}, V^{SR}, or K determines uniquely the Γ_+^F characteristic. The relationship between, K, V^{FF}, V^{SR}, and ξ_+^F is given by

$$K = \frac{V^{SR}}{V^{FF}} = 1 + \frac{(c_1^{FF} - c_2^{FF}\xi_+^F)(\alpha K_1 \xi_+^F + K_2)}{(\alpha - 1)\xi_+^F} \tag{10}$$

where $\alpha = H_2/H_1$ is the separation factor. When the solvent removal capacity is used as a design criterion, ξ_+^F can be solved explicitly from Eq. (10). In contrast, when V^{FF} or V^{SR} is selected as a starting point, ξ_+^F must be solved numerically. It is shown that when K or V^{SR} increases, V^{FF} increases and ξ_+^F decreases [1].

When the slope of the characteristic Γ_+^F corresponding on the steady state is solved, the shape of the rear part of the chromatogram is known. The four cut times and the steady state feed composition can be predicted by using the following approach. At first, the cut time t_{B2} is chosen equal to the time of complete elution of the feed pulse. For Langmuir isotherm, the resulting expression is

$$t_{B2} = t_0(1 + \phi H_2) + \Delta t^F \tag{11}$$

where the duration of the feed pulse is given by $\Delta t^F = V^F/Q$ with Q being the volumetric flow rate.

To find the cut time t_{B1} the rear part of the chromatogram is integrated backwards. Starting at time $t = t_{B2}$, the amounts $m_i^j(t)$ are calculated until the purity constraint of the product fraction B, Eq. (7), is satisfied exactly. Depending on p_2^B, there exist two possibilities for the location of the cut point $B1$. When p_2^B is high, the cut point is located on the mixed wave while for low p_2^B values it lies on the feed plateau. The limit for these two cases, $p_{2,\mathrm{limit}}^B$, is given in Appendix A, Eq. (A.11). In addition, it is shown that the cut point $B1$ relative to the end of the feed pulse $\tau_{B1} = t_{B1} - \Delta t^F$ is independent of the volume of feed pulse. The design is based on Eq. (A.21) when $p_2^B \geq p_{2,\mathrm{limit}}^B$ and on Eq. (A.15) when $p_2^B < p_{2,\mathrm{limit}}^B$.

Once the cut times t_{B1} and t_{B2} are solved, also the mass in product fraction B is known from the backwards integration. If V^{FF} or V^{SR} are not used as a design criterion, they are solved from the global mass balance of the second component. Because no waste stream is allowed, the resulting expressions are

$$V^{FF} = \frac{m_2^B}{c_2^{FF} Y_2} = \frac{Q \int_{t_{B1}}^{t_{B2}} c_2 dt}{c_2^{FF} Y_2} \tag{12}$$

$$V^{SR} = K V^{FF} \tag{13}$$

where the yield Y_2 is calculated from the purity constraints as shown in Eq. (9). Explicit expression for V^{FF} is given in Appendix A, Eqs. (A.16) and (A.22).

The end time of fraction A, t_{A2}, is determined from volume balances

$$t_{A2} = t_{B1} - \Delta t^F + \frac{V^{FF} - V^{SR}}{Q} = \tau_{B1} + \frac{V^{FF} - V^{SR}}{Q} \tag{14}$$

As seen in the equation, also t_{A2} is independent of the volume of the feed pulse.

The steady state feed composition is solved from the mass balance around the feed node

$$c_i^F = \frac{c_i^R V^R + c_i^{FF} V^{FF}}{V^F} \quad \text{for } i = (1, 2) \tag{15}$$

where V^R is the volume of recycle fraction and c_i^R is the volume-average concentration of component i given by

$$V^R = V^F - V^{FF} + V^{SR} \tag{16}$$

$$c_i^R = \frac{Q \int_{t_{A2}}^{t_{B1}} c_i dt}{V^R} \quad \text{for } i = (1, 2) \tag{17}$$

When V^F is relatively low, the cut time t_{A2} is located on the mixed wave and the steady state feed concentrations decrease with increasing V^F. For high V^F values, t_{A2} is located on the feed plateau and the steady state feed composition is independent of V^F. The limit for these two cases is derived in Appendix B. The steady state feed composition can be calculated analytically by using Eqs. (A.7), (A.8), (A.26) and (A.27).

As a final step, the remaining cut time t_{A1} is chosen equal to the retention time of the pure component 1 shock. If the feed pulse is large enough, the plateau of pure first component (Q) prevails and the cut time t_{A1} is given by

$$t_{A1} = t_0 \left(1 + \phi \frac{q_1^{\mathrm{eq}}(c_1^Q, 0)}{c_1^Q}\right) \tag{18}$$

In the case of sufficiently small feed pulse, the plateau is eroded completely and the exact value of t_{A1} can be calculated analytically by using the equations or the free software given in [18].

3. Operating regions for SSR–SR process

3.1. Solvent removal constraints

As mentioned in Section 2.4, SSR–SR process has the following two freely adjustable operating parameters: (1) the volume of feed pulse into the column and (2) the volume of fresh feed (or alternatively the volume of removed solvent or the solvent removal capacity). The region of feasible operating parameters depends on the process configuration and the extent of solvent removal which is often limited by different factors. The solvent removal constraints

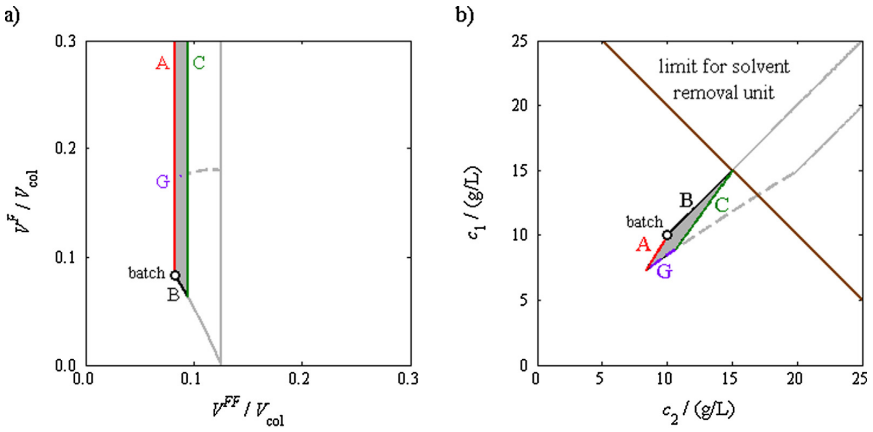

Fig. 4. (a) Regions of feasible operating parameters and (b) regions of feasible steady state feed compositions for SSR–SR configuration I (solvent removal from fresh feed) when the limit for solvent removal unit is $c_1^{FF'} + c_2^{FF'} \leq 30$ g/L. Grey lines: operating regions without solvent removal constraints. Same fresh feed concentrations, isotherm parameters, phase ratio, and purity constraints as in Fig. 3.

can be divided in the following two categories: (1) maximum concentration achievable in the solvent removal unit (*e.g.* solubility, osmotic pressure, or vapour pressure limit) and (2) maximum concentration of the solution fed into the column (*e.g.* solubility or viscosity limit). In this work, the discussion is limited to continuous constraints that can be expressed in form

$$g_1(c_1^j, c_2^j) \leq 0 \quad \text{for } j = (FF', R', F) \tag{19}$$

$$g_2(c_1^F, c_2^F) \leq 0 \tag{20}$$

where the limit for the maximum concentration of the solution in the solvent removal unit is given by function g_1 and the limit for the maximum concentration of the column feed is given by function g_2. By using the notation in Fig. 3 we have $j = FF'$ for configuration I, whereas for configuration II, $j = R'$, and for configuration III, $j = F$.

In the following Sections 3.2–3.4, the operating regions of the three SSR–SR configurations and batch chromatography integrated with solvent removal are derived for the case when the maximum concentration of the solvent removal unit, Eq. (19), is the limiting factor. The regions of corresponding steady state feed compositions on the hodograph plane can be constructed by using the design method reviewed in Section 2.4. The discussion is not limited to any special concentration limit type but is valid for arbitrary constraints. It is worth noting that the operating regions in the case of no solvent removal constraints derived in [1] are obtained as a limiting value by setting $g_1 \leq \infty$.

In SSR–SR configuration III, the composition of the outlet stream of the solvent removal unit is equal to the column feed. This means that the operating limits caused by the constraints for the maximum concentration of the column feed are obtained for all SSR–SR options from the approach derived in Section 3.4 by replacing the limit g_1 with limit g_2. In addition, the operating regions for the cases when both the maximum concentration of solution in the solvent removal unit and in the column feed limits the operation can be solved by combining different limits. This issue is discussed in Section 3.5.

3.2. SSR–SR configuration I and batch chromatography with solvent removal

An example of the operating region of SSR–SR configuration I for the case when the maximum concentration achievable in the solvent removal unit, Eq. (19), limits the operation is shown in Fig. 4a. The region is a half-open domain limited by the following three lines (1) lower limit for V^{FF} that corresponds to the operation of conventional SSR chromatography (limit A), (2) lower limit for V^F that corresponds to the operation of classical batch chromatography with solvent removal (limit B), and (3) upper limit for V^{FF} that depends on the solvent removal constraint (limit C). As to the maximum V^F, there is no upper limit because the volume of the recycle fraction can be increased indefinitely. However, when V^F is relatively high, the beginning of the recycle fraction, t_{A2}, is located on the feed plateau. Part of the feed plateau is recycled and the operation is suboptimal. The maximum V^F with which the feed plateau is not recycled is denoted in Fig. 4 by violet dashed line (limit G). As to the hodograph plane, Fig. 4b, the limit corresponds on the minimum steady state feed composition of SSR–SR process [1]. An explicit equation to calculate the limiting V^F for a given V^{FF} is given in Appendix B, Eq. (B.2).

Calculation of the lower limit for V^{FF} (limit A in Fig. 4) is based on the fact that in SSR–SR process, the volume of fresh feed increases when the volume of removed solvent increases. The minimum V^{FF} is thus obtained when $V^{SR} = 0$. As already mentioned, this corresponds to the operation of conventional SSR process. Under ideal conditions, the volume of fresh feed that can be processed in SSR chromatography is independent of V^F and equal to that of classical batch process [16]. The operating region of SSR process is thus a straight vertical line starting from the operating point of classical batch chromatography (black circle in Fig. 4). The corresponding V^{FF} can be calculated with the design method reviewed in Section 2.4 by setting $K = 0$ and using Eq. (12).

In SSR–SR process, V^F increases linearly when the volume of the recycle fraction increases [1]. The lower limit of V^F (limit B) is obtained when $V^R = 0$ which corresponds to the operation of batch chromatography with solvent removal from fresh feed. On the hodograph plane, the steady state feed composition is located on the line that passes through the origin and *FF* (black solid line in Fig. 4b). To construct the limit on the (V^{FF}, V^F) plane, the solvent removal capacity K is varied from 0 to the upper limit $K_{\text{limit C}}$ (see below the calculation of $K_{\text{limit C}}$). The corresponding V^{FF} and V^{SR} values are solved by using the design method described in Section 2.4, Eqs. (12) and (13). The desired V^F is then obtained from the volume balance by setting $V^R = 0$ which yields $V^F = V^{FF} - V^{SR}$.

The upper limit for V^{FF} is obtained when maximum amount of solvent is removed. As to the hodograph plane, this means that point *FF*′ is located on the concentration constraint (Fig. 4b).

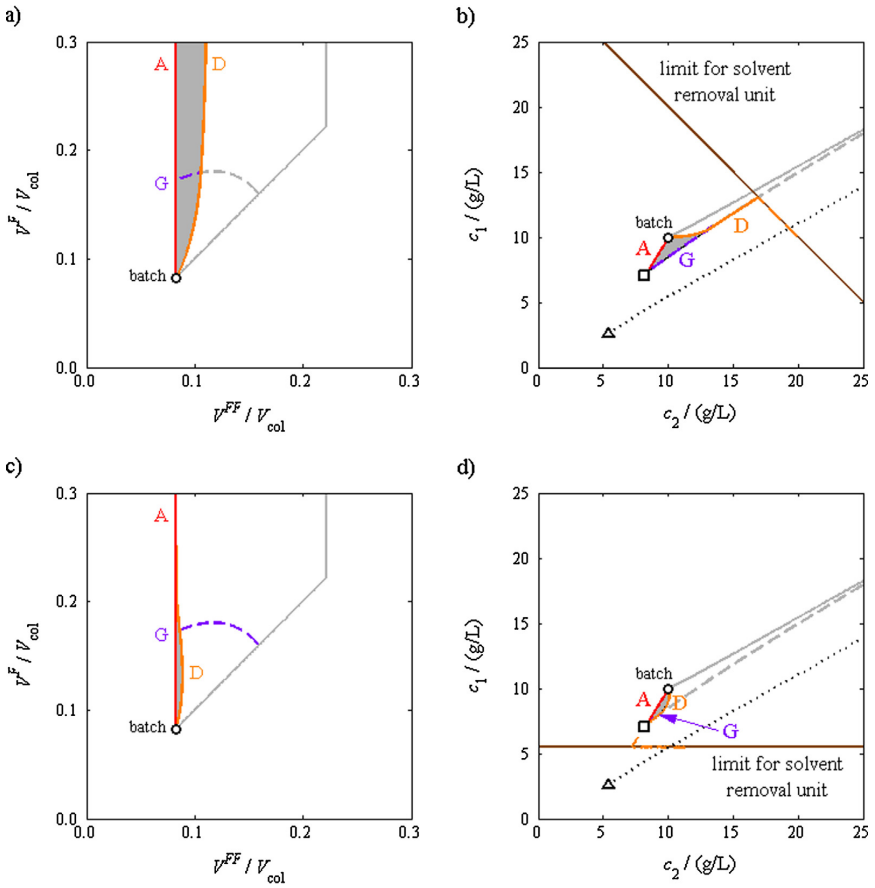

Fig. 5. (a) Regions of feasible operating parameters and (b) regions of feasible steady state feed compositions for SSR–SR configuration II (solvent removal from recycle fraction) when the limit for solvent removal unit is $c_1^{R'} + c_2^{R'} \leq 30$ g/L. (c) Regions of feasible operating parameters and (d) regions of feasible steady state feed compositions for SSR–SR configuration II when the limit for solvent removal unit is $c_1^{R'} \leq 6$ g/L. Grey lines: operating regions without solvent removal constraints. Black triangle: minimum R in SSR process. Black square: maximum R in SSR process. Black dotted line: lower limit for R in SSR–SR process II. Orange dashed line: R' corresponding upper limit for V^{FF} in SSR–SR process II. Same fresh feed concentrations, isotherm parameters, phase ratio, and purity constraints as in Fig. 3. (For interpretation of the references to color in figure legend, the reader is referred to the web version of the article.)

To calculate the maximum V^{FF}, the intersection of the operation line of the solvent removal unit, $c_1 = (c_1^{FF}/c_2^{FF})c_2$, and the solvent removal constraint, Eq. (19), is first solved. The point will henceforth be denoted as $(c_{2,\text{limit C}}^{FF'}, c_{1,\text{limit C}}^{FF'})$. When the solvent removal constraint is linear, a simple analytic expression for the intersection is obtained. In the general case, the point must be solved numerically.

Once the point $(c_{2,\text{limit C}}^{FF'}, c_{1,\text{limit C}}^{FF'})$ is known, the corresponding solvent removal capacity is obtained from the mass balance around the solvent removal unit

$$K_{\text{limit C}} = \frac{c_{i,\text{limit C}}^{FF'} - c_i^{FF}}{c_{i,\text{limit C}}^{FF'}} \tag{21}$$

Finally, the volume of fresh feed is calculated by using Eq. (12).

It is interesting to note that when the solvent removal constraint tends towards infinity, the limiting solvent removal capacity $K_{\text{limit C}}$ tends towards 1. In other words, in the case of no solvent removal limitations, the upper limit for V^{FF} is achieved when $V^{FF} = V^{SR}$ (grey vertical line in Fig. 4a). As to the hodograph plane, this means that the steady state feed composition cannot be located on such a characteristic Γ_+ that has a slope lower than c_1^{FF}/c_2^{FF}.

3.3. SSR–SR configuration II

Examples of the regions of feasible operating parameters for SSR–SR configuration II are shown in Fig. 5. The shape of the operating region depends on the location of the limit for maximum concentration achievable in the solvent removal unit, Eq. (19), with respect to the limits for the minimum and maximum recycle fraction composition in the case of SSR–SR process II without solvent removal constraints. The upper limit for R is equal to the minimum steady state feed composition (limit G in Fig. 5b and d). The lower limit for R (black dotted line in Fig. 5b and d) is in turn obtained from Eq. (17) by using V^{FF} and V^F values that corresponds on the lower limit for V^F in the case of no solvent removal constraints, *i.e.* $V^F = V^{FF}$ (grey line in Fig. 5a and b). The minimum, $R_{\text{min}}^{\text{SSR}}$, and maximum, $R_{\text{max}}^{\text{SSR}}$, recycle fraction compositions in the conventional SSR process are denoted in Fig. 5b and d by black triangle and black square, respectively.

Fig. 5a and b represents the case where the maximum concentration reachable in the solvent removal unit is higher than R^{SSR}_{max}. On the (V^{FF}, V^F) plane, the operating region is a half-open region limited by the operating line of conventional SSR chromatography (limit A) and the upper limit of V^{FF} (limit D). As in the case of SSR–SR configuration I, the upper limit for V^{FF} is obtained when as much solvent as possible is removed. On the hodograph plane, the composition of the concentrated recycle fraction R' is thus located on the solvent removal constraint (orange dashed line in Fig. 5b). The point R' is related to the average recycle fraction composition R by

$$\frac{V^{SR}}{V^R} = \frac{c_i^{R'} - c_i^R}{c_i^{R'}} \tag{22}$$

The upper limit for V^{FF} can be constructed on the (V^{FF}, V^F) plane by varying the composition R' on the solvent removal constraint curve and by solving the corresponding V^{FF} and V^F from the system of Eqs. (12), (13), (16), (17) and (22). However, the system remains implicit and it must be solved numerically. In this work, the limit is calculated by using the following numerical approach. At first, the volume of feed pulse into the column is varied upward from the value of V^F that corresponds on the operation of classical batch chromatography. For each V^F, the corresponding solvent removal capacity is then calculated by using a numerical root-finding algorithm to find the values of K with which $g_1(c_1^{R'}(K), c_2^{R'}(K)) = 0$ where $c_i^{R'}(K)$ is solved from Eq. (22). Finally, the corresponding fresh feed volumes are calculated from Eq. (12).

As seen in Eq. (22), the ratio V^{SR}/V^R tends towards unity when the solvent removal constraint tends towards infinity. In the case of no solvent removal limitations, the upper limit of V^{FF} is thus obtained when $V^{SR} = V^R$, *i.e.* $V^F = V^{FF}$ (grey line with slope 1 in Fig. 5a and c). However, when V^{FF} is sufficiently high, the recycle fraction composition approaches infinity independent of V^F (grey vertical line in Fig. 5a and c). At the same time, the cut time t_{A2} approaches the retention time of a non-retained component t_0 [1]. An explicit equation to calculate the corresponding V^{FF} is given in Appendix C.

In Fig. 5c and d, the solvent removal constraint is located between R^{SSR}_{min} and R^{SSR}_{max}. With relatively low V^F, the point R in SSR–SR process is located below the solvent removal constraint and operation of SSR–SR configuration II is feasible. When the volume of feed pulse increases, the volume-average composition of the recycle fraction increases and becomes higher than the solvent removal limit. The SSR–SR II can no longer be operated. The upper limit for V^{FF} can be constructed by using the same numerical approach as in the previous case. However, when V^F is high, $g_1(c_1^R(K = 0), c_2^R(K = 0)) > 0$, and the function g_1 has no root. This corresponds to the condition where the operation of SSR–SR process II is not possible.

In the last case, the solvent removal constraint lies below the minimum recycle fraction composition. The operation of SSR–SR configuration II is not feasible independent of the volume of feed pulse.

3.4. SSR–SR configuration III

Fig. 6 shows examples of the regions of feasible operating parameters for SSR–SR configuration III. The shape of the operating region depends on the location of the limit for maximum concentration achievable in the solvent removal unit, Eq. (19), with respect to the region of feasible steady state feed compositions for SSR–SR process III without solvent removal constraints (grey lines in Fig. 6).

Fig. 6a and b represents the case where the fresh feed composition is lower than the concentration constraint for the solvent removal unit. On the hodograph plane (Fig. 6b), the solvent removal constraint intersects the upper (limit B) and the lower (limit G) limits for F but not the operating line of conventional SSR chromatography (limit A). As to the (V^{FF}, V^F) plane (Fig. 6a), the upper limit for V^{FF} (limit E) is larger than the volume of fresh feed than can be processed in the conventional SSR process independent of V^F.

The limit for maximum V^{FF} is again obtained when as much solvent as possible is removed. On the hodograph plane (Fig. 6b), this corresponds on the condition where the steady state feed composition is located on the solvent removal constraint. To construct the upper limit for V^{FF} into the (V^{FF}, V^F) plane (Fig. 6a), the point ($c^F_{2,\text{limit E}}$, $c^F_{1,\text{limit E}}$) is varied along the solvent removal constraint within the limits for feasible steady state feed composition in the case of no solvent removal constraints. The corresponding ξ^F_+ is calculated from Eq. (A.3), ω_1^F from Eq. (A.1), ω_2^F from Eq. (A.2), K from Eq. (10), V^{FF} from Eq. (12), and t_{A2} from Eq. (14). Finally, the volume of feed pulse into the column is solved from Eq. (15) by setting $c_i^F = c^F_{i,\text{limit E}}$ which yields

$$V^F = \left[\mu - 2\left(\omega_1^F + \sqrt{(\omega_1^F)^2 - \mu\omega_1^F + \frac{Q(t_{A2} - t_0)}{\sigma}}\right)\right]\sigma\omega_1^F \tag{23}$$

where σ and μ are auxiliary parameters given by

$$\sigma = \frac{(1-\varepsilon)\omega_2^F}{H_1 H_2} V_{\text{col}} \tag{24}$$

$$\mu = 2\omega_1^{B1} + \left(1 - \frac{c_1^{FF}}{c_2^{FF}}\frac{H_1}{H_2}\frac{1}{\xi_+^F}\right)\frac{(H_2 - \omega_1^{B1})^2}{(H_2 - H_1)Y_2} \tag{25}$$

When V^F is relatively high, the cut time t_{A2} is located on the feed plateau (limit G) and the steady state feed composition is independent of the V^F as already mentioned in Section 2.4. On the (V^{FF}, V^F) plane, the upper limit for V^{FF} is thus a straight vertical line above the limit G. The corresponding steady state feed composition is located at the intersection of the solvent removal constraint and the limit G (Fig. 6b).

When the solvent removal constraint tends towards infinity, the maximum V^{FF} tends towards a certain finite value [1]. The upper limit of V^{FF} is a straight vertical line and equal to the upper limit of V^{FF} for SSR–SR configuration II (grey vertical line in Fig. 6a and c). As already mentioned, an explicit equation to calculate the limit is given in Appendix C.

In the second case, the solvent removal constraint intersects the operating line of conventional SSR process (limit A). An example is shown in Fig. 6c and d. When V^F is relatively small, the steady state feed composition is higher than the maximum concentration achievable in the solvent removal unit and the SSR–SR configuration III cannot be operated. For high V^F, the feed composition is located below the solvent removal limit and the operation is feasible. The upper limit for V^{FF} can be constructed on the (V^{FF}, V^F) plane by using the same approach as in the previous case.

In the third case, the solvent removal constraint does not intersect the region of F in the case of SSR–SR process III without solvent removal constraints. The lower limit for steady state feed composition (limit G) in the case of no solvent removal constraints is higher than the maximum concentration reachable in the solvent removal unit. The operation of SSR–SR configuration III is not feasible.

3.5. Combination of operating limits

In Sections 3.2–3.4, the operating regions of SSR–SR configurations were derived for the case when only the maximum concentration reachable in the solvent removal unit limits the operation. Next, the following two issues will be discussed (1) the operation is limited by the constraint for maximum concentration of the solution fed into the column and (2) the operation is limited by both the constraint for maximum concentration reachable in

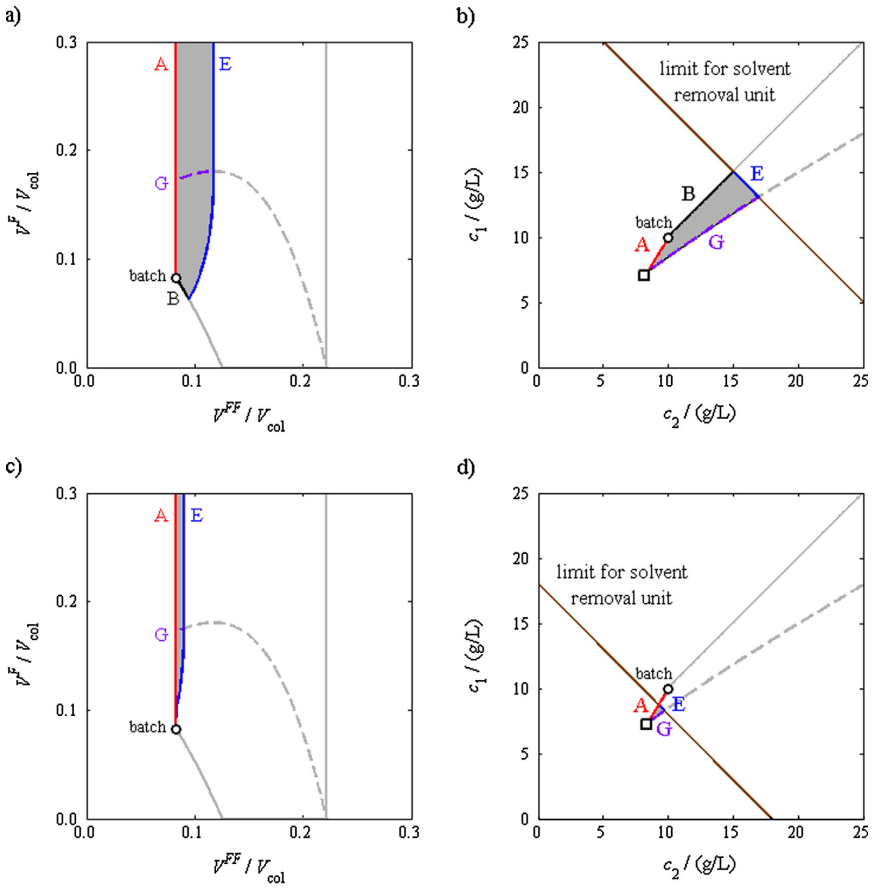

Fig. 6. (a) Regions of feasible operating parameters and (b) regions of feasible steady state feed compositions for SSR–SR configuration III (solvent removal from mixed fraction) when the limit for solvent removal unit is $c_1^F + c_2^F \leq 30$ g/L. (c) Regions of feasible operating parameters and (d) regions of feasible steady state feed compositions for SSR–SR configuration III when the limit for solvent removal unit is $c_1^F + c_2^F \leq 18$ g/L. Grey lines: operating regions without solvent removal constraints. Same fresh feed concentrations, isotherm parameters, phase ratio, and purity constraints as in Fig. 3.

the solvent removal unit and the constraint for maximum concentration of the solution fed into the column. Examples of these two cases are shown in Fig. 7.

Fig. 7a and b displays the case where the limit for maximum concentration of the column feed is $c_1^F + c_2^F \leq 45$ g/L. In SSR–SR configuration III, the composition of the outlet stream of the solvent removal unit is equal to the column feed. The operating region for SSR–SR process III is thus obtained by using the approach described in Section 3.4 by replacing the limit for solvent removal unit, Eq. (19), by limit for column feed, Eq. (20). On the (V^{FF}, V^F) plane, the operating domain is a half-open region limited by lines A, B and E (Fig. 7a).

The operating regions of SSR–SR configurations I and II are intersections of the corresponding operating regions without solvent removal constraints (grey lines in Fig. 7a and b) and the operating region of SSR–SR configuration III. When V^F is relatively small, the operation of SSR–SR process I is limited by the maximum concentration of the column feed (limit E in Fig. 7a and b). For sufficiently large V^F, on the other hand, the steady state feed concentration reachable in the SSR–SR process I is smaller than the limit for column feed because large recycle fraction dilutes the feed solution. The upper limit for V^{FF} is equal to the corresponding limit without concentration constraints (limit C in Fig. 7a and b).

In the case of the SSR–SR configuration II, relatively small V^F values lead to steady state feed concentrations that are lower than the constraint for maximum column feed. The upper limit for V^{FF} is equal to the corresponding limit without concentration constraints (limit D in Fig. 7a and b). When the volume of feed pulse increases, the steady state feed concentrations on the limit D increase. For sufficiently large V^F, the operation is thus limited by the constraint for column feed (limit E in Fig. 7a and b).

Fig. 7c and d show the case when both the constraint for solvent removal unit ($c_1^j + c_2^j \leq 45$ g/L) and the constraint for the column feed ($c_1^F + c_2^F \leq 30$ g/L) limit the operation. The operation region for SSR–SR III is now obtained by using the approach described in Section 3.4 and the stricter of the two constraints g_1 and g_2. The operation domains of SSR–SR configurations I and II are in turn intersections the corresponding operating regions when only the solvent removal constraint limits operation (grey lines in Fig. 7c and d) and the region when the operation is limited by the constraint for column feed. The behaviour is very similar as in the previous case. When V^F is relatively small the operation of SSR–SR process I

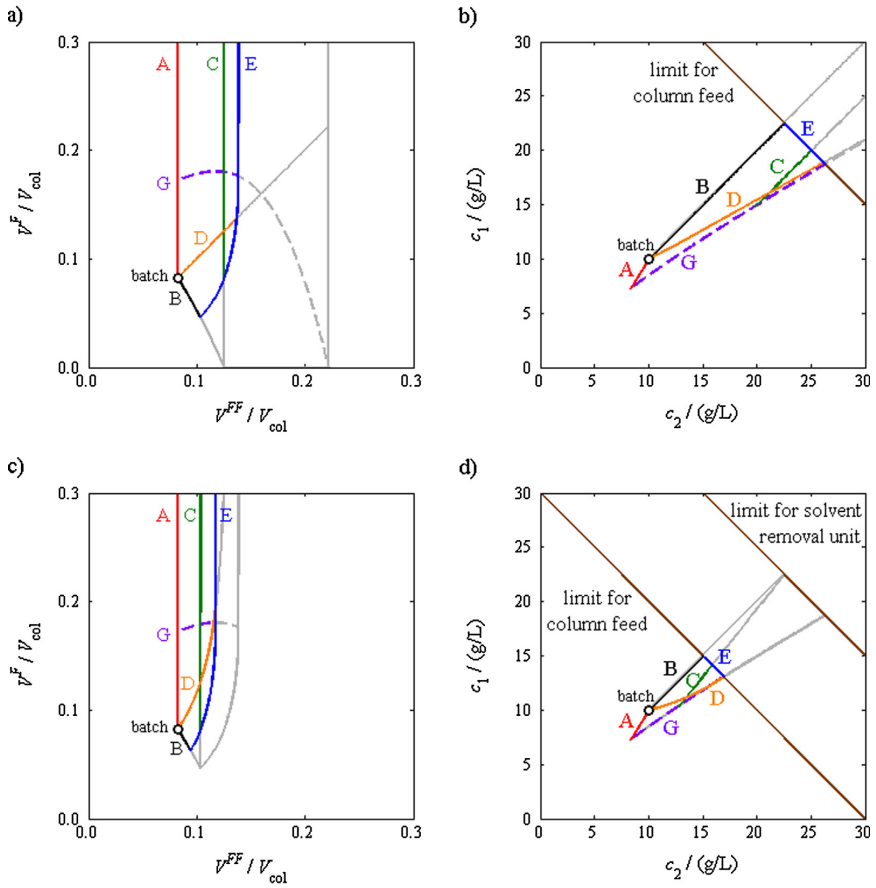

Fig. 7. (a) Regions of feasible operating parameters and (b) regions of feasible steady state feed compositions for different SSR–SR configurations when the limit for column feed is $c_1^F + c_2^F \leq 45$ g/L. (c) Regions of feasible operating parameters and (d) regions of feasible steady state feed compositions for different SSR–SR configurations when the limit for solvent removal unit is $c_1^j + c_2^j \leq 45$ g/L ($j = FF', R', F$) and the limit for column feed is $c_1^F + c_2^F \leq 30$ g/L. Same fresh feed concentrations, isotherm parameters, phase ratio, and purity constraints as in Fig. 3.

is limited by the maximum feed concentration in the column (limit E in Fig. 7c and d), while for large V^F the constraint for solvent removal limits the operation (limit C in Fig. 7c and d). For SSR–SR configuration II opposite behaviour is again observed.

4. Performance evaluation: case studies

The calculation method presented above is applied to study the performances of the three SSR–SR configurations under ideal conditions. The following two case studies are investigated: (1) separation of mandelic acid enantiomers and (2) separation of EMD 53986 enantiomers.

4.1. Performance parameters

The process performance is evaluated in terms of productivity, *PR*, and specific eluent consumption, *EC*. The productivity is defined as the total amount of components in the desired product fractions divided by the cycle time, Δt_{cycle}, and the column volume, V_{col}

$$PR = \frac{m_1^A + m_2^B}{\Delta t_{cycle} V_{col}} = \frac{(Y_1 c_1^{FF} + Y_2 c_2^{FF}) V^{FF}}{\Delta t_{cycle} V_{col}} \quad (26)$$

It is assumed that the process is operated with "stacked injections" such that the elution profiles of consecutive cycles do not overlap but there is no gap between them either. The cycle time is thus given by

$$\Delta t_{cycle} = t_{B2} - t_{A1} \quad (27)$$

The specific eluent consumption is given by the ratio between the amount of eluent used in a chromatographic cycle, V_{eluent}, and the amount of products

$$EC = \frac{V_{eluent}}{m_1^A + m_2^B} = \frac{Q\Delta t_{cycle} - V^F}{(Y_1 c_1^{FF} + Y_2 c_2^{FF}) V^{FF}} = \frac{Q(\tau_{B2} - t_{A1})}{(Y_1 c_1^{FF} + Y_2 c_2^{FF}) V^{FF}} \quad (28)$$

In practice, the removed solvent can be used as eluent to reduce the need of fresh eluent as shown in Fig. 1. In addition, also the solvent removal capacity affects the separation costs and could be considered as a third performance parameter. In the following discussion, however, it is assumed that an equal solvent removal capacity is applied in all process configurations. If it is not possible to remove solvent from the recycle or feed fractions, the solvent is removed from the product fractions. The definition of *EC* used here is thus justified, and it allows showing that solvent removal may

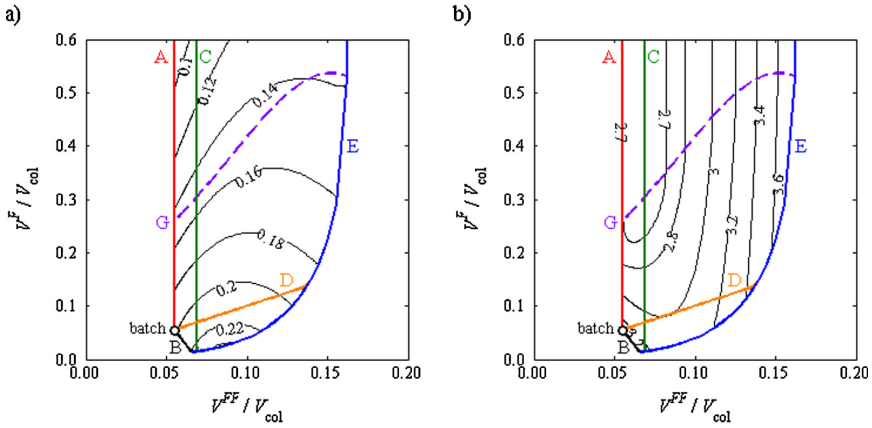

Fig. 8. Regions of feasible operating parameters for separation of mandelic acid enantiomers with (a) productivity contour lines and (b) eluent consumption contour lines. Fresh feed concentrations: $c_1^{FF} = c_2^{FF} = 1.0$ g/L. Purity constraints: $p_1^A = p_2^B = 0.95$.

decrease the eluent consumption even when removed solvent is not reused as eluent.

4.2. Separation of mandelic acid enantiomers

The adsorption equilibrium of mandelic acid enantiomers in water–acetic acid–acetonitrile (86.4:9.1:4.5, v/v), 0.05 mol/L ammonium acetate (pH = 3.0) mobile phase on nucleodex β-OH stationary phase follows competitive Langmuir isotherm model [19]. The isotherm parameters at 20 °C for the less absorbed *S*(+)-enantiomer are $K_1 = 0.1111$ L/g and $N_1 = 72.5$ g/L and for the more absorbed *R*(−)-enantiomer $K_2 = 0.1222$ L/g and $N_2 = 70.6$ g/L. The separation factor is thus relatively small, $\alpha = 1.07$. The overall void fraction of the bed is 0.756.

The solubility of the mandelic acid enantiomers in the considered mobile phase is relatively high (more than 50 g/L) [19]. The maximum total concentration of the column feed is limited by the fact that pH must be stabilized to avoid significant change of the adsorption equilibrium and decrease of selectivity [20]. For the given specific buffer concentration pH starts to change when the total mandelic acid concentrations exceeds 10 g/L [19].

The regions of feasible operating parameters on the (V^{FF}, V^F) plane are shown in Fig. 8. The fresh feed concentrations are $c_1^{FF} = c_2^{FF} = 1.0$ g/L and the purity constraints $p_1^A = p_2^B = 0.95$. Productivity and specific eluent consumption are displayed as contour lines that show the points with equal value of the performance parameters.

As observed in Fig. 8, the SSR–SR configuration III, *i.e.* solvent removal from the column feed, has the widest range of feasible operating parameters (boundaries: A–B–E). For SSR–SR configuration I (solvent removal from the fresh feed; boundaries: A–B–C), the maximum achievable V^{FF} is 59% smaller than for SSR–SR III. This is because for relatively high V^{FF} values the required V^{SR} is higher than V^{FF} and enough solvent cannot be removed from the fresh feed. In the case of SSR–SR configuration II (solvent removal from the recycle fraction; boundaries: A–D–E), the volume of recycle fraction is smaller than the required V^{SR} when the volume of feed pulse is relatively low. For sufficiently large V^F, the recycle fraction becomes large enough and the operation is possible.

For a given volume of fresh feed and thus for a given solvent removal capacity, the productivity decreases when the volume of feed pulse increases. This stem from prolonged cycle time due to increased volume of recycle fraction. For relatively low V^F values (below limit G in Fig. 8), the increase in V^R decreases the steady state feed concentrations and slows down the propagation velocity of the first shock. As a result, the cut time t_{A1} value can be adjusted later and the eluent consumption decreases until it levels off when the feed plateau is recycled. The results are congruent with the findings of Sainio and Kaspereit [16] for conventional SSR chromatography and the findings of Siitonen et al. [1] for SSR–SR process without solvent removal constraints.

When the volume of feed pulse is constant, the upper limit for the volume of fresh feed is reached with maximum solvent removal capacity. The productivity, however, goes through maximum and the eluent consumption goes through minimum when the volume of fresh feed and the solvent removal capacity increase. This can be explained by the fact that the solvent removal increases steady state feed concentrations and speeds up the propagation velocity of the first shock. This leads to prolonged cycle time which counterbalances the increase of the volume of fresh feed.

Fig. 9a shows the productivity and the eluent consumption on the operating limits, *i.e.* when maximum amount of solvent is removed. In the cases of conventional SSR process (red line in Fig. 9) and SSR–SR configuration I (green line in Fig. 9), *PR* and *EC* decreases monotonically with increasing V^F because the cycle time increases but the volume of fresh feed remains constant. For SSR–SR configurations II and III (orange and blue lines in Fig. 9), V^{FF} depends on V^F. When V^F is relatively low, productivity slightly increases with increasing V^F due to increase in V^{FF}. For high V^F values, the cycle time increases significantly and productivity starts to decrease. It is also observed that for all SSR–SR configurations, maximum *PR* is obtained when the process is operated at the solvent removal constraint. To obtain minimum *EC*, in contrast, maximum solvent removal capacity should not be applied.

In Fig. 9b the overall process performance consisting of *PR* and *EC* is displayed by using Pareto frontiers. The Pareto curves show the maximum productivity achievable with certain eluent consumption. In the case of all three SSR–SR configurations, a trade-off between *PR* and *EC* is clearly required. For example, when the SSR–SR process III is optimized with respect to maximum productivity, eluent consumption is 17.6% higher than achievable minimum eluent consumption.

As can be expected, SSR–SR configuration III is the most efficient one due to largest operating region. It leads to 4.4% higher productivity with 5.7% lower eluent consumption than batch process with a similar solvent removal unit when the processes are optimized with respect to productivity. Due to ideal conditions, however, here

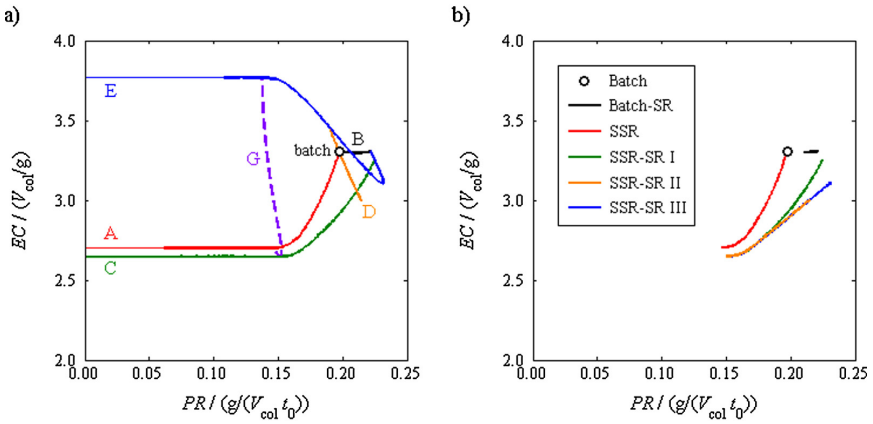

Fig. 9. Performance of different process configurations for separation of mandelic acid enantiomers. (a) Process performance on the operating limits. (b) Pareto frontiers of different configurations. Same fresh feed concentrations and purity constraints as in Fig. 8. (For interpretation of the references to color near the citation of this figure, the reader is referred to the web version of the article.)

the benefit is much smaller compared to those reported under strongly non-ideal conditions by Hellstén et al. [11] for separation of glucose and galactose and Kaspereit and Sainio [3] for separation of two cycloketones. In simple terms, the performance of batch operation (with or without solvent removal) is much more strongly affected by dispersion than SSR chromatography. In fact, if SSR and batch were operated with the same fresh feed amount under non-ideal conditions, SSR would produce a higher purity for two reasons. Firstly, in SSR the overlapping parts of the chromatogram that were affected by dispersion are not collected into the product fractions but recycled, whereas in batch operation the purity constraints can be met only by decreasing the fresh feed injection volume. Secondly, SSR schemes are less sensitive to dispersive effects due to higher column overloading. As a result, the advantages of SSR operation are emphasized when the column efficiency is low.

As to the SSR–SR configuration I, it slightly outperforms batch–SR process in terms of maximum productivity. This is because the concentrations of the column feed instead of the operation of the solvent removal unit limit the amount of solvent removal. In the case of SSR–SR I, fresh feed can be concentrated over the pH stability limit and diluted with recycle fraction. The maximum productivity of SSR–SR configuration II is smaller than that of other SSR–SR processes because operation with relatively small recycle fraction volumes, and thus small feed pulse volumes, is not possible.

4.3. Separation of EMD 53986 enantiomers

The adsorption equilibrium of EMD 53986 enantiomers in 100% ethanol on amylose-tris(3,5-dimethylphenylcarbamate) stationary phase is characterized by modified competitive Langmuir model [21]. One of the enantiomers can be used as a precursor for a pharmaceutical calcium sensitizing agent whereas the other has no such activity. In this work, the modified Langmuir isotherms are approximated with competitive Langmuir model. The resulting isotherm parameters at 25 °C are $K_1 = 0.067$ L/g, $N_1 = 112.3$ g/L, $K_2 = 0.251$ L/g, and $N_2 = 72.8$ g/L. The separation factor, $\alpha = 2.34$, is now much larger compared to the separation of mandelic acid enantiomers. The total void fraction of the bed is 0.72.

The maximum concentration reachable in the solvent removal unit and the maximum concentration of column feed are limited by the solubility of EMD 53986 enantiomers in ethanol. The solubility curve shown in Fig. 11 is interpolated from the solubility data reported by Ströhlein et al. [22]. The curve is symmetric with respect to line $c_1 = c_2$ and its shape is characteristic for enantiomer systems that form a racemic compound. The solubility of the pure enantiomer is about 3.5 g/L and the solubility of 1:1 mixture about 8 g/L. The eutectic compositions are $c_1 = 10.45$ g/L, $c_2 = 0.55$ g/L and $c_1 = 0.55$ g/L, $c_2 = 10.45$ g/L.

The operating regions for the case $c_1^{FF} = c_2^{FF} = 1.0$ g/L and $p_1^A = p_2^B = 0.99$ are shown in Figs. 10 and 11. As expected, the SSR–SR configuration III has again the widest operating region. Due to high separation factor, however, the range of the volume of fresh feed and the volume of feed pulse are now about one order of magnitude larger than in the separation of mandelic acid enantiomers. As to the image of the operating regions on the hodograph plane, high separation factor leads to very narrow operating regions. This is because the pure second component plateau is now relatively high and the recycle fraction composition is very close to the feed composition even when the volume of feed pulse is small. The limit for recycling feed plateau, and thus the lower limit of the steady state

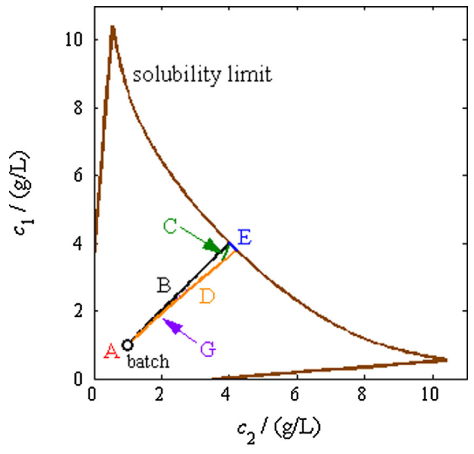

Fig. 10. Regions of feasible steady state feed compositions on the hodograph plane for separation of EMD 53986 enantiomers. Fresh feed concentrations: $c_1^{FF} = c_2^{FF} = 1.0$ g/L. Purity constraints: $p_1^A = p_2^B = 0.99$.

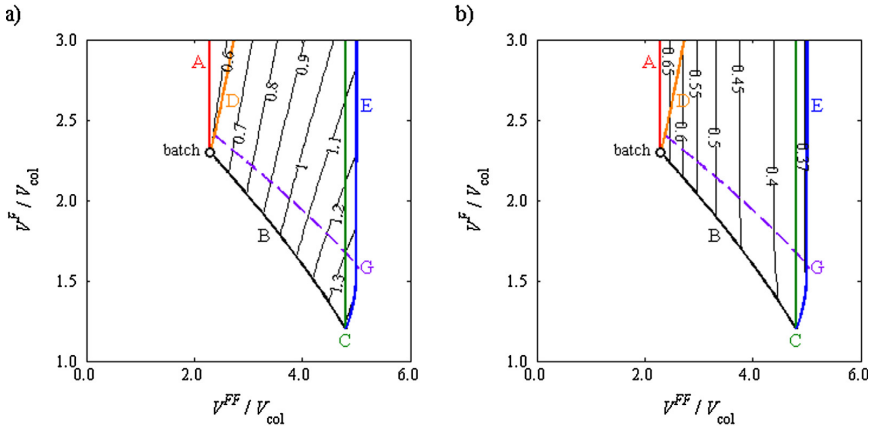

Fig. 11. Regions of feasible operating parameters for separation of EMD 53986 enantiomers with (a) productivity contour lines and (b) eluent consumption contour lines. Same fresh feed concentrations and purity constraints as in Fig. 10.

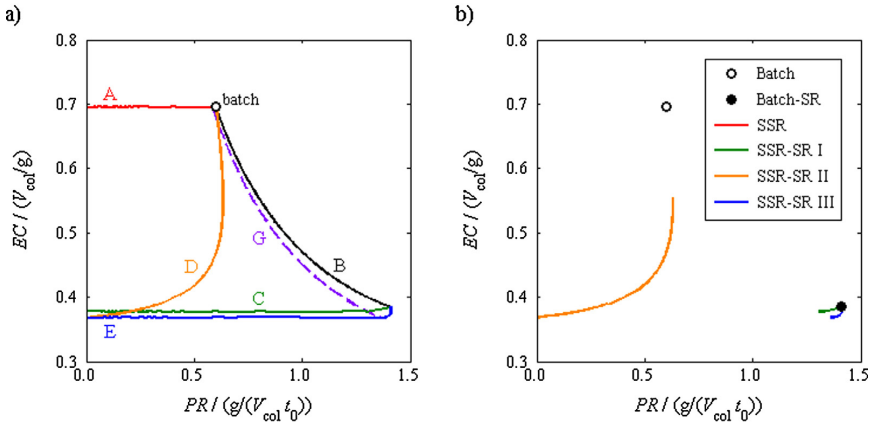

Fig. 12. Performance of different process configurations for separation of EMD 53986 enantiomers. (a) Process performance on the operating limits. (b) Pareto frontiers of different configurations. Same fresh feed concentrations and purity constraints as in Fig. 10.

feed composition (limit G in Figs. 11 and 12), is achieved when V^F is only slightly increased from the value of V^F for batch process with solvent removal (black solid line in Figs. 10 and 11).

When the volume of fresh feed is constant, productivity and eluent consumption decrease with increasing volume of feed pulse. The behaviour is similar to that of separation of mandelic acid enantiomers. In contrast, when the volume of feed pulse is constant, productivity increases and eluent consumption decreases monotonically with increasing volume of fresh feed. Maximum productivities, minimum eluent consumptions and the whole Pareto fronts of different SSR–SR configurations are obtained on the solvent removal limit as seen in Fig. 12. This is explained by the fact that the relatively large volume of feed pulse that is caused by high separation factor leads to long cycle time. For this reason, the effect of decreased retention time of the first shock due to increased feed concentrations on the cycle time, and thus on the productivity and the eluent consumption, is smaller than in the separation of mandelic acid.

It is observed in Fig. 12b that the most efficient process configurations are SSR–SR III, SSR–SR I, and batch–SR. In all these cases, optimal steady state feed composition with respect to productivity lies on the solubility limit and relatively small feed pulse is beneficial. For classical batch chromatography and conventional SSR process, maximum productivity is about 60% lower and minimum eluent consumption about 80% higher than for SSR–SR operation. This is due to low fresh feed concentrations in the conventional processes. In the case of SSR–SR configuration II, the volume of recycle fraction must be increased significantly to increase the volume of fresh feed per cycle. This leads to relatively low eluent consumption but also to low productivity due to prolonged cycle time.

5. Conclusions

The effect of solvent removal constraints on the operation and performance of mixed-recycle steady state recycling chromatography with an integrated solvent removal unit was investigated within the frame of the equilibrium theory. A design method was developed for calculation of regions of feasible operating parameters under arbitrary solvent removal limitations and purity requirements for different SSR–SR configurations. The following two types of concentration constraints were considered: (1) maximum concentration achievable in the solvent removal unit

(*e.g.* solubility, osmotic pressure, or vapor pressure limit) and (2) maximum concentration of the solution fed into the chromatographic column (*e.g.* solubility or viscosity limit). The approach is applicable for binary systems that follow competitive Langmuir adsorption isotherm model. For SSR–SR configurations where solvent is removed from the fresh feed or from the column feed the design equations are explicit. In the case of solvent removal from the recycle fraction, one numerical root-finding step is needed.

The design method presented here is based on the ideal model of chromatography with assumption of infinite column efficiency. For this reason, it is most applicable when the column efficiency is high. However, we believe that the proposed approach can be used in many practical applications to predict the preliminary operating parameters which can be later fine-tuned by using detailed simulations.

The design equations were applied to study the performance of the three SSR–SR configurations in two case studies. Separation of mandelic acid enantiomers and separation of EMD 53986 enantiomers were used as model systems. It was observed that maximum productivity is always obtained when the fresh feed, recycle, or column feed fraction is concentrated on the solvent removal limit. The behaviour of the eluent consumption, in contrast, depends on the isotherm parameters and the solvent removal constraint. In addition, it was demonstrated that SSR–SR process yields higher productivity and/or lower eluent consumption than conventional SSR process or batch chromatography that employs a similar solvent removal unit. The benefit under ideal conditions studied here was smaller than that reported by Hellstén et al. [11] for separation of glucose and galactose under strongly non-ideal conditions.

Acknowledgements

Financial support from Graduate School in Chemical Engineering (GSCE), Finland, and Academy of Finland (grant 252688) are gratefully acknowledged.

Appendix A. Derivation of explicit design equations

In this appendix, explicit equations for the cut time τ_{B1}, the volume of fresh feed, the steady state feed composition and the volume-average steady state recycle fraction composition are derived. The derivation is based on the following variable transform from concentrations (c_1, c_2) to characteristic parameters (ω_1, ω_2) introduced by Mazzotti [14]:

$$\omega_1 = \frac{\left(\xi_- + h\right) H_2}{\xi_- + h\alpha} \tag{A.1}$$

$$\omega_2 = \frac{\left(\xi_+ + h\right) H_2}{\xi_+ + h\alpha} \tag{A.2}$$

where $h = (H_1K_2)/(H_2K_1)$. The slopes of the Γ_+ and Γ_- characteristics denoted by ξ_+ and ξ_-, respectively, are given by

$$\xi_+ = \frac{-\eta + \sqrt{\eta^2 + 4K_1K_2H_1H_2c_1c_2}}{2K_1H_2c_2} \tag{A.3}$$

$$\xi_- = \frac{-\eta - \sqrt{\eta^2 + 4K_1K_2H_1H_2c_1c_2}}{2K_1H_2c_2} \tag{A.4}$$

with $\eta = H_1(1 + K_2c_2) - H_2(1 + K_1c_1)$. It has been shown that there exists a one-to-one mapping between the concentrations (c_1, c_2) and the two characteristic parameters (ω_1, ω_2). The concentrations are given by

$$c_1 = \frac{-H_2(\omega_1 - H_1)(\omega_2 - H_1)}{\omega_1\omega_2(H_2 - H_1)K_1} \tag{A.5}$$

$$c_2 = \frac{H_1(\omega_1 - H_2)(\omega_2 - H_2)}{\omega_1\omega_2(H_2 - H_1)K_2} \tag{A.6}$$

It is worth noting that the notations Γ_1 and Γ_2 used in Mazzotti [14] correspond to the notations Γ_+ and Γ_- used here and in Rhee et al. [13]. In addition, the characteristic parameters defined by Eqs. (A.1) and (A.2) fulfil the conditions $\omega_1 = H_2a$ and $\omega_2 = H_2b$, where a and b are the parameters used in Rhee et al. [13].

As mentioned in Section 2.4, τ_{B1} and V^{FF} depend on the slope of the Γ_+^F characteristic only while the steady state feed and recycle fraction concentrations depend on ξ_+^F and the volume of feed pulse. Depending on p_2^B and V^F, there exist three possibilities for the locations of the cut points $A2$ and $B1$. When p_2^B is relatively high, the cut point $B1$ is located on the mixed wave. The cut point $A2$ lies on the mixed wave or on the feed plateau depending on the size of V^F. For sufficiently low p_2^B values both t_{A2} and t_{B1} are located on the feed plateau independent of V^F.

When t_{A2} and t_{B1} lie on the feed plateau, the volume-average composition of the recycle fraction is equal to the steady state feed composition. On the hodograph plane, the steady state feed composition must lie on the intersection of the characteristic Γ_+^F and the line that passes through the origin and the fresh feed composition FF. The steady state feed and recycle fraction concentrations are thus given by

$$c_1^F = c_1^R = \frac{\xi_+^F(H_2 - H_1)}{\left[\xi_+^F(c_2^{FF}/c_1^{FF}) - 1\right](H_2K_1\xi_+^F + H_1K_2)} \tag{A.7}$$

$$c_2^F = c_1^R = \frac{c_2^{FF}}{c_1^{FF}}c_1^F \tag{A.8}$$

To solve the limiting purity $p_{2,\mathrm{limit}}^B$, whether the cut point $B1$ is located on the mixed wave or on the feed plateau, the amounts of components 1 and 2 that elutes in the tail of the chromatogram after the end of the feed plateau, t_l, are considered. Explicit equations derived by Siitonen et al. [23] are given by

$$m_1^{\mathrm{tail}} = \frac{(1-\varepsilon)(\omega_2^F - H_1)(H_1 - \omega_1^F)^2}{K_1H_1(H_2 - H_1)}V_{\mathrm{col}} \tag{A.9}$$

$$m_2^{\mathrm{tail}} = \frac{(1-\varepsilon)(H_2 - \omega_2^F)(H_2 - \omega_1^F)^2}{K_2H_2(H_2 - H_1)}V_{\mathrm{col}} \tag{A.10}$$

In the above equations, ω_1^F and ω_2^F are ω-values at the feed state. These are calculated from the steady state feed concentrations in the case when B1 lies on the feed plateau by using Eqs. (A.1) and (A.2). Substitution of the Eqs. (A.9) and (A.10) into the definition of p_2^B, Eq. (7), yields to the following expression for the limiting purity

$$p_{2,\mathrm{limit}}^B = \left(1 + \frac{p_1^{FF}}{1 - p_1^{FF}}\frac{H_1 - \omega_1^F}{H_2 - \omega_1^F}\right)^{-1} \tag{A.11}$$

It is worth noting that when $\xi_+^F \le c_1^{FF}/c_2^{FF}$, the characteristic Γ_+^F and the line that passes through the origin and the fresh feed composition do not intersect. In that case, the cut point $B1$ lies always on the mixed wave independent of the purity constraint p_2^B.

When the cut point $B1$ is located on the feed plateau, *i.e.* $p_2^B < p_{2,\mathrm{limit}}^B$ and $\xi_+^F > c_1^{FF}/c_2^{FF}$, the amounts of components 1 and 2 in fraction B are given by

$$m_1^B(\tau_{B1}) = (\tau_l - \tau_{B1})c_1^FQ + m_1^{\mathrm{tail}} \tag{A.12}$$

$$m_2^B(\tau_{B1}) = (\tau_l - \tau_{B1})c_2^FQ + m_2^{\mathrm{tail}} \tag{A.13}$$

where τ_l is the end of the feed plateau relative to the end of the feed pulse

$$\tau_l = \left[1 + \frac{\phi(\omega_1^F)^2\omega_2^F}{H_1H_2}\right]t_0 \tag{A.14}$$

To solve the cut time τ_{B1}, m_1^B and m_2^B are eliminated from the system of Eqs. (A.12), (A.13) and (7)

$$\tau_{B1} = \tau_I - \frac{m_2^{\text{tail}} - \left[p_2^B/(1-p_2^B)\right] m_1^{\text{tail}}}{\left[p_2^B/(1-p_2^B)\right] c_1^F - c_2^F} \frac{1}{Q} \tag{A.15}$$

The volume of fresh feed is calculated by substituting the expression of m_2^B, Eq. (A.13), into Eq. (12)

$$V^{FF} = \frac{(\tau_I - \tau_{B1}) c_2^F Q + m_2^{\text{tail}}}{c_2^{FF} Y_2} \tag{A.16}$$

When the cut point $B1$ is located on the mixed wave, $p_2^B \geq p_{2,\text{limit}}^B$ or $\xi_+^F \leq c_1^{FF}/c_2^{FF}$, equations for $m_1^B(\tau_{B1})$ and $m_2^B(\tau_{B1})$ given by [23] are

$$m_1^B(\tau_{B1}) = \frac{(1-\varepsilon)(\omega_2^F - H_1)(H_1 - \omega_1^{B1})^2}{K_1 H_1 (H_2 - H_1)} V_{\text{col}} \tag{A.17}$$

$$m_2^B(\tau_{B1}) = \frac{(1-\varepsilon)(H_2 - \omega_2^F)(H_2 - \omega_1^{B1})^2}{K_2 H_2 (H_2 - H_1)} V_{\text{col}} \tag{A.18}$$

where ω_1^{B1} is ω_1-value at the cut point $B1$. Explicit expression for ω_1^{B1} is solved by eliminating m_1^B and m_2^B from system of Eqs. (A.17), (A.18) and (7) which yields

$$\omega_1^{B1} = \frac{H_1 - H_2 \lambda}{1 - \lambda} \tag{A.19}$$

where λ is an auxiliary parameter given by

$$\lambda = \sqrt{\frac{1 - p_2^B}{p_2^B} \frac{K_1 H_1 (H_2 - \omega_2^F)}{K_2 H_2 (\omega_2^F - H_1)}} \tag{A.20}$$

The cut time $B1$ relative to the end of the feed pulse is calculated from the propagation velocity of the mixed wave

$$\tau_{B1} = \left[1 + \frac{\phi (\omega_1^{B1})^2 \omega_2^F}{H_1 H_2}\right] t_0 \tag{A.21}$$

The volume of fresh feed is solved by substituting Eq. (A.18) into Eq. (12)

$$V^{FF} = \frac{(1-\varepsilon)(H_2 - \omega_2^F)(H_2 - \omega_1^{B1})^2}{K_2 H_2 (H_2 - H_1) c_2^{FF} Y_2} V_{\text{col}} \tag{A.22}$$

To derive equations for the steady state feed concentrations, location of the cut point $A2$ must be considered. When the volume of feed pulse is relatively low, t_{A2} lies on the mixed wave while for high V^F values it is located on the feed plateau. The limit for these two cases is derived in Appendix B, Eq. (B.2).

When t_{A2} is located on the mixed wave, $V^F \leq V_{\text{limit G}}^F$, ω_1-value at the cut point $A2$ is solved from the propagation velocity of the Γ_+^F characteristic which yields

$$\omega_1^{A2} = \sqrt{\frac{H_1 H_2}{\phi t_0 \omega_2^F} \left(t_{A2} - t_0 - \frac{V^F}{Q}\right)} \tag{A.23}$$

The amount of component i in the recycle fraction, *i.e.* integral term in Eq. (17), is obtained from the difference between m_i that elutes from column after t_{A2} and m_i that elutes from column after t_{B1}. These values are solved from Eqs. (A.17) and (A.18) by substituting corresponding ω_1-values, ω_1^{A2} and ω_1^{B1}, into them. The resulting expressions for the volume-average recycle fraction concentrations are given by

$$c_1^R = \frac{\frac{(1-\varepsilon)(\omega_2^F - H_1)V_{\text{col}}}{K_1 H_1 (H_2 - H_1)} \left[(H_1 - \omega_1^{A2})^2 - (H_1 - \omega_1^{B1})^2\right]}{V^F - V^{FF} + V^{SR}} \tag{A.24}$$

$$c_2^R = \frac{\frac{(1-\varepsilon)(H_2 - \omega_2^F)V_{\text{col}}}{K_2 H_2 (H_2 - H_1)} \left[(H_2 - \omega_1^{A2})^2 - (H_2 - \omega_1^{B1})^2\right]}{V^F - V^{FF} + V^{SR}} \tag{A.25}$$

and for the steady state feed concentrations by

$$c_1^F = \frac{\frac{(1-\varepsilon)(\omega_2^F - H_1)V_{\text{col}}}{K_1 H_1 (H_2 - H_1)} \left[(H_1 - \omega_1^{A2})^2 - (H_1 - \omega_1^{B1})^2\right] + c_1^{FF} V^{FF}}{V^F} \tag{A.26}$$

$$c_2^F = \frac{\frac{(1-\varepsilon)(H_2 - \omega_2^F)V_{\text{col}}}{K_2 H_2 (H_2 - H_1)} \left[(H_2 - \omega_1^{A2})^2 - (H_2 - \omega_1^{B1})^2\right] + c_2^{FF} V^{FF}}{V^F} \tag{A.27}$$

When t_{A2} is located on the feed plateau, *i.e.* $V^F > V_{\text{limit G}}^F$, the steady state feed composition is independent of V^F [1]. The steady state feed concentrations are calculated from Eqs. (A.26) and (A.27) by setting $V^F = V_{\text{limit G}}^F$.

Appendix B. Explicit equation for the limit G

In this appendix, an equation to calculate the limiting volume of feed pulse whether the cut point $A2$ is located on the mixed wave or on the feed plateau (limit G) is derived. As mentioned in Appendix A, t_{A2} may locate on the mixed wave only in the case when the cut point $B1$ lies on the mixed wave. For this reason, the following discussion is limited to case where $p_2^B \geq p_{2,\text{limit}}^B$ or $\xi_+^F \leq c_1^{FF}/c_2^{FF}$.

When t_{A2} is located on the mixed wave, the concentration of component 2 at time t_{A2} can be solved by substituting the equation of ω_1^{A2}, Eq. (A.23), into the relationship between c_2 and ω-values, Eq. (A.6). Some rearrangement gives

$$c_2(t_{A2}) = \frac{H_1 (H_2 - \omega_2^F)}{K_2 \omega_2^F (H_2 - H_1)} \left(\sqrt{\frac{\phi t_0 \alpha \omega_2^F}{t_{A2} - t_0 - V^F/Q}} - 1\right) \tag{B.1}$$

In the limiting case, t_{A2} is equal to the end of the feed plateau, t_I, and $c_2(t_{A2}) = c_2^F$. The volume of feed pulse is solved from pair of Eqs. (A.27) and (B.1) which yields

$$V^F = 2Q(t_{A2} - t_0) - \frac{\sigma\mu^2 - \sqrt{\sigma\mu^2 \left[\sigma\mu^2 - 4Q(t_{A2} - t_0)\right]}}{2} \tag{B.2}$$

In the above equation, σ and μ are auxiliary parameters that can be calculated by using Eqs. (24) and (25), respectively.

Appendix C. Explicit equation for maximum V^{FF} of SSR–SR configurations II and III in the case of no solvent removal constraint

In this appendix, an equation to calculate the upper limit for the volume of fresh feed for SSR–SR configurations II and III (limit E) in the case of no solvent removal constraints is derived. As mentioned, in Section 3.3, the limit is obtained when the cut time t_{A2} tends towards t_0. Setting $t_{A2} = t_0$ into Eq. (14) yields

$$\tau_{B1} - t_0 + (1 - K)\frac{V^{FF}}{Q} = 0 \tag{C.1}$$

In the above equation, variables τ_{B1}, K, and V^{FF} depend on the slope of the Γ_+^F characteristic only. By substituting the equations of τ_{B1}, Eq. (A.21), K, Eq. (10), and V^{FF}, Eq. (A.22), into Eq. (C.1) and by solving ξ_+^F from the resulting equation, the following expression is

obtained

$$\xi_+^F = \left\{ \frac{\sqrt{((1-p_2^B)/p_2^B)\alpha Y_2} + \sqrt{(\alpha-1)\left[(c_1^{FF}/c_2^{FF})(\alpha+Y_2-1) - ((1-p_2^B)/p_2^B)\alpha Y_2\right]}}{\alpha+Y_2-1} \right\}^2 \tag{C.2}$$

Once ξ_+^F is solved, the solvent removal capacity that corresponds on the limit E without solvent removal constraints is calculated from Eq. (10) and the volume of fresh feed from Eq. (A.22).

References

[1] J. Siitonen, T. Sainio, M. Kaspereit, Sep. Purif. Technol. 78 (2011) 21.
[2] A. Seidel-Morgenstern, G. Guiochon, AIChE J. 39 (1993) 809.
[3] M. Kaspereit, T. Sainio, Chem. Eng. Sci. 66 (2011) 5428.
[4] M. Bailly, D. Tondeur, Chem. Eng. Sci. 37 (1982) 1199.
[5] C.M. Grill, J. Chromatogr. A 796 (1998) 101.
[6] G. Paredes, H.-K. Rhee, M. Mazzotti, Ind. Eng. Chem. Res. 45 (2006) 6289.
[7] S. Abdelmoumen, L. Muhr, M. Bailly, O. Ludemann-Hombourger, Sep. Sci. Technol. 41 (2006) 2639.
[8] S. Nimmig, M. Kaspereit, Chem. Eng. Process. 67 (2013) 89.
[9] M. Bechtold, S. Makart, M. Heinemann, S. Panke, J. Biotechnol. 124 (2006) 146.
[10] N. Wagner, M. Fuereder, A. Bosshart, S. Panke, M. Bechtold, Org. Process Res. Dev. 16 (2012) 323.
[11] S. Hellstén, J. Siitonen, M. Mänttäri, T. Sainio, J. Chromatogr. A 1251 (2012) 122.
[12] H.-K. Rhee, R. Aris, N.R. Amundson, First-Order Partial Differential Equations. Theory and Application of Single Equations, vol. I, Dover Publications, New York, 2001.
[13] H.-K. Rhee, R. Aris, N.R. Amundson, First-Order Partial Differential Equations. Theory and Application of Hyperbolic Systems of Quasilinear Equations, vol. II, Dover Publications, New York, 2001.
[14] M. Mazzotti, Ind. Eng. Chem. Res. 45 (2006) 5332.
[15] A. Rajendran, M. Mazzotti, Ind. Eng. Chem. Res. 50 (2011) 352.
[16] T. Sainio, M. Kaspereit, Sep. Purif. Technol. 66 (2009) 9.
[17] M. Kaspereit, K. Gedicke, V. Zahn, A.W. Mahoney, A. Seidel-Morgenstern, J. Chromatogr. A 1092 (2005) 43.
[18] J. Siitonen, T. Sainio, J. Chromatogr. A 1218 (2011) 6379.
[19] M. Kaspereit, P. Jandera, M. Škavrada, A. Seidel-Morgenstern, J. Chromatogr. A 944 (2002) 249.
[20] P. Jandera, M. Skavrada, K. Klemmova, V. Backovska, G. Guiochon, J. Chromatogr. A 917 (2001) 123.
[21] A. Jupke, A. Epping, H. Schmidt-Traub, J. Chromatogr. A 944 (2002) 93.
[22] G. Ströhlein, M. Schulte, J. Strube, Sep. Sci. Technol. 38 (2003) 3353.
[23] J. Siitonen, T. Sainio, A. Rajendran, J. Chromatogr. A 1286 (2013) 55.

Article V

Chemical Engineering Science 122 (2015) 436–451

Contents lists available at ScienceDirect

Chemical Engineering Science

journal homepage: www.elsevier.com/locate/ces

Unified design of chromatographic separation processes

Jani Siitonen, Tuomo Sainio *

Lappeenranta University of Technology, Skinnarilankatu 34, FI-53850 Lappeenranta, Finland

HIGHLIGHTS

- Unified design method for chromatographic separation processes is presented.
- The approach is demonstrated both under ideal and non-ideal conditions.
- The method enables predicting optimal and robust operating conditions.
- Operating parameters of one setup can be utilized for the design of other setups.
- SSR and SMB can be designed with a single pulse injection using unified design.

ARTICLE INFO

Article history:
Received 20 April 2014
Received in revised form
4 September 2014
Accepted 2 October 2014
Available online 13 October 2014

Keywords:
Batch chromatography
Steady state recycling
Cross-current chromatography
Simulated moving bed
Triangle theory
Process design

ABSTRACT

A unified method is developed for the designing preparative chromatographic processes of various types. The method allows, for example, generalizing the established triangle theory of counter-current simulated moving bed technique for other single and multi-column chromatographic schemes including (1) classical batch chromatography, (2) mixed-recycle steady state recycling chromatography, (3) cross-current chromatography, and (4) mixed-recycle cross-current recycling chromatography. The approach allows direct prediction of the range of feasible dimensionless operating parameters that lead to complete separation of a binary feed mixture. By using the equilibrium theory of chromatography, explicit design equations are derived for systems that follow linear or competitive Langmuir isotherm model. It is shown that under ideal conditions the boundaries of the dimensionless operating parameters are identical for all studied process concepts, except for the upper limit of a parameter that is related to the regeneration of the fluid phase in the case of Langmuir isotherm. The practical relevance of the unified design method is demonstrated with numerical simulations. It is shown that even under non-ideal conditions the counter-current SMB can be designed with good accuracy based on a single pulse injection to a batch column, especially for relatively low purity requirements.

1. Introduction

Preparative liquid chromatography is a highly selective separation technique that is successfully applied for isolation and purification of a wide variety of substances in the pharmaceutical, fine chemical and food industries. To meet the diverse industrial demands several process schemes have been developed and applied. They can be roughly categorized to single column fixed bed techniques, such as classical batch chromatography and different recycling schemes, to continuous counter-current multi-column techniques, such as simulated moving bed chromatography (SMB) and its various modifications, and to continuous cross-current techniques, such as annular chromatography (AC) and carousel multi-column setup (CMC).

The choice of the best process configuration is typically a trade-off between the process performance, robustness, flexibility, implementation time, and investments costs. The classical fixed bed batch chromatography is a common setup in many fine chemical and pharmaceutical applications because it is versatile, provides multiple product fractions, and allows rapid method development. The simplicity of the concept is counter-balanced by low productivity, high eluent consumption and/or low recovery yield. The performance of batch process can be improved by using different single column recycling techniques or the multi-column SMB scheme. The most promising recycling concept is steady state recycling chromatography (SSR) that can be operated in different injection modes such as mixed-recycle mode (Bailly and Tondeur, 1982), closed-loop mode (Grill, 1998), segmented recycling (Charton, 1995), or a combination of different modes (Charton et al., 1994). The SMB process assures a continuous feed flow and high performance but is rather complex and has high investment costs. It is applied widely for the separation of petrochemicals

* Corresponding author. Tel.: +358 40 3578683.
E-mail address: tuomo.sainio@lut.fi (T. Sainio).

http://dx.doi.org/10.1016/j.ces.2014.10.004
0009-2509/

(Ruthven and Ching, 1989), sugars (Bubnik et al., 2004), and fine chemicals, particularly enantiomers of chiral compounds (Rajendran et al., 2009). As to the cross-current concepts, the annular chromatography is not gained an industrial breakthrough due to rather complex implementation and/or negligible performance benefit compared to the batch process (Guiochon et al., 2006), whereas the CMC concept is applied, for example, in ion exchange (Huckman et al., 2001; Virolainen et al., 2014) and multi-step solvent gradient (Antos 2009; Bochenek et al., 2013) separations.

The design of chromatographic processes is often challenging due to dynamic character of the separation. For this reason, a wide range of models with different levels of complexity are used. A well-established equilibrium theory of chromatography considers the influence of phase equilibrium only while all dispersive effects are neglected. The model forms a system of partial differential equations that can be solved by the method of characteristics leading in many cases of interest to simple algebraic equations. The theory helps to analyse and understand both the fixed bed and the multi-column chromatographic separations. It is used in many practical applications to predict the preliminary operating parameters which are later fine-tuned by detailed simulations.

Golshan-Shirazi and Guiochon (1989a) have applied the equilibrium theory to optimize the classical batch chromatography. They derived explicit equations to predict the feed loading and the cut times that lead to 100% product purities and recovery yields, *i.e.* touching band operation, for binary systems that follow competitive Langmuir isotherm model. They provided also analytical equations to calculate the optimal operating parameters that correspond to arbitrary purity constraints when generation of waste fraction is allowed. Recently, Siitonen et al. (2013) have extended the method for operation without generation of waste stream. In addition, the analytical solution of the ideal model has been used to analyse the batch chromatography under practically relevant non-ideal conditions by combining it with a simple model of band broadening (*e.g.* Knox and Pyper, 1986; Golshan-Shirazi and Guiochon, 1989b).

As to the mixed-recycle SSR process, Bailly and Tondeur (1982) have applied the equilibrium theory to predict the optimal cut times that lead to 100% product purities. Later, Sainio and Kaspereit (2009) extended the method for less than 100% purity constraints and provided a short-cut design approach (Kaspereit and Sainio, 2011) for non-ideal conditions to estimate the preliminary cut times that can be fine-tuned by detailed simulations (Hellstén and Sainio, 2012). For other SSR operation modes, there exist only methods that are based on detailed dynamic process models or skilful interpretation of experiments (*e.g.* Grill, 1998).

In the design of SMB applications, the equilibrium theory based triangle method introduced by Storti et al. (1993) has become a standard tool during the past two decades. The method allows calculating the optimal operating parameters for a given separation task. In addition, it specifies a range of adjustable operating parameters leading to pure products, which help to analyse the process robustness. The theory has been elaborated for most of the relevant types of adsorption isotherms (Mazzotti et al., 1994, 1996, 1997a, 1997b; Gentilini et al., 1998; Migliorini et al., 2000; Mazzotti, 2006a, 2006b), for less than 100% purity constraints (Kaspereit et al., 2007; Rajendran 2008), and for the modified SMB techniques such as gradient operation (Mazzotti et al., 1997c; Migliorini et al., 2001; Abel et al., 2002, 2004), three fraction separations (Paredes et al., 2004), and the enriched extract SMB (Paredes et al., 2006).

The cross-current chromatographic processes, especially annular chromatography, have been analysed by several authors (Giddings 1962; Wankat, 1977; Goto and Goto, 1987; Thiele et al., 2001). It has been shown that the steady state two-dimensional cross-current chromatography is formally analogous to the classical time dependent one-dimensional fixed bed process when the dispersion in the direction of the solid flow is neglected. For this reason, the design methods developed originally for the fixed processes can be applied for the cross-current concepts too.

Although the equilibrium theory has been successfully applied for the design of fixed bed, cross-current, and counter-current processes, their design approaches, including the calculation procedure and the way of representing the results, are quite different from each other. This is mainly because the design parameters of the process schemes are apparently totally different. As a result, generalization of the information related to the choice of feasible operating parameters for one chromatographic configuration to the design of other process schemes is often difficult due to lack of universal conversion rules especially in the case of non-linear competitive adsorption behaviour.

Another research gap concerning the design of fixed bed and cross-current chromatographic processes is that almost all of the design methods developed so far allow the calculation of the optimal operating parameters only. In contrast to the triangle theory design of SMB applications, the range of the feasible operating parameters is rarely discussed. This makes it difficult to find a robust operating point, especially in the cases of recycling schemes, due to interactions between the operating parameters.

The aim of this work is to unify the design methodology of chromatographic separation processes. For this purpose, a method applicable for design of (1) classical fixed bed batch chromatography, (2) mixed-recycle SSR chromatography, (3) cross-current chromatography, such as annular chromatography or multi-column carousel setup, and (4) mixed-recycle cross-current recycling chromatography is presented. Explicit equations are derived to calculate the regions of feasible operating parameters that lead to complete separation of a binary mixture that follows linear or competitive Langmuir adsorption isotherm model. It is shown that the process configurations can be designed by using an identical set of dimensionless operating boundaries. Possible extensions and application areas of the unified design method are proposed and discussed. The practical relevance of the work is twofold. First, the results and methodology concerning the choice of optimal and robust operating conditions for SMB process (Mazzotti et al., 1997a) can be extended for fixed bed and cross-current schemes. Second, the analogy between process configurations allows converting the feasible operating parameters obtained for one scheme to the operating parameters of other schemes, which simplifies the design of recycling and multi-column processes. This is demonstrated by showing with numerical simulations that counter-current SMB process can be designed based on a single pulse injection to a batch column.

2. Process configurations

Schematic setups of the process configurations studied in this work are shown in Figs. 1–3. Principles of the process options are described extensively in the literature. The interested reader is referred to (Guiochon et al., 2006) for details of batch chromatography, to (Sainio and Kaspereit, 2009; Kaspereit and Sainio, 2011) for details of steady state recycling chromatography, to (Rajendran et al., 2009) for details of counter-current chromatography, and to (Bochenek et al., 2013; Thiele et al., 2001) for details of cross-current schemes.

Classical fixed bed batch chromatography (Fig. 1a) can be used for separation of both binary and multi-component mixtures. In addition, different cutting strategies can be applied depending on if generation of waste fraction is allowed or not. In this work, only

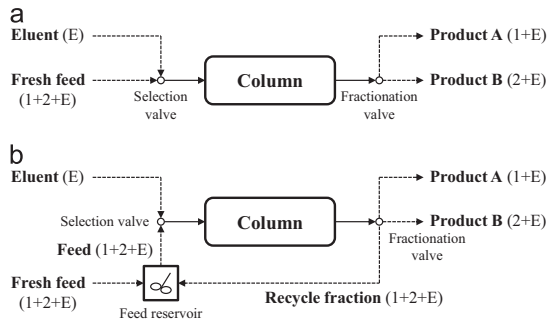

Fig. 1. Schematic setup of (a) a classical batch chromatography and (b) a mixed-recycle steady state recycling chromatography.

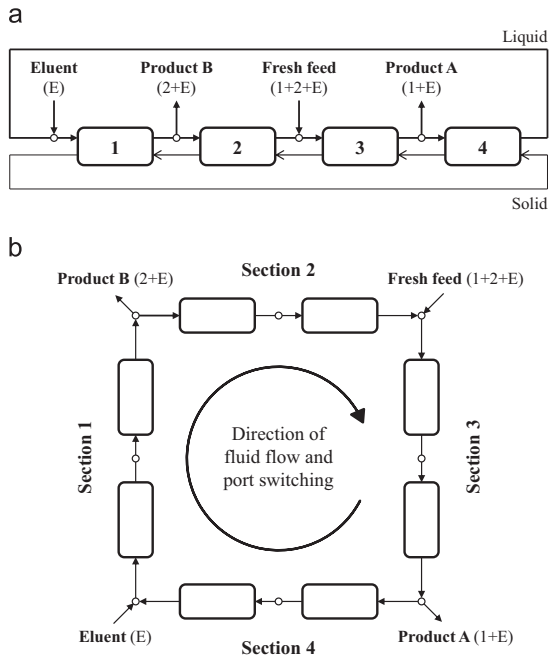

Fig. 2. Schematic setup of (a) a four-section true moving bed chromatography and (b) a four-section simulated moving bed chromatography.

the binary separation without generation of waste fraction is discussed.

In steady state recycling process, illustrated in Fig. 1b, the volume of the feed pulse into the column is typically larger than in batch chromatography. This leads to only partial separation of the target components. The pure leading and trailing sections of the elution profile are collected as products, while the unresolved middle part is recycled. In the mixed-recycle mode, the whole recycle fraction is collected in the feed reservoir, mixed with fresh feed, and then introduced back into the column.

In counter-current chromatography, the fluid and solid phases flow in opposite directions. The operation mode can be implemented continuously with the true moving bed (TMB) technique (Fig. 2a) or in a discontinuous manner by using the simulated moving bed (SMB) scheme (Fig. 2b) where the counter-current movement is mimicked by switching the inlet and outlet ports of series of conventional fixed bed columns. In practice, however,

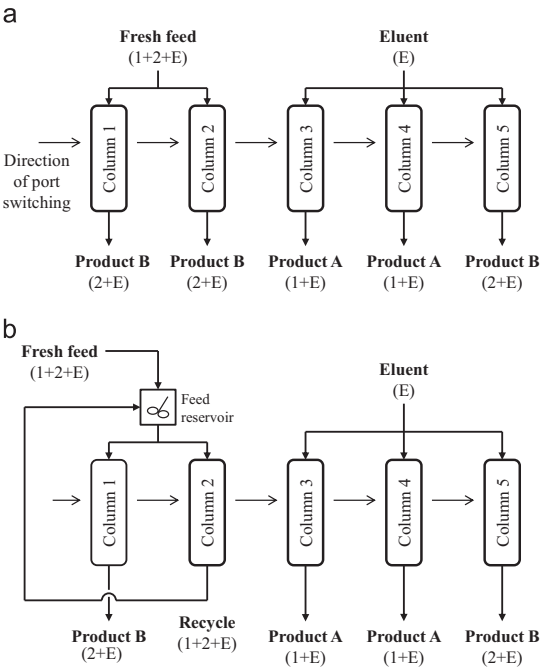

Fig. 3. Schematic setup of (a) a cross-current multi-column carousel chromatography and (b) a mixed-recycle cross-current multi-column carousel chromatography.

TMB is not feasible concept because the movement of solid phase causes mixing and attrition, and SMB setup is preferred.

In cross-current chromatography separation is achieved by employing two spatial directions. The fluid phase flow in cross-wise direction with respect to the solid phase, which leads to time independent steady state. The true cross-current operation can be implemented in annular chromatography (AC) and simulated cross-current operation in carousel multi-column setup (CMC). In practice, the carousel multi-column setup shown in Fig. 3 is more feasible option because the implementation of annular technique is rather complex. The two-dimensional cross-current chromatography is formally analogous to the classical one-dimensional time dependent fixed bed process (see *e.g.* Wankat, 1977). Physically, the analogy is most obvious for the carousel type multi-column setup where each individual column is operated in exactly the same way as a single column. For this reason, also the recycling scheme similar to the fixed bed SSR process can be easily implemented (Fig. 3b).

3. Process models

Within the frame of the equilibrium theory, it is assumed that the mass transfer resistance and the dispersive effects are negligible and the fluid velocity is constant along the column. The material balance for an individual component i in the fixed bed column is given by

$$\frac{\partial c_i}{\partial \gamma}+\frac{\partial}{\partial \tau}\left(c_i+Fq_i^{eq}\right)=0 \quad \text{for} \quad i=(1,\ 2) \tag{1}$$

where c_i is the fluid phase concentration of solute i, q_i^{eq} is the solid phase concentration that is in equilibrium with the fluid phase, and $F=(1-\varepsilon)/\varepsilon$ is the phase ratio with ε being the total void

fraction of the bed. The dimensionless time, τ, and the dimensionless space variable, γ, are given by $\tau=(u^L t)/y_{\mathrm{col}}$ and $\gamma=y/y_{\mathrm{col}}$, where u^L is the interstitial fluid velocity, t is the time, y_{col} is the column length, and y is the column axial coordinate.

To describe the counter-current chromatography true moving bed model is used. Each section is modelled as a moving bed where the fluid flows with an interstitial velocity u_j^L and the solid phase with a velocity u^S in the opposite direction. This leads to the following material balance

$$\frac{\partial}{\partial\gamma}\left(\frac{u_j^L}{Fu^S}c_i-q_i^{\mathrm{eq}}\right)+\frac{\partial}{\partial\tau}(c_i+Fq_i^{\mathrm{eq}})=0 \quad \text{for} \quad i=(1,\ 2) \quad j=(1,\ldots,4) \tag{2}$$

The dimensionless time is given by $\tau=(Fu^S t)/y_{\mathrm{col}}$. The SMB and TMB modes can be considered to be equivalent and yield to similar separation performance when the following two equivalence relationships are satisfied

$$Q_j^{\mathrm{SMB}}=Q_j^{\mathrm{TMB}}+\frac{Q^S}{F} \tag{3}$$

$$\frac{V_{\mathrm{col}}}{t^*}=\frac{Q^S}{(1-\varepsilon)} \tag{4}$$

In the above equations, Q_j is the volumetric flow rate of the fluid phase in section j, $Q^S=(1-\varepsilon)A_{\mathrm{col}}u^S$ is the volumetric flow rate of the solid phase with A_{col} being the cross-sectional area of the column, V_{col} is the column volume, and t^* is the switch time in the SMB unit.

In the case of cross-current true moving bed model, it is assumed that the fluid flows with an interstitial velocity u_y^L in the direction y, and both the solid phase and the fluid phase moves with a velocity $u_x^S=u_x^L$ in the direction x that is perpendicular to y. The material balance describing the solute movement is

$$F\varphi\frac{\partial c_i}{\partial\gamma}+\frac{\partial}{\partial\chi}(c_i+Fq_i^{\mathrm{eq}})=0 \quad \text{for} \quad i=(1,\ 2) \tag{5}$$

where $\gamma=y/y_{\mathrm{col}}$ and $\chi=x/x_{\mathrm{col}}$ are the dimensionless spatial coordinates. The dimensionless cross-flow velocity, φ, is defined as

$$\varphi=\frac{Q_y^L}{Q_x^S}=\frac{1}{F}\frac{x_{\mathrm{col}}}{y_{\mathrm{col}}}\frac{u_y^L}{u_x^S} \tag{6}$$

where Q_y^L and Q_x^S are the volumetric flow rates of the fluid phase in the y-direction and the solid phase in the x-direction, respectively.

In the case of annular chromatography, χ corresponds to the angular coordinate and φ to term $u_y^L/(Fy_{\mathrm{col}}w)$ where w is the angular velocity. For simulated cross-current process, *i.e.* multi-column carousel unit, the conversion rules are given by

$$\frac{N}{N_{\mathrm{col}}}=\chi \tag{7}$$

$$\tau^*=\frac{F\varphi}{N_{\mathrm{col}}} \tag{8}$$

where N/N_{col} is the proportion of columns to the total number of columns, N_{col}, and $\tau^*=(u_y^L t^*)/y_{\mathrm{col}}$ is the dimensionless switch time. As shown by Wankat (1977), the two-dimensional time independent cross-flow model, Eq. (5), is formally analogous to the one-dimensional time dependent fixed bed model, Eq. (1), with transform

$$\tau=F\varphi\chi \tag{9}$$

To solve the models, Eqs. (1), (2), and (5), the equilibrium relationship between the solid phase loading and the fluid phase concentration is needed. In this work, linear

$$q_i^{\mathrm{eq}}=H_i c_i \quad \text{for} \quad i=(1,\ 2) \tag{10}$$

and binary competitive Langmuir adsorption isotherm model

$$q_i^{eq}=\frac{H_i c_i}{1+K_1c_1+K_2c_2} \quad \text{for } i=(1,\ 2) \tag{11}$$

are considered. In the above equations, H_i and K_i are the Henry constant and the equilibrium parameter of component i, respectively. In the following discussion, it is assumed that the component 1 is less strongly absorbed one, *i.e.* $\alpha=H_2/H_1>1$ with α being the separation factor.

The equilibrium model forms a set of homogeneous quasilinear partial differential equations. In the case of linear and Langmuir isotherm models, it can be solved analytically for constant initial and boundary conditions by the method of characteristics (Rhee et al., 2001a, 2001b; Mazzotti, 2006c; Rajendran and Mazzotti 2011; Golshan-Shirazi and Guiochon, 1989c). It is worth noting that the equations derived originally for the fixed bed chromatography can be applied also for the cross-current process by using the transform given in Eq. (9).

4. Unified design method for chromatographic separation processes

4.1. General specifications

Several kinds of dimensionless operating parameters have been used in designing chromatographic separation processes. These include, for example, dimensionless cut times and dimensionless flow rate ratios. The main idea of the unified design approach is to establish a set of rules how the dimensionless parameters should be defined in order to bring the feasible design spaces of apparently totally different chromatographic process configurations to a comparable form. We present such rules and then present a collection of useful dimensionless operating parameters for batch, SSR, cross-flow, and counter-current TMB and SMB processes.

In the following discussion, it is assumed that the column dimensions and the fresh feed concentrations are fixed and the packing properties and the isotherm parameters are known. A binary mixture is separated in isocratic mode into two product fractions such that no waste fraction is generated.

Since the triangle theory of counter-current chromatography, developed by Storti et al. (1993), Mazzotti et al. (1997a), has proven extremely useful, the said set of rules will be devised such that the design spaces of the other processes can also be represented on a plane of two operating parameters.

For counter-current, batch, and classical cross-current chromatography, let us select four m-parameters, m_1, m_2, m_3, and m_4 to represent the dimensionless operating parameters. For SSR and cross-current recycling schemes, recycling provides one additional degree of freedom denoted as m_R.

The first rule for defining the parameters is that volumes of fresh feed, m_{FF}, and eluent, m_E, that are introduced into the process during a chromatographic cycle or switch with respect to the volume of the solid phase in the column are given by

$$m_{FF}=m_3-m_2 \tag{12}$$

$$m_E=m_1-m_4 \tag{13}$$

and the amounts of products A and B per cycle or switch with respect to the amount of the solid phase in the column are obtained as follows:

$$m_A=m_3-m_4 \tag{14}$$

Table 1
Definitions of m-parameters for counter-current, fixed bed, and cross-current process configurations. For batch and cross-current chromatography without recycling $m_R=0$.

Parameter	Counter-current TMB	Counter-current SMB	Batch and SSR	Cross-current
m_1	$\frac{Q_1^{\mathrm{TMB}}}{Q^s}$ (1.1)	$\frac{Q_1^{\mathrm{SMB}}t^*-\varepsilon V_{\mathrm{col}}}{(1-\varepsilon)V_{\mathrm{col}}}$ (1.5)	$\frac{Q(t_{B2}-\Delta t_F)-\varepsilon V_{\mathrm{col}}}{(1-\varepsilon)V_{\mathrm{col}}}=\frac{\tau_{B2}-\Delta\tau_F-1}{F}$ (1.9)	$\frac{F\varphi(\chi_{B2}-\Delta\chi_F)-1}{F}$ (1.14)
m_2	$\frac{Q_2^{\mathrm{TMB}}}{Q^s}$ (1.2)	$\frac{Q_2^{\mathrm{SMB}}t^*-\varepsilon V_{\mathrm{col}}}{(1-\varepsilon)V_{\mathrm{col}}}$ (1.6)	$\frac{Q(t_{B1}-\Delta t_F)-\varepsilon V_{\mathrm{col}}}{(1-\varepsilon)V_{\mathrm{col}}}=\frac{\tau_{B1}-\Delta\tau_F-1}{F}$ (1.10)	$\frac{F\varphi(\chi_{B1}-\Delta\chi_F)-1}{F}$ (1.15)
m_3	$\frac{Q_3^{\mathrm{TMB}}}{Q^s}$ (1.3)	$\frac{Q_3^{\mathrm{SMB}}t^*-\varepsilon V_{\mathrm{col}}}{(1-\varepsilon)V_{\mathrm{col}}}$ (1.7)	$\frac{Qt_{A2}-\varepsilon V_{\mathrm{col}}}{(1-\varepsilon)V_{\mathrm{col}}}=\frac{\tau_{A2}-1}{F}$ (1.11)	$\frac{F\varphi\chi_{A2}-1}{F}$ (1.16)
m_4	$\frac{Q_4^{\mathrm{TMB}}}{Q^s}$ (1.4)	$\frac{Q_4^{\mathrm{SMB}}t^*-\varepsilon V_{\mathrm{col}}}{(1-\varepsilon)V_{\mathrm{col}}}$ (1.8)	$\frac{Qt_{A1}-\varepsilon V_{\mathrm{col}}}{(1-\varepsilon)V_{\mathrm{col}}}=\frac{\tau_{A1}-1}{F}$ (1.12)	$\frac{F\varphi\chi_{A1}-1}{F}$ (1.17)
m_R			$\frac{V_R}{(1-\varepsilon)V_{\mathrm{col}}}=\frac{\tau_{B1}-\tau_{A2}}{F}$ (1.13)	$\varphi(\chi_{B1}-\chi_{A2})$ (1.18)

$$m_B = m_1 - m_2 \tag{15}$$

The system of Eqs. (12)–(15) does not uniquely define the set of parameters m_1, m_2, m_3, and m_4, but one of them must be specified independently. Therefore, the second rule requires that one of the four m-parameters has identical numerical value for all processes under some conditions. Here we have chosen the definition of m_1 parameter such that its lower limit is equal for all process configurations under ideal conditions and 100% purity of first eluted compound in the limiting case of infinite dilution. The resulting definitions of m-parameters for the studied process schemes are given in Table 1. It is worth noting that, in all cases, proper selection of m_2 and m_3 values ensures the desired separation of the feed mixture, whereas m_1 and m_4 are related to the regeneration of the solid and fluid phases, respectively.

The dimensionless operating parameters allow expressing the feasible separation domain in scale independent form. The boundaries of the region for each process concept can be calculated by considering how the configuration should be operated to achieve the desired separation. The design criteria can be expressed in the following general form:

$$m_{1,\,\mathrm{min}} \le m_1 \tag{16}$$

$$m_{2,\,\mathrm{min}} \le m_2 \le m_{2,\,\mathrm{max}} \tag{17}$$

$$m_{3,\,\mathrm{min}} \le m_3 \le m_{3,\,\mathrm{max}} \tag{18}$$

$$m_4 \le m_{4,\,\mathrm{max}} \tag{19}$$

$$m_R \ge 0 \tag{20}$$

In general case, the lower and upper bounds of all m-values depend on the values of other m-parameters, the adsorption isotherm parameters, the fresh feed concentrations, and the column efficiency. However, when m_1 and m_4 are selected such that they ensure complete regeneration of solid and fluid phases, the limits become independent of them.

In the following Sections 4.2–4.4, a procedure to calculate the operating boundaries for batch, mixed-recycle SSR, and cross-current chromatography with or without recycling will be described. Analytical design equations to predict the range of feasible operating parameters that lead to complete separation of a binary feed mixture under ideal conditions will be derived for systems that follow (1) linear or (2) competitive Langmuir adsorption isotherm model.

4.2. Batch chromatography

4.2.1. Operating parameters

For classical batch chromatography, there exist the following five freely adjustable operating parameters: (1) the duration of the feed pulse, $\Delta\tau_F$, (2) the beginning of the product fraction A, τ_{A1}, (3) the end of the product fraction A, τ_{A2}, which is equal to the beginning of the product fraction B, τ_{B1}, (4) the end of the product fraction B, τ_{B2}, and (5) the volumetric flow rate of the fluid phase, $Q=\varepsilon A_{\mathrm{col}}u^L$. To derive the design equations the operating parameters are expressed as dimensionless m-parameters given by Eqs. (1.9)–(1.12).

Each m_j^{batch} value denotes the difference between the volume of the fluid phase that elutes from the column before a given cut point and the volume of the fluid phase in the column with respect to the volume of the solid phase. The end and the beginning of the product fraction B are expressed relative to the end of the feed pulse, Eqs. (1.9) and (1.10), while the end and the beginning of the product fraction A are expressed relative to the beginning of the feed pulse, Eqs. (1.11) and (1.12).

Under ideal conditions, the fluid phase flow rate does not affect the boundaries of m-parameters. It can be selected independently, *e.g.* such that given pressure constraint is not exceed. The duration of the feed pulse and the cut points are given by

$$\Delta\tau_F = F\left(m_3^{\mathrm{batch}} - m_2^{\mathrm{batch}}\right) \tag{21}$$

$$\tau_{A1} = Fm_4^{\mathrm{batch}} + 1 \tag{22}$$

$$\tau_{A2} = \tau_{\mathrm{B1}} = Fm_3^{\mathrm{batch}} + 1 \tag{23}$$

$$\tau_{\mathrm{B2}} = F\left(m_1^{\mathrm{batch}} + m_3^{\mathrm{batch}} - m_2^{\mathrm{batch}}\right) + 1 = Fm_1^{\mathrm{batch}} + 1 + \Delta\tau_F \tag{24}$$

The cycle time, *i.e.* the time between consecutive injections is given by

$$\Delta\tau_{\mathrm{cycle}} = \tau_{B2} - \tau_{A1} \tag{25}$$

4.2.2. Linear isotherm

For linear isotherm, the propagation velocity of component i is independent of concentrations

$$\frac{d\gamma}{d\tau} = \frac{1}{1+FH_i} \quad \text{for} \quad i=(1,\ 2) \tag{26}$$

The beginning, τ_{Ri}, and the end, τ_{Ei}, of the individual elution profiles are thus given by

$$\tau_{Ri} = 1 + FH_i \quad \text{for} \quad i=(1,\ 2) \tag{27}$$

$$\tau_{Ei} = 1 + FH_i + \Delta\tau_F \quad \text{for} \quad i=(1,\ 2) \tag{28}$$

To obtain 100% product purities and recovery yields the following four constraints for the cut times must be satisfied: (1) the beginning time of the product fraction A, τ_{A1}, must be lower than or equal to the retention time of the first component, τ_{R1}, (2) the end time of the product fraction A, τ_{A2}, must be lower than

or equal to the retention time of the second component, τ_{R2}, (3) the beginning time of the product fraction B, τ_{B1}, must be higher than or equal to the time of complete elution of the first component, τ_{E1}, and (4) the end time of the product fraction B, τ_{B2}, must be higher than or equal to the time of complete elution of the second component, τ_{E2}. As already mentioned, in batch process without generation of waste or recycle stream, the end of the product fraction A is equal to the beginning of the product fraction B. The above constraints can thus be expressed as follows:

$$\tau_{A1} \le \tau_{R1} \tag{29}$$

$$\tau_{R2} \ge \tau_{A2} = \tau_{B1} \ge \tau_{E1} \tag{30}$$

$$\tau_{B2} \ge \tau_{E2} \tag{31}$$

In addition, the duration of the feed pulse must be positive:

$$\Delta\tau_F > 0 \tag{32}$$

By substituting the expressions for the duration of the feed pulse and the cut points, Eqs. (21)–(24), as well as the equations for the retention and complete elution times, Eqs. (27) and (28), into Eqs. (29)–(32), the following constraints for m_j^{batch} are obtained:

$$H_2 \le m_1^{\text{batch}} \tag{33}$$

$$H_1 \le m_2^{\text{batch}} < m_3^{\text{batch}} \le H_2 \tag{34}$$

$$m_4^{\text{batch}} \le H_1 \tag{35}$$

The constraints of m-parameters for classical batch chromatography given by Eqs. (33)–(35) are fully identical to those of SMB process reported in (Storti et al., 1993). This means that the maximum amounts of fresh feed that can be processed in the batch process during a cycle and in the SMB process during a switch, given by Eq. (12), are equal. As will be shown below, this conclusion is valid also for other process configurations and for systems with Langmuir isotherm.

The operating boundaries of m_2 and m_3 parameters are conveniently represented on the (m_2, m_3) plane shown in Fig. 4. The triangle shape domain 1, limited by the straight lines ab, bw, and

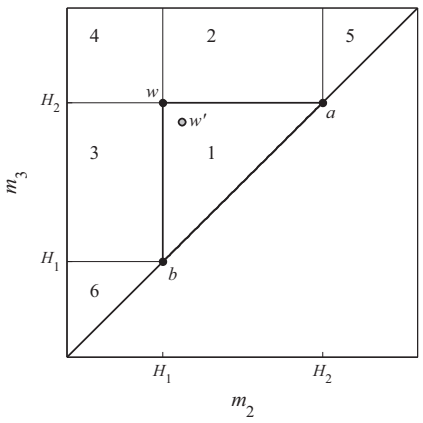

Fig. 4. Separation regions for SMB, batch, SSR, cross-current, and cross-current recycling processes under linear conditions. (1) Complete separation region; (2) pure product B and impure product A; (3) pure product A and impure product B; (4) both products are impure; (5) product A is flooded with the fresh feed and product B with the eluent; (6) product A is flooded with the eluent and product B with the fresh feed. Point w': a robust operating point inside the complete separation region (see Section 6.1).

Table 2
Characteristic points on the boundary of the complete separation region on the (m_2, m_3) plane for SMB, batch, SSR, cross-current, and cross-current recycling processes in the case of a Langmuir isotherm.

Point	m_2	m_3
a	H_2	H_2
b	H_1	H_1
r	$\frac{(\omega_1^{FF})^2}{H_2}$	$\frac{\omega_2^{FF}[\omega_2^{FF}(H_1-\omega_1^{FF})+\omega_1^{FF}(H_2-H_1)]}{H_1(H_2-\omega_1^{FF})}$
w	$\frac{\omega_1^{FF}H_1}{H_2}$	$\frac{\omega_2^{FF}[H_1(H_1-\omega_1^{FF})+\omega_1^{FF}(H_2-H_1)]}{H_1(H_2-\omega_1^{FF})}$

aw, corresponds to the complete separation region where the purities of both product fractions are equal to 100%. In the region 2 above the line aw, the product B is pure while the product A is contaminated by component 2. Similarly, the region 3 on the left hand side of line bw denotes the case where the product A is pure and the product B is contaminated by component 1. The operating points in region 4 on the top left lead to the case where both products are polluted. Finally, the region 5 refers to a situation where the product A and B are flooded with the fresh feed and the eluent, respectively, while the region 6 denotes the opposite case.

4.2.3. Langmuir isotherm

For Langmuir isotherm, the time of complete elution of component 2 is equal to that under linear conditions

$$\tau_{E2} = 1 + FH_2 + \Delta\tau_F \tag{36}$$

Since the cut time τ_{B2} must be higher than or equal to τ_{E2}, the design criterion for m_1^{batch} is given by

$$H_2 \le m_1^{\text{batch}} \tag{37}$$

The region of feasible m_2^{batch} and m_3^{batch} parameters depends on the isotherm parameters and the fresh feed concentrations. Detail derivation of the equations to calculate the boundaries of the region is given in Appendix A. The derivation is based on a variable transform from concentrations (c_1, c_2) to characteristic parameters (ω_1, ω_2) defined as the roots of the following quadratic equation such that $\omega_2 > \omega_1$

$$(1+K_1c_1+K_2c_2)\omega^2 - [H_1(1+K_2c_2)+H_2(1+K_1c_1)]\omega + H_1H_2 = 0 \tag{38}$$

The resulting equations are reported in Tables 2 and 3, and an example of the operating boundaries on the (m_2, m_3) plane is displayed in Fig. 5. The equations, and thus the operating domain, are identical to those of SMB process given in (Mazzotti et al., 1997a).

The complete separation region on the (m_2, m_3) plane, shown in Fig. 5, is now distorted triangle. Its boundary consists of three straight lines, ab, bw, and rw and one curve ar. In the case of batch chromatography, the size of the feed pulse is directly proportional to the difference $(m_3^{\text{batch}} - m_2^{\text{batch}})$. The components are separated complete when the operating point on the (m_2, m_3) plane is located below the line that is parallel to the diagonal and passes through the point w. The curve ar in Fig. 5 corresponds to the condition where the duration of the feed pulse is so small that the pure second component plateau is eroded completely. Corresponding chromatogram is shown in Fig. 6a. The cut time τ_{A2} (or τ_{B1}) is equal to the beginning of the second component band, τ_{R2}. In the line rw, the duration of the feed pulse is larger and the second component plateau prevails (Fig. 6b). The cut time τ_{A2} is again equal to τ_{R2}. The maximum duration of the feed pulse is obtained in the point w that corresponds to the touching band operation (Fig. 6c). The line bw, in turn, stand for the case where the cut time τ_{A2} is equal to the end of the first component profile τ_{E1} (Fig. 6d). The duration of the feed pulse decreases when the

Table 3
Equations to calculate the boundaries of the complete separation region on the (m_2, m_3) plane for SMB, batch, SSR, cross-current, and cross-current recycling processes in the case of a Langmuir isotherm.

Line *ab*	$m_3 = m_2$ (3.1)
Line *ar*	$m_3 = m_2 + \frac{\left(\sqrt{H_2} - \sqrt{m_2}\right)^2}{K_2 c_2^{FF}}$ (3.2)
Line *rw*	$m_3 = \frac{\omega_1^{FF}\omega_2^{FF}(H_2 - H_1) + m_2 H_2 (H_1 - \omega_1^{FF})}{H_1 (H_2 - \omega_1^{FF})}$ (3.3)
Line *wb*	$m_3 = \frac{H_1(H_2 - H_1) - m_2[H_2 - H_1(1 + K_2 c_2^{FF})]}{H_1 K_2 c_2^{FF}}$ (3.4)

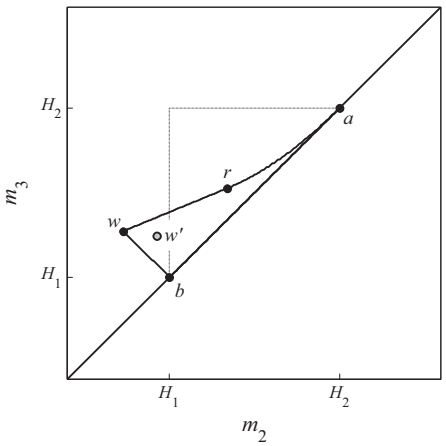

Fig. 5. Complete separation region in SMB, batch, SSR, cross-current, and cross-current recycling processes for the case of a Langmuir isotherm (solid line). The separation region under linear conditions is shown as a reference (dashed line). Point *w'*: a robust operating point inside the complete separation region (see Section 6.1). Fresh feed concentrations: $c_1^{FF} = c_2^{FF} = 5$ g/L. Isotherm parameters: $H_1 = 2.0$, $H_2 = 2.5$, $K_1 = 0.020$ L/g, and $K_2 = 0.025$ L/g.

operating point moves towards point *b*. The second component plateau is eroded or not depending on the size of the feed pulse, *i.e.* the difference $\left(m_3^{\text{batch}} - m_2^{\text{batch}}\right)$.

The operating points above the complete separation region, *i.e.* above the line *arw*, lead again to a pure product *B* but a contaminated product *A*. The left hand side of line *bw* corresponds to the operation where the product *A* is pure and the product *B* is contaminated. On the operating points at the top left of the (m_2, m_3) plane, the purities of both product fractions are less than 100%.

The upper limit for m_4^{batch} is solved piecewise depending on whether the plateau on the top of the first component band is eroded or not. Explicit criterion for the plateau erosion is given by

$$\left(m_3^{\text{batch}} - m_2^{\text{batch}}\right) = \frac{\omega_1^{FF}\omega_2^{FF}(H_2 - \omega_1^{FF})(H_1 - \omega_1^{FF})}{H_1 H_2 (\omega_2^{FF} - \omega_1^{FF})} \tag{39}$$

When the difference between m_3^{batch} and m_2^{batch} values is higher than the limit given by Eq. (39), *i.e.* the duration of the feed pulse is relatively high, the first component plateau prevails and the retention time of the first shock, τ_{R1}, is calculated by using an equation derived by Golshan-Shirazi and Guiochon (1989c). In this case, the upper limit of m_4^{batch} is equal to ω_1^{FF}. In the case of relatively small feed pulse, the plateau erodes completely and the exact values of τ_{R1} and $m_{4,\,\max}^{\text{batch}}$ is solved analytically by using the equations or the free software given in Siitonen and Sainio (2011).

In contrast to the limits for m_1^{batch}, m_2^{batch}, and m_3^{batch} parameters, the upper boundary for m_4^{batch} is not identical to that of SMB concept.

4.3. Steady state recycling chromatography

4.3.1. Operating parameters

In SSR process, there exists one more degree of freedom than in batch mode. The freely adjustable operating parameters are the duration of the feed pulse into the column, the four cut times τ_{A1}, τ_{A2}, τ_{B1}, τ_{B2}, and the fluid flow rate. The cut points *A*1 and *A*2 relative to beginning of the feed pulse and the cut points *B*1 and *B*2 relatively to end of the feed pulse are expressed as dimensionless *m*-parameters identically to the case of batch process, Eqs. (1.9)–(1.12). The dimensionless volume of the recycle fraction, m_R^{SSR}, is given by Eq. (1.13).

The conversion rules from dimensionless *m*-parameters back to the duration of the feed pulse and the four cut times are

$$\Delta\tau_F = F\left(m_3^{\text{SSR}} - m_2^{\text{SSR}} + m_R^{\text{SSR}}\right) \tag{40}$$

$$\tau_{A1} = F m_4^{\text{SSR}} + 1 \tag{41}$$

$$\tau_{A2} = F m_3^{\text{SSR}} + 1 \tag{42}$$

$$\tau_{B1} = F\left(m_3^{\text{SSR}} + m_R\right) + 1 = F m_2^{\text{SSR}} + 1 + \Delta\tau_F \tag{43}$$

$$\tau_{B2} = F\left(m_1^{\text{SSR}} + m_3^{\text{SSR}} - m_2^{\text{SSR}} + m_R\right) + 1 = F m_1^{\text{SSR}} + 1 + \Delta\tau_F \tag{44}$$

4.3.2. Linear isotherm

In the case of linear isotherm, the propagation velocities of the solutes are independent of the concentrations. The beginning, τ_{Ri}, and the end, τ_{Ei}, of the individual elution profiles are thus given by Eqs. (27) and (28) also for SSR process even through the steady state feed composition may be unequal to the feed composition of classical batch process. To achieve 100% product purities the following criteria for the cut times, the amount of the fresh feed, and the volume of the recycle fraction must be satisfied: $\tau_{A1} \le \tau_{R1}$, $\tau_{A2} \le \tau_{R2}$, $\tau_{B1} \ge \tau_{E1}$, $\tau_{B2} \ge \tau_{E2}$, $m_{FF}^{\text{SSR}} > 0$, and $m_R^{\text{SSR}} > 0$. The constraints for the cut times are equal to the case of batch process except the fact that the end of the product fraction *A* is no longer equal to the beginning of the product fraction *B*.

To calculate the range of feasible *m*-parameters the expressions for the duration of the feed pulse and the cut times in the case of SSR process, Eqs. (40)–(44), and the equations for the retention and complete elution times, Eqs. (27) and (28), are substituted into the above inequalities. This yields to the following constraints:

$$H_2 \le m_1^{\text{SSR}} \tag{45}$$

$$H_1 \le m_2^{\text{SSR}} < m_3^{\text{SSR}} \le H_2 \tag{46}$$

$$m_4^{\text{SSR}} \le H_1 \tag{47}$$

As observed, all the lower and upper limits for m^{SSR} parameters are independent of m_R^{SSR}. In addition, the constraints are identical to those of SMB and batch processes (Fig. 4).

4.3.3. Langmuir isotherm

For Langmuir isotherm, it has been shown that the rear part of the chromatogram remains unaltered from cycle to cycle when the mixed recycle SSR process is run to steady state (Bailly and Tondeur 1982; Sainio and Kaspereit 2009). In addition, the rear part of the steady state chromatogram is independent of m_R^{SSR} and equal to that of batch process. Due to this behaviour, the end of the elution profile of the second component can be calculated with

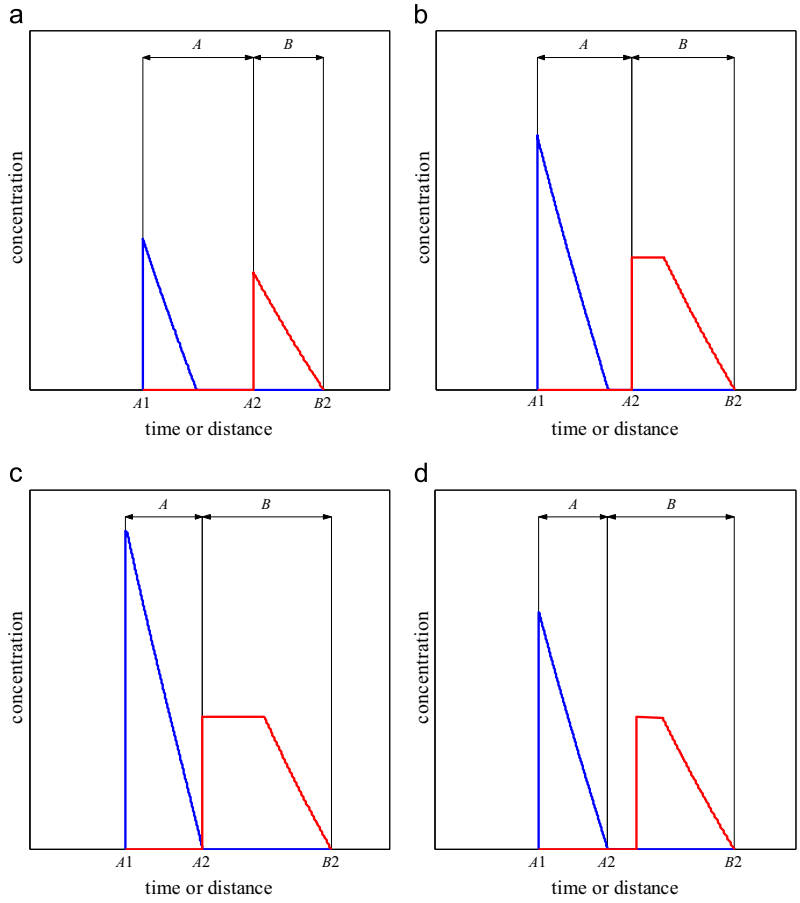

Fig. 6. Individual elution profiles and fraction collection in batch (abscissa is time) and cross-current chromatography without recycling (abscissa is spatial coordinate in the direction of the solid flow). (a) The operating point is located in line *ar* (m_2=2.204, m_3=2.278). (b) The operating point is located in line *rw* (m_2=2.019, m_3=2.201). (c) The operating point is located in point *w* (m_2=1.864, m_3=2.136). (d) The operating point is located in line *bw* (m_2=1.919, m_3=2.081). Same fresh feed concentrations and isotherm parameters as in Fig. 5. The elution profiles are calculated analytically with the free software given in Siitonen and Sainio (2011).

Eq. (36) and the constraint for m_1 given in Eq. (37) is valid for SSR concept too. Moreover, the complete separation region on the (m_2, m_3) plane is independent of m_R^{SSR} and identical to those of batch process and counter-current chromatography (Tables 2 and 3 and Fig. 5). Detail derivation of the operating boundaries is given in Appendix A.

In the case of SSR process, the line *ar* on the (m_2, m_3) plane (Fig. 5) corresponds to the case where τ_{A2} is equal to τ_{R2} and τ_{B1} is located on the pure second component wave (Fig. 7a). This means that a part of the pure second component fraction is recycled. Along the line *rw*, τ_{A2} is again equal to τ_{R2}, but τ_{B1} lies on the pure second component plateau (Fig. 7b). The maximum amount of fresh feed is achieved in the point *w* where $\tau_{A2}=\tau_{R2}$ and $\tau_{B1}=\tau_{E1}$ (Fig. 7c). In this case, no pure fractions are recycled. The line *bw*, corresponds to the case where the cut time τ_{B1} is equal to τ_{E1} (Fig. 7d). The cut point τ_{A2} is located on the pure first component wave or on the pure first component plateau. A part of the pure first component fraction is thus recycled.

To solve the upper limit for m_4^{SSR} the steady state feed concentrations, c_1^F and c_2^F, are needed. They depend on m_2^{SSR}, m_3^{SSR}, and m_R^{SSR}. In principle, they can be solved from the following set of equations:

$$c_i^F V_F = c_i^{FF} V_{FF} + c_i^R V_R \quad \text{for} \quad i=(1,\ 2) \tag{48}$$

$$c_i^R = \frac{\int_{\tau_{A2}}^{\tau_{B1}} c_i(\tau)\mathrm{d}\tau}{\tau_{B1}-\tau_{A2}} \quad \text{for} \quad i=(1,\ 2) \tag{49}$$

where c_i^R is the volume-average recycle fraction concentration of solute *i*. The individual elution profiles, $c_i(\tau)$, depend on the steady state feed concentrations and the duration of the feed pulse. They can be calculated by using the analytical solution of the equilibrium model (Golshan-Shirazi and Guiochon, 1989c; Siitonen and Sainio, 2011).

In general case, explicit solution of the set of Eqs. (48) and (49) is very difficult if not impossible because a quartic equation needs to be solved in order to find the amount of component 1 in the recycle fraction. For this reason, numerical methods are recommended to find the steady state feed concentrations. For example,

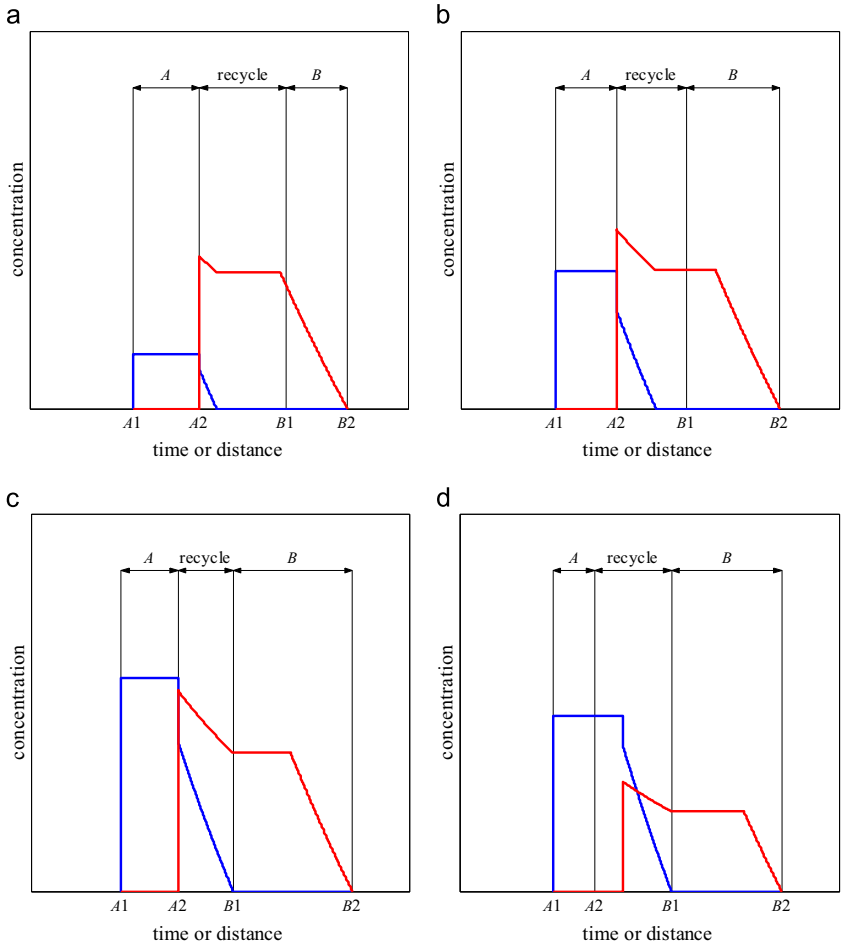

Fig. 7. Steady state elution profiles and fraction collection in SSR (abscissa is time) and cross-current recycling chromatography (abscissa is spatial coordinate in the direction of the solid flow). (a) The operating point is located in line *ar* (m_2=2.204, m_3=2.278, m_R=0.422). (b) The operating point is located in line *rw* (m_2=2.019, m_3=2.201, m_R=0.355). (c) The operating point is located in point *w* (m_2=1.864, m_3=2.136, m_R=0.296). (d) The operating point is located in line *bw* (m_2=1.919, m_3=2.081, m_R=0.407). Same fresh feed concentrations and isotherm parameters as in Fig. 5. The elution profiles are calculated analytically with the free software given in Siitonen and Sainio (2011).

c_1^F and c_2^F can be searched by calculating the chromatograms analytically from cycle to cycle until the periodic steady state is reached. In every cycle, the recycle fraction composition can be computed by integrating the chromatogram numerically, for example, with trapezoidal rule. As an alternative, numerical multidimensional root-finding algorithms can be applied to find c_1^F and c_2^F.

Once the steady state feed concentrations are found, the upper limit for m_4^{SSR} can be solved by using the same procedure as in the case of batch chromatography. When m_R^{SSR} is large enough, the cut point τ_{A2} is located on the pure first component plateau, and the upper limit of m_4^{SSR} is identical to that of SMB process derived in (Mazzotti et al., 1997a) as shown in Appendix B.

Value of $m_{4,\,\max}$ is always higher for SSR process than for batch scheme. This is because the feed concentrations into the column are lower due to diluted recycle fraction. As a result, the propagation velocity of the first shock decreases, the retention time of the shock increases, and thus a higher value for τ_{A1} can be chosen.

4.4. Cross-current chromatography

4.4.1. Operating parameters

For classical cross-current chromatography, the freely adjustable operating parameters are the width of the feed section, $\Delta\chi_F$, the three cut points, χ_{A1}, $\chi_{A2}=\chi_{B1}$, χ_{B2}, and either the volumetric flow rate of the fluid phase in the *y*-direction, Q_y^L, or the volumetric cross-flow velocity of the solid phase in the *x*-direction, Q_x^S. In the case of cross-current recycling chromatography, one can also choose the volume of the recycle fraction and thus the end of the product fraction *A*, χ_{A2}, is not equal to the beginning of the product fraction *B*, χ_{B1}. The operating parameters can be expressed as dimensionless *m*-parameters given by Eqs. (1.14)–(1.18) where $m_R^{\mathrm{cross}}=0$ for classical cross-current process without recycling.

To ensure that there is no gap between the consecutive chromatographic cycles $\chi_{B2}-\chi_{A1}$ must be equal to unity ($x_{B2}-x_{A1}=x_{\mathrm{col}}$). This means that the dimensionless cross-flow velocity defined by Eq. (6), *i.e.* the relationship between Q_y^L and

Q_x^S, must be selected as follows:

$$\varphi = m_1^{\text{cross}} - m_2^{\text{cross}} + m_3^{\text{cross}} - m_4^{\text{cross}} + m_R^{\text{cross}} \tag{50}$$

For a given φ, the width of the feed section and the cut points are given by

$$\Delta\chi_F = \frac{(m_3^{\text{cross}} - m_2^{\text{cross}} + m_R^{\text{cross}})}{\varphi} \tag{51}$$

$$\chi_{A1} = \frac{Fm_4^{\text{cross}} + 1}{F\varphi} \tag{52}$$

$$\chi_{A2} = \frac{Fm_3^{\text{cross}} + 1}{F\varphi} \tag{53}$$

$$\chi_{B1} = \frac{F(m_3^{\text{cross}} + m_R^{\text{cross}}) + 1}{F\varphi} = \frac{Fm_2^{\text{cross}} + 1}{F\varphi} + \Delta\chi_F \tag{54}$$

$$\chi_{B2} = \frac{F(m_1^{\text{cross}} + m_3^{\text{cross}} - m_2^{\text{cross}} + m_R^{\text{cross}}) + 1}{F\varphi} = \frac{Fm_1^{\text{cross}} + 1}{F\varphi} + \Delta\chi_F \tag{55}$$

4.4.2. Linear isotherm

In the case of cross-current chromatography, the propagation velocity of component i for linear isotherm is given by

$$\frac{d\gamma}{d\chi} = \frac{F\varphi}{1 + FH_i} \quad \text{for} \quad i = (1,\ 2) \tag{56}$$

This yields to the following expression for the beginning, χ_{Ri}, and the end, χ_{Ei}, of the individual elution profiles

$$\chi_{Ri} = \frac{1 + FH_i}{F\varphi} \quad \text{for} \quad i = (1,\ 2) \tag{57}$$

$$\chi_{Ei} = \frac{1 + FH_i}{F\varphi} + \Delta\chi_F \quad \text{for} \quad i = (1,\ 2) \tag{58}$$

To achieve complete separation the following set of design criteria must be fulfilled: $\chi_{A1} \le \chi_{R1}$, $\chi_{A2} \le \chi_{R2}$, $\chi_{B1} \ge \chi_{E1}$, $\chi_{B2} \ge \chi_{E2}$, $m_{FF}^{\text{cross}} > 0$, and $m_R^{\text{cross}} \ge 0$ where $\chi_{A2} = \chi_{B1}$ and $m_R^{\text{cross}} = 0$ for cross-current chromatography without recycling. The boundaries of m^{cross} parameters are solved by substituting Eqs. (51)–(55), (57), and (58) into the above inequalities. Some re-arrangement gives

$$H_2 \le m_1^{\text{cross}} \tag{59}$$

$$H_1 \le m_2^{\text{cross}} < m_3^{\text{cross}} \le H_2 \tag{60}$$

$$m_4^{\text{cross}} \le H_1 \tag{61}$$

As can be expected, the constraints are identical to the cases of fixed bed and counter-current processes (Fig. 4). This is understandable since the cross-current processes are analogous to the corresponding fixed bed schemes with transform given by Eq. (9).

4.4.3. Langmuir isotherm

Because the cross-current processes are analogous to the corresponding fixed bed schemes, the constraints for m-parameters are identical also in the case of Langmuir isotherm. The operating boundaries can be calculated by using the procedure described in Sections 4.2.3 and 4.3.3. Derivation of the design equations, not shown here, is analogous to the fixed bed case with the transform given by Eq. (9).

The lower limit for m_1^{cross} is again equal to H_2 whereas the operating region on the (m_2, m_3) plane depends on the fresh feed concentrations and the isotherm parameters (Fig. 5). The upper limit for m_4^{cross} is, in turn, a function of m_2^{cross}, m_3^{cross}, m_R^{cross}, fresh feed concentrations and isotherm parameters. For the recycling scheme, $m_{4,\,\max}^{\text{cross}}$ is larger than for the classical cross-current process due to dilution of the feed concentrations into the column.

5. Validation of the design equations

To validate the design equations, the operating boundaries predicted by the equilibrium theory were compared with detailed simulations under ideal conditions. The comparison was performed by applying both linear and Langmuir isotherm models, small and large separation factors (1.1–3.0) as well as small and large m_R values (0–2) such that all cases mentioned in Sections 4.2–4.4 were covered.

In the simulation study, m_2 and m_3 values were varied within an interval [0, H_2]. For each combination of m_2, m_3 values, operation of each process configuration were simulated by using the free software (Siitonen and Sainio, 2011) that gives the analytical solution of the ideal model (Golshan-Shirazi and Guiochon, 1989c; Siitonen and Sainio, 2011) to calculate the chromatograms until periodic steady state was reached. The lower limit for m_1 value
and the upper limit for m_4 value were calculated from the end and the beginning of the steady state chromatogram, respectively. Finally, the purities of the product fractions were computed by integrating the steady state chromatogram numerically with trapezoidal rule.

The results of the explicit design equations and the simulation study showed a fully agreement. An example of the comparison on the (m_2, m_3) plane is shown in Fig. 8. It is seen that the points corresponding to 100% purity level nicely fall within the boundaries predicted by the explicit equations. The boundaries of m_1 and m_4 were obtained with accuracy of eight decimals.

6. Utilization of the unified design method

6.1. Selection of optimal and robust operating conditions

The unified design method can be applied to select the optimal and robust operating conditions for fixed bed and cross-current schemes in the same manner that has been employed earlier for the design of SMB unit (Storti et al., 1993; Mazzotti et al., 1994, 1996, 1997a, 1997b; Gentilini et al., 1998; Migliorini et al., 2000; Mazzotti, 2006a, 2006b; Kaspereit et al., 2007; Rajendran 2008) and its modifications (Mazzotti et al., 1997c; Migliorini et al., 2001; Abel et al., 2002, 2004; Paredes et al., 2004, 2006). In all process concepts, the maximum productivity and the minimum specific eluent consumption are achieved when the operating point on the (m_2, m_3) plane is located on the vertex of the triangle (point w in Figs. 4 and 5) and m_1 and m_4 are set equal to their lower and upper limits, respectively. As mentioned in Section 4, for classical batch and cross-current concepts, this corresponds to the operation with touching bands. In the recycling concepts, only the unresolved middle zone between the pure component bands is recycled, not any pure component fractions.

It should be noted that the productivities of the studied process configurations are not necessarily identical even if the optimal m-parameters are. In fact, it is not even possible to compare the process productivities in an unbiased manner under ideal conditions, because the column lengths and the dimensional flow rates cannot be optimized. An analysis of performances of different process schemes under ideal conditions is given as Supplementary material. It is demonstrated that for linear systems, all process configurations have equal eluent consumption, whereas in the case of Langmuir isotherm, the counter-current SMB and the recycling schemes outperform other studied configurations. In

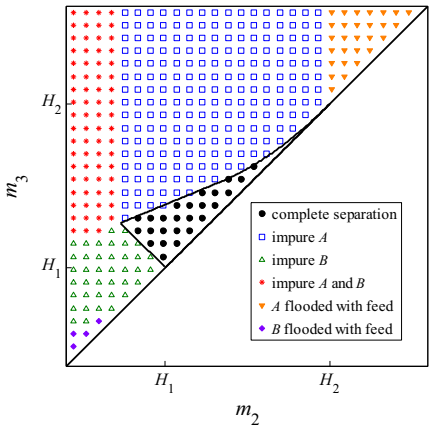

Fig. 8. Comparison of complete separation regions predicted by using the explicit equations (lines) and detailed simulations with the equilibrium model (symbols). The same results are valid for batch, SSR, and cross-current schemes. Same fresh feed concentrations and isotherm parameters as in Fig. 5.

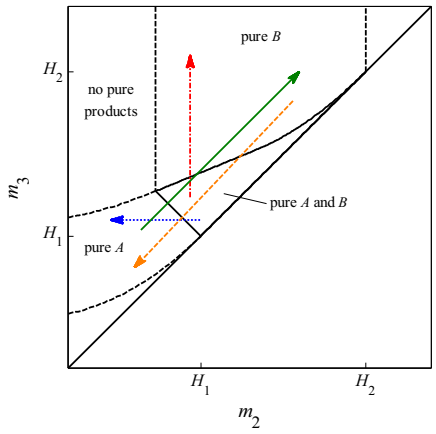

Fig. 9. Effect of the amount of fresh feed, the cut points, and the fluid low rate to the position of the operating point for batch, SSR, and cross-current chromatography with or without recycling. Blue dotted arrow: the amount of fresh feed increases, while the dimensional cut points relative to the beginning of the feed pulse and the fluid flow rate are constant. Red dash-dot arrow: the amount of fresh feed increases, while the dimensional cut points relative to the end of the feed pulse and the fluid flow rate are constant. Green solid arrow: the cut points $A2$ and $B1$ increase, while the duration of the feed pulse, the fluid flow rate, the size of the recycle fraction, and the cut points $A1$ and $B2$ are constant. Orange dashed arrow: the fluid flow rate decreases, while the dimensional duration of the feed pulse and the dimensional cut times are constant. (For interpretation of the references to color in this figure legend, the reader is referred to the web version of this article.)

terms of productivity, on the other hand, the batch chromatography and the cross-current chromatography without recycling are the best options when the flow rates are limited by an equal pressure drop constraint and the column lengths are identical.

To make the separation more robust the operating point must be chosen inside the complete separation region, not on the boundary. The final choice of the operating conditions is thus a trade-off between different performance characteristics and robustness. Examples of robust operating points are denoted by w' in Figs. 4 and 5. The minimum recommended distance between the operating point and the boundaries of the complete region separation depends on the size of the expected perturbations. Availability of the novel, explicit equations for prediction of the operating boundaries allows analysing the effect of various disturbances on the robustness of batch, SSR and cross-current schemes as well as operating the units safely closer the optimum conditions. Since the limits for m_2 and m_3 parameters are identical for all studied process configurations, the results concerning the influence of fresh feed concentrations on the shape of the complete separation region and thus on the process robustness reported earlier for the SMB process (Mazzotti et al., 1997a) must be valid for the fixed bed and cross-current schemes too.

6.2. Analysis of process operation

The triangle theory enables also analysing the effect of different operating parameters on the product purities and hence understanding analogies between the process configurations. The influences of the amount of fresh feed, the location of the cut points, and the fluid flow rate on the operation of batch, SSR, and cross-current setups are demonstrated in Fig. 9. A similar analysis for SMB process is given in (Rajendran et al., 2009). It is worth noting that the influence of chancing m-parameters on the product purities is qualitatively the same whatever the adsorption isotherm and the column efficiency.

The amount of fresh feed increases in all process options when the difference $(m_3^{\text{batch}} - m_2^{\text{batch}})$ is increased, *i.e.* the operating point is shifted further away from the diagonal. When the amount of fresh feed is increased such that the cut points relative to the beginning of the feed pulse as well as the fluid flow rate are kept constant, m_1 and m_2 decreases linearly, while m_3 and m_4 remain constant. The operating point moves along a horizontal line from right to left on the (m_2, m_3) plane (blue dotted arrow in Fig. 9). When the line crosses the complete separation region, one or both of the two product purities decrease. In addition, the lower limit of m_1 is violated when the amount of fresh feed is too high leading to the contamination of product A. The behaviour is similar to that observed in SMB process when Q_{FF} is increased and t^*, Q_A, Q_B, Q_3, and Q_4 are kept constant.

Increasing the amount of fresh feed while keeping the fluid flow rate and the cut points relative to end of the feed pulse constant leads to increase of m_3 and m_4. In this case, m_1 and m_2 remain constant, and the operating point moves upward a vertical line on the (m_2, m_3) plane (red dash-dot arrow in Fig. 9). As to the SMB unit, this corresponds to increasing Q_{FF} while keeping t^*, Q_A, Q_B, Q_1, and Q_2 constant.

When the middle cut points $A2$ and $B1$ are changed, while keeping the amount of fresh feed, the size of the recycle fraction, and the fluid flow rate constant, the operating point moves along the line that is parallel to the diagonal (green solid arrow in Fig. 9). If the values of the cut points $A2$ and $B1$ are too low, the product B is impure, whereas too high values of $A2$ and $B1$ lead to the contamination of the product A. The behaviour is similar to that observed in SMB unit when the product flow rates, Q_A and Q_B, change and Q_{FF} remain constant.

Finally, the effect of fluid flow rate on the location of the operating point when the dimensional cut points, the dimensional duration of the feed pulse, and the solid flow rate in cross-current setups are constant is represented by orange dashed arrow in Fig. 9. The distance between the diagonal and the line depends on the absolute values of the cut points and the duration of the feed pulse. The purities of the products A and B are decreased when the flow rate is too high or too low, respectively. In addition, the values of m_1 and m_4 increase as the fluid flow rate increases. As a result, the upper bound of m_4 is violated when the fluid flow rate is too high. This leads to the contamination of product B. As to the operation of SMB unit, the behaviour corresponds to chancing the switch time, while keeping the dimensional flow rates constant.

6.3. Correspondence of experimentally determined operating parameters

When the isotherm parameters are not known, but the isotherms are of linear or Langmuir type, the analogy between the design criteria can be utilized to approximate the feasible operating conditions for all studied process configurations by using the information obtained for one setup. In addition, shortcut design approaches developed originally for one process configuration can be exploited for the design of other process schemes as well. For example, the volume of feed pulse and the cut times that lead to desired separation in batch chromatography can be estimated with a simple, recently developed shortcut method (Siitonen et al., 2013). The predicted dimensional operating parameters can be converted to dimensionless m-values (Eqs. (1.9)–(1.12)) and finally to dimensional operating parameters of SMB, SSR, and cross-current units. The dimensional flow rates of SMB process can be solved from Eqs. (1.5)–(1.8), the cut points of SSR process from Eqs. (40)–(44), and the width of the feed section and the cut points of cross-current setup from Eqs. (51)–(55). In the cases of the recycling schemes, the procedure corresponds to the shortcut design method of fixed bed SSR process proposed by Kaspereit and Sainio (2011) and gives estimations of m_1, m_2, m_3, and m_4 values, whereas the size of the recycle fraction must be optimized independently.

The predictions of the unified design method are exact only under ideal conditions so the approach is most applicable for high efficient systems. Under strongly non-ideal conditions deviations between the process configurations are expected because the role of dispersive effects depends on the mutual direction of the solid and fluid flows and the column loading. In addition, the fluid flow rates and thus the column efficiencies in different configurations cannot be fully matched because four different flow rates are used in the four zones of the counter-current units, while the fluid flow rate is constant in the fixed bed and cross-current schemes.

To demonstrate the applicability of the unified design method for transferring information from one setup to another under strongly non-ideal conditions, a numerical simulation study was carried out. The feasible m-parameters corresponding to given purity constraints were first estimated by employing a shortcut design approach of fixed bed units that is based on a simple procedure applied to a single conventional chromatogram (Siitonen et al., 2013; Kaspereit and Sainio, 2011). The dimensional operating parameters of SMB scheme were then calculated by using Eqs. (1.5)–(1.8), and the obtained parameters were applied to simulate the steady state purities. For SSR process, m_R was selected such that the feed plateau was not eroded completely during elution. This provides minimum eluent consumption for a given set of m_1, m_2, m_3, and m_4 parameters without significant decrease in productivity (Kaspereit and Sainio, 2011). In the case of SMB schemes, the total bed length and the average fluid flow rate in sections 1–4 were set equal to the column length and the fluid flow rate of single-column processes, respectively. The total pressure drop in SMB columns was thus equal to that of fixed bed mode. The parameters m_1 and m_4 were selected such they guaranteed complete regeneration of solid and fluid phases because the shortcut design method does not consider overlapping between the consecutive chromatograms. All simulations were carried out by employing the transport-dispersive model with the solid film linear driving force (LDF) approximation to describe the effects of finite mass transfer rate and axial dispersion (for more details, see *e.g.* Guiochon et al., 2006). The number of theoretical plates in fixed bed column, determined under linear conditions for the less strongly adsorbed component, was 200. The parameters of the two generic model systems as well as the conditions of the shortcut design are summarized in Table 4.

Table 4
Parameters for the model system used in the simulation study.

Parameter	System 1	System 2
Fresh feed concentration of component 1, c_1^{FF} (g/L)	4.0	
Fresh feed concentration of component 2, c_2^{FF} (g/L)	4.0	
Total bed length, $N_{col}L_{col}$ (cm)	84.0	
Column diameter, D_{col} (cm)	2.5	
isotherm parameters		
K_1 (L/g)	0.025	
H_1	2.5	
K_2 (L/g)	0.035	0.050
H_2	3.5	5.0
Total void fraction of the bed, ε	0.7	
Axial dispersion coefficient, D_{ax} (cm^2/min)	0.213	
Mass transfer coefficient of component 1, k_1(1/min)	6.0	
Mass transfer coefficient of component 2, k_2(1/min)	6.0	
Fluid flow rate in the single-column processes, Q (mL/min)	12.5	
Volume of the feed pulse in the short-cut design, V_F^{design} (mL)	600	

The predicted m-parameters as well as the achieved purities of the product fractions A and B (p_1^A and p_2^B, respectively) are given in Table 5. It is seen that the design approach works best when the purity constraints are low and the separation factor is large. This is because these conditions provide large column loading that makes the thermodynamic effects more predominant.

The deviations observed in the cases of high target purities can be explained by two different factors. First, the single-column shortcut method provides systematically a slightly too optimistic estimation for m_{FF} and thus for m_3 as reported in (Siitonen et al., 2013; Kaspereit and Sainio, 2011). Consequently, the purity of the first eluting component is lower than the target. It is well known that this purity is very sensitive to selection of m_3 due to non-linear phase equilibrium. The purity p_1^A can hence be easily increased by slightly decreasing m_3. Second, the unified conversion rules derived in this contribution do not guarantee identical purities for all process configurations under non-ideal conditions because the units tolerate dispersive effects differently. As a result, the counter-current SMB schemes lead to higher product purities when identical m-parameters are used, and the shortcut approach works even better for them than for the single-column units.

Finally, it is interesting to note that the differences between the product purities obtained in SSR and SMB 1-1-1-1 units are generally relatively small. This implies that the operating points on the (m_2, m_3) plane with which the target purities are matched exactly in these two configurations are most probably very close to each other as well. It is thus expected that the unified conversion rules provide best results when they are applied to transfer result between SSR and SMB 1-1-1-1 configurations. This property is very useful, in particular when the feasible operating conditions for one scheme are known and the operating parameters for the other one are needed.

7. Possible extensions of the method

The explicit design equations derived in Section 4 are valid in the case of ideal conditions for complete separation of a binary feed mixture that follows linear or competitive Langmuir adsorption isotherm model. In principle, the approach could be also applied to more complex cases. However, it is possible that the dimensionless operating limits are not always identical for all process configurations.

First, the design method described in Section 4 can be extended to the cases where the target purities are less than 100%. The reduced purities can be achieved by using two different strategies

Table 5
Application of the single-column short-cut design method for different process configurations and purity requirements. Simulation parameters are given in Table 4.

Case	System 1						System 2					
	A		B		C		A		B		C	
Target purities	p_1^A	p_2^B	p_1^A	p_2^B	p_1^A	p_2^B	p_1^A	p_2^B	p_1^A	p_2^B	p_1^A	p_2^B
	0.980	0.980	0.900	0.900	0.800	0.800	0.980	0.980	0.900	0.900	0.800	0.800
Predicted m-parameters												
m_1	5.050		5.050		5.050		6.840		6.840		6.840	
m_2	2.842		2.280		1.870		2.337		1.784		1.283	
m_3	3.141		3.001		3.095		3.959		4.088		4.479	
m_4	1.300		1.300		1.300		1.310		1.310		1.310	
Achieved purities	p_1^A	p_2^B	p_1^A	p_2^B	p_1^A	p_2^B	p_1^A	p_2^B	p_1^A	p_2^B	p_1^A	p_2^B
Batch	0.781	0.962	0.822	0.879	0.783	0.792	0.936	0.977	0.891	0.898	0.800	0.800
SSR	0.813	0.985	0.843	0.902	0.787	0.801	0.944	0.980	0.893	0.901	0.799	0.800
SMB 1-1-1-1	0.841	0.983	0.867	0.913	0.797	0.809	0.948	0.971	0.896	0.895	0.802	0.798
SMB 1-2-2-1	0.885	1.000	0.887	0.977	0.800	0.842	0.987	0.998	0.901	0.923	0.801	0.801

depending on whether the consecutive chromatograms are allowed to overlap or not. In restrictive case, the process is operated such that the chromatograms do not overlap, and the constraints for m_1 and m_4 parameters derived in Section 4 are satisfied. Based on this assumption, a design method has been developed to calculate the cut times that lead to arbitrary target purities both for batch (Siitonen et al., 2013) and SSR (Sainio and Kaspereit 2009; Kaspereit and Sainio 2011) process in the case of Langmuir isotherm. The dimensionless m-parameters can be calculated from the cut times by using Eqs. (1.9)–(1.12). It has been shown in (Sainio and Kaspereit, 2009) that there is only a unique combination of cut times t_{A2} and t_{B1}, and thus m_2 and m_3 values, for which given purity constraints are matched exactly. The same approach can be easily extended to linear isotherm systems. In the case of non-restrictive design, overlapping between the consecutive chromatograms is allowed. It is expected that the separation region on the (m_2, m_3) plane depends now on m_1, m_4, and m_R. However, there are no analytical equations available to calculate the elution profiles of overlapping cycles, and explicit design equations have not been derived. As already mentioned, it is possible that the operating boundaries corresponding to reduced purity constraints are not identical for all process concepts.

Second, dispersive effects such as axial dispersion and mass transfer resistances play often an important role on the separation dynamics. In this case, the general criteria on the operating parameters, Eqs. (16)–(20), are still valid. The range of feasible m-values can be calculated by employing the simulation approach that has been used earlier for the design of SMB unit (Migliorini et al., 1999) and in this work for the validation of the design equations (see Section 5). The operating boundaries on the (m_2, m_3) plane can be plotted by contouring the region where high product purities, *e.g.* 99.9%, are achieved. The model to calculate the elution profiles can be selected case by case. In the case of non-ideal conditions, the fluid flow rate often affect the degree of dispersive effects and hence on the range of feasible m-parameters. It is generally known that the number of theoretical plates required to achieve a desired separation in batch process is higher than those of SMB and SSR schemes (see *e.g.* Strube et al., 1998; Jupke et al., 2002). It is thus expected that the complete separation region of batch process on the (m_2, m_3) plane shrinks most rapidly when the column efficiency decreases.

Thirdly, the approach described in Section 4 can be applied to derive design equations for other isotherm models which are amenable to the treatment based on the equilibrium theory such as modified Langmuir, bi-Langmuir, and generalized Langmuir isotherms. Explicit solution of all the design constraints, however, is not guaranteed. For more complex isotherm models than mentioned above, for which analytical solution of the equilibrium model is not available, the operating bounds can be searched by using the same simulation procedure as in the case of non-ideal conditions.

Fourthly, the triangle theory can be extended to other fixed bed and cross-current operation strategies such as other recycling schemes, gradient elution, ternary separation, and recently introduced bypass operation (Siitonen et al., 2012). In addition, the approach can be applied to design hybrid process concepts where chromatography is integrated with other unit operations such as SSR chromatography with an integrated solvent removal unit, SSR–SR (Siitonen et al., 2011; Hellstén et al., 2012; Siitonen and Sainio, 2014), or a combination of fixed bed chromatography, racemization, and solvent removal (Nimmig and Kaspereit, 2013).

8. Conclusions

The equilibrium theory of chromatography was applied to extend the triangle theory for the design of batch, steady state recycling, cross-current, and cross-current recycling processes. The method allows predicting the region of the feasible operating parameters that lead to complete separation of a binary mixture, not only the optimal operating point. Explicit design equations were derived for systems with linear or competitive Langmuir adsorption isotherms. The design approach can be extended for reduced purity constraints, for other isotherms that are amenable to the treatment based on the equilibrium theory, for other operation modes such as gradient and bypass operation, and for chromatography-based hybrid separation units.

The unified design method enables understanding the similarities and differences between different operation modes, especially the influence of non-linear phase equilibrium on the separation performance. Under linear conditions, the boundaries of the feasible dimensionless operating parameters are identical for all studied fixed bed and cross-current concepts and equal to those of counter-current SMB unit. In the case of Langmuir isotherm, the complete separation region on the (m_2, m_3) plane and the lower limit of m_1 are independent of the applied configuration whereas the upper limit of m_4 depends on the process scheme as well as the volume of the recycle fraction. For all concepts, the maximum amount of fresh feed that can be processed during a chromatographic cycle or switch is equal. However, any conclusions about the productivities of the processes cannot be made because optimization of the column length is not possible within the framework of the equilibrium theory.

The observed equality between the complete separation regions under ideal conditions allows extending the results

reported earlier for the SMB unit concerning the choice of the optimal and robust operating conditions (Mazzotti et al., 1997a) for the fixed bed and cross-current schemes. The theory enables analysing the effect of different variables, such as fresh feed concentrations and isotherm parameters, on the shape of the complete separation region and hence on the process robustness. In addition, the unified design method can be utilized to find the feasible operating parameters for all studied process schemes when the operating parameters of one configuration are known. This simplifies the design of multi-column counter-current and cross-current schemes as well as fixed bed recycling chromatography.

The derived design equations are limited to the ideal conditions with assumption of infinite column efficiency. This means that the theory is most applicable for high performance systems, while some conclusions may not be valid for systems of moderate or low efficiency. However, the method provides deep understanding of the main characteristics of chromatographic processes that is applicable also for practically relevant non-ideal case where the dispersive effects play a significant role. Under these conditions, the general design criteria are still valid, and the effect of column efficiency can be analysed by using a similar approach as in the design of SMB unit (Migliorini et al., 1999).

Acknowledgement

Financial support from Academy of Finland (grant no. 252688) and Graduate School in Chemical Engineering (Finland) are gratefully acknowledged.

Appendix A. Derivation of explicit equations to calculate the complete separation region on the (m_2, m_3) plane in the case of Langmuir isotherm for batch and SSR processes

In this appendix, explicit equations to calculate the complete separation region on the (m_2, m_3) plane for batch chromatography and for steady state recycling chromatography in the case of competitive Langmuir adsorption isotherm model are derived. All the required equations for $\omega_i(\tau)$ used in this appendix are provided by Rajendran and Mazzotti (2011).

Derivation of the operating boundaries is based on the fact that for Langmuir isotherm the rear part of the chromatogram is independent of the volume of the feed pulse into the column both in the case of classical batch chromatography and mixed mode SSR process (Bailly and Tondeur 1982; Sainio and Kaspereit, 2009). The amount of component 2 that is collected in the product fraction B, n_2^B, depends on the cut time τ_{B1} and hence m_2, but not on $\Delta\tau_F$. It can be thus expressed in form $n_2^B = f(m_2)$. Once n_2^B is known, the amount of fresh feed that is introduced into the process during a chromatographic cycle is solved from the mass balance around the feed node which yields

$$m_{FF} = \frac{n_2^B}{(1-\varepsilon)c_2^{FF}V_{\mathrm{col}}} \tag{A.1}$$

Finally, m_3 is solved from Eq. (12)

$$m_3 = m_2 + m_{FF} \tag{A.2}$$

The boundary *ar* on the (m_2, m_3) plane (Fig. 5) corresponds to the case where the beginning of the product fraction B, τ_{B1}, is located on the pure second component wave, *i.e.* Γ_- characteristic (Figs. 6a and 7a). The amount of component 2 that is collected in the product fraction B is solved by integrating Γ_- characteristic from the cut point τ_{B1} to the end of the profile. Along the wave ω_1 remains constant at value H_1. The relationship between the cut time τ_{B1} and the corresponding ω_2^{B1} value is obtained from the propagation velocity of the Γ_- characteristic:

$$\tau_{B1} = 1 + \frac{F(\omega_2^{B1})^2}{H_2} + \Delta\tau_F \tag{A.3}$$

The concentration profile of component 2 is integrated by using the substitution $t = f(\omega_2)$. The resulting expression for n_2^B is given by

$$\begin{aligned} n_2^B &= \varepsilon V_{\mathrm{col}} \int_{\tau_{B1}}^{\tau_{B2}} c_2(\tau)\ \mathrm{d}\tau = \varepsilon V_{\mathrm{col}} \int_{\omega_2(\tau_{B1})}^{\omega_2(\tau_{B2})} c_2(\tau(\omega_2))\tau'(\omega_2)\ \mathrm{d}\omega_2 \\ &= \frac{1}{K_2}\left[\sqrt{H_2} - \sqrt{\frac{\tau_{B1} - \Delta\tau_F - 1}{F}}\right]^2 (1-\varepsilon)V_{\mathrm{col}} \end{aligned} \tag{A.4}$$

To solve the amount of fresh feed, the relationship between m_2-value and the cut time τ_{B1}, Eq. (1.10), is substituted into Eq. (A.4) and the resulting expression is substituted into Eq. (A.1). Some rearrangement gives

$$m_{FF} = \frac{\left(\sqrt{H_2} - \sqrt{m_2}\right)^2}{K_2 c_2^{FF}} \tag{A.5}$$

The equation for the boundary *ar* is obtained by substituting Eq. (A.5) into Eq. (A.2) which yields

$$m_3 = m_2 + \frac{\left(\sqrt{m_2} - \sqrt{H_2}\right)^2}{K_2 c_2^{FF}} \tag{A.6}$$

In the line *rw*, the cut point τ_{B1} is located on the pure second component plateau (Figs. 6b and 7b). To calculate the amount of component 2 in product fraction B the rear part of the elution profile is integrated piecewise. Again, along the pure second component wave, ω_1 parameter remains constant and the substitution $t = f(\omega_2)$ is used. In the pure second component plateau, c_2 is constant and the integral term is replaced by $c_2(\tau_P)(\tau_P - \tau_{B1})$, where $c_2(\tau_P)$ is the concentration of component 2 at the pure second component plateau and τ_P is the end of the pure second component plateau given by Golshan-Shirazi and Guiochon (1989c)

$$\tau_P = 1 + \frac{F(\omega_2^{FF})^2}{H_2} + \Delta\tau_F \tag{A.7}$$

The resulting expression for n_2^B is

$$\begin{aligned} n_2^B &= \varepsilon V_{\mathrm{col}}\left[\int_{\tau_{B1}}^{\tau_P} c_2(\tau)\ \mathrm{d}\tau + \int_{\tau_P}^{\tau_{B2}} c_2(\tau)\ \mathrm{d}\tau\right] \\ &= \varepsilon V_{\mathrm{col}}\left[c_2(\tau_P)(\tau_P - \tau_{B1}) + \int_{\omega_2(\tau_P)}^{\omega_2(\tau_{B2})} c_2(\tau(\omega_2))\tau'(\omega_2)\ \mathrm{d}\omega_2\right] \\ &= \varepsilon V_{\mathrm{col}}\left[\frac{(H_2 - \omega_2^{FF})}{\omega_2^{FF}K_2}\left(1 + \frac{F(\omega_2^{FF})^2}{H_2} + \Delta\tau_F - \tau_{B1}\right) + \frac{F(H_2 - \omega_2^{FF})^2}{H_2 K_2}\right] \end{aligned} \tag{A.8}$$

To solve the amount of fresh feed Eq. (1.10) is substituted into expression of n_2^B, Eq. (A.8), and the resulting equation is substituted into Eq. (A.1)

$$m_{FF} = \frac{\omega_1^{FF}(H_2 - H_1)(\omega_2^{FF} - m_2)}{H_1(H_2 - \omega_1^{FF})} \tag{A.9}$$

The boundary *rw* is obtained by substituting Eq. (A.9) into Eq. (A.2)

$$m_3 = \frac{\omega_1^{FF}\omega_2^{FF}(H_2 - H_1) + m_2 H_2(H_1 - \omega_1^{FF})}{H_1(H_2 - \omega_1^{FF})} \tag{A.10}$$

The boundary *bw* corresponds to the lower limit of the cut time τ_{B1}. It is obtained when τ_{B1} is equal to the end of the elution profile of the first component, τ_{E1}. Expression for τ_{E1} depends on the

resolution between the elution bands. In batch chromatography, the components are completely separated in the column to achieve 100% product purities (Fig. 6d). The cut time τ_{B1} is given by

$$\tau_{B1} = \tau_{E1} = 1 + FH_1\left(1 - \frac{K_2 c_2^{FF} V^{FF}}{(H_2 - H_1)(1-\varepsilon)V_{\mathrm{col}}}\right) + \Delta\tau_F \tag{A.11}$$

To calculate the amount of fresh feed the above Eq. (A.11) is substituted into the definition of m_2 parameter, Eq. (1.10), and V^{FF} is solved. The resulting equation is

$$m_{FF} = \frac{(H_2 - H_1)(H_1 - m_2)}{H_1 K_2 c_2^{FF}} \tag{A.12}$$

Substitution of Eq. (A.12) into Eq. (A.2) leads to the following expression for m_3 parameter:

$$m_3 = \frac{H_1(H_2 - H_1) - m_2\left[H_2 - H_1\left(1 + K_2 c_2^{FF}\right)\right]}{H_1 K_2 c_2^{FF}} \tag{A.13}$$

In the case of SSR chromatography, the components are typically not completely separated. The end of the first component band, and thus the cut time τ_{B1}, is equal to the beginning of the second component plateau (Fig. 7d). The cut time τ_{B1} is given by

$$\tau_{B1} = \tau_{E1} = 1 + \frac{F\omega_2^F H_1}{H_2} + \Delta\tau_F \tag{A.14}$$

where ω_2^F corresponds to the steady state feed composition. The amount of component 2 in the product fraction B is obtained by integrating piecewise the elution profile of the second component

$$\begin{aligned} n_2^B &= \varepsilon V_{\mathrm{col}}\left[\int_{\tau_{B1}}^{\tau_P} c_2(\tau)\ \mathrm{d}\tau + \int_{\tau_P}^{\tau_{B2}} c_2(\tau)\ \mathrm{d}\tau\right] \\ &= \varepsilon V_{\mathrm{col}}\left[c_2(\tau_P)(\tau_P - \tau_{B1}) + \int_{\omega_2(\tau_P)}^{\omega_2(\tau_{B2})} c_2(\tau(\omega_2))\tau'(\omega_2)\ \mathrm{d}\omega_2\right] \\ &= \frac{(H_2 - \omega_2^F)(H_2 - H_1)}{H_2 K_2}(1-\varepsilon)V_{\mathrm{col}} \end{aligned} \tag{A.15}$$

The amount of fresh feed is solved from the set of Eqs. (1.10), (A.1), (A.14), and (A.15) which yields

$$m_{FF} = \frac{(H_2 - H_1)(H_1 - m_2)}{H_1 K_2 c_2^{FF}} \tag{A.16}$$

As seen by comparing Eqs. (A.16) and (A.12), the amount of fresh feed as a function m_2 along the line bw in SSR process is equal to that of batch process. For this reason, also the relationship between m_3 and m_2 parameters must be identical and given by Eq. (A.13).

Finally, equations to calculate the critical points, a, b, r, and w, are solved from intersections of the lines ab, rw, bw, and the curve ar. This leads to equations reported in Table 2.

Appendix B. Derivation of an explicit equation to calculate the upper limit of m_4 for SSR process in the case of Langmuir isotherm and large recycle fraction

The upper limit of m_4 for SSR process in the case of Langmuir isotherm and large recycle fraction can be solved from the mass balance of the first component. When m_R^{SSR} is large and the cut point τ_{A2} is located on the pure first component plateau, the amount of component 1 in the product fraction A is given by

$$n_1^A = \varepsilon V_{\mathrm{col}} c_1^A(\tau_{A2} - \tau_{R1}) \tag{B.1}$$

where c_1^A is the plateau concentration of component 1. At steady state, this quantity must be equal to the amount of component 1 that is introduced into the process during a cycle which yields

$$c_1^A(\tau_{A2} - \tau_{R1}) = Fc_1^{FF}(m_3 - m_2) \tag{B.2}$$

The relationship between τ_{R1} and c_1^A is given by the propagation velocity of the first shock (Golshan-Shirazi and Guiochon, 1989c)

$$\tau_{R1} = 1 + \frac{FH_1}{1 + K_1 c_1^A} \tag{B.3}$$

To solve the upper limit of m_4^{SSR}, c_1^A is solved from Eq. (B.3) and substituted into Eq. (B.2). The cut point $\tau_{A1}$is set equal to τ_{R1} and solved from the resulting equation. This yields to the following boundary for m_4^{SSR}

$$\begin{aligned} m_4^{\mathrm{SSR}} \le \frac{1}{2}\{ & m_3^{\mathrm{SSR}} + H_1 + K_1 c_1^{FF}(m_3^{\mathrm{SSR}} - m_2^{\mathrm{SSR}}) \\ & - \sqrt{\left[m_3^{\mathrm{SSR}} + H_1 + K_1 c_1^{FF}(m_3^{\mathrm{SSR}} - m_2^{\mathrm{SSR}})\right]^2 - 4m_3^{\mathrm{SSR}} H_1}\Big\} \end{aligned} \tag{B.4}$$

The above constraints is identical to that of SMB process given in (Mazzotti et al., 1997a).

Appendix C. Supporting information

Supplementary data associated with this article can be found in the online version at http://dx.doi.org/10.1016/j.ces.2014.10.004.

References

Abel, S., Mazzotti, M., Morbidelli, M., 2002. Solvent gradient operation of simulated moving beds I. Linear isotherms. J. Chromatogr. A 944, 23–39.

Abel, S., Mazzotti, M., Morbidelli, M., 2004. Solvent gradient operation of simulated moving beds 2. Langmuir isotherms. J. Chromatogr. A 1026, 47–55.

Antos, D., 2009. Gradient Techniques in Preparative Chromatography: Modeling and Experimental Realization. Lambert Academic Publishing, Saarbrücken.

Bailly, M., Tondeur, D., 1982. Recycle optimization in non-linear productive chromatography—I Mixing recycle with fresh feed. Chem. Eng. Sci. 37, 1199–1212.

Bochenek, R., Marek, W., Pią tkowski, W., Antos, D., 2013. Evaluating the performance of different multicolumn setups for chromatographic separation of proteins on hydrophobic interaction chromatography media by a numerical study. J. Chromatogr. A 1301, 60–72.

Bubnik, Z., Pour, V., Gruberova, A., Starhova, H., Hinkova, A., Kadlec, P., 2004. Application of continuous chromatographic separation in sugar processing. J. Food Eng. 61, 509–513.

F. Charton, Optimisation des coupes et recyclages en chromatographie preparative industrielle, Ph.D. Thesis, Institut National Polytechnique de Lorraine, Nancy, 1995.

Charton, F., Bailly, M., Guiochon, G., 1994. Recycling in preparative liquid chromatography. J. Chromatogr. A 687, 12–31.

Gentilini, A., Migliorini, C., Mazzotti, M., Morbidelli, M., 1998. Optimal operation of simulated moving-bed units for non-linear chromatographic separations II. Bi-Langmuir isotherm. J. Chromatogr. A 805, 37–44.

Giddings, J.C., 1962. Theoretical basis for a continuous, large-capacity gas chromatographic apparatus. Anal. Chem. 34, 37–39.

Golshan-Shirazi, S., Guiochon, G., 1989a. Theory of optimization of the experimental conditions of preparative elution using the ideal model of liquid chromatography. Anal. Chem. 61, 1276–1287.

Golshan-Shirazi, S., Guiochon, G., 1989b. Theory of optimization of the experimental conditions of preparative elution chromatography: optimization of the column efficiency. Anal. Chem. 61, 1368–1382.

Golshan-Shirazi, S., Guiochon, G., 1989c. Analytical solution for the ideal model of chromatography in the case of a pulse of a binary mixture with competitive Langmuir isotherm. J. Phys. Chem. 93, 4143–4157.

Goto, M., Goto, S., 1987. Continuous separation using an annular chromatograph with rotating inlet and outlet. J. Chem. Eng. Jpn. 20, 598–603.

Grill, C.M., 1998. Closed-loop recycling with periodic intra-profile injection: a new binary preparative chromatographic technique. J. Chromatogr. A 796, 101–113.

Guiochon, G., Felinger, A., Shirazi, D.G., Katti, A.M., 2006. Fundamentals of Preparative and Nonlinear Chromatography, second ed. Academic Press, Amsterdam.

Hellstén, S., Sainio, T., 2012. Steady state recycling chromatography in acid–sugar separation on an ion-exchange resin. Sep. Sci. Technol 47, 2358–2365.

Hellstén, S., Siitonen, J., Mänttäri, M., Sainio, T., 2012. Steady state recycling chromatography with an integrated solvent removal unit—separation of glucose and galactose. J. Chromatogr. A 1251, 122–133.

Huckman, M.E., Latheef, I.M., Anthony, R.G., 2001. Designing a commercial ion-exchange carousel to treat DOE wastes using CST granules. AIChE J 47, 1425–1431.

Jupke, A., Epping, A., Schmidt-Traub, H., 2002. Optimal design of batch and simulated moving bed chromatographic separation processes. J. Chromatogr. A 944, 93–117.

Kaspereit, M., Sainio, T., 2011. Simplified design of steady-state recycling chromatography under ideal and nonideal conditions. Chem. Eng. Sci. 66, 5428–5438.
Kaspereit, M., Seidel-Morgenstern, A., Kienle, A., 2007. Design of simulated moving bed processes under reduced purity requirements. J. Chromatogr. A 1162, 2–13.
Knox, J.H., Pyper, H.M., 1986. Framework for maximizing throughput in preparative liquid chromatography. J. Chromatogr. 363, 1–30.
Mazzotti, M., 2006b. Equilibrium theory based design of simulated moving bed processes for a generalized Langmuir isotherm. J. Chromatogr. A 1126, 311–322.
Mazzotti, M., 2006a. Design of simulated moving bed separations: generalized Langmuir isotherm. Ind. Eng. Chem. Res. 45, 6311–6324.
Mazzotti, M., 2006c. Local equilibrium theory for the binary chromatography of species subject to a generalized Langmuir isotherm. Ind. Eng. Chem. Res. 45, 5332–5350.
Mazzotti, M., Storti, G., Morbidelli, M., 1994. Robust design of countercurrent adsorption separation processes: 2. Multicomponent systems. AIChE J. 40, 1825–1842.
Mazzotti, M., Storti, G., Morbidelli, M., 1996. Robust design of countercurrent adsorption separation processes: 3. Nonstoichiometric systems. AIChE J. 42, 2784–2796.
Mazzotti, M., Storti, G., Morbidelli, M., 1997c. Supercritical fluid simulated moving bed chromatography. J. Chromatogr. A 786, 309–320.
Mazzotti, M., Storti, G., Morbidelli, M., 1997a. Optimal operation of simulated moving bed units for nonlinear chromatographic separations. J. Chromatogr. A 769, 3–24.
Mazzotti, M., Storti, G., Morbidelli, M., 1997b. Robust design of countercurrent adsorption separation processes: 4. Desorbent in the feed. AIChE J. 43, 64–72.
Migliorini, C., Gentilini, A., Mazzotti, M., Morbidelli, M., 1999. Design of simulated moving bed units under nonideal conditions. Ind. Eng. Chem. Res. 38, 2400–2410.
Migliorini, C., Mazzotti, M., Morbidelli, M., 2000. Robust design of countercurrent adsorption separation processes: 5. Nonconstant selectivity. AIChE J. 46, 1384–1399.
Migliorini, C., Wendlinger, M., Mazzotti, M., Morbidelli, M., 2001. Temperature gradient operation of a simulated moving bed unit. Ind. Eng. Chem. Res. 40, 2606–2617.
Nimmig, S., Kaspereit, M., 2013. Continuous production of single enantiomers at high yields by coupling single column chromatography, racemization, and nanofiltration. Chem. Eng. Process. 67, 89–98.
Paredes, G., Abel, S., Mazzotti, M., Morbidelli, M., Standler, J., 2004. Analysis of a simulated moving bed operation for three-fraction separations (3F-SMB). Ind. Eng. Chem. Res. 43, 6157–6167.
Paredes, G., Rhee, H.-K., Mazzotti, M., 2006. Design of simulated-moving-bed chromatography with enriched extract operation (EE-SMB): Langmuir isotherms. Ind. Eng. Chem. Res. 45, 6289–6301.
Rajendran, A., 2008. Equilibrium theory-based design of simulated moving bed processes under reduced purity requirements Linear isotherms. J. Chromatogr. A 1185, 216–222.
Rajendran, A., Mazzotti, M., 2011. Local equilibrium theory for the binary chromatography of species subject to a generalized Langmuir isotherm. 2. Wave interactions and chromatographic cycle. Ind. Eng. Chem. Res. 50, 352–377.
Rajendran, A., Paredes, G., Mazzotti, M., 2009. Simulated moving bed chromatography for the separation of enantiomers. J. Chromatogr. A 1216, 709–738.
Rhee, H.-K., Aris, R., Amundson, N.R., 2001b. First-order partial differential equations. Theory and Application of Hyperbolic Systems of Quasilinear Equations, vol. II. Dover Publications, New York, NY.
Rhee, H.-K., Aris, R., Amundson, N.R., 2001a. First-order partial differential equations. Theory and Application of Single Equations, vol. I. Dover Publications, New York, NY.
Ruthven, D.M., Ching, C.B., 1989. Counter-current and simulated counter-current adsorption separation processes. Chem. Eng. Sci. 44, 1011–1038.
Sainio, T., Kaspereit, M., 2009. Analysis of steady state recycling chromatography using equilibrium theory. Sep. Purif. Technol. 66, 9–18.
Siitonen, J., Sainio, T., 2011. Explicit equations for the height and position of the first component shock for binary mixtures with competitive Langmuir isotherms under ideal conditions. J. Chromatogr. A 1218, 6379–6387.
Siitonen, J., Sainio, T., 2014. Steady state recycling chromatography with solvent removal—effect of solvent removal constraints on process operation under ideal conditions. J. Chromatogr. A 1341, 15–30.
Siitonen, J., Sainio, T., Kaspereit, M., 2011. Theoretical analysis of steady state recycling chromatography with solvent removal. Sep. Purif. Technol. 78, 21–32.
Siitonen, J., Sainio, T., Rajendran, A., 2012. Bypass chromatography—design and analysis of an improved strategy for operating batch chromatography processes. J. Chromatogr. A 1230, 77–92.
Siitonen, J., Sainio, T., Rajendran, A., 2013. Design of batch chromatography for separation of binary mixtures under reduced purity requirements. J. Chromatogr. A 1286, 55–68.
Storti, G., Mazzotti, M., Morbidelli, M., Carrà, S., 1993. Robust design of binary countercurrent adsorption separation processes. AIChE J. 39, 471–492.
Strube, J., Haumreisser, S., Schmidt-Traub, H., Schulte, M., Ditz, R., 1998. Comparison of batch elution and continuous simulated moving bed chromatography. Org. Process Res. Dev. 2, 305–319.
Thiele, A., Falk, T., Tobiska, L., Seidel-Morgenstern, A., 2001. Prediction of elution profiles in annular chromatography. Comput. Chem. Eng. 25, 1089–1101.
Virolainen, S., Suppula, I., Sainio, T., 2014. Continuous ion exchange for hydrometallurgy: Purification of Ag(I)–NaCl from divalent metals with aminomethylphosphonic resin using counter-current and cross-current operation. Hydrometallurgy 142, 84–93.
Wankat, P.C., 1977. The relationship between one-dimensional and two-dimensional separation processes. AIChE J. 23, 859–867.

Article VI

Siitonen, J., Mänttäri, M., Seidel-Morgenstern, A., Sainio, T., Robustness of steady state recycling chromatography with an integrated solvent removal unit, submitted to *Journal of Chromatography A* on October 2014.

Robustness of steady state recycling chromatography with an integrated solvent removal unit

submitted by

Jani Siitonen[a], Mika Mänttäri[a], Andreas Seidel-Morgenstern[b], and Tuomo Sainio[a*]

[a] Lappeenranta University of Technology, Skinnarilankatu 34, FI–53850 Lappeenranta, Finland

[b] Max Planck Institute for Dynamics of Complex Technical Systems, Sandtorstrasse 1, DE–39106 Magdeburg, Germany

[*] Corresponding author. E-mail Tuomo.Sainio@lut.fi. Telephone: +358403578683

ABSTRACT

The robustness of a hybrid separation process where the performance of mixed-recycle steady state recycling chromatography is enhanced by integrating it with a solvent removal unit is analysed theoretically and by means of numerical simulations. The equilibrium theory of chromatography is applied to derive equations for boundaries of feasible operating parameters in such a hybrid process. Visualization of the feasible operating parameter ranges helps in analysing the influence of various physical and process parameters of robustness of an operating point. It is observed that process robustness can be improved by adjusting the solvent removal capacity or the cut times. When the solvent removal capacity increases, the region of feasible cut times becomes narrower due to increased non-linearity of the system. This makes it more difficult to maintain robust operation.

Keywords: steady state recycling, solvent removal, robustness, equilibrium theory, unified design

1 Introduction

One of the most promising approaches to improve the performance of preparative and large scale chromatographic separations is process integration where two or more unit operations are combined. Many potential chromatography-based hybrid concepts have been proposed such as coupling of chromatography with crystallization [1–9], chemical reactions [10–17], partial solvent removal [18–22], or combinations of them [23, 24].

Robust design and operation of the hybrid separation processes is challenging due to interactions between the coupled units. In industrial applications, the processes must tolerate at least to some extent fluctuations in the uncontrollable process variables and chemico-physical properties. Such fluctuations may originate, for example, from contamination or chemical modification of the stationary phase in the chromatographic unit that leads to changes in the adsorption behaviour, from enzyme inactivation that decreases the conversion in the reactor, or from membrane fouling that affects the permeate flux and the membrane retention in solvent removal. The fluctuations in the individual unit operations propagate through the system, and affect the performance of the whole integrated process. This is the case especially for integrated processes with internal recycle streams.

Process integration, on the other hand, provides also new, alternative ways to enhance process robustness. For example, it has been recently demonstrated that robustness of hybrid process concepts where SMB chromatography is coupled with crystallization and solvent removal [9] or chemical reaction and solvent removal [17] can be improved by manipulating the solvent removal rate. There is thus an obvious need to understand how different operating parameters of coupled units interact with each other.

The robustness of classical multi-column simulated moving bed (SMB) scheme has been conveniently analysed by using the established triangle theory [25, 26] that is based on the equilibrium theory of chromatography with an assumption of infinite column efficiency. The method allows predicting the range of feasible operating parameters that lead to desired separation. It has been applied successfully for the design of SMB process both in the cases of stand-alone separations [27, 28] and coupled processes, such as combination of SMB unit with crystallization [6], bioreactor [15], or partial solvent removal [19].

The robustness studies of single column chromatographic schemes have commonly been based on numerical simulations employing, for example, fractional design [29, 30] or stochastic methods [31]. In contrast, almost all of the theoretical studies have been focused on the selection of the optimal operating parameters only, whereas robustness has been rarely analysed using equilibrium theory. The recently introduced Unified Design approach [32] facilitates presenting the operating parameter spaces of batch, steady state recycling (SSR), and cross-current chromatographic schemes in the same way as in the triangle theory of counter-current chromatography. The Unified Design approach therefore enables selecting robust operating parameters for the chromatographic separation unit also in hybrid processes.

In this work, we will focus on analysing the robustness of a hybrid separation process where mixed-recycle SSR chromatography is integrated with a solvent removal unit (SSR–SR) [20]. In SSR–SR concept, the internal recycling stream of SSR unit is concentrated by removing part of the solvent, for example, with membrane filtration or evaporation. This leads to increased productivity and decreased eluent consumption as demonstrated in [20–22]. In earlier works [20, 22], a method has been developed to calculate the optimal cut times as well

as the range of feasible solvent removal capacity and the volume of the feed pulse that corresponds to arbitrary purity and solvent removal constraints by using the equilibrium theory of chromatography. The robustness of SSR–SR concept has not been analysed in detail until now.

The main objective of this contribution is to provide a theoretical frame for robust design of SSR–SR units. For this purpose, the Unified Design approach [32] is used to present the method developed earlier for the design of SSR–SR setup [20, 22] in a form analogous to the triangle theory in order to analyse the robustness of the SSR–SR process. The effect of solvent removal capacity on the range of feasible cut times is of special interest. The influence of dispersive effects on the operation of SSR–SR process is studied by means of numerical simulations. The separation of EMD 53986 enantiomers is used as a model system.

2 SSR–SR process

A schematic setup of SSR–SR concept studied in this work is illustrated in Fig. 1. The process is based on the mixed-recycle SSR scheme. At periodic time intervals, a pulse of feed mixture with known duration, Δt_F, is introduced into a chromatographic column and eluted isocratically with solvent *S*, called eluent. The column effluent is fractionated into a product fraction *A* containing an excess of the less adsorbed component 1 (between t_{A1} and t_{A2}), an unresolved recycle fraction *R* (between t_{A2} and t_{B1}), and a product fraction *B* containing an excess of the more retained component 2 (between t_{B1} and t_{B2}). The recycle fraction is directed to an intermediate reservoir and mixed with fresh feed *FF*. To increase the performance of a stand-alone SSR process the mixture is concentrated by partially removing solvent from it, *e.g.* with membrane filtration or evaporation, and the concentrated mixture is introduced into the column feed tank *F*. The solvent removal unit is operated in a continuous manner. In the case of membrane filtration, part of the membrane concentrate, called retentate, can be recycled back to the inlet of the membrane unit. This allows maintaining the cross-flow velocity across the membrane to prevent concentration polarization irrespective of other process parameters which can vary with time or feed composition.

It is worth noting that there exist also several other ways to implement an SSR–SR process. As an alternative to the concentration of the mixture of fresh feed and recycle streams, solvent can be removed directly from the recycle fraction or from the fresh feed before mixing [20]. The removed solvent can be used as eluent to reduce the need of fresh eluent provided that the removed solvent is pure. Moreover, it is possible to direct the concentrated solution from the solvent removal unit back to the intermediate mixing tank and use that reservoir as a feed tank for the chromatographic step. This reduces the number of needed reservoirs but causes back-dilution. In this study, we will focus on the concept shown in Fig. 1 since it typically offers the highest productivity [21, 22]. The theory discussed in Section 5, however, is applicable for analysing the robustness of other SSR–SR configurations as well.

The most common industrial solvent removal methods are evaporation, distillation, and pressure driven membrane filtration processes such as ultrafiltration, nanofiltration, and reverse osmosis. In all solvent removal methods, there may occur some fouling and/or scaling that affect the process stability. Membrane fouling may be a severe problem, especially in the filtration of organic macromolecules or colloidal particles. The solutes deposit onto the membrane surface or into the membrane pores and decreases the filtration flux over time. As to the evaporation, fouling and scaling of heating surfaces may impede the heat transfer and so decrease the solvent removal capacity. Fouling and scaling can be

reduced by cleaning, appropriate choice of the membrane properties and the filtration module or the evaporator type, and controlling the operating conditions.

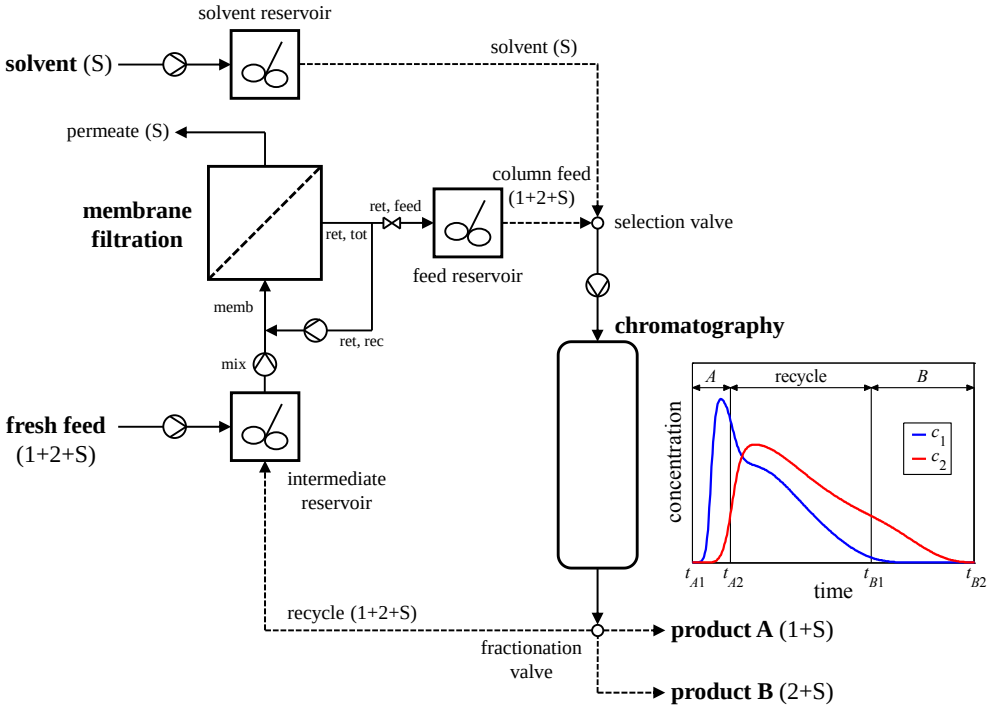

Fig. 1. Schematic setup of an SSR–SR process configuration where recycle fraction and fresh feed are mixed before membrane filtration. The membrane unit is operated in a feed and bleed mode. Solid line: continuous flow. Dashed line: discontinuous flow.

3 Process models

In this study, two different process models are used. The theoretical analysis of process robustness (Section 5) is based on the equilibrium theory of chromatography with an assumption of infinite column efficiency. The analysis is not limited to any special solvent removal method, but is valid as far as the solute yields in the solvent removal unit are complete, *i.e.* removed solvent is pure. To study the influence of dispersive effects on the selection of robust operating parameters (Section 6), a non-ideal process model is used, taking into account the role of mass transfer resistance and axial dispersion. To model the solvent removal unit, it is assumed that membrane filtration is applied to remove solvent.

3.1 Ideal process model

In the ideal model of chromatography, the mass transfer resistance and the dispersive effects are neglected and the fluid velocity along the column is assumed to be constant. The mass balance for an individual solute *i* is given by

$$\frac{\partial c_i}{\partial t} + u\frac{\partial c_i}{\partial x} + F\frac{\partial q_i^{\mathrm{eq}}}{\partial t} = 0 \qquad i = (1, 2) \tag{1}$$

where c_i is the fluid phase concentration of solute i, q_i^{eq} is the stationary phase concentration that is in equilibrium with the fluid phase, F is the phase ratio ($F = (1-\varepsilon)/\varepsilon$ with ε being the total void fraction of the bed), u is the interstitial velocity ($u = L_{col}/t_0$ with L_{col} being the column length and t_0 being the retention time of a non-retained component), t is the time, and x is the column axial coordinate. The discussion in Section 5 is limited to binary systems that follow the competitive Langmuir adsorption isotherm model

$$q_i^{\mathrm{eq}} = \frac{N_i K_i c_i}{1 + K_1 c_1 + K_2 c_2} \tag{2}$$

where N_i and K_i are the saturation capacity and the equilibrium parameter of solute i, respectively.

The initial and boundary conditions of the model are given by

$$c_i(x, t = 0) = 0 \quad \text{for } 0 \le x \le L_{col} \tag{3}$$

$$c_i(x = 0, t) = c_i^F \quad \text{for } 0 \le t \le \Delta t_F \tag{4}$$

$$c_i(x = 0, t) = 0 \quad \text{for } t > \Delta t_F \tag{5}$$

In theoretical analysis presented in Section 5, it is assumed that the concentrations of the solutes i = (1, 2) in the feed reservoir, c_i^F, are constant during an injection. In addition, it is assumed that the solvent removal unit works ideally such that the removed solvent is pure. The column feed concentrations are calculated from the following mass balances:

$$c_i^F = \frac{c_i^{FF} V_{FF} + c_i^R V_R}{Q_{col} \Delta t_F} \tag{6}$$

$$V_{FF} = V_F - V_R + V_{SR} \tag{7}$$

$$V_R = (t_{B1} - t_{A2}) Q_{col} \tag{8}$$

$$V_{SR} = \Delta t_{cycle} Q_{SR} \tag{9}$$

In the above equations, c_i^{FF} is concentration of solute i in the fresh feed, c_i^R is the volume-average concentration of solute i in the recycle fraction, V_{FF} is the volume of fresh feed introduced into the process during a chromatographic cycle, V_R is the volume of recycle fraction, Q_{col} is the volumetric flow rate of fluid phase in the column, V_{SR} is the volume of removed solvent per cycle, Q_{SR} is the solvent removal rate, and Δt_{cycle} is the cycle time, *i.e.* the time interval between the subsequent feed pulses, given by

$$\Delta t_{cycle} = t_{B2} - t_{A1} \tag{10}$$

The model equations form a system of two homogeneous quasilinear partial differential equations. When Riemann boundary conditions (see Eqs. (3)–(5)) are used, the model can be solved analytically by the method of characteristics (see *e.g.* [33–36]).

3.2 Non-ideal process model

In the non-ideal process model, a transport-dispersive model with the solid film linear driving force model is applied to describe the finite mass transfer rate in the chromatographic column. The component mass balances are given by

$$\frac{\partial c_i}{\partial t} + u\frac{\partial c_i}{\partial x} + F\frac{\partial q_i}{\partial t} = D_{\text{ax}}\frac{\partial^2 c_i}{\partial x^2} \tag{11a}$$

$$\frac{\partial q_i}{\partial t} = k_i\left(q_i^{\text{eq}} - q_i\right) \tag{11b}$$

where D_{ax} is the axial dispersion coefficient and k_i is the mass transfer coefficient of solute i. The initial and boundary conditions of Eq. (11) are given by Eqs. (3)–(5).

The transport of solvent and solutes through the membrane are described by solution–diffusion model, and the concentration polarization effect is neglected. In practice, however, any other membrane model could be used as well. The solvent flux, J_S, and the solute flux, J_i, are given by

$$J_S = B_S\left(\Delta P_{memb} - \Delta\pi\right) \tag{12}$$

$$J_i = B_i\left(c_i^{memb} - c_i^{perm}\right) \tag{13}$$

where B_S and B_i are the permeabilities of solvent and solute i, respectively, ΔP_{memb} is the transmembrane pressure, $\Delta\pi$ is the osmotic pressure, c_i^{memb} is the concentration of solute i in the membrane feed, and c_i^{perm} is the concentration of solute i in the permeate. The osmotic pressure is described by van't Hoff equation which is applicable for dilute low molecular weight solutions considered in this work (for more details see e.g. [37]):

$$\Delta\pi = RT\sum\left(c_i^{memb} - c_i^{perm}\right) \tag{14}$$

where R is the gas constant and T is the temperature. The solvent removal rate and the permeate concentrations are given by

$$Q_{SR} = Q_{perm} = A_{memb}J_S \tag{15}$$

$$c_i^{perm} = \frac{J_i}{J_S} \tag{16}$$

where A_{memb} is the membrane surface area.

The flow rates into the membrane unit, Q_{memb}, the total retentate, $Q_{ret,tot}$, and the retentate that is fed from the membrane unit to the column feed tank, $Q_{ret,feeed,}$ are calculated from the following volume balances:

$$Q_{memb} = Q_{mix} + Q_{ret,rec} \tag{17}$$

$$Q_{ret,tot} = Q_{memb} - Q_{perm} \tag{18}$$

$$Q_{ret,feed} = Q_{ret,tot} - Q_{ret,rec} \tag{19}$$

where Q_{mix} is the flow rate from the intermediate mixing tank to the solvent removal unit and $Q_{ret,rec}$ is the flow rate of the recycled retentate. The solute concentrations in the streams are given by

$$c_i^{memb} = \frac{c_i^{perm} Q_{perm} + c_i^{ret,tot} Q_{ret,tot}}{Q_{memb}} \tag{20}$$

$$c_i^{ret,tot} = c_i^{ret,feed} = \frac{c_i^{mix} Q_{mix} - c_i^{perm} Q_{perm}}{Q_{ret,feed}} \tag{21}$$

To model the eluent (*E*), column feed (*F*), and mixed fraction (*mix*) reservoirs, perfect mixing is assumed. This yield to the following material balances:

$$\frac{dV^j}{dt} = \sum Q_{in}^j - \sum Q_{out}^j \tag{22}$$

$$\frac{dn_i^j}{dt} = \frac{d\left(V^j c_i^j\right)}{dt} = \sum Q_{in}^j c_{i,in}^j - \sum Q_{out}^j c_{i,out}^j \tag{23}$$

where V^J, n_i^j, and c_i^j denotes the volume of solution, the amount of solute *i*, and the concentration of solute *i* in the reservoir *j*, respectively.

The model equations were implemented in Matlab and solved with finite difference methods by discretizing the time and the column axial coordinates. The transport-dispersive model of chromatography, Eqs. (11a) and (11b), were integrated by using an explicit backward-forward scheme, where the axial dispersion term is approximated numerically by the step size in the spatial discretization. For the reservoirs mass balances, Eqs (22) and (23), the Euler method was applied.

4 Design specifications

In the following discussion, it is assumed that the dimensions of the chromatographic column and the fresh feed concentrations are fixed and the packing properties and the isotherm parameters are known. A binary mixture is separated in isocratic mode into two fractions with user-given purity requirements. The purity constraints of the fractions are defined as follows:

$$p_1^A = \frac{n_1^A}{n_1^A + n_2^A} \tag{24}$$

$$p_2^B = \frac{n_2^B}{n_1^B + n_2^B} \tag{25}$$

where p_i^j is the purity of component i in the fraction j = (A, B), and n_i^j is the amount of component i in the fraction j.

For the SSR–SR process, there exist the following freely adjustable operating parameters: (1) the duration of the feed pulse into the chromatographic column, Δt^F, (2) the four fractionation times t_{A1}, t_{A2}, t_{B1}, and t_{B2}, (3) the volumetric flow rate of the mobile phase in the column, Q_{col}, and (4) alternatively the volumetric flow rate of removed solvent, Q_{SR}, or the amount of fresh feed processed during a chromatographic cycle, V_{FF}. In accordance with the Unified Design approach [32], these operating parameters are expressed in dimensionless form that allows representing the design space in the same way as in the triangle theory of counter-current chromatography (see *e.g.* [26, 38, 39]) as follows:

$$m_1 = \frac{t_{B2} - \Delta t_F - t_0}{F t_0} = \frac{Q_{col}\left(t_{B2} - \Delta t_F\right) - \varepsilon V_{col}}{\left(1-\varepsilon\right) V_{col}} \tag{26}$$

$$m_2 = \frac{t_{B1} - \Delta t_F - t_0}{F t_0} = \frac{Q_{col}\left(t_{B1} - \Delta t_F\right) - \varepsilon V_{col}}{\left(1-\varepsilon\right) V_{col}} \tag{27}$$

$$m_3 = \frac{t_{A2} - t_0}{F t_0} = \frac{Q_{col} t_{A2} - \varepsilon V_{col}}{\left(1-\varepsilon\right) V_{col}} \tag{28}$$

$$m_4 = \frac{t_{A1} - t_0}{F t_0} = \frac{Q_{col} t_{A1} - \varepsilon V_{col}}{\left(1-\varepsilon\right) V_{col}} \tag{29}$$

$$m_R = \frac{t_{B1} - t_{A2}}{F t_0} = \frac{V_R}{\left(1-\varepsilon\right) V_{\mathrm{col}}} \tag{30}$$

$$K_{SR} = \frac{V_{SR}}{V_{FF}} = \frac{Q_{SR} \Delta t_{cycle}}{V_{FF}} \tag{31}$$

where V_{col} is the column volume. Parameters m_1, m_2, m_3, and m_4 denote the dimensionless fractionation points, m_R is the volume of the recycle fraction with respect to the volume of the stationary phase, and K_{SR} is dimensionless solvent removal capacity. The beginning and the end of the product fraction A (m_3 and m_4) are expressed in time relative to the beginning of the feed pulse whereas the beginning and the end of the product fraction B (m_1 and m_2) are given in time relative to the end of the feed pulse. The dimensionless amount of fresh feed processed per cycle is given by

$$m_{FF} = \frac{V_{FF}}{\left(1-\varepsilon\right) V_{col}} = \frac{\left(m_3 - m_2\right)}{\left(1 - K_{SR}\right)} \tag{32}$$

In order to achieve positive fresh feed flow, m_2 must be lower than m_3 when $K_{SR} < 1$, and larger than m_3 when $K_{SR} > 1$. In a special case of $K_{SR} = 1$, m_2 and m_3 must be equal, right hand side of Eq. (32) has no defined value, and m_{FF} must be chosen independently.

For a given mobile phase flow rate, the duration of the feed pulse, the four cut times, and the solvent removal rate can be calculated as follows:

$$\Delta t_F = \frac{V_F}{Q_{col}} = F t_0 \left(m_3 - m_2 + m_R \right) \tag{33}$$

$$t_{A1} = t_0 \left(F m_4 + 1 \right) \tag{34}$$

$$t_{A2} = t_0 \left(F m_3 + 1 \right) \tag{35}$$

$$t_{B1} = t_0 \left(F m_2 + 1 \right) + \Delta t_F \tag{36}$$

$$t_{B2} = t_0 \left(F m_1 + 1 \right) + \Delta t_F \tag{37}$$

$$Q_{SR} = \frac{(1-\varepsilon) V_{col}}{\Delta t_{cycle}} K_{SR} m_{FF} \tag{38}$$

The extent of solvent removal is often limited by various factors. The maximum concentration achievable in the membrane filtration unit may be limited by solubility of the components or, if solubility is high, osmotic pressure. The maximum concentration of the column feed, on the other hand, may be limited by solubility or viscosity. When the solvent is removed from the column feed (Fig. 1), the solvent removal constraints can be expresses in the following general form:

$$g\left(c_1^F, c_2^F \right) \leq 0 \tag{39}$$

5 Robust design of SSR–SR process under ideal conditions

The design of mixed-recycle SSR and SSR–SR processes based on the equilibrium theory of chromatography has been discussed extensively elsewhere [20, 22, 32, 40]. Here only the most relevant aspects and novel developments are summarized. The design method is then applied to analyse the robustness of SSR–SR unit.

The design procedure of SSR–SR process has two steps. The first task is to select the dimensionless solvent removal capacity and volume of the recycle fraction. Alternatively, one can choose the amount of fresh feed that is processed during a chromatographic cycle and the volume of the feed pulse. Equations to calculate the range of feasible operating conditions that corresponds to arbitrary purity and solvent removal constraints under ideal conditions have been derived in [20, 22]. In the original works, the operation region is represented on a dimensional (V_{FF}, V_F) plane, but equations to calculate the corresponding solvent removal capacity and the volume of the recycle fraction have also been provided. When K_{SR} and m_R are chosen, the corresponding V_{FF} and V_F can be calculated form Eqs. (32) and (33), respectively.

The second design step is to select the cut times. The boundaries of the feasible cut points can be given in dimensionless form that is analogous to the criteria of the dimensionless flow rate ratios applied in the triangle theory of multi-column SMB process. Explicit equations to calculate the optimal cut times with which user-given purity requirements are exactly matched have been derived for SSR process in [40] and for SSR–SR process in [20]. Recently, Siitonen and Sainio [32] have extended the approach for predicting the whole range of cut times that lead to complete separation of a binary mixture in batch or SSR process. It has been shown [32] that the boundaries of dimensionless cut times of SSR process are identical to the boundaries of dimensionless flow rates of SMB process.

The feasible range of dimensionless cut times is conveniently represented on (m_2, m_3) plane shown in Fig. 2. The complete separation region, where the purities of both product fractions are 100%, is a triangle-like domain limited by three straight lines *ab*, *bw*, *rw*, and a curve *ar*. In general case, the shape and size of the complete separation region depends on the fresh feed concentrations, isotherm parameters, solvent removal capacity, and volume of the recycle fraction. In the case of competitive Langmuir isotherm and ideal conditions, however, the boundaries become independent of m_R [32].

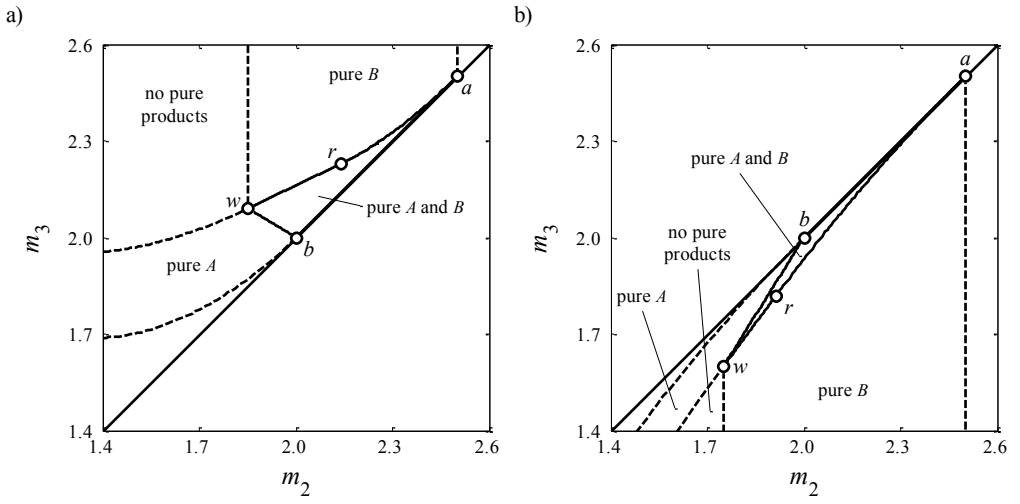

Fig. 2. Complete separation region in SSR–SR process on the (m_2, m_3) plane under ideal conditions. Solvent removal capacity: (a) K_{SR} = 0.2, (b) K_{SR} = 1.3. Fresh feed concentrations: $c_1^{FF} = c_2^{FF}$ = 5 g/L. Isotherm parameters: H_1 = 2.0, H_2 = 2.5, K_1 = 0.020 L/g, and K_2 = 0.025 L/g.

In practice, the boundaries of the complete separation space of SSR–SR process on the (m_2, m_3) plane can be calculated with the equations of SSR chromatography by replacing the value of a characteristic parameter ω_2 at fresh feed state by ω_2 that corresponds to the slope $\tilde{\xi}_+^F$ of Γ_+ characteristic passing through the steady state feed composition when no pure products are recycled (denoted as $\tilde{\omega}_2^F$) [20, 22]. Explicit equations that have not published before to calculate the range of m_2, m_3, and m_{FF} that lead to complete separation for SSR–SR process are summarized in Table 1. In the case of K_{SR} = 0, the equations reduce to those reported in [32] except that the equations for lines *bw* and *rw*, Eqs. (1.4) and (1.5), are expressed in

different form compared to the original work to make the expressions simpler for SSR–SR scheme.

Table 1 Equations to calculate the boundaries of the complete separation region on the (m_2, m_3) and (m_2, m_{FF}) planes for SSR–SR processes.

slope $\tilde{\xi}_+^F$	$\tilde{\xi}_+^F = \dfrac{\eta + \sqrt{\eta^2 - 4K_1K_2H_1H_2c_1^{FF}c_2^{FF}}}{2K_1H_2c_2^{FF}}$	(1.1)
	with $\eta = (1-K_{SR})(H_2 - H_1) + K_1H_2c_1^{FF} + K_2H_1c_2^{FF}$	
$\tilde{\omega}_2^F$ -value:	$\tilde{\omega}_2^F = \dfrac{K_2H_1 + K_1H_2\tilde{\xi}_+^F}{K_2 + K_1\tilde{\xi}_+^F}$	(1.2)
line *ar*:	$m_{FF} = \dfrac{\left(\sqrt{H_2} - \sqrt{m_2}\right)^2}{K_2c_2^{FF}}$, $m_3 = (1-K_{SR})\dfrac{\left(\sqrt{H_2} - \sqrt{m_2}\right)^2}{K_2c_2^{FF}} + m_2$	(1.3)
line *rw*:	$m_{FF} = \dfrac{(H_2 - \tilde{\omega}_2^F)(\tilde{\omega}_2^F - m_2)}{\tilde{\omega}_2^F K_2c_2^{FF}}$, $m_3 = (1-K_{SR})\dfrac{(H_2 - \tilde{\omega}_2^F)(\tilde{\omega}_2^F - m_2)}{\tilde{\omega}_2^F K_2c_2^{FF}} + m_2$	(1.4)
line *bw*:	$m_{FF} = \dfrac{(H_2 - H_1)(H_1 - m_2)}{H_1K_2c_2^{FF}}$, $m_3 = (1-K_{SR})\dfrac{(H_2 - H_1)(H_1 - m_2)}{H_1K_2c_2^{FF}} + m_2$	(1.5)
point *a*:	$m_2 = H_2$, $m_{FF} = 0$, $m_3 = H_2$	(1.6)
point *b*:	$m_2 = H_1$, $m_{FF} = 0$, $m_3 = H_1$	(1.7)
point *r*:	$m_2 = \dfrac{(\tilde{\omega}_2^F)^2}{H_2}$, $m_{FF} = \dfrac{(H_2 - \tilde{\omega}_2^F)^2}{K_2H_2c_2^{FF}}$, $m_3 = (1-K_{SR})m_{FF} + m_2$	(1.8)
point *w*:	$m_2 = \dfrac{\tilde{\omega}_2^F H_1}{H_2}$, $m_{FF} = \dfrac{(H_2 - \tilde{\omega}_2^F)(H_2 - H_1)}{K_2H_2c_2^{FF}}$, $m_3 = (1-K_{SR})m_{FF} + m_2$	(1.9)

The optimal operating parameters of SSR–SR process discussed in previous works [20, 22] are very sensitive to various kinds of disturbances because they are commonly located on the boundary of the feasible operating region. Firstly, perturbations in the flow rates or in the cut points and uncertainties in the estimation of the column dimensions or the total void fraction of the bed may modify the dimensionless operating parameters and the operating point may move outside the feasible region. Secondly, perturbations in the fresh feed concentrations and inaccuracies in the estimation of isotherm parameters alter the shape and the location of the feasible operating region. The actual feasible separation region differs from the operating domain predicted by the design equations, and it may not include the selected operating point. In both cases, the purity constraints are not satisfied. On the other hand, fluctuations in the

solvent removal capacity, in the fresh feed concentrations, or in the recycle fraction composition may lead to violation of the solvent removal constraints. As a result, the components may precipitate in the unit, the osmotic pressure may become excessively high leading to significant decrease in the membrane flux, or the viscosity of the feed solution may increase too much leading to viscous fingering or too high pressure drop.

The developed design methods can be used to select the robust operating conditions for SSR–SR process. The robustness of the concept can be improved by adjusting the solvent removal rate or the cut points. The effect of K_{SR} on the process robustness is demonstrated in Fig. 3 and 4. It is seen that the adjustment of the solvent removal rate affects the process robustness in two different ways. Firstly, when the solvent removal rate decreases, the feed concentrations in the column decrease (Fig. 3). As a result, the solvent removal constraints, such as solubility, osmotic pressure, or viscosity limits, are not violated so easily. The upper limit of K_{SR} depends on the volume of the recycle fraction. When m_R is relatively low (below the dotted line in Fig. 3), the feed plateau is not recycled and the steady state feed concentrations decrease with increasing m_R due to dilution of recycle stream. At the same time, the upper limit of K_{SR} increases. When m_R is high and part of the feed plateau is recycled, the steady state feed concentrations as well as the upper limit of K_{SR} are independent of m_R.

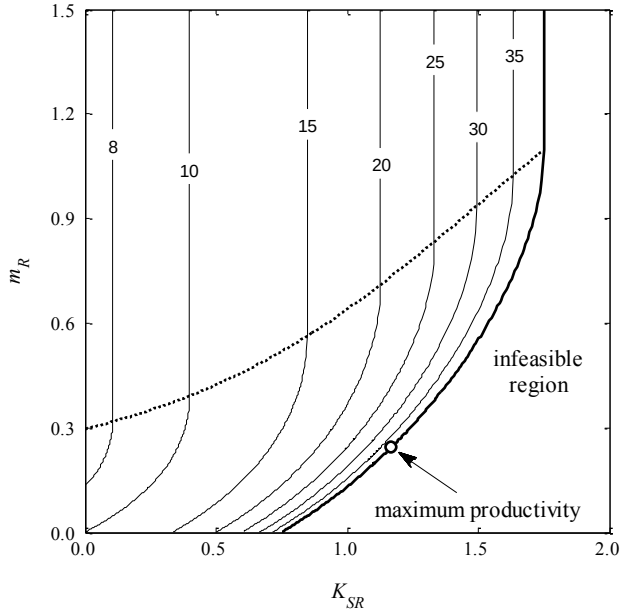

Fig. 3. Region of feasible K_{SR} and m_R values for SSR–SR process when the solvent removal constraint is $c_1^F + c_2^F \leq 40$ g/L . The contour lines show the total steady state feed concentration. The steady state feed concentrations are independent of m_R when the feed plateau is recycled (above the dotted line). Same fresh feed concentrations and isotherm parameters as in Fig. 2.

Secondly, the solvent removal rate has a significant effect on the shape of the region of feasible cut times (Fig. 4). When $K_{SR} < 1$, *i.e*. the amount of removed solvent is lower than the amount of processed fresh feed, the feasible operating region on the (m_2, m_3) plane is located above the diagonal $m_3 = m_2$ (Fig. 4a). On the other hand, when $K_{SR} > 1$, positive fresh feed flow is achieved with $m_2 > m_3$. In a special case of $K_{SR} = 1$, the operating region on the (m_2, m_3) plane shrinks to the diagonal. In that case, it is more convenient to use (m_2, m_{FF}) plane instead of (m_2, m_3) coordinates (Fig. 4b). It is interesting to note that the complete separation regions with different K_{SR} values overlap on the (m_2, m_{FF}) plane such that the operating domain with a given K_{SR} always covers the regions with lower K_{SR} values. When K_{SR} and thus the column feed concentrations increase, the operation region on the (m_2, m_3) and (m_2, m_{FF}) planes becomes narrower due to increased non-linearity of the system. This makes it more difficult to find robust cut times with which the distance from the operation boundaries is large enough.

To select the robust cut times, the operating point on the (m_2, m_3) plane must be adjusted towards the diagonal from its optimal value. At the same time, the amount of fresh feed processed with a given amount of eluent decreases. As a result, the recycle fraction becomes more dilute and the solvent removal constraints are not violated so easily when the dimensionless solvent removal capacity is kept constant. In practice, it is also beneficial for robustness to adjust the beginning of the product fraction *A*, m_4, and the end of the product fraction *B*, m_1, such that a small safety gap exists between the consecutive chromatograms.

The (m_2, m_3) plot helps to select the direction in which it is beneficial to shift the operating point to make the process more robust. The direction depends strongly on non-linearity of the system, *i.e*., the fresh feed concentrations, the isotherm parameters, and the solvent removal capacity. When the solvent removal capacity and the fresh feed concentrations are relatively low, m_2 must be increased and m_3 decreased. The increase in m_2 with respect to the decrease in m_3 must be the stronger the higher the steady state feed concentrations are. Under very non-linear conditions, both m_2 and m_3 must be increased.

Finally, it is worth noting that when the solvent removal rate decreases or the cut times on the (m_2, m_3) plane are adjusted towards the diagonal, the amount of processed fresh feed decreases. Moreover, adjustment of m_1 and m_4 values to obtain longer safety gap between the consecutive chromatograms increases the cycle time. In all cases, the process productivity decreases and the specific eluent consumption increases. The selection of the operating parameters is thus always a trade-off between the process performance and robustness.

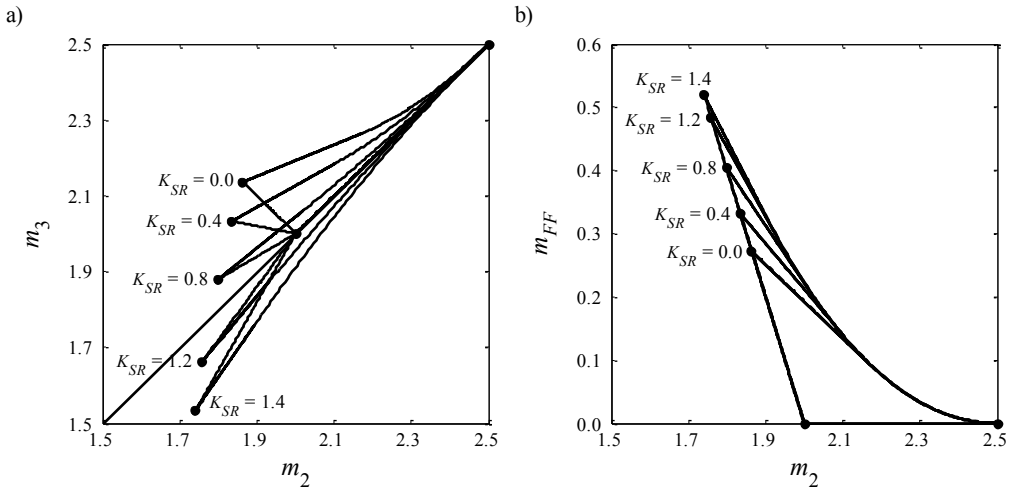

Fig. 4. Effect of solvent removal capacity on the shape of the complete separation region (a) on the (m_2, m_3) plane and (b) on the (m_2, m_{FF}) plane. Same fresh feed concentrations and isotherm parameters as in Fig. 2.

6 Operation of SSR–SR process under non-ideal conditions

The effect of finite column efficiency on the operation of SSR–SR process was studied by means of numerical simulations by using the non-ideal process model described in Section 3.2. The separation of EMD 53986 enantiomers was used a model case. The selection of robust m_2 and m_3 parameters were of special interest since it is the most critical step in the design procedure. For this reason, m_1 and m_4 were selected with a sufficient safety margin that guarantees that the consecutive chromatograms did not overlap. For SSR and SSR–SR schemes, the volume of the recycle fraction was chosen such that the feed plateau prevailed. This provides minimum eluent consumption for a given solvent removal capacity without significant decrease in productivity [22, 41].

The adsorption equilibrium of EMD 53986 enantiomers in 100% ethanol on amylose-tris(3,5-dimethylphenylcarbamate) stationary phase is characterized by modified competitive Langmuir model [42]. In this study, the modified Langmuir isotherms were approximated with competitive Langmuir model. The resulting isotherm parameters as well as other simulation parameters are summarized in Table 2. The separation factor of the system is relatively high, $\alpha = H_2/H_1 = 2.34$.

To study the influence of dispersive effects on the process operation, the mass transfer coefficients were varied between 4.32–163.2 min^{-1}. As to the number of theoretical plates of the column, *NTP*, determined under linear conditions for the less strongly adsorbed component, this corresponds to variation from 50 to 500 plates.

In SSR–SR scheme, the dimensionless solvent removal capacity K_{SR}, *i.e.* the amount of removed solvent with respect to the processed fresh feed, was kept constant at 0.625. In the optimal operating point predicted by the equilibrium theory, the total steady state feed concentration increased to the level of 6.2–6.4 g/L. The solute retention in the membrane filtration was assumed to be 0.98.

Table 2 Parameters for EMD 53986 model system.

Parameter	Value
fresh feed concentrations, c_i^{FF} (g/L)	1.5
column length, L_{col} (cm)	15.0
column diameter, D_{col} (cm)	1.0
isotherm parameters:	
K_1 (L/g)	0.067[a]
N_1 (g/L)	112.3[a]
K_2 (L/g)	0.251[a]
N_2 (g/L)	72.8[a]
total void fraction of the bed, ε	0.72[b]
axial dispersion coefficient, D_{ax} (cm^2/min)	0.036
mass transfer coefficients, k_i (min^{-1})	4.32–163.2
eluent flow rate, (mL/min)	1.8
membrane area, A_{memb} (cm^2)	4.37–84.6
solvent permeability, B_S (L/(m^2 h bar))	0.5
solute permeability, B_i (L/(m^2 h))	0.1
effective pressure, $\Delta P_{memb} - \Delta\pi$ (bar)	10.0

[a] best fit of Langmuir isotherm model to the isotherm data in [42]
[b] value from [42]

The effect of limited column efficiency on the size and shape of the complete separation region for batch, SSR, and SSR–SR processes is demonstrated in Figs. 5–7. The domains where the purities of both product fractions are more than 99% are denoted by black circles. As expected, the separation region under non-ideal conditions approaches the ideal region predicted by the equilibrium theory when the column efficiency is relatively high (Figs. 5a, 6a, and 7a). When the column efficiency decreases, the operating regions corresponding to given purity values shrink and higher deviations from the ideal case are observed. It is worth noting that the model system studied here is characterized by a relatively high separation factor. It is expected that the complete separation region would shrink more rapidly with decreasing column efficiency when the separation factor is low.

As seen in Figs. 5–7, the bottom left corners of the complete regions shrink most rapidly when the column efficiency decreases. This is because the tail of first component band broadens easily due to dispersion, and contaminates the product *B*. The behaviour is similar to that reported earlier for SMB process in [43], which is as expected based on the results obtained by Siitonen and Sainio using the Unified Design method [32]. In practice, this means that it is most beneficial to make the processes more robust by decreasing the amount processed fresh feed m_{FF}, while keeping the value of m_3 near its upper limit.

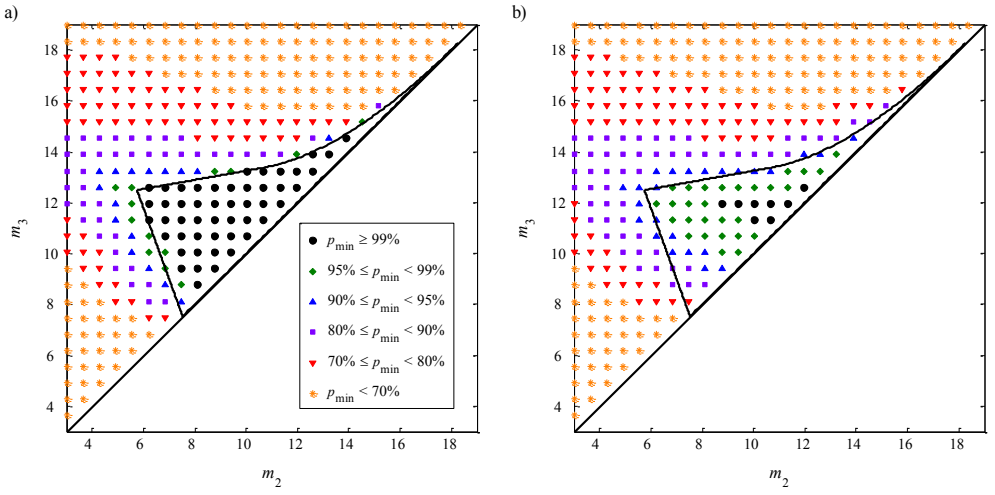

Fig. 5. Product purities for separation of EMD 53986 enantiomers in batch chromatography. Symbols: product purities under non-ideal conditions when (a) NTP_1 = 500 and (b) NTP_1 = 50. Solid line: complete separation region under ideal conditions.

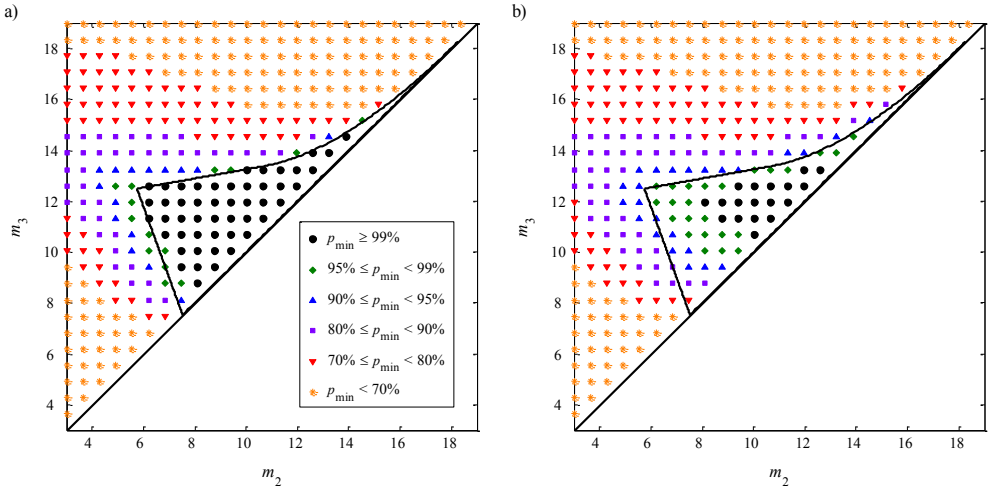

Fig. 6. Product purities for separation of EMD 53986 enantiomers in SSR chromatography. Symbols: product purities under non-ideal conditions when (a) NTP_1 = 500 and (b) NTP_1 = 50. Solid line: complete separation region under ideal conditions.

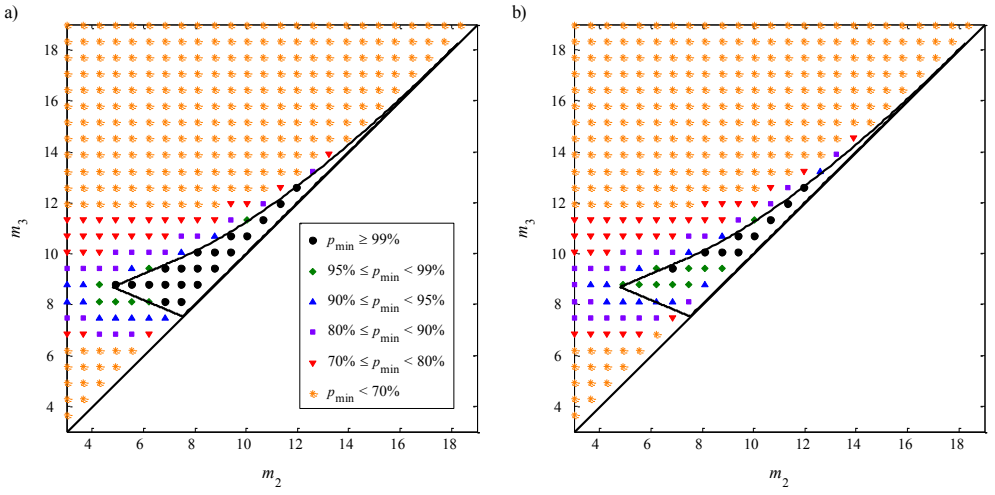

Fig. 7. Product purities for separation of EMD 53986 enantiomers in SSR–SR process. Symbols: product purities under non-ideal conditions when (a) $NTP_1 = 500$ and (b) $NTP_1 = 50$. Solid line: complete separation region under ideal conditions.

When $NTP_1 = 50$ and the processes are operated in their optimal operating points of the ideal complete separation regions (*i.e.* in the vertexes of the triangles shown in Figs. 5b, 6b, and 7b), the achieved product purities are in batch process $p_1^A = 0.955$, $p_2^B = 0.945$, in SSR process $p_1^A = 0.966$, $p_2^B = 0.950$, and in SSR–SR process $p_1^A = 0.986$, $p_2^B = 0.950$. The relatively high purities can be explained by the relatively large separation factor. It enables to use large column loadings even in batch process, which make the separations less sensitive to dispersive effects. The highest product purities are obtained in SSR–SR scheme even though its complete separation region predicted by the equilibrium theory is the narrowest one. This is because the steady state feed concentrations are higher than in SSR process, and the thermodynamic effects are thus more predominant.

7 Conclusion

In this work, the robustness of mixed-recycle SSR chromatography with an integrated solvent removal unit was investigated theoretically and by means of numerical simulations. The equilibrium theory and the Unified Design approach were applied to investigate the selection of robust operating conditions under ideal conditions. The influence of column efficiency on the product purities was evaluated quantitatively by using the separation of EMD 53986 enantiomers as a model system.

The theoretical analysis revealed that the process robustness can be improved by adjusting the solvent removal capacity or the cut times. When the solvent removal capacity decreases, the region of feasible cut times becomes wider due to increased linearity of the system, and it is easier to find the robust operating conditions that lead to desired product purities. At the same time, the steady state feed concentrations decrease, and the solvent removal constraints, *e.g.* solubility of the components, are not violated so easily. The other option to increase the process robustness is to adjust the cut times such that the amount of fresh feed decreases. The

direction in which the cut times must be tuned depends strongly on the non-linearity of the system. In both options, however, the process productivity decreases and the eluent consumption increases as demonstrated in earlier works [20–22]. The selection of operating parameters is thus a trade-off between the process robustness and performance.

In the simulation study, it was demonstrated that the shapes and locations of the complete separation regions for batch, SSR, and SSR–SR processes approach those predicted by the equilibrium theory when the column efficiency is relatively high. As expected, the influence of finite column efficiency on the product purities is the higher the lower the column loading is. It was observed that the SSR–SR scheme is less sensitive to finite column efficiency than conventional SSR process due to higher steady state feed concentrations.

As demonstrated with the EMD 53986 model system, dispersive effects have a significant influence on the product purities, and they cannot be neglected in the process design. However, we believe that the equilibrium theory based analysis presented in this work provides general guidelines for selection of robust operating conditions for SSR–SR process and helps to understand the effect of different process parameters on the process robustness.

References

[1] B.-G. Lim, C.-B. Ching, R.B. Tan, S.-C. Ng, Recovery of (−)-praziquantel from racemic mixtures by continuous chromatography and crystallisation, Chem. Eng. Sci., 50 (1995) 2289–2298.

[2] H. Lorenz, P. Sheehan, A. Seidel-Morgenstern, Coupling of simulated moving bed chromatography and fractional crystallisation for efficient enantioseparation, J. Chromatogr. A, 908 (2001) 201–214.

[3] G. Ströhlein, M. Schulte, J. Strube, Hybrid processes: design method for optimal coupling of chromatography and crystallization units, Sep. Sci. Technol., 38 (2003) 3353–3383.

[4] K.Y. Fung, K.M. Ng, C. Wibowo, Synthesis of chromatography-crystallization hybrid separation processes, Ind. Eng. Chem. Res., 44 (2005) 910–921.

[5] M. Kaspereit, K. Gedicke, V. Zahn, A. W. Mahoney, A. Seidel-Morgenstern, Shortcut method for evaluation and design of a hybrid process for enantioseparations, J. Chromatogr. A, 1092 (2005) 43–54.

[6] M. Kaspereit, Separation of enantiomers by a process combination of chromatography and crystallization, PhD thesis, Otto von Guericke University, Magdeburg, Shaker Verlag, Aachen, Germany, 2006.

[7] M. Amanullah, M. Mazzotti, Optimization of a hybrid chromatography-crystallization process for the separation of Tröger's base enantiomers, J. Chromatogr. A, 1107 (2006) 36–45.

[8] H. Kaemmerer, Z. Horvath, J. W. Lee, M. Kaspereit, R. Arnell, M. Hedberg, B. Herschend, M. J. Jones, K. Larson, H. Lorenz, A. Seidel-Morgensten, Separation of racemic bicalutamide by an optimized combination of continuous chromatography and selective crystallization, Org. Process Res. Dev., 16 (2012) 331–342.

[9] S. Swernath, M. Kaspereit, A. Kienle, Dynamics and control of coupled continuous chromatography and crystallization processes for the production of pure enantiomers, Chem. Eng. Technol., 36 (2013) 1417–1429.

[10] K. Hashimoto, S. Adachi, H. Noujima, Y. Ueda, A new process combining adsorption and enzyme reaction for producing higher-fructose syrup, Biotechnol. Bioeng., 25 (1983) 2371–2393.

[11] M. Bechtold, S. Makart, M. Heinemann, S. Panke, Integrated operation of continuous chromatography and biotransformations for the generic high yield production of fine chemicals, J. Biotechnol., 124 (2006) 146–162.

[12] M. Kaspereit, J. García Palacios, T. Meixús Fernández, A. Kienle, Systematic design of production processes for enantiomers with integration of chromatography and racemisation reactions, Comput. Aided Chem. Eng., 25 (2008) 97–102.

[13] J. García Palacios, M. Kaspereit, A. Kienle, Integrated simulated moving bed processes for production of single enantiomers, Chem. Eng. Technol., 34 (2011) 688–698.

[14] J. García Palacios, B. Kramer, A. Kienle, M. Kaspereit, Experimental validation of a new integrated simulated moving bed process for the production of single enantiomers, J. Chromatogr. A, 1218 (2011) 2232–2239.

[15] N. Wagner, M. Fuereder, A. Bosshart, S. Panke, M. Bechtold, Practical aspects of integrated operation of biotransformation and SMB separation for fine chemical synthesis, Org. Process Res. Dev., 16 (2012) 323–330.

[16] S. Nimmig, M. Kaspereit, Continuous production of single enantiomers at high yields by coupling single column chromatography, racemization, and nanofiltration, Chem. Eng. Process., 67 (2013) 89–98.

[17] S. Swernath, M. Kaspereit, A. Kienle, Coupled continuous chromatography and racemization processes for the production of pure enantiomers, Chem. Eng. Technol., 37 (2014) 643–651.

[18] S. Abdelmoumen, L. Muhr, M. Bailly, O. Ludemann-Hombourger, The M3C process: a new multicolumn chromatographic process integrating a concentration step. I—the equilibrium model, Sep. Sci. Technol., 41 (2006) 2639–2663.

[19] G. Paredes, H.-K. Rhee, M. Mazzotti, Design of simulated-moving-bed chromatography with enriched extract operation (EE-SMB): Langmuir isotherms, Ind. Eng. Chem. Res., 45 (2006) 6289–6301.

[20] J. Siitonen, T. Sainio, M. Kaspereit, Theoretical analysis of steady state recycling chromatography with solvent removal, Sep. Purif. Technol., 78 (2011) 21–32.

[21] S. Hellstén, J. Siitonen, M. Mänttäri, T. Sainio, Steady state recycling chromatography with an integrated solvent removal unit – Separation of glucose and galactose, J. Chromatogr. A, 1251 (2012) 122–133.

[22] J. Siitonen, T. Sainio, Steady state recycling chromatography with solvent removal—Effect of solvent removal constraints on process operation under ideal conditions, J. Chromatogr. A, 1341 (2014) 15–30.

[23] S.R. Perrin, W. Hauck, E. Ndzie, J. Blehaut, O. Ludemann-Hombouger, R.-M. Nicoud, W.H. Pirkle, Purification of difluoromethylornithine by global process optimization: coupling of chemistry and chromatography with enantioselective crystallization, Org. Process Res. Dev., 11 (2007) 817–824.

[24] J. von Langermann, M. Kaspereit, M. Shakeri, H. Lorenz, M. Hedberg, M. J. Jones, K. Larson, B. Herschend, R. Arnell, E. Temmel, J.-E. Bäckvall, A. Kienle, A. Seidel-Morgenstern, Design of an integrated process of chromatography, crystallization and racemization for the resolution of 2',6'-pipecoloxylidide (PPX), Org. Process Res. Dev., 16 (2012) 343−352.

[25] G. Storti, M. Mazzotti, M. Morbidelli, S. Carrà, Robust design of binary countercurrent adsorption separation processes, AIChE J., 39 (1993) 471–492.

[26] M. Mazzotti, G. Storti, M. Morbidelli, Optimal operation of simulated moving bed units for nonlinear chromatographic separations, J. Chromatogr. A, 769 (1997) 3–24.

[27] E. Francotte, P. Richert, M. Mazzotti, M. Morbidelli, Simulated moving bed chromatographic resolution of a chiral antitussive, J. Chromatogr. A, 796 (1998) 239–248.

[28] M. Pedeferri, G. Zenoni, M. Mazzotti, M. Morbidelli, Experimental analysis of a chiral separation through simulated moving bed chromatography, Chem. Eng. Sci., 54 (1999) 3735–3748.

[29] N. Jakobsson, M. Degerman, B. Nilsson, Optimization and robustness analysis of a hydrophobic interaction chromatography step, J. Chromatogr. A, 1099 (2005) 157–166.

[30] K. Westerberg, E.B. Hansen, M. Degerman, T.B. Hansen, B. Nilsson, Model-based process challenge of an industrial ion-exchange chromatography step, Chem. Eng. Technol., 35 (2012) 183–190.

[31] E.J. Close, J.R. Salm, D.G. Bracewell, E. Sorensen, A model based approach for identifying robust operating conditions for industrial chromatography with process variability, Chem. Eng. Sci., 116 (2014) 284–295.

[32] J. Siitonen, T. Sainio, Unified design of chromatographic separation processes, Chem. Eng. Sci., 122 (2015) 436–451.

[33] H.-K. Rhee, R. Aris, N.R. Amundson, First-Order Partial Differential Equations. Theory and Application of Single Equations, vol. I, Dover Publications, New York, 2001.

[34] H.-K. Rhee, R. Aris, N.R. Amundson, First-Order Partial Differential Equations. Theory and Application of Hyperbolic Systems of Quasilinear Equations, vol. II, Dover Publications, New York, 2001.

[35] S. Golshan-Shirazi, G. Guiochon, Analytical solution for the ideal model of chromatography in the case of a pulse of a binary mixture with competitive Langmuir isotherm, J. Phys. Chem., 93 (1989) 4143–4157.

[36] J. Siitonen, T. Sainio, Explicit equations for the height and position of the first component shock for binary mixtures with competitive Langmuir isotherms under ideal conditions, J. Chromatogr. A, 1218 (2011) 6379–6387.

[37] M. Mulder, Basic Principles of Membrane Technology, Kluwer Academic Publishers, Dordrecht, Netherlands, 1996.

[38] A. Gentilini, C. Migliorini, M. Mazzotti, M. Morbidelli, Optimal operation of simulated moving-bed units for non-linear chromatographic separations II. Bi-Langmuir isotherm, J. Chromatogr. A, 805 (1998) 37–44.

[39] M. Mazzotti, Equilibrium theory based design of simulated moving bed processes for a generalized Langmuir isotherm, J. Chromatogr. A, 1126 (2006) 311–322.

[40] T. Sainio, M. Kaspereit, Analysis of steady state recycling chromatography using equilibrium theory, Sep. Purif. Technol., 66 (2009) 9–18.

[41] M. Kaspereit, T. Sainio, Simplified design of steady-state recycling chromatography under ideal and nonideal conditions, Chem. Eng. Sci., 66 (2011) 5428–5438.

[42] A. Jupke, A. Epping, H. Schmidt-Traub, Optimal design of batch and simulated moving bed chromatographic separation processes, J. Chromatogr. A, 944 (2002) 93–117.

[43] C. Migliorini, A. Gentilini, M. Mazzotti, M. Morbidelli, Design of simulated moving bed units under nonideal conditions, Ind. Eng. Chem. Res., 38 (1999) 2400-2410.

ACTA UNIVERSITATIS LAPPEENRANTAENSIS

576. LANKINEN, JUKKA. Local features in image and video processing – object class matching and video shot detection. 2014. Diss.

577. AL-SAEDI, MAZIN. Flexible multibody dynamics and intelligent control of a hydraulically driven hybrid redundant robot machine. 2014. Diss.

578. TYSTER, JUHO. Power semiconductor nonlinearities in active d*u*/d*t* output filtering. 2014. Diss.

579. KERÄNEN, JOONA. Customer value assessment in business markets. 2014. Diss.

580. ALEXANDROVA, YULIA. Wind turbine direct-drive permanent-magnet generator with direct liquid cooling for mass reduction. 2014. Diss.

581. HUHTALA, MERJA. PDM system functions and utilizations analysis to improve the efficiency of sheet metal product design and manufacturing. 2014. Diss.

582. SAUNILA, MINNA. Performance management through innovation capability in SMEs. 2014. Diss.

583. LANA, ANDREY. LVDC power distribution system: computational modelling. 2014. Diss.

584. PEKKARINEN, JOONAS. Laser cladding with scanning optics. 2014. Diss.

585. PELTOMAA, JYRKI. The early activities of front end of innovation in OEM companies using a new FEI platform as a framework for renewal. 2014. Diss.

586. ROZHANSKY, IGOR. Resonant tunneling effects in semiconductor heterostructures. 2014. Diss.

587. PHAM, THUY DUONG. Ultrasonic and electrokinetic remediation of low permeability soil contaminated with persistent organic pollutants. 2014. Diss.

588. HOKKANEN, SANNA. Modified nano- and microcellulose based adsorption materials in water treatment. 2014. Diss.

589. HINKKANEN, JUHA. Cooperative strategy in emerging markets – analysis of interfirm R&D cooperation and performance in Russian manufacturing companies. 2014. Diss.

590. RUSKOVAARA, ELENA. Entrepreneurship education in basic and upper secondary education – measurement and empirical evidence. 2014. Diss.

591. IKÄHEIMONEN, TUULI. The board of directors as a part of family business governance – multilevel participation and board development. 2014. Diss.

592. HAJIALI, ZUNED. Computational modeling of stented coronary arteries. 2014. Diss.

593. UUSITALO, VILLE. Potential for greenhouse gas emission reductions by using biomethane as road transportation fuel. 2014. Diss.

594. HAVUKAINEN, JOUNI. Biogas production in regional biodegradable waste treatment – possibilities for improving energy performance and reducing GHG emissions. 2014. Diss.

595. HEIKKINEN, JANNE. Vibrations in rotating machinery arising from minor imperfections in component geometries. 2014. Diss.

596. GHALAMCHI, BEHNAM. Dynamic analysis model of spherical roller bearings with defects. 2014. Diss.

597. POLIKARPOVA, MARIIA.Liquid cooling solutions for rotating permanent magnet synchronous machines. 2014. Diss.

598. CHAUDHARI, ASHVINKUMAR. Large-eddy simulation of wind flows over complex terrains for wind energy applications. 2014. Diss.

599. PURHONEN, MIKKO. Minimizing circulating current in parallel-connected photovoltaic inverters. 2014. Diss.

600. SAUKKONEN, ESA. Effects of the partial removal of wood hemicelluloses on the properties of kraft pulp. 2014. Diss.

601. GUDARZI, DAVOOD. Catalytic direct synthesis of hydrogen peroxide in a novel microstructured reactor. 2014. Diss.

602. VALKEAPÄÄ, ANTTI. Development of finite elements for analysis of biomechanical structures using flexible multibody formulations. 2014. Diss.

603. SSEBUGERE, PATRICK. Persistent organic pollutants in sediments and fish from Lake Victoria, East Africa. 2014. Diss.

604. STOKLASA, JAN. Linguistic models for decision support. 2014. Diss.

605. VEPSÄLÄINEN, ARI. Heterogenous mass transfer in fluidized beds by computational fluid dynamics. 2014. Diss.

606. JUVONEN, PASI. Learning information technology business in a changing industry landscape. The case of introducing team entreneurship in renewing bachelor education in information technology in a university of applied sciences. 2014. Diss.

607. MÄKIMATTILA, MARTTI. Organizing for systemic innovations – research on knowledge, interaction and organizational interdependencies. 2014. Diss.

608. HÄMÄLÄINEN, KIMMO. Improving the usability of extruded wood-plastic composites by using modification technology. 2014. Diss.

609. PIRTTILÄ, MIIA. The cycle times of working capital: financial value chain analysis method. 2014. Diss.

610. SUIKKANEN, HEIKKI. Application and development of numerical methods for the modelling of innovative gas cooled fission reactors. 2014. Diss.

611. LI, MING. Stiffness based trajectory planning and feedforward based vibration suppression control of parallel robot machines. 2014. Diss.

612. KOKKONEN, KIRSI. From entrepreneurial opportunities to successful business networks – evidence from bioenergy. 2014. Diss.

613. MAIJANEN-KYLÄHEIKO, PÄIVI. Pursuit of change versus organizational inertia: a study on strategic renewal in the Finnish broadcasting company. 2014. Diss.

614. MBALAWATA, ISAMBI SAILON. Adaptive Markov chain Monte Carlo and Bayesian filtering for state space models. 2014. Diss.

615. UUSITALO, ANTTI. Working fluid selection and design of small-scale waste heat recovery systems based on organic rankine cycles. 2014. Diss.

616. METSO, SARI. A multimethod examination of contributors to successful on-the-job learning of vocational students. 2014. Diss.